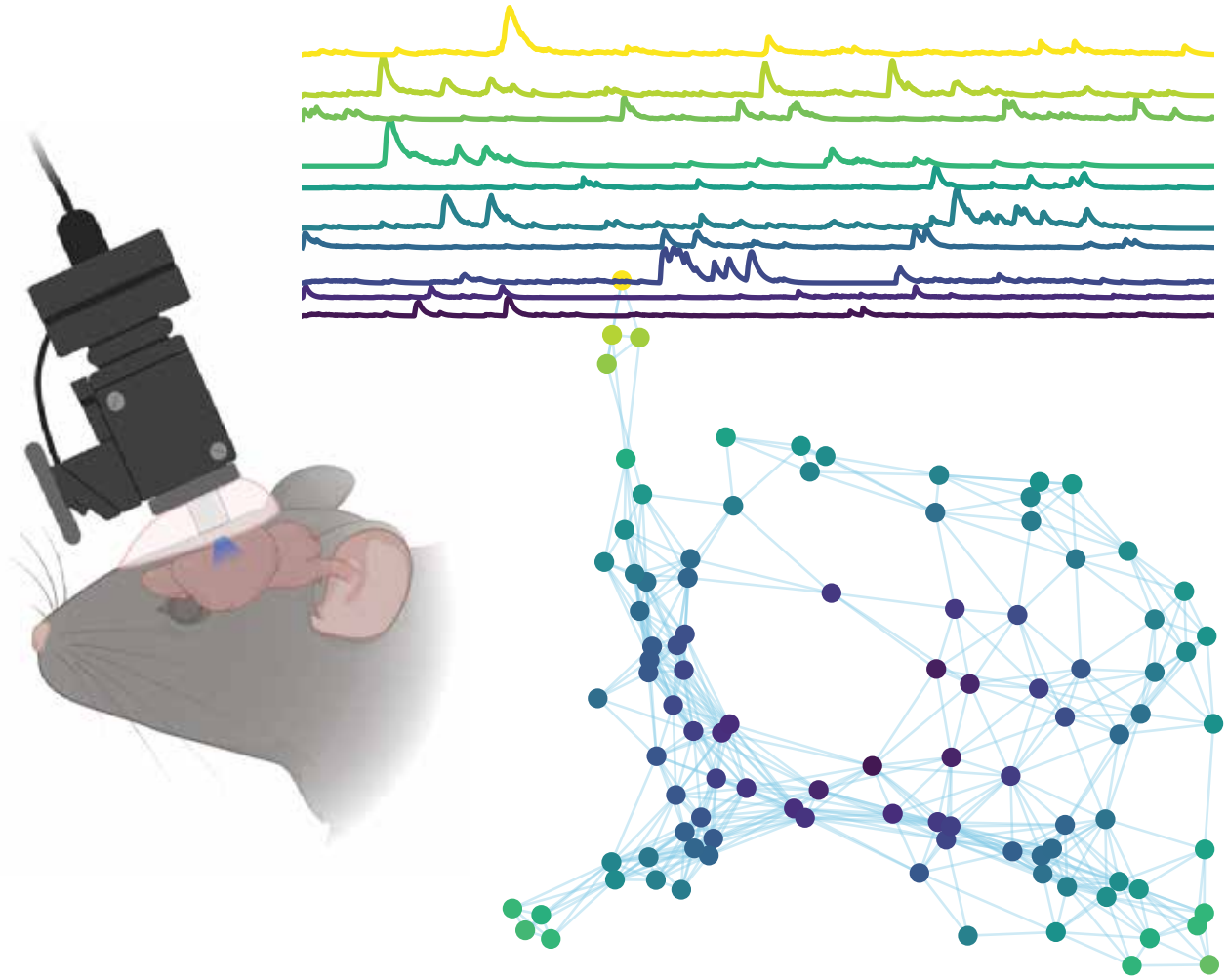
Neuronal activity in dorsal CA1 drives memory consolidation and depends on Arc/Arg3.1

Abdurahman Hassan Abdurahman Kuku

Dissertation Zur Erlangung des akademischen Grades
des Doktors der Naturwissenschaften (Dr.rer.nat.) an der Universität Hamburg,
2025



Universität Hamburg
DER FORSCHUNG | DER LEHRE | DER BILDUNG

Neuronal activity in dorsal CA1 drives memory consolidation and depends on Arc/Arg3.1

Dissertation

Zur Erlangung des akademischen Grades

des Doktors der Naturwissenschaften (Dr.rer.nat.)

des Fachbereichs Biologie,

der Fakultät für Mathematik, Informatik und Naturwissenschaften,

der Universität Hamburg

vorgelegt von

Abdurahman Hassan Abdurahman Kuku

aus Rabak, Sudan

Hamburg, 2025

1st Gutachter: Dr. Ora Ohana

2nd Gutachter: Prof. Dr. Christian Lohrs

Die Arbeit wurde im Zeitraum von Februar 2021 bis Februar 2025 im Institut für Molekulare und Zelluläre Kognition, und von Februar 2025 bis Mai 2025 der Abteilung für Neurochirurgie, des Universitätsklinikum Hamburg-Eppendorf, unter der Anleitung von Herrn Prof. Dietmar Kuhl und Frau Dr. Ora Ohana angefertigt.

Date of disputation: 29 August 2025

Eidesstattliche Versicherung:

Hiermit versichere ich an Eides statt, die vorliegende Dissertationsschrift selbst verfasst und keine anderen als die angegebenen Hilfsmittel und Quellen benutzt zu haben.

Sofern im Zuge der Erstellung der vorliegenden Dissertationsschrift generative Künstliche Intelligenz (gKI) basierte elektronische Hilfsmittel verwendet wurden, versichere ich, dass meine eigene Leistung im Vordergrund stand und dass eine vollständige Dokumentation aller verwendeten Hilfsmittel gemäß der Guten wissenschaftlichen Praxis vorliegt. Ich trage die Verantwortung für eventuell durch die gKI generierte fehlerhafte oder verzerrte Inhalte, fehlerhafte Referenzen, Verstöße gegen das Datenschutz- und Urheberrecht oder Plagiate.

Affidavit:

I hereby declare and affirm that this doctoral dissertation is my own work and that I have not used any aids and sources other than those indicated.

If electronic resources based on generative artificial intelligence (gAI) were used in the course of writing this dissertation, I confirm that my own work was the main and value-adding contribution and that complete documentation of all resources used is available in accordance with good scientific practice. I am responsible for any erroneous or distorted content, incorrect references, violations of data protection and copyright law or plagiarism that may have been generated by the gAI.

Ich versichere, dass dieses gebundene Exemplar der Dissertation und das in elektronischer Form eingereichte Dissertationsexemplar (über den Docata-Upload) und das bei der Fakultät (zuständiges Studienbüro bzw. Promotionsbüro Physik) zur Archivierung eingereichte gedruckte gebundene Exemplar der Dissertationsschrift identisch sind.

I, the undersigned, declare that this bound copy of the dissertation and the dissertation submitted in electronic form (via the Docata upload) and the printed bound copy of the dissertation submitted to the faculty (responsible Academic Office or the Doctoral Office Physics) for archiving are identical.

Hamburg, Datum | Date

Table of Contents

Abbreviations I
List of Figures III
List of Tables V
Graphical Abstract VI
Abstract VII
Zusammenfassung XII
1 Introduction 2
1.1 Memory Systems 3
1.2 Episodic Memory 3
1.2.1 Encoding of memory engram 6
1.2.2 Engram consolidation 7
1.2.3 Engram Retrieval 8
1.2.4 Recognition and Modification of Engrams 9
1.2.5 Tracking Engram Neuron 10
1.3 Synaptic Plasticity and Memory Formation 11
1.3.1 Arc/Arg3.1 12
1.3.2 Arc/Arg3.1 is localized in synapses and regulates synaptic plasticity 12
1.3.3 Arc/Arg3.1 function in behavior 13
1.4 Study aim 14
2 Methods and Materials 17
2.1 Animals 17
2.2 Surgeries 17
2.2.1 Stereotaxic virus injection 18
2.2.2 Implantation of the grin lens 18
2.3 Behavioral Experiments and Calcium Imaging 19
2.3.1 Open Field Test 20
2.3.2 Contextual Fear Conditioning 20
2.4 Calcium Imaging data Acquisition and Processing 22
2.4.1 Source Extraction 22
2.4.2 Place Cells detection 24
2.4.3 Correlated calcium activity graph theory analysis 25
2.4.4 Defining Shock, Tone, Freeze, and Mobility Neuron 26
2.4.5 Neuronal index discrimination 26
2.5 Acquisition and processing of local field potentials and Action Potentials 27
2.5.1 Spike Sorting 27

2.5.2 Cell Type Classification 28
2.6 Key resources table 28
2.7 Statistical Analysis 29
3 Results 31
3.1 Preprocessing of Calcium Imaging Data 31
3.1.1 Motion Correction 32
3.1.2 Source Extraction 33
3.1.3 Random Forest Classifier 35
3.1.4 Neural Activity 37
3.2 Arc/Arg3.1 KO Mice Exhibit Reduced Exploratory Behavior over days 39
3.2.1 Distance Moved 39
3.2.2 Summary of Open Field Exploration 41
3.3 Calcium Dynamics in dCA1 and the Emergence of Place Cell 41
3.3.1 Reduced Calcium Spikes and Events in Arc/Arg3.1 KO 41
3.3.2 Absence of Small Calcium Events in Arc/Arg3.1 KO 43
3.3.3 Identification of Place Cells 46
3.3.4 Reactivation and remapping of place cells 49
3.3.5 Summary Open Field Test 52
3.4 Conserved Electrical Spike Activity in Arc/Arg3.1 KO 53
3.5 Neural Activity Dynamics Are Largely Preserved During Fear Memory Acquisition in Arc/Arg3.1 KO 55
3.5.1 Intact Behavioral Response During Contextual Fear Memory Acquisition in Arc/Arg3.1 KO 56
3.5.2 Episode-Specific Neural Activity Modulation During Fear Memory Acquisition Is Mostly Intact in Arc/Arg3.1 KO 59
3.5.3 Contextual Fear Conditioning Significantly Suppresses Neuronal Activity 62
3.5.4 Differential Neuronal Responses to Shock and Tone Stimuli 65
3.5.5 Impact of Shock on Behavior-Specific Neuronal Population Dynamics 70
3.5.6 Contextual Fear Conditioning Drives Remapping of Place Cells 75
3.5.7 Summary of Fear Memory Acquisition 76
3.6 Disrupted Retrieval of Conditioned Fear Memory in Arc/Arg3.1 KO 78
3.6.1 Impaired Behavioral Response in Recent and Remote Memory in Arc/Arg3.1 KO 78
3.6.2 Impaired Modulation of Neural Activity in Memory Retention in Arc/Arg3.1 KO 80
3.6.3 Behavior-Specific Neuronal Population Dynamics during the CFC 82

3.6.4 Lack of Context-Dependent Modulation of Place Field Coverage in Arc/Arg3.1 KO 83
3.6.5 Coordinated Neural Activity is Impaired in Arc/Arg3.1 KO 84
3.7 High-Excitability Identification and Tracking of Engram Neurons 87
3.7.1 Neural Reactivation Unaffected in Arc/Arg3.1 KO 87
3.7.2 Loss of Coordinated Neural Activity in Arc/Arg3.1 KO in reactivated neurons 90
3.7.3 Reactivation of Shock and Tone-Responsive Neurons 92
3.7.4 Slight Reactivation of Place Cells 94
4 Discussion 98
4.1 Arc/Arg3.1 KO Mice Exhibit Reduced Exploratory Behavior in the Open Field Test 98
4.2 Context-Dependent Modulation in Neural Activity 99
4.2.1 Disrupted Translation of Neural Activity to Calcium Signaling in Arc/Arg3.1 KO 99
4.2.2 Downregulation of Neural Activity after Conditioning 100
4.2.3 Impaired Context-Dependent Neuronal Activity in Arc/Arg3.1 KO 102
4.2.4 Impaired Formation of Coordinated Activity in Arc/Arg3.1 KO 102
4.2.5 Coordinated Activity May be Supported by Early and Late Arc/Arg3.1 Expression 103
4.3 dCA1 Sensory Encoding Remains Almost Intact in Arc/Arg3.1 KO 104
4.3.1 Place Cell Development in a Non-Aversive Environment Unaffected in Arc/Arg3.1 KO 105
4.3.2 Expansion of Place Field Coverage Drives Context-Dependent Memory 105
4.3.3 Mobility Neurons Exhibit Context-Dependent Variability 106
4.3.4 Conserved Freeze Neuron Activity in Arc/Arg3.1 KO 107
4.3.5 Intact Encoding of Conditioned and Unconditioned Stimuli in Arc/Arg3.1 KO 108
4.4 How does Arc/Arg3.1 affect context encoding and memory: a model 108
4.5 Experiment Limitation 109
5 Future Perspectives 110
6 Supplementary 113
6.1 Supplementary tables 113
6.2 Statement of Contributions 131
6.3 Acknowledgments 132
7 Reference 133

Abbreviations

Arc/Arg3.1	Activity-Regulated Cytoskeletal-associated protein/ Activity-Regulated Gene 3.1
AUC	Area under curve
BLA	Basolateral amygdala
CaM	Calmodulin
CC	Clustering Coefficient
CeA	Central Amygdala
CFC	Contextual Fear Conditioning
CREB	Cyclic AMP Response Element-binding Protein
CS	Conditioned Stimuli
DG	Dentate Gyrus
Dox	Doxycycline
DV	Dorsal / Ventral
EC	Entorhinal Cortex
fEPSP	Field Excitatory Postsynaptic Potential
GECIs	Genetically Encoded Calcium Indicators
GLM	Generalized Linear Model
GRIN	Gradient Index
IDPS	Inscopix Data Processing Software
IEGs	Immediate Early Genes
IEI	inter-event interval
ISI	Inter Spike interval
KO	knockout
LA	Lateral Amygdala
LAvl	Ventral Lateral Nucleus of the Lateral Amygdala
LFP	Local Field Potentials
LTD	long-term depression
LTM	long-term memory
LTP	long-term potentiation
MAPKs	mitogen-activated protein kinases
mEPSCs	miniature excitatory postsynaptic currents
mGluR1s	group 1 metabotropic glutamate receptors
MI	Mutual Information
miniscopes	head-mounted miniaturized microscopes
mRNA	messenger Ribonucleic acid
MTT	Multiple Trace Theory
MWM	Morris water maze
NAcc	nucleus accumbens
nAChR	nicotinic acetylcholine receptors
NI	nucleus incertus
NMDARs	N-methyl-D-aspartate receptor
NMI	Neuronal Modulation Index
OB	olfactory bulb

ODNs	oligodeoxynucleotides
OFT	Open Field Task
ORF	open reading frame
PCA	Principal Component Analysis
PFC	prefrontal cortex
PSD	postsynaptic density
REM	rapid eye moments
ROIs	regions of interest
RSC	retrosplenial cortex
SK	sensory cortex
SNR	Signal to noise Ratio
STM	Short term memory
SWRs	sharp-wave ripples
SWS	Slow wave sleep
TRPCC	transient receptor potential type C channels
tTA	tetracycline transactivator
US	unconditioned stimulus
UTR	untranslated region
VGCC	voltage-gated calcium channels
WT	Wildtype
2ST-Sidak	Two-sample t-tests with Sidak correction for multiple comparisons

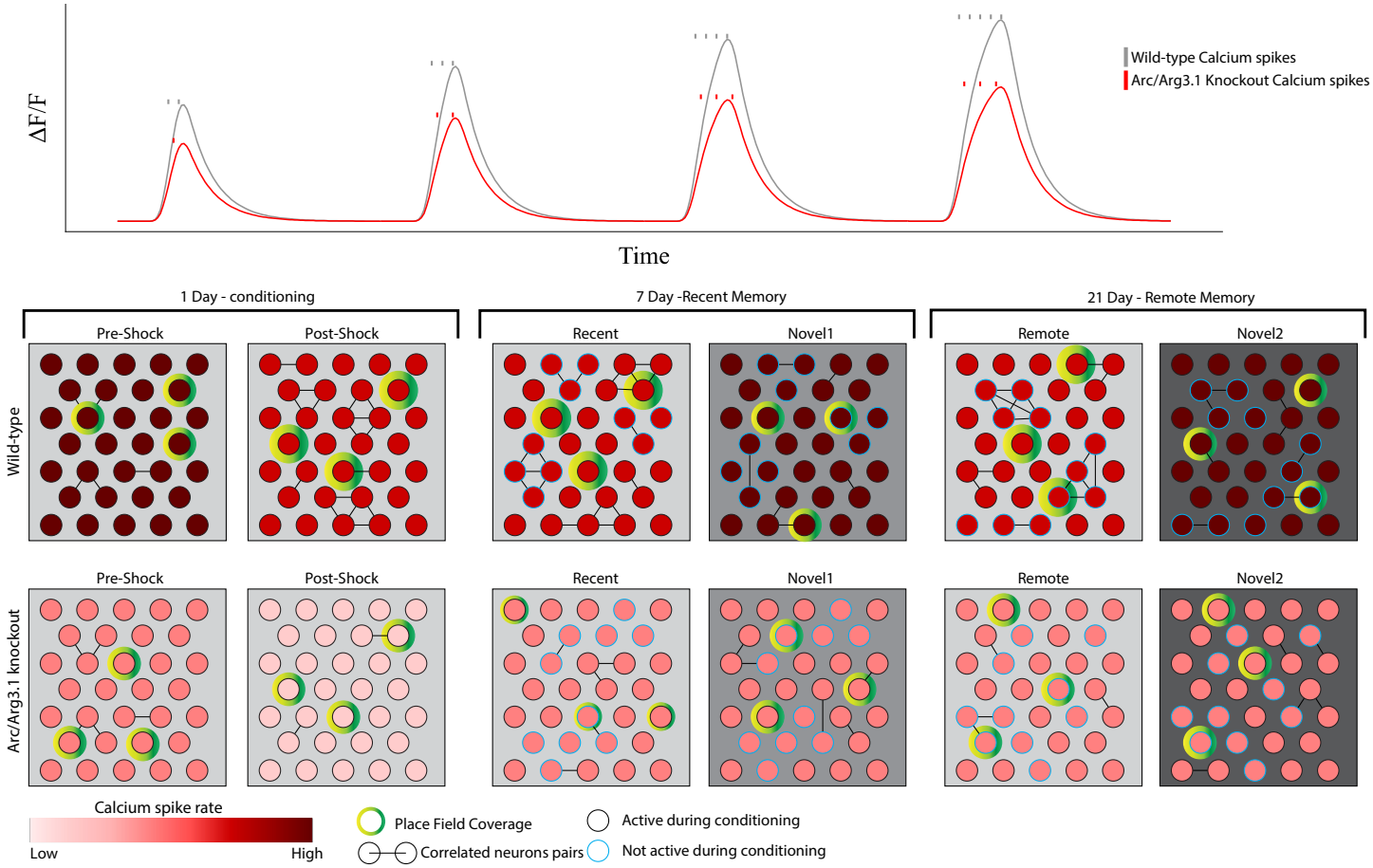
List of Figures

Figure 1.2-1 A canonical view of the memory engram for each stage of memory 6
Figure 1.2-2 Engram studies. 10
Figure 1.3-1 Arc/Arg3.1 on synaptic plasticity. 13
Figure 3.1-1 *In vivo* calcium imaging of dCA1 neurons expressing GCaMP8m in freely behaving mice. 32
Figure 3.1-2 Motion Correction of Calcium Imaging Data. 33
Figure 3.1-3 CNMFe parameters exploration. 34
Figure 3.1-4 Manual correction of spatial footprints and traces. 36
Figure 3.1-5 Performance and Feature Importance of the Random Forest Model. 37
Figure 3.1-6 Representation of Calcium Activity. 38
Figure 3.2-1 Total distance traveled. 40
Figure 3.3-1 Number of neurons and their calcium spike rate in the open field task. 42
Figure 3.3-2 Various methods for quantifying calcium activity. 43
Figure 3.3-3 Calcium spikes' amplitude and bursting index. 44
Figure 3.3-4 Calcium Burst. 45
Figure 3.3-5 Example of a place cell in the open field. 47
Figure 3.3-6 Place cells during the open field exploration task. 48
Figure 3.3-7 Proportion of reactivated neurons in OFT-day2 and OFT-day3. 50
Figure 3.3-8 Place cell remapping in the OFT. 51
Figure 3.4-1 Local field potential recording in the CA1 53
Figure 3.4-2 Example of an isolated neuron. 54
Figure 3.4-3 Firing rate of excitatory and inhibitory neurons. 55
Figure 3.5-1 Contextual fear conditioning paradigm 56
Figure 3.5-2 CFC: Behavioral response to fear conditioning. 57
Figure 3.5-3 Calcium spike rates during fear acquisition. 60
Figure 3.5-4 dF/F trace of inhibited or excited neurons post-conditioning. 63
Figure 3.5-5 Calcium spike rate of excited and inhibited neurons post-conditioning. 64
Figure 3.5-6 Shock-and tone-neurons. 67
Figure 3.5-7 The proportion of inhibited versus excited tone- and shock-neurons. 69
Figure 3.5-8 Mobility and freeze-neurons neurons. 72
Figure 3.5-9 Remapping of freeze- and mobility-neurons post conditioning 74
Figure 3.5-10 Place cells remap in the pre- to post-shock session. 75
Figure 3.6-1 Freezing behavior in recent and remote memory test. 79
Figure 3.6-2 Neurons recorded during the CFC and their calcium spike rate. 81
Figure 3.6-3 Mobility and freeze-neurons during the CFC sessions. 83
Figure 3.6-4 Place cell dynamics during the CFC sessions. 84
Figure 3.6-5 Example of correlated neurons 85
Figure 3.6-6 Calcium spike activity correlation 86
Figure 3.7-1 Neuron Reactivation A) 88
Figure 3.7-2 Calcium spike rate of Engram neurons 89
Figure 3.7-3 Correlated pairs within engram neurons 91
Figure 3.7-4 Reactivation of tone and shock neurons 93
Figure 3.7-5 Place cell reactivation from the conditioning session 95
Figure 3.7-6 Place cell reactivation from the Recent session 96

List of Tables

Stats-table 1 Distance travelled with and without a miniscope 113
Stats-table 2 Mice with a miniscope 113
Stats-table 3 WT-control miniscope effect 113
Stats-table 4 Arc/Arg3.1-knockout miniscope effect 114
Stats-table 5 Fraction of neurons active in a given day 114
Stats-table 6 Calcium spike rate: 2-way ANOVA for Genotype X OFT-days 114
Stats-table 7 Proportion of Place cells over days 115
Stats-table 8 Place field size over days: 2-way ANOVA for Genotype X OFT-days 115
Stats-table 9 Calcium rate place cells vs non-place cells 115
Stats-table 10 Freezing percentage over the different conditioning episodes 116
Stats-table 11 Freeze bouts duration: 2-way ANOVA for Genotype X episodes 117
Stats-table 12 Frequency of freeze bouts for each episodes 118
Stats-table 13 Inter-freezing bout-interval: 2-way ANOVA for Genotype X episodes 120
Stats-table 14 Calcium spike rates during the conditioning episodes 120
Stats-table 15 NMI of calcium spike rates 121
Stats-table 16 NMI of excited neurons 122
Stats-table 17 NMI of inhibited neurons: 123
Stats-table 18 Freezing percentage over the different CFC days 124
Stats-table 19 2 Freeze bouts duration 125
Stats-table 20 Number of freezing bouts 126
Stats-table 21 Firing rate during each session of CFC 127
Stats-table 22 Calcium rate place cells vs non-place cells 128
Stats-table 23 Correlated pairs across the sessions 128
Stats-table 24 Correlation coefficient for the conditioning sessions 129
Stats-table 25 Calcium Spike rate of reactivated neurons 130

Graphical Abstract



Abstract

Learning and memory are fundamental aspects of human cognition, encompassing complex processes that facilitate the encoding, consolidation, and retrieval of information and experiences that are essential for survival, adaptation, and abstract thinking. Despite decades of rigorous research, understanding the mechanisms behind memory encoding and consolidation remains a significant challenge. On the molecular level, novel gene transcription initiated during memory acquisition starts a cascade of molecular and cellular events concluding with structural and functional modulations of neurons, synapses, and memory-relevant neural networks. On a systemic level, a prevalent and re-emerging theory suggests that memories are integrated into engrams, which consist of groups of neurons (engram neurons) that are active during learning and are reactivated during memory retrieval. At the heart of this hypothesis lies the assumption that the collective activity pattern of engram neurons constitutes the very code of the stored information and contains distinctive elements setting it apart it from other acquired memories. The replay of these activity patterns can revoke the specific memory. Recent development of miniaturized head-mounted microscopes, so called miniscopes, combined with genetically-encoded calcium indicators (GECIs), provides a platform for recording the simultaneous activity of hundreds of individual neurons in the brains of freely behaving animal models. A surge of recent studies utilizing these techniques, provided invaluable information on neural activity supporting memory acquisition and retrieval. Nonetheless, many fundamental questions remain unanswered, in particular, what activity patterns and possibly engrams, support the persistence of memories over long-periods of time while maintaining their specificity? How does the process of molecular consolidation affect the emergence and time-dependent evolution of memory engrams and their activity?

The aim of this thesis is to address these questions by employing miniscopes and GECI technologies to perform longitudinal calcium imaging from mice performing a contextual fear memory task over several weeks. To unveil the contribution of molecular consolidation to formation and time-dependent evolution of memory engrams, I chose to investigate Arc/Arg3.1 KO mice, which fully lack the ability to consolidate long-term memory.

The activity-regulated cytoskeleton-associated protein Arc/Arg3.1 is coded by the immediate-early gene (IEG) ARC/ARG3.1, known for its central role in memory. Arc/Arg3.1 expression in the hippocampus is low under baseline activity, but is rapidly and strongly upregulated by plasticity-inducing stimuli, novel experience, learning and memory retrieval. Previous work

from our lab and others, demonstrated that genetic deletion or inhibition of ARC/ARG3.1, resulted in failure to stabilize synaptic plasticity and a concurrent loss of long-term memories. Given the importance of the hippocampus to episodic memory and its dynamic expression of Arc/Arg3.1, we chose to investigate neural activity and memory engrams in the dorsal CA1 (dCA1) region.

We injected jGCaMP8m, a fast and sensitive GECI into the dCA1 of adult mice and implanted GRIN lenses for chronic imaging. The Inscopix miniscope and acquisition system were used to acquire calcium signals in vivo. Calcium imaging data were pre-processes to remove noise and motion artifacts. Calcium imaging data were motion-corrected within and between all imaging sessions of the longitudinal study. We conducted source extraction to obtain footprints of individual neurons and extracted their calcium traces, which were further refined with the aid of a Random Forest model. Finally, calcium traces were deconvolved into Calcium spikes using the OASIS algorithm. Calcium spikes were then used to identify place cells and neurons responsive to shock, tone, freezing, and mobility. Additionally, we conducted multi-electrode in vivo recordings from urethane-anesthetized mice in dorsal CA1, to examine action potential firing in WT and KO mice.

In part 1, we evaluated exploratory behavior in an open field arena, to examine possible influence of the surgical procedure and the tethering of the miniaturized microscopes on mice behavior. We found no significant differences in exploratory behavior between non-implanted and implanted mice, confirming preservation of native behavior under the imaging conditions. In all mice, exploratory activity in the same arena, declined on subsequent testing days, a sign of natural habituation. We noted stronger habituation in the KO mice.

Interestingly, calcium activity rates were lower in dCA1 of KO mice compared with WT littermates. Reduced calcium activity was associated with smaller amplitudes and shorter durations of complex calcium events but not with their numbers. Deconvolution of calcium events indicated a decrease in the number of spikes contributing to each event. Since calcium events result primarily from action-potential mediated influx through voltage dependent calcium channels, both reduction in action potential firing rates and alterations in calcium influx, might be responsible for the reduced calcium activity in the KO mice. We tested this possibility by recording extracellularly, action potentials (spikes) in dCA1 of urethane-anesthetized mice. We observed similar firing rates in KO and WT neurons, pointing towards the intriguing possibility of altered calcium influx regulation in the KO mice, as the source of reduced calcium spike activity.

A central function of CA1, is to encode location through place activity of its neurons. We thus analyzed calcium spikes for signs of place cell activity. Our findings reveal that KO mice contain slightly lower percentage of place cells, with similar place field size but weaker tuning, compared to WT. Across the three testing days, Place cells displayed higher and more stable activity rates, compared to other neurons for both WT and KO. Remapping of place cells between testing days was predominant in both genotypes, with non-significantly increased stability of WT neurons. In total, these findings show rather subtle differences between WT and KO place cell properties, indicating that despite the difference in calcium spike activity, Arc/Arg3.1 KO mice, maintained basic ability for functional space encoding in dCA1.

The second and major part of the thesis, investigates the link between neural activity and memory consolidation over long time periods. Implanted WT and KO mice underwent contextual fear conditioning and were tested in the conditioning context and in a novel context twice: 7 days (recent memory) and 21 (remote memory) days after conditioning. Firstly, we asked how WT and KO mice encoded contextual, sensory and behavior-associated information during the conditioning session. Behavioral analysis showed prolonged freezing in all mice following conditioning, reaffirming successful fear conditioning in WT and KO mice, as previously reported. Analysis of the simultaneously recorded calcium traces revealed a widespread reduction in calcium activity rates after the conditioning, that was particularly pronounced in the WT neurons. In both genotypes, activity rates decreased in two-thirds of the neurons but increased in the remaining third. We identified neurons with heightened responses to either tone or shock stimuli or to both. In both WT and KO mice, tone and shock neurons constituted, each, roughly 9% of all neurons and dual-responding neurons less than 1%. No significant differences were detected in the distribution of stimulus-responsive neurons between KO and WT neurons, or in their averaged population activity. Examination of the post-conditioning activity of these neurons, revealed that contrary to the overall inhibition of CA1 neurons, most tone-responsive neurons were excited in WT and KO mice alike. Divergent modulations were observed for the shock-responsive neurons, that were largely inhibited in the WT, but excited in the KO mice. During pre- and post-shock periods, mice engaged in two types of behavior: movement as an exploratory activity and freezing, signifying risk assessment, anxiety and fear. The proportion of time mice engaged with each behavior, changed dramatically after conditioning. We classified neurons, as either mobility- or freezing-responsive when their activity rates were significantly increased during concurrent behavior. Neurons without significantly preferred responses were classified as “others”. Prior to conditioning (Pre-shock), the distribution of neuronal classes was overall similar among WT and KO mice, constituting of a minority of freeze-neurons

followed by a larger fraction of mobility neurons and a majority of neurons classified as others. In the post-conditioning episode, freezing bouts increased in number and duration and concordantly the number of freezing-responsive neurons. An even stronger modulation was observed for the mobility-neurons, most of which lost their preferred response altogether. One interpretation of these findings is that, fear-induced freezing is largely supported by removal of mobility-related activity, in addition to recruitment of fear-related activity. The similarity of these activity modulations among WT and KO, reflects their similar behavioral responses. Analysis of place cell activity was performed also for the conditioning context, showing similar fractions of place cells in WT and KO, and for both genotypes, only a small subset of neurons maintained their classification as place cells across both pre- and post-shock episodes (less the 2%).

In summary, analysis of calcium-spike activity, revealed similar fractions of tone, shock, mobility, freezing and place cell specific neurons, in WT and KO mice, suggesting that despite reduced activity rates in KO neurons, encoding of these functional properties, emerged independently of Arc/Arg3.1 presence and remained sufficiently efficient to support the rapid aversive learning observed in the Arc/Arg3.1 KO mice. To our surprise, conditioning silenced the majority of neurons in dCA1 of both genotypes.

We next investigated neural activity patterns during recent and remote memory recall. As shown in the first chapter, WT mice showed significantly higher percentage freezing in the conditioning context during recent and remote tests, but much weaker freezing in the novel contexts, indicating successful formation of strong and specific context memory. In contrast, the KO mice displayed weak and indiscriminate freezing in the conditioning and novel contexts, indicating their inability to consolidate the memory. Analysis of the collective population calcium activity, revealed a distinct pattern associated with the detection of familiar and novel environments. When WT mice were placed in the familiar conditioning-environment, the hippocampus calcium activity was reduced but significantly increased when the mice were placed shortly afterwards in a novel environment; this pattern was entirely absent in KO mice. We investigated the degree of correlation between neurons in the same mice, classifying significant ones as correlation partners. Analysis of WT mice, revealed a stark increase in the number of correlation-partners in the familiar conditioning-environment but not in the novel ones. Again, this coactivation signature was absent in KO neurons. Place cell activity displayed a similar modulation in WT mice, where their numbers and activity rates dropped in the familiar- but increased in the novel contexts. A similar but weaker pattern of place cell recruitment and activity was observed in KO mice. A striking difference between WT and KO became apparent

upon analysis of the place field size: whereas in WT the field size increased after shock and was retained in the familiar context but reduced in the novel, the exact opposite modulation was observed in KO place cells. These findings confirm that place cells activity, contributes to distinction between familiar and novel environment up to three weeks post conditioning. Moreover, these findings suggest that while formation of place cells was not strongly affected by the loss of Arc/Arg3.1 in the KO mice, their modulation along the process of memory consolidation, was strongly altered.

Finally, we attempted to detect neural engrams that encode the conditioning context and are reliably reactivated during recent and remote memory tests. We also expected such engrams to differ significantly from those active in the unfamiliar contexts. We explored two engram definitions based on their heightened activity, either during the pre-shock episode or the during recent memory test in the familiar context. The number of reactivated neurons, based on either engram-definition was similar among genotypes and environments. However, activity rates of neurons allocated to the engram and their correlation values, displayed a significant environment-dependent modulation in WT mice but not in KO neurons. In total, our exploration of putative memory engrams supports the notion that highly active neurons are more likely to be allocated into the engram. However, it also suggests that rates and correlations of activity contribute most significantly to a memory signature rather than the size or identity of specific neurons.

In total, this thesis presents new findings on activity and functional encoding in Arc/Arg3.1 KO mice and sheds new light on the neural activity code underlying long-term memory consolidation. These include the following:

1. Arc/Arg3.1 regulates activity-dependent calcium influx in the hippocampus.

2. The emergence and formation of neurons encoding sensory, spatial, and behavioral information in dCA1 are independent of Arc/Arg3.1 plasticity.

3. Enhanced activity rates and neural synchronization underlie successful memory retrieval and distinguish familiar from novel information.

4. Modulation of activity rates and neural synchronization along the process of memory consolidation is driven by Arc/Arg3.1 expression in the brain.

Zusammenfassung

Lernen und Gedächtnis sind grundlegende Bestandteile menschlicher Kognition. Sie umfassen komplexe Prozesse welche für das Überleben, Adaptionen und abstraktes Denken essenziell sind. Hierzu zählen die Kodierung, Konsolidierung und der Abruf von Informationen und Erfahrungen. Trotz jahrzehntelanger intensiver Forschung sind die zugrundeliegenden Mechanismen der Kodierung und Konsolidierung des Gedächtnisses bis heute unbekannt. Auf molekularer Ebene setzt eine neue Gentranskription während des Gedächtniserwerbs eine Kaskade molekularer und zellulärer Ereignisse in Gang welche in einer strukturellen und funktionellen Modulation von Neuronen, Synapsen und gedächtnisrelevanten neuronalen Netzwerken resultiert. Auf der systemischen Ebene schlägt eine weit verbreitete Theorie vor, dass Erinnerungen in Engramme codiertwerden. Diese Engramme bestehen aus Gruppen von Neuronen (En-grammneuronen), welche während des Lernens aktiv sind und beim Abrufen von Erinnerungen reaktiviert werden. Im Mittelpunkt der Theorie steht die Annahme, dass das kollektive Aktivitätsmuster der Engrammneuronen den eigentlichen Code der gespeicherten Information darstellt und charakteristische Elemente enthält, welche sie von anderen erworbenen Erinnerungen un-terscheiden. Die Wiederholung dieser Aktivitätsmuster kann die spezifische Erinnerung wie-derherstellen. Die jüngste Entwicklung miniaturisierter kopfgetragener Mikroskope, so genann-ter Miniskope, in Verbindung mit genetisch kodierten Kalziumindikatoren (GECIs) bietet eine Plattform für die gleichzeitige Aufzeichnung der Aktivität von Hunderten einzelner Neuronen im Gehirn frei agierender Tiermodelle. Eine Reihe neuerer Studien, bei denen diese Techniken zum Einsatz kamen, lieferten wichtige Informationen über die neuronale Aktivität, die den Erwerb und das Abrufen von Gedächtnisinhalten unterstützt. Dennoch bleiben viele grundlegen-de Fragen unbeantwortet. Insbesondere die Frage, welche Aktivitätsmuster und potenzielle Engramme die Persistenz von Erinnerungen über lange Zeiträume hinweg unterstützen und dabei ihre Spezifität erhalten? Eine weitere bislang unbeantwortete Frage ist inwiefern sich der Prozess der molekularen Konsolidierung auf die Entstehung und zeitabhängige Entwicklung von Gedächtnis-Engrammen und deren Aktivität auswirkt?

Ziel dieser Arbeit ist es, diese Fragen zu beantworten, indem Miniskope und GECI-Technologien eingesetzt werden. Diese ermöglichen eine longitudinale Kalziumbildgebung anhand dieser die neuronale Aktivität von Mausmodellen, während kontextuelle Furchtge-dächtnisaufgaben über mehrere Wochen verfolgt werden kann. Um den Beitrag der molekula-ren Konsolidierung zur Bildung und zeitabhängigen Entwicklung von Gedächtnis-Engrammen

aufzudecken, habe ich mich für die Untersuchung von Arc/Arg3.1 KO-Mäusen entschieden, denen die Fähigkeit zur Konsolidierung des Langzeitgedächtnisses vollständig fehlt.

Das aktivitätsregulierte Zytoskelett-assoziierte Protein Arc/Arg3.1 wird durch das Immediate-Early-Gen (IEG) ARC/ARG3.1 kodiert, das für seine zentrale Rolle im Gedächtnis bekannt ist. Die Expression von Arc/Arg3.1 im Hippocampus ist bei Grundaktivität gering, wird aber durch plastizitätsfördernde Reize, neue Erfahrungen, Lernen und Gedächtnisabruf schnell und stark hochreguliert. Frühere Arbeiten unserer Arbeitsgruppe und anderer haben gezeigt, dass die genetische Deletion oder Inhibition von ARC/ARG3.1, zu einer fehlenden Stabilisierung der synaptischen Plastizität und zu einem gleichzeitigen Verlust des Langzeitgedächtnisses führt. Angesichts der Bedeutung des Hippocampus für das episodische Gedächtnis und seiner dynamischen Expression von Arc/Arg3.1 haben wir uns entschieden, die neuronale Aktivität und die Gedächtnis-Engramme in der dorsalen CA1-Region (dCA1) zu untersuchen.

Wir injizierten jGCaMP8m, ein schnelles und empfindliches GECI, in die dCA1 von adulten-Mäusen und implantierten GRIN-Linsen für die chronische Bildgebung. Das Inscopix-Miniskop und das Aufnahmesystem wurden zur Erfassung von Kalziumsignalen in vivo ver-wendet. Die Kalzium-Bilddaten wurden vorverarbeitet, um Rauschen und Bewegungsartefakte zu entfernen. Die Kalzium-Bilddaten wurden innerhalb und zwischen allen Bildgebungssitzun-gen der Längsschnittstudie bewegungskorrigiert. Wir führten eine Quellenextraktion durch, um Fußabdrücke einzelner Neuronen zu erhalten, und extrahierten deren Kalziumspuren, die mit Hilfe eines Random Forest-Modells weiter verbessert wurden. Schließlich wurden die Kalziumspuren mit Hilfe des OASIS-Algorithmus zu Kalziumspikes dekonvolviert. Die Kalziumspikes wurden dann zur Identifizierung von Ortszellen und Neuronen verwendet, die auf Schock, Tonus, Einfrieren und Mobilität reagieren. Zusätzlich führten wir in vivo Multi-Elektroden-Aufnahmen von Mäusen im dorsalen CA1 durch, um das Feuern von Aktionspo-tentialen bei WT- und KO-Mäusen zu untersuchen.

Im ersten Teil des Projektes untersuchten wir das Erkundungsverhalten in einer offenen Feldarena, um mögliche Einflüsse des chirurgischen Eingriffs und der Anbringung der Miniaturmikroskope auf das Verhalten der Mäuse zu untersuchen. Wir fanden keine signifikanten Unterschiede im Erkundungsverhalten zwischen nicht-implantierten und implantierten Mäusen, welches die Bewahrung des natürlichen Verhaltens unter den Bildgebungsbedingungen bestätigt. Bei allen Mäusen nahm die Erkundungsaktivität in derselben Arena an den folgenden Testtagen ab, welches ein Zeichen für die natürliche Gewöhnung ist. Wir stellten eine stärkere Gewöhnung bei den KO-Mäusen fest.

Interessanterweise waren die Kalziumaktivitätsraten in dCA1 von KO-Mäusen im Vergleich zu WT-Wurfgeschwistern geringer. Die geringere Kalziumaktivität ging mit kleineren Amplituden und kürzeren Dauern komplexer Kalziumereignisse einher, nicht aber mit deren Anzahl. Die Dekonvolution der Kalziumereignisse zeigte eine Abnahme der Anzahl von Spikes, die zu jedem Ereignis beitragen. Da Kalziumereignisse in erster Linie aus dem durch Aktionspotenziale vermittelten Einstrom von Kalziumionen durch spannungsabhängige Kalziumkanäle resultie-ren, könnten sowohl eine Verringerung der Feuerfrequenz von Aktionspotenzialen als auch Veränderungen des Kalziumeinstroms für die verringerte Kalziumaktivität in den KO-Mäusen verantwortlich sein. Wir testeten diese Möglichkeit durch extrazelluläre Aufzeichnungen von Aktionspotenzialen (Spikes) in dCA1 von mit Urethan betäubten Mäusen. Wir beobachteten ähnliche Feuerfrequenzen in KO- und WT-Neuronen, welches auf eine veränderte Regulierung des Kalziumeinstroms in den KO-Mäusen als Ursache für die verringerte Kalziumspike-Aktivität hindeutet.

Eine zentrale Funktion der CA1-Region besteht darin, durch die Ortsaktivität seiner Neuronen den Ort zu kodieren. Daher haben wir die Kalziumspikes auf Anzeichen von Ortszellenaktivität untersucht. Unsere Ergebnisse zeigen, dass KO-Mäuse einen geringfügig niedrigeren Prozentsatz an Ortszellen mit einer ähnlichen Größe des Ortsfeldes, aber einer schwächeren Abstimmung im Vergleich zu WT-Mäusen aufweisen. Über die drei Testtage hinweg zeigten die Ortszellen höhere und stabilere Aktivitätsraten im Vergleich zu anderen Neuronen, sowohl bei WT als auch bei KO-Mäusen. Das Neuzuordnung von Ortszellen zwischen den Testtagen war bei beiden Genotypen vorherrschend, wobei die Stabilität der WT-Neuronen nicht signifikant erhöht war. Insgesamt zeigen diese Ergebnisse eher subtile Unterschiede zwischen der WT- und KO-Ortszellen, was darauf hindeutet, dass in Arc/Arg3.1 KO-Mäuse trotz des Unterschieds in der Kalziumspike-Aktivität die grundlegende Fähigkeit zur funktionellen Raumkodierung in dCA1 erhalten blieb.

Im zweiten Teil der Arbeit wird der Zusammenhang zwischen neuronaler Aktivität und Gedächtniskonsolidierung über lange Zeiträume untersucht. Implantierte WT- und KO-Mäuse wurden einer kontextuellen Angstkonditionierung unterzogen und jeweils zweimal im konditionierenden Kontext und in einem neuen Kontext getestet: 7 Tage (rezentes Gedächtnis) und 21 Tage (Remote Gedächtnis) nach der Konditionierung. Zunächst untersuchten wir, wie WT- und KO-Mäuse während der Konditionierung kontextuelle, sensorische und verhaltensbezoge-ne Informationen kodierten. Die Verhaltensanalyse zeigte bei allen Mäusen ein verlängertes Einfrieren nach der Konditionierung, was die erfolgreiche Angstkonditionierung bei WT- und KO-

Mäusen bestätigt. Die Analyse der simultan aufgezeichneten Kalzium Daten signale zeigten eine Verringerung der Kalziumaktivitätsraten nach der Konditionierung, welches insbeson-dere bei den WT-Neuronen ausgeprägt war. Bei beiden Genotypen nahmen die Aktivitätsraten in zwei Dritteln der Neuronen ab, während diese in dem verbleibenden Drittel zunahmen. Wir konnten Neuronen identifizieren, welche verstärkte Reaktionen entweder auf Ton- oder Schockreize oder auf beides zeigten. Sowohl bei den WT- als auch bei den KO-Mäusen betrug der Anteil der Neuronen, welche auf Ton- und Schockreize reagierten, jeweils etwa 9 % aller Neuronen, während der Anteil der Neuronen mit doppelter Reaktion weniger als 1 % betrug. Es wurden keine signifikanten Unterschiede in dem Vorkommen der auf die Reize reagierenden Neuronen zwischen KO- und WT-Neuronen oder in ihrer gemittelten Populationsaktivität festgestellt. Die Untersuchung der Aktivität dieser Neuronen nach der Konditionierung ergab, dass im Gegensatz zur allgemeinen Inhibition der CA1-Neuronen die meisten tonreagierenden Neuronen sowohl bei WT- als auch bei KO-Mäusen aktiv waren. Die Modulationen der auf die Schocks reagierenden Neuronen unterschied sich zwischen WT- und KO-Mäusen. Während die Neuronen der WT-Mäuse weitgehend inhibiert wurden, wurden diese bei den KO-Mäusen aktiviert. Das Verhalten der Mäuse vor und nach dem Schock zeigte zwei Arten Reaktionen: Bewegung als Erkundungsaktivität und Einfrieren als Zeichen für Risikobewertung, Angst und Furcht. Der Anteil der Zeit, in der die Mäuse jedes Verhalten ausübten, änderte sich nach der Konditionierung deutlich. Wir klassifizierten Neuronen als entweder auf Bewegung oder auf Einfrieren reagierend, wenn ihre Aktivitätsraten während des gleichzeitigen Verhaltens signifikant erhöht waren. Neuronen ohne signifikant bevorzugte Reaktionen wurden als "andere" klassifiziert. Vor der Konditionierung (Prä-Schock) war die Verteilung der Neuronen-Klassen bei WT- und KO-Mäusen vergleichbar und bestand aus einer Minderheit von Freeze-Neuronen, einem etwas größeren Anteil von Mobilitäts-Neuronen und einer Mehrheit von Neu-ronen, die als "andere" klassifiziert wurden. In der Postkonditionierungsepisode erhöhten sich Anzahl und Dauer der Freezing-Bouts und damit auch die Anzahl der Neuronen, die auf Free-zing reagieren. Eine noch stärkere Modulation wurde bei den Mobilitätsneuronen beobachtet, von denen die meisten ihre bevorzugte Reaktion gänzlich verloren. Eine Interpretation dieser Ergebnisse ist, dass das angstinduzierte Einfrieren weitgehend durch die Beseitigung der mobi-litätsbezogenen Aktivität zusätzlich zur Rekrutierung der angstbezogenen Aktivität unterstützt wird. Die Ähnlichkeit dieser Aktivitätsmodulationen bei WT und KO spiegelt ihre ähnlichen Verhaltensreaktionen wider. Die Analyse der Ortszellenaktivität wurde auch für den Konditio-nierungskontext durchgeführt und zeigte ähnliche Anteile von Ortszellen in WT und KO. In-beiden

Genotypen behielt nur eine kleine Untergruppe von Neuronen ihre Klassifizierung als Ortszellen sowohl vor als auch nach den Schockepisoden bei (weniger als 2%).

Zusammenfassend lässt sich sagen, dass die Analyse der Kalzium-Spike-Aktivität ähnliche Anteile an tonus-, schock-, mobilitäts-, gefrier- und ortsspezifischen Neuronen in WT- und KO-Mäusen ergab. Dieses deutet darauf hin, dass die Kodierung dieser funktionellen Eigenschaften trotz reduzierter Aktivitätsraten in den KO-Neuronen unabhängig von der Anwesenheit von Arc/Arg3.1 entstand und ausreichend effizient blieb, um das schnelle aversive Lernen zu unterstützen, das bei den Arc/Arg3.1-KO-Mäusen beobachtet wurde. Ein unerwartetes Resultat der Konditionierung war die Inhibition der Mehrheit der Neuronen in dCA1 in beider Genotypen.

Als nächstes untersuchten wir die neuronalen Aktivitätsmuster während des Abrufs des rezenter - und Ferngedächtnisses. Wie im ersten Kapitel gezeigt, zeigten WT-Mäuse einen signifikant höheren Prozentsatz des Einfrierens im konditionierenden Kontext während rezenter und Fern tests, aber ein viel schwächeres Einfrieren in den neuen Kontexten, was auf eine erfolgreiche Bildung eines starken und spezifischen Kontextgedächtnisses hindeutet. Im Gegensatz dazu zeigten die KO-Mäuse ein schwaches und wahlloses unspezifisches Einfrieren in den konditionierenden und neuen Kontexten, was auf ihre Unfähigkeit zur Gedächtniskonsolidierung hinweist. Die Analyse der kollektiven Kalziumaktivität der Population zeigte ein unterschiedliches Muster, das mit der Erkennung von vertrauten und neuen Umgebungen verbunden war. Wenn WT-Mäuse in die vertraute Konditionierungsumgebung gebracht wurden, war die Kalziumaktivität im Hippocampus reduziert, aber signifikant erhöht, wenn die Mäuse in eine neue Umgebung gebracht wurden; dieses Muster war bei den KO-Mäusen nicht vorhanden. Wir untersuchten den Grad der Korrelation zwischen Neuronen in denselben Mäusen und klassifizierten signifikante Neuronen als Korrelationspartner. Die Analyse von WT-Mäusen ergab einen deutlichen Anstieg der Zahl der Korrelationspartner in der vertrauten Konditionierungsumgebung, nicht aber in der neuen Umgebung. Auch diese Koaktivierungssignatur fehlte bei KO-Neuronen. Die Aktivität der Ortszellen zeigte eine ähnliche Modulation in WT-Mäusen, wo ihre Anzahl und Aktivitätsrate in der vertrauten Umgebung abnahm, aber in der neuen Umge-bung zunahm. Ein ähnliches, aber schwächeres Muster der Rekrutierung und Aktivität von Ortszellen wurde bei KO-Mäusen beobachtet. Ein auffälliger Unterschied zwischen WT- und KO-Mäusen zeigte sich bei der Analyse der Größe des Ortsfeldes: Die Größe des Feldes nach dem Schock nahm in den WT-blieb die Größe konstant Mausen zu. Im vertrauten Kontext , während sie im neuen Kontext hingegen abnahm. Bei den KO-Ortszellen wurde eine entge-gengesetzte Modulation beobachtet. Diese Ergebnisse bestätigen, dass die Aktivität der Ortszellen bis zu drei

Wochen nach der Konditionierung zur Unterscheidung zwischen vertrauter und neuer Umgebung beiträgt. Außerdem deuten diese Ergebnisse darauf hin, dass die Bildung von Ortszellen durch den Verlust von Arc/Arg3.1 in den KO-Mäusen zwar nicht stark beeinträchtigt wurde, ihre Modulation im Verlauf der Gedächtniskonsolidierung jedoch stark verändert war.

Schließlich versuchten wir, neuronale Engramme zu identifizieren, die den Konditionierungskontext kodieren und bei Tests des rezenter - und Ferngedächtnisses zuverlässig reaktiviert werden. Wir erwarteten, dass sich solche Engramme signifikant von denen unterscheiden, die in ungewohnten Kontexten aktiv sind. Wir untersuchten zwei Engrammdefinitionen auf der Grundlage ihrer erhöhten Aktivität, entweder während der Episode vor dem Schock oder während des Tests des Kurzzeitgedächtnisses im vertrauten Kontext. Die Anzahl der reaktivierten Neuronen war bei beiden Engramm-Definitionen in den verschiedenen Genotypen und Umgebungen ähnlich. Die Aktivitätsraten der Neuronen, die dem Engramm zugeordnet waren, und ihre Korrelationswerte zeigten jedoch eine signifikante umweltabhängige Modulation bei WT-Mäusen, nicht aber bei KO-Neuronen. Insgesamt deutet dies darauf hin, dass hochaktive Neuronen mit größerer Wahrscheinlichkeit dem Engramm zugeordnet werden. Zudem zeigt dieses, dass Aktivitätsraten und -korrelationen am stärksten zu einer Gedächtnissignatur beitragen und nicht die Größe oder Identität spezifischer Neuronen

In dieser Arbeit werden neue Erkenntnisse über die Aktivität und die funktionelle Kodierung in Arc/Arg3.1 KO-Mäusen vorgestellt, die ein neues Licht auf den neuronalen Aktivitätscode werfen, der der Konsolidierung des Langzeitgedächtnisses zugrunde liegt. Dazu gehören die folgenden:

1. Arc/Arg3.1 reguliert den aktivitätsabhängigen Kalziumeinstrom im Hippocampus.

2. Die Entstehung und Bildung von Neuronen, die sensorische, räumliche und verhaltensbezogene Informationen in dCA1 kodieren, sind unabhängig von der Arc/Arg3.1-Plastizität.

3. Erhöhte Aktivitätsraten und neuronale Synchronisation liegen einem erfolgreichen Gedächtnisabruf zugrunde und unterscheiden bekannte von neuen Informationen.

4. Die Modulation der Aktivitätsraten und der neuronalen Synchronisation während des Prozesses der Gedächtniskonsolidierung wird durch die Expression von Arc/Arg3.1 im Gehirn gesteuert.

Introduction

1 Introduction

Learning and memory, the foundation of human cognition, are intricate processes that facilitate the acquisition, storage, and retrieval of information, which are crucial for survival, adaptation, and complex thought. These processes shape individual identities, influence behavior, and underlie cultural and social interactions. The ability to generalize one's past experiences to novel situations and extrapolate learned principles beyond their original context is a defining characteristic of intelligence. Without memory, there would be no accumulated knowledge, problem-solving ability, or capacity for long-term planning.

An important feature of the brain is its remarkable flexibility, allowing it to identify patterns, recognize regularities, and use previous memories in new contexts. This generalization process is essential for adaptive behavior and is vital for survival. For instance, once an individual learns that fire is dangerous, they can apply this knowledge to novel situations without placing their hand into the fire(Dunsmoor & Paz, 2015).

However, excessive generalization can be destructive. In pathological cases, such as post-traumatic stress disorder, overgeneralized fear responses lead to heightened anxiety, fear, and avoidance behaviors in a safe environment (Dunsmoor & Paz, 2015).

In contrast, having specific memories is essential for accurate recall and effective action. Such memories help people differentiate between similar yet distinct experiences, like identifying a friendly dog compared to a threatening one. A lack of specificity can hinder learning, as observed in Alzheimer’s disease, where individuals find it difficult to remember detailed information while still holding onto vague impressions (Perry & Hodges, 1999). On the other hand, too much specificity can be hindering, causing rigid thinking and reduced flexibility and adaptability. This is evident in disorders such as obsessive-compulsive disorder and autism spectrum disorder, where overly specific memories can disrupt flexible cognitive processes(Breijyeh & Karaman, 2020).

Grasping how memories are encoded, stabilized, and retrieved over time, along with memory's flexibility and specificity, is one of nature's marvels that has captivated countless scientists, including Abdurahman Hassan Abdurahman Kuku and colleagues.

In this study, we aim to contribute to this larger puzzle by studying the Immediate Early Gene (IEGs) Arc/Arg3.1 (Activity-Regulated Cytoskeletal-associated protein/ Activity-Regulated Gene 3.1) (Link et al., 1995; Lyford et al., 1995) in learning and memory. Arc/Arg3.1 is

recognized for its crucial role in regulating synaptic plasticity and modulating synaptic strength (Plath et al., 2006).

1.1 Memory Systems

Learning and memory are fundamental processes that enable organisms to adapt to their environment by encoding, consolidating, and retrieving information. Memory, defined as the storage and use of learned information in the brain, is necessary to modulate behavior and is critical for animals' adaptation to their environments and survival (Ortega-de San Luis & Ryan, 2022).

Memory is commonly divided into two types, short-term memory (STM), where information is held for a short period, and long-term memory (LTM), which involves converting information into stable neural representations that can be retrieved after long periods (Squire & Wixted, 2011). LTM is further divided into explicit (declarative) and implicit (non-declarative) memory, which are distinguished based on the level of conscious awareness involved in retrieving. Declarative memory encompasses episodic (events) and semantic (facts) memory, primarily relying on the hippocampus and medial temporal lobe structures (Eichenbaum, 2017a). In contrast, non-declarative memory involves procedural learning, skill acquisition, and habits, which are associated with the striatum and cerebellum (Doyon & Benali, 2005).

Episodic memory has been studied in the context of fear memory using animal models. Fear, a common behavior, impacts a significant portion of the global population, often resulting in both physical and psychological distress (Raber et al., 2019). This reality is something we encounter daily through news and our environment (Tunney et al., 2021). Fear is vital for survival, making it a key focus of research in learning and memory. Here, the term "fear memory" describes how animal models learn, store, and retrieve fear-related behaviors. In animal research, fear learning is typically assessed using Pavlovian conditioning, which examines the relationship between environmental changes (conditioned stimulus, CS) and a fear-inducing event (usually footshocks, the unconditioned stimulus, US) (Izquierdo et al., 2016).

1.2 Episodic Memory

Contextual fear conditioning is a widely used paradigm in memory research and serves as an example of episodic memory (LeDoux, 2003; LeDoux, 2014). In this paradigm, an animal is placed in a distinct environment and exposed to an aversive stimulus, such as a mild foot shock. After a single exposure, the animal learns to associate the environment with the aversive

experience and will exhibit fear behavior, manifesting as freezing (unconditioned response), when re-exposed to the same context. Fear memories engage specialized brain circuits that enhance learning and memory consolidation. The major brain regions involved in fear memory include the amygdala, hippocampus, prefrontal cortex, hypothalamus, and periaqueductal gray(LeDoux, 1994). Each of these structures plays a distinct and important role in encoding, consolidating, retrieving, and regulating fear-related memories.

The hippocampus has long been recognized as essential for the formation of new episodic memories. Studies on amnesic patients, including the well-documented case of Henry Molaison (H.M.), have demonstrated that hippocampal damage leads to severe deficits in acquiring new episodic memories while sparing remote memories and procedural learning(Scoville & Milner, 2000). Demonstrating the important role of the hippocampus in encoding and the early stages of consolidation of episodic memories. On the other hand, the prefrontal cortex plays a key role in higher-level cognitive control functions that facilitate memory retrieval, integration, and long-term retention(Miller & Cohen, 2001). The relationship between these two areas is essential for the efficient encoding, gradual consolidation, and context-appropriate retrieval of memories(Eichenbaum, 2017b).

The hippocampus' role in encoding new episodic memories is binding together different elements of the "event", including sensory, spatial, and temporal information (O'Keefe & Krupic, 2021; Smith & Mizumori, 2006). This process is supported by the trisynaptic circuit, which involves projections from the entorhinal cortex (EC) to the dentate gyrus (DG), which in turn projects to CA3 and subsequently to CA1(Kesner & Hunsaker, 2010). Various types of sensory information, including visual, auditory, and somatosensory inputs from the neocortex, are relayed to the EC and subsequently to the DG. The DG is particularly important for pattern separation, a process that ensures similar experiences are stored as distinct memories(Schmidt et al., 2012), like the example with the friendly vs threatening dog. This function helps to reduce interference between overlapping experiences. CA3 is involved in pattern completion, allowing the retrieval of entire memory traces based on partial cues(Gold & Kesner, 2005). CA1 serves as an integrative hub, refining and relaying processed information to the prefrontal cortex and other cortical regions. The dCA1 in rodents has been found to be particularly important for spatial memory and episodic retrieval (Morris et al., 1990). In contrast, the vCA1 is more strongly associated with emotional and motivational aspects of a memory. This functional differentiation pinpoints the diverse contributions of different hippocampal subregions to episodic memory processes(Maren, 1999).

The amygdala is the primary structure responsible for processing emotionally significant memories, particularly those related to fear. It receives sensory input from the thalamus and cortex and plays a crucial role in associating neutral stimuli with aversive events, e.g., fear conditioning(McGaugh, 2004). Within the amygdala, the basolateral amygdala (BLA) encodes the association between a conditioned stimulus (e.g., a tone) and an unconditioned stimulus (e.g., a shock) (Balleine et al., 2003), while the central amygdala (CeA) coordinates the behavioral expression of fear responses(LeDoux et al., 1988).

The amygdala interacts closely with both the hippocampus and prefrontal cortex to modulate fear memory (Izquierdo et al., 2016). While the amygdala is essential for forming and retrieving fear associations, contextual fear memories depend on the hippocampus, which encodes the environmental context in which the fearful event occurred. Studies using hippocampal lesions or optogenetic inhibition of hippocampal neurons demonstrated that animals with hippocampal dysfunction fail to associate the environment with a fearful memory event. Providing evidence that the hippocampus is crucial for the formation of the contextual representation(Phillips & LeDoux, 1992). In contrast, cued fear conditioning, in which an animal associates a discrete auditory or visual cue with the aversive stimulus, does not require the hippocampus and is instead primarily dependent on the amygdala (Kim & Fanselow, 1992; Phillips & LeDoux, 1992).

Initially, episodic memories are dependent on the hippocampus, but over time, they become more reliant on distributed neocortical regions, through memory consolidation (Eichenbaum, 2017b). One of the key mechanisms underlying memory consolidation is hippocampal replay, a phenomenon in which neural activity patterns observed during learning are reactivated during rest and sleep (Lee & Wilson, 2002; Louie & Wilson, 2001). This process is tightly linked to sharp-wave ripples (SWRs), which are brief bursts of high-frequency oscillatory activity occurring in the hippocampus (Buzsáki et al., 1983). Some evidence supports a role for SWRs in facilitating information transfer between the hippocampus and prefrontal cortex, allowing for the gradual integration of episodic memories into long-term storage (Buzsáki, 2015).

Although essential to brain function, determining how to identify a memory in the brain remains largely unanswered. A widespread and re-emerging theory suggests that memories integrate into engrams (Figure 1.2-1). An engram comprises a group of neurons that are active during the learning process. These neurons undergo both biochemical and physical changes, allowing them to store information in a stable state, which can later be reactivated during memory retrievals (Eichenbaum, 2016).

The engram is often viewed as a hypothetical biological entity that we are just starting to grasp. As the community grows, the terminology and ideas used to explore the connection between the brain and memory will likely evolve alongside advancements in experimental tools, data, and analysis methods (Choucry et al., 2024).

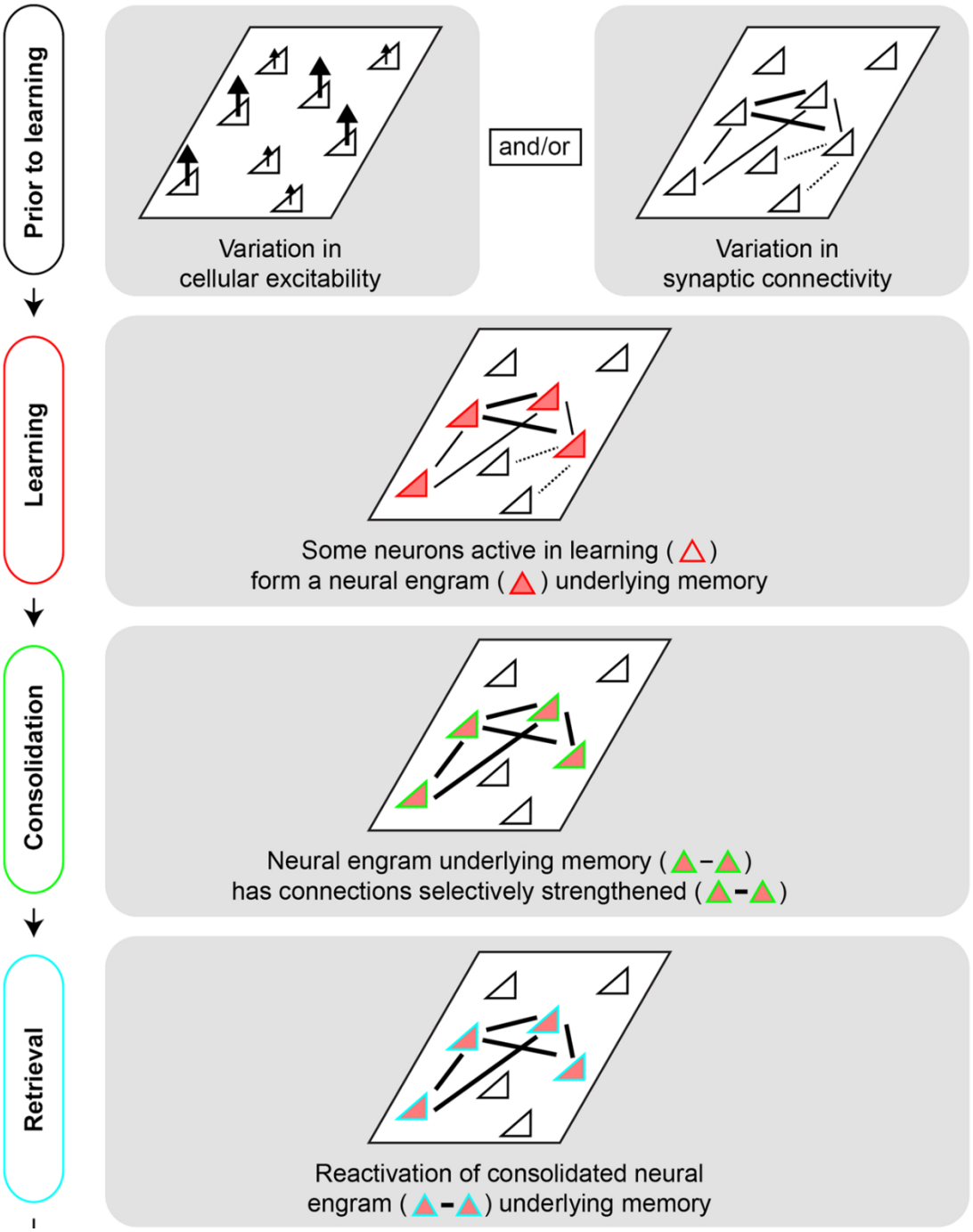


Figure 1.2-1 A canonical view of the memory engram for each stage of memory (Modified from (Bostancıklıoğlu, 2020))

1.2.1 Encoding of memory engram

Memory encoding is a versatile process that converts sensory information into neural representations. The term "engram" denotes the physical changes in the nervous system that occur in specific neurons after a learning experience. The selection of neurons into an engram is influenced by individual intrinsic characteristics of the neurons, particularly their excitability (Choucry et al., 2024; Han et al., 2009).

Research indicates that neurons with greater excitability tend to be more active while learning new experiences, making them more likely to become part of an engram(Figure 1.2-1) (Han et al., 2009). One important regulatory element in this context is the cyclic AMP response element-binding protein (CREB), which affects neuronal activity across various subcortical and cortical areas. CREB plays a vital role in determining which neurons become incorporated into an engram. Notably, neurons exhibiting increased CREB activity are preferentially included in an engram (Kim et al., 2014), whereas those lacking CREB activity are less likely to be incorporated into the memory engram (Han et al., 2007; Yiu et al., 2014).

The distribution of neurons involved in an engram reflects the complex link between neuronal traits and memory formation. Variations in neural excitability over time critically influence which specific subsets of neurons are recruited for memory encoding. Additionally, it ensures that the same neurons are not repeatedly chosen for every given memory engram. (Benito & Barco, 2010).

1.2.2 Engram consolidation

For episodic events to be remembered, they must undergo a process known as consolidation, which stabilizes and stores memory engrams for the long term. The initial phase of memory consolidation is known as synaptic consolidation (Dudai, 2004). Synaptic consolidation relies on intricate mechanisms of gene expression and new protein synthesis. That will strengthen synaptic connections between neurons that were active during the learning experience, e.g., engram neurons. IEGs, such as Arc/Arg3.1 and c-Fos, play a crucial role in this process, as they promote the synaptic plasticity necessary for long-term potentiation (LTP) and long-term depression (LTD), the fundamental mechanisms underlying strengthening and weakening of synaptic connections, respectively (Bramham et al., 2008).

Over time, the stabilized memory engrams undergo systems consolidation, characterized by a reorganization of memory storage. Memories are transferred and integrated into the neocortex (Dudai, 2004). Initially, memories are dependent on the hippocampus, but over time, they start to

shift their reliance toward cortical regions, particularly the medial prefrontal cortex. This transition appears to occur predominantly during offline states, especially during sleep, when the hippocampus engages in neuronal replay, accompanied by sharp-wave ripples. These events are thought to facilitate the "training" of cortical networks, effectively transferring the encoded episodic details from the hippocampus to the neocortex (Eichenbaum, 2017b; Frankland & Bontempi, 2005; Klinzing et al., 2019).

The details and mechanisms involved in memory engram consolidation continue to be a topic of discussion among researchers. The Multiple Trace Theory (MTT) offers a model that suggests that episodic memory engrams do not completely shift from the hippocampus to the neocortex over time (Nadel & Moscovitch, 1997). Rather, MTT postulates that every time an engram is accessed, the memory is re-stabilized through a reconsolidation process that relies on protein synthesis within the hippocampal–neocortical network. This approach improves the memory engram's overall representation rather than relocating it entirely to cortical regions, and it also weakens unused memories. This distribution strategy ensures that episodic memories still depend on the hippocampus and highlights the role of retrieval-driven plasticity in memory retention. Unlike the standard consolidation theory, which outlines a complete gradual migration of memory representations from the hippocampus to the neocortex(Frankland & Bontempi, 2005).

1.2.3 Engram Retrieval

Once an engram has been consolidated at both synaptic and systemic levels, it is "available" for memory retrieval (Tonegawa et al., 2015). Several crucial factors influence the success of this retrieval process. According to the encoding specificity principle, successful memory retrieval is dictated by the extent to which the context (or cues) at retrieval match those encountered during encoding. This principle comprises two main concepts: context-dependent memory and state-dependent memory. Context-dependent memory refers to the idea that external environmental cues, such as the location or social environment in which a memory was formed, play a vital role in facilitating retrieval (Ramirez et al., 2013). State-dependent memory emphasizes the importance of the individual's internal neurophysiological state during retrieval, which should ideally align with the state at the time of encoding for optimal memory retrieval (Liu et al., 2012).

It was found that retrieval of a context memory preferentially reactivates CA1 engram neurons that were active during memory encoding. Memory retrieval will, therefore, be successful to the extent that the brain recapitulates patterns of neural activity that were present during memory

encoding. It has been demonstrated that inhibiting engram neurons greatly hinders the retrieval of a memory, even in the right context where the memory was formed (Tanaka et al., 2014). On the other hand, the artificial activation of these engram neurons typically enhances the retrieval process, leading to recall even in contexts unrelated to the original (Ramirez et al., 2013). These insights have been validated across various behavioral tasks and within multiple brain regions. Reinforcing the notion that an engram formed during the encoding process, and subsequently reinforced during consolidation and re-consolidation, is essential for memory retrieval. This also further supports the MTT, demonstrating that memories are stored across different brain regions in distinct engrams (Roy et al., 2022).

1.2.4 Recognition and Modification of Engrams

“Engram neurons" refer to groups of neurons that form essential components of a specific memory engram. They might also play crucial roles in engrams related to other memories. Engram neurons are (1) activated by a learning experience, (2) modified physically or chemically as a result, and (3) reactivated when stimuli from that experience (or its components) are encountered again, facilitating memory retrieval(Josselyn & Tonegawa, 2020). Initially, there was discouragement in the search for engrams within neurobiology, stemming from Richmond Semon, who coined the term "engram," and later mainly due to Karl Lashley's failed experiments to locate these engrams. This led to a significant abandonment of searching for the engrams. However, advancements in molecular biology and imaging techniques in the late 20th and early 21st century have led to the identification of some kind of engram neurons. The TetTag mouse model, along with neuronal activity markers like c-Fos and Arc/Arg.31, facilitated the identification of engram neurons(Navabpour et al., 2020; Reijmers et al., 2007). TetTag mice are genetically engineered to allow targeting of neurons involved in memory formation using a tetracycline-controlled transcriptional activation (Tet-off) system. In the TetTag system, the tetracycline transactivator (tTA) is expressed under the control of an IEG promoter. Upon neuronal activation, the IEG promoter drives the expression of tTA. Tet-off systems work by withdrawing doxycycline (Dox), this withdrawal of dox allows the tetracycline transactivator (tTA) to bind to the TetO promoter and drive the expression of a fluorescent reporter (e.g., GFP) or functional effectors (e.g., Channelrhodopsins, a ligate gate ion channel, for optogenetics (Liu et al., 2012) or designer receptor exclusively activated by designer drugs receptors for chemogenetics (Garner et al., 2012)) allowing permanently tagging these neurons. After the tagging window, Dox is reintroduced to prevent further labeling, ensuring that only neurons activated during the specified time period remain marked as part of the engram (Reijmers et al., 2007). Three categories of studies provide evidence for the

existence of engrams (Figure 1.2-2). Observational studies, which link the activation of specific cell groups to memory expression; loss-of-function studies, which determine the necessity of certain neurons' activation for particular memory behaviors; and gain-of-function studies, demonstrate that activating specific neurons can provoke memory retrieval (Bostancıklıoğlu, 2020).

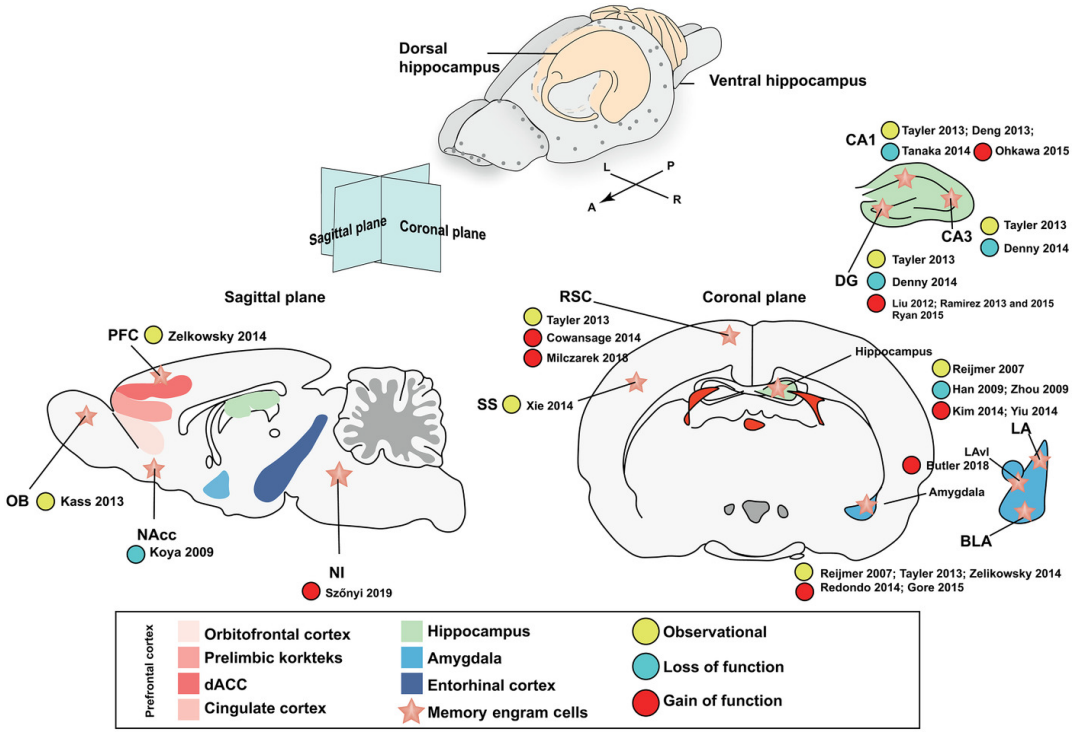


Figure 1.2-2 Engram studies. The anatomical locations of memory engram cell groups in the rat brain are identified through three types of studies: observational, loss-of-function, and gain-of-function. The key areas highlighted include the basolateral amygdala (BLA), lateral amygdala (LA), ventral lateral nucleus of the lateral amygdala (LAvl), nucleus accumbens (NAcc), nucleus incertus (NI), olfactory bulb (OB), prefrontal cortex (PFC), retrosplenial cortex (RSC), and sensory cortex (SK). (Copied with permission from (Bostancıklıoğlu, 2020))

1.2.5 Tracking Engram Neuron

Activity-dependent promoters/proteins have been widely employed for targeting engram neurons, but they have limitations. The uses a Tet-off system relies on the washout of doxycycline to induce the tagging of experience-activated neurons. The withdrawal of Dox usually happens at least 24 hours before the task/event. As a result, the temporal resolution of tagging is not strictly limited to the time of the specific task/event, such as conditioning. Since the tagging window is a magnitude larger than the specific task, no guarantee exists for suppressed IEGs expression, even with preventive measures. This results in an inflated estimation of neurons encoding a particular task/event.

Recent developments in *in vivo* head-mounted miniaturized microscopes (miniscopes) have

introduced a novel approach to studying engram neurons. By directly monitoring the activity of neurons through genetically encoded calcium indicators (GECIs) before, during, and after learning. Particularly in relation to episodic memory, the miniscope allows the observation of engram neurons' trajectory from before encoding, during encoding, consolidation, and retrieval.

Early studies with the miniscopes described how the more separated in time the memories for two contexts were, the less overlapping their engrams are in the hippocampal region CA1 (Cai et al., 2016). This aligns with the CREB experiment, indicating that if two events occur within 6 hours following the induction of CREB, the two engrams are likely to overlap (Rashid et al., 2016). Triggering the activation of one engram, may in turn activate the second engram (Reijmers et al., 2007). Further research by (Jimenez et al., 2020) using the miniscope revealed that during memory retrieval in a contextual fear memory task, a group of vCA1 neurons became linked to shock-encoding neurons. Moreover, the degree of correlated activity in this group corresponded to the strength of the memory.

Mocle et al. expand on the concept that neurons that become part of a memory engram exhibit a higher excitability compared to non-engram neurons (Mocle et al., 2024). Specifically, they demonstrated that engram neurons exhibited greater activity than non-engram neurons three hours before training but not from 24 hours to five days before training. Sub-engrams that were more active before training were allocated to the engram, and their functional correlation increased during training. Therefore, both neuronal excitability and pre-configured functional correlation mediate allocation to an engram.

Ghandour et al. established a unique imaging system that combines miniscope imaging and engram tagging (Ghandour et al., 2019). They identify engram neurons using the photoconvertible fluorescent protein Kikume Green Red and the c-fos-tet-tag system, which allowed them to extract the characteristics of engram activity by visualizing and discriminating between engram and non-engram neurons. They demonstrated that engram neurons exhibited greater synchronization than non-engram neurons, both during the task and in the subsequent sleep and retrieval sessions, which supports the importance of sleep in memory consolidation.

1.3 Synaptic Plasticity and Memory Formation

Throughout the life of a memory engram, synaptic plasticity plays a crucial role. Synaptic plasticity, which refers to the capacity of synapses to either strengthen or weaken based on activity, serves as a core mechanism for learning and memory (Neves et al., 2008). LTP and LTD are two primary forms of synaptic plasticity, allowing for experience-dependent modifications in

neural circuits (Citri & Malenka, 2008). LTP involves the persistent strengthening of synapses following high-frequency stimulation, whereas LTD involves synaptic weakening through low-frequency stimulation (Bliss & Lømo, 1973; Citri & Malenka, 2008; Neves et al., 2008).

The activation of IEGs is critical in regulating synaptic plasticity. These genes are rapidly transcribed in response to neuronal activity, they do not require new protein synthesis. IEGs are essential for converting external stimuli into molecular and cellular responses, including changes in gene expression. These changes are crucial for the structural and functional adaptations of synapses that support memory engrams (Minatohara et al., 2016).

1.3.1 Arc/Arg3.1

Activity-regulated cytoskeleton-associated (Arc) / Activity-regulated gene 3.1(Arg3.1) is a unique IEG, as the Arc/Arg3.1 gene encodes for an effector protein and not a transcription factor, as other IEGs (Bramham et al., 2010). Two groups independently identified Arc/Arg3.1 as a gene induced by synchronous activity and seizures in the hippocampus in 1995 (Link et al., 1995; Lyford et al., 1995). It is highly conserved among mammals, situated on chromosome 15, 7, and 8 in the mouse, rat, and human, respectively. The Arc/Arg3.1 gene contains a single coding exon that encodes a protein of 396 amino acids with a predicted molecular weight of 55 kDa, and a 3′ untranslated region (UTR) with two introns that are spliced to form the mature Arc/Arg3.1 messenger RNA (mRNA). Arc/Arg3.1 has no known alternative splice variations. Arc/Arg3.1 mRNA is induced by synaptic activity and trafficked rapidly to dendrites, where it accumulates and undergoes local translation.
Arc/Arg3.1 has been implicated in many canonical cellular models of excitatory neuron synaptic plasticity, including LTP (Guzowski et al., 2000; Messaoudi et al., 2007), LTD (Park et al., 2008; Waung et al., 2008) and homeostatic synaptic scaling(Gao et al., 2010; Shepherd et al., 2006). Arc/Arg3.1 gene deletion in mice leads to deficits in circuit plasticity (Gao et al., 2018; McCurry et al., 2010; Wang et al., 2006) and impairments in learning and memory (Guzowski et al., 2000; Messaoudi et al., 2007; Plath et al., 2006)

1.3.2 Arc/Arg3.1 is localized in synapses and regulates synaptic plasticity

Studies have identified multiple signaling pathways that mediate Arc/Arg3.1 induction, particularly those involving calcium influx, mitogen-activated protein kinases (MAPKs) (Waltereit et al., 2001), and cAMP response element-binding protein (CREB) (Ying et al., 2002) (Figure

1.3-1). During resting states Arc/Arg3.1 is typically transcribed at low levels , with AMPAR activation further suppressing its expression (Rao et al., 2006). In contrast, activation of the BDNF TrkB receptor (Ying et al., 2002), group 1 metabotropic glutamate receptors (mGluR1s) (Park et al., 2008; Waung et al., 2008), muscarinic acetylcholine receptors (Teber et al., 2004), and NMDA receptors (NMDARs) (Oswald Steward & Paul F Worley, 2001) following heightened neuronal activity associated with learning leads to a significant increase in Arc/Arg3.1 transcription. Arc/Arg3.1 mRNA is detectable within 5 minutes from stimulation. Arc/Arg3.1 mRNA is immediately transported to dendrites, accumulating at synaptic sites for local translation(Steward et al., 1998; Oswald Steward & Paul F. Worley, 2001).

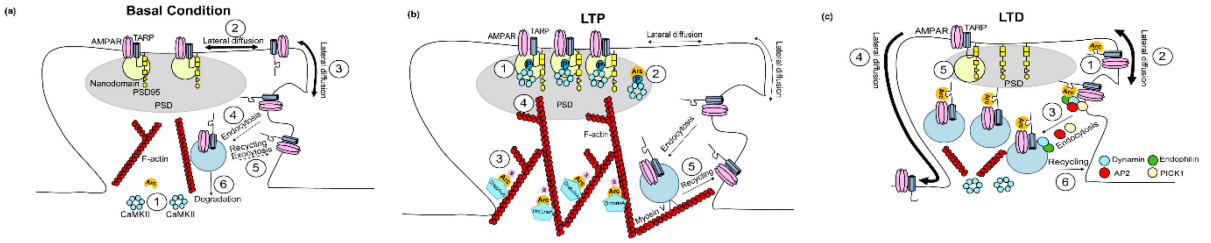


Figure 1.3-1 Arc/Arg3.1 on synaptic plasticity. Schematic representation illustrating some of the main mechanisms underlying Arc/Arg3.1 effects on synaptic plasticity (Copied with permission from (Zhang & Bramham, 2021))

The dual role of Arc/Ar3.1 in both LTP((Guzowski et al., 2000; Messaoudi et al., 2007; Plath et al., 2006)) and LTD ((Plath et al., 2006; Waung et al., 2008)) highlights its function as a key regulator of experience-dependent plasticity, ensuring that neural circuits remain flexible yet stable over time. During LTP, Arc/Arg3.1 supports synaptic strengthening by stabilization of F-actin, whereas during LTD, Arc/Arg3.1 facilitates AMPAR endocytosis (Chowdhury et al., 2006), contributing to synaptic weakening (Figure 1.3-1).

1.3.3 Arc/Arg3.1 function in behavior

Arc/Arg3.1's importance in LTP and LTD highlights its crucial functional role in learning and memory. Arc/Arg3.1-deficient mice have deficits in memory task performance that require memory consolidation (LTM) (Gao et al., 2018; Guzowski et al., 2000; Guzowski et al., 2006; Plath et al., 2006), which is not evident when mice are tested within shorter times in STM tasks.

For example, as shown by (Plath et al., 2006), Arc/Arg3.1 KO mice learned new behavioral tasks in a similar manner to control WT mice but could not consolidate the new memories. During contextual fear memory acquisition, both genotypes formed a short-lasting association. However, when tested for fear memory 24 hours after conditioning (Plath et al., 2006) or 1

week later (Gao et al., 2018), WT mice showed high levels of freezing in the training environment and in a neutral environment when confronted with the conditioning tone (e.g. constrained stimuli). In contrast, KO mice showed drastically lower levels of freezing to both stimuli, indicating impaired context- and cue-dependent long-term memory formation

The impairment was also evident in the object recognition task. After 10 minutes of exposure to an object, both KO and wild-type mice show equal preferences for a novel object compared to the original, suggesting that KO mice are capable of acquiring and retaining memory within this brief period. However, after 24 hours, WT mice continued to prefer a novel object, while KO mice did not show any preference (Managò et al., 2016; Plath et al., 2006).

Deficits in learning were also reported for more complex spatial tasks, such as the Morris water maze (MWM). Where both WT and KO showed an overall decline in the length of the swim path during the learning. However, in contrast to WT, the KO mice failed to improve performance during the late learning days. During the memory test, which was 1 week after the learning was completed, WT showed a persistent search within the target zone and a significantly higher number of target-annulus crossings compared to KO (Gao et al., 2018; Plath et al., 2006).

Memory consolidation was also shown to be disrupted by infusions of Arc/Arg3.1 antisense oligodeoxynucleotides (ODNs) administered before or after training of different memory tasks (Korb & Finkbeiner, 2011). For example, Guzowski et al. showed that intrahippocampal infusion of Arc/Arg3.1 antisense ODNs, prior to training, did not affect animals' ability to learn the MWM spatial task. However, the ODNS drastically impaired the animals' ability in the memory test 2 days after the end of training. Also, Arc/Arg3.1 antisense ODNs delivered immediately after training but not 8 hours later caused a similar impairment in the memory test (Guzowski et al., 2000). Similar results were also observed in contextual fear conditioning when the infusion of ODNs happens before the conditioning (Czerniawski et al., 2011).

1.4 Study aim

Although Arc/Arg3.1 is recognized for its critical role in synaptic plasticity and memory consolidation, its impact on the organization of neuronal activity reflecting learning and memory remains insufficient. This thesis aims to fill this gap by utilizing *in vivo* miniscope calcium imaging and Arc/Arg3.1 knockout to investigate how neuronal activity is related to changes in learning and memory during the encoding and retrieval processes. By integrating behavioral tests, this research seeks to reveal the role of Arc/Arg3.1 in encoding and retrieval of memory over time.

- To investigate the influence of Arc/Arg3.1 on hippocampal neural activity during exploratory behavior.
- To examine the role of Arc/Arg3.1 in the formation and stability of hippocampal place cells under both neutral and aversive conditions
- To determine if Arc/Arg3.1 affects the hippocampus' ability to encode sensory information.
- To investigate the impact of Arc/Arg3.1-driven plasticity on engram consolidation and the retrieval of episodic memory.

Method and Materials

2 Methods and Materials

2.1 Animals

Adult male and female mice, aged 3-6 months, were group-housed in a controlled vivarium environment with an inverted 12:12 light/dark cycle (dark period: 8:00–20:00). The mice were maintained under standard conditions, including a temperature of 23 ± 1°C, 40-50% humidity, and unrestricted access to food and water. Mice were housed in groups with one or two littermates, whenever possible, and remained in these groups throughout the experiments. All experimental procedures were conducted in strict compliance with German and European Community regulations on the protection of experimental animals and received approval from the local authorities of the City of Hamburg.

In this study, we employed the conventional Arc/Arg3.1 knockout (KO) and wild-type littermates (WT). The mice were used for *in vivo* electrophysiological recordings and *in vivo* calcium imaging experiments, combined with behavioral tests.

The generation of mice was achieved following the method previously published (Plath et al., 2006). In summary, vectors containing a neomycin resistance cassette, flanked by two loxP sites, were inserted at position +2690 into the second intron, where Arc/Arg3.1 ORF was flanked by inserting a third loxP site at position -1720. These vectors were electroporated into embryonic stem cells and exposed to transient Cre recombinase expression. This process resulted in clones where the open reading frame (ORF) of the gene was either deleted (Arc/Arg3.1$^{-/-}$, KO) or flanked by two LoxP sites (Arc/Arg3.1$^{fl/fl}$).

2.2 Surgeries

Mice used for *in vivo* calcium imaging underwent two stereotaxic surgeries. The first surgery was to inject a virus encoding for a calcium indicator (pGP-AAV-syn-jGCaMP8m-WPRE, (Zhang et al., 2023)) into the dorsal CA1(dCA1). A second surgery was performed 10-14 days later to implant the grin lens in the dCA1. To ensure appropriate postoperative care, mice were single-housed for at least 24 hours following the implantation surgery and returned to their original home cages.

At the end of the experiment, all injected mice were euthanized and perfused, and their brains were extracted for post hoc histology.

2.2.1 Stereotaxic virus injection

During the operation, carprofen and buprenorphine were applied systemically (1.5 mg/kg, s.c.) to provide pain relief and general analgesia. The operations were performed under aseptic conditions. Mice were first anesthetized with isoflurane (3-5% in oxygen) for 2 minutes and placed in a stereotaxic frame (Kopf Instruments). Once the mouse was head-fixed, the anesthesia was maintained with isoflurane (1.5-2% in oxygen) applied through a nose-mask. The mouse's body temperature was maintained at 37°C by a feedback-controlled heating pad via a rectal thermometer. The eyes were protected with ointment (Vidisec) and covered by thick paper to protect them from direct light. The head was shaved, the skin was disinfected with betadine, followed by 70% ethanol, then lidocaine was applied to numb the skin. A midline incision was made to expose the skull, and the surgical coordinates were established by levelling the skull between the lambda and bregma. Using a dental drill fitted with a 0.5 mm bill bit (FST), a hole was created at the coordinates (AP: -2.0 mm, ML: ±1.5 mm), corresponding to the dCA1. A computer-driven injector (Neurostar) was used to inject small volumes of virus solution through a specialized Hamilton syringe (Neurosyringe, 1 ml volume). The virus was injected into the dCA1 of the right hemisphere (AP: -2.0 mm, ML: +1.5 mm, DV: -1.6 mm). A total of 1 µl virus-solution was injected at a rate of 0.1 µl/min, in two steps (0.5µl/step): first at a depth (DV) of -1.6 mm and then at -1.5 mm. After a 10-minute pause following the second injection, the needle was slowly retracted. The incision in the skin was sutured, and the mice received an injection of carprofen/saline (5 mg/kg, subcutaneously) for pain relief and hydration, which was administered for 3 days. Following surgery, mice were allowed to recover in a clean cage placed over a heating mat, until they exhibited normal mobility and feeding behavior. Additionally, soft food mixed with Metacam(meloxicam) was provided for the first 3 days.

2.2.2 Implantation of the grin lens

The second surgery involved the implantation of a gradient index (GRIN) lens (Inscopix Inc, measuring 1 mm in diameter and 4 mm in length) in the dCA1. The GRIN lens was integrated with a baseplate for the miniscope.
All the steps leading up to the craniotomy were performed according to the virus injection procedure.

After making a midline incision, the skull was cleaned with 3% hydrogen peroxide, followed by saline. The skull surface was scored in a checkerboard pattern using a scalpel blade to enhance

adhesion for the dental cement. In a few cases, a stabilizing screw were inserted diagonally into the skull, positioned in front of the craniotomy site. The surgical coordinates were determined after leveling the skull between the lambda and bregma. After leveling, the coordinates were marked at (AP: -2.0 mm, ML: +1.5 mm, DV), which corresponded to the virus injection coordinates. A 2 mm trephine (FST) drill bit was employed to create a hole at the marked coordinates. The dura mater was carefully removed using a cotton swab and a 30G needle, gently scraping around the craniotomy site to detach any remaining dura and to clean the area of bone debris. Throughout the procedure, the craniotomy site was kept moist with cold saline. Using a (30G / 27G) blunt needle under low vacuum pressure and constant irrigation with cold saline, the cortex overlying the dCA1 region was aspirated in a circular movement. Aspiration was stopped after the medial-lateral fibers of the corpus callosum were removed, exposing the anterior-posterior fibers. In case of any bleeding, Gelfoam (GelfoamTM, Henry Schein) and cold saline were applied for 2 to 5 minutes to achieve hemostasis.
Then, the skull was thoroughly dried with a cotton swab, except for the craniotomy area, which remained moist with saline. The GRIN lens was carefully lowered to the surface of the brain using stereotaxic, targeting the coordinates (AP: -2.0 mm, ML: -1.5 mm, DV: -1.3 mm). Kwik-Sil (World Precision Instruments) was applied to seal any gaps between the edge of the skull and the GRIN lens. The lens was then secured to the skull using multiple layers of dental cement (C&B Metabond, Parkell), with each layer allowed to dry for 5 minutes before the next one was applied. For some mice, the final layer was made using Paladur dental cement (Heraeus Kulzer). A blunt 20G needle and syringe were utilized to apply the dental cement. Some mice needed suturing of the skin around the implant.

Following the operation, mice received subcutaneous injections of a carprofen/saline solution (5 mg/kg). This was repeated twice within the first 24 hours and then additionally once every 24 hours for 48 hours to manage their pain. During the first 3 days, they were provided with soft food mixed with metacam (meloxicam). The mice underwent a recovery period of 14 to 21 days before participating in the behavioral experiments.

2.3 Behavioral Experiments and Calcium Imaging

All mice participated in a series of behavioral experiments conducted in the following order: Open Field Task (OFT) followed by Contextual Fear Conditioning (CFC).

Before the first behavioral experiment (Open Field), the mice were handled for 10 to 15 minutes daily, for four consecutive days. During this handling period, they were gently picked up and allowed to explore the experimenter's hand and arm, helping them become accustomed to human contact.

A dummy miniscope was used for 10 minutes daily over the four days to help familiarize the mice. On the first day of habituation, the mice were placed under light anesthesia while the dummy miniscope was attached. During the subsequent habituation sessions, which took place in the experimental room, the mice remained awake. They were lightly restrained in the experimenter's hand to ensure the proper attachment of the dummy miniscope.

The dummy miniscope was secured to the baseplate, and the mice were allowed to explore a holding cage for 10 minutes. This holding cage acted as temporary housing for the mice prior to their placement in the experimental arena, and it was also the location where the miniscope settings were configured.

2.3.1 Open Field Test

The specific testing apparatus was placed at the center of a 2m diameter space separated by white curtains from the lab, to minimize non-specific visual cues. Prior to each experiment and between mice, the apparatus was wiped-clean with ethanol (70%) to reduce olfactory interference.

The OFT arena was a square box measuring 42 cm x 40 cm x 40 cm, constructed from opaque white forex plates. It was illuminated with warm white light at an intensity of approximately 10 lux. Mice were placed at the center of the arena and allowed to explore for 10 minutes over three consecutive days. Their positions were recorded by a video camera (Basler acA1920-40gc) at a frequency of 20-25 Hz and automatically tracked using Ethovision software (Noldus XT 16).

Behavioral parameters were extracted from the OFT to conduct a comprehensive analysis of locomotor activity, anxiety-like behaviors, and cognitive performance. In the OFT, locomotor activity was assessed using metrics such as total distance traveled, and the amount of time spent in the center of the arena.

2.3.2 Contextual Fear Conditioning

Two days prior to the conditioning session, mice were acclimated to a holding room for at least two hours each day to minimize stress. Conditioning and memory testing were performed in a specialized apparatus (Fear Conditioning System, TSE Systems, Germany) consisting of a box equipped with a metal grid surrounded by a frame of light sensors for automatic detection of mouse position. Light, sound, electrical shocks as well as video recording are controlled and monitored automatically via the TSE software.

On the day of conditioning, the mice were placed in a square conditioning chamber measuring 20 cm by 20 cm. The chamber had transparent plastic walls, a stainless-steel grid floor, white lighting, constant white noise, and an ethanol odor. This environment was referred to as The Context. After a 3-minute exploration period (Pre-shock), the mice were exposed to a high-frequency tone (10 kHz, 70 dB) for 30 seconds, which was paired with a 2-second electric foot shock (0.5 mA) during the final 2 seconds of the tone. This tone-shock pairing was repeated after a 60-second interval. Following the second tone-shock pairing, the mice remained in the chamber for an additional 3-minute period (Post-Shock) before returning to their home cages. The chamber was cleaned with 70% ethanol between mice.

Memory recall was assessed on two probe days: 7 (Recent Memory test) and 21 (Recent Memory test) days after conditioning. During each probe day, context memory retrieval was first evaluated by placing the mice back in The Context for 3 minutes. After a minimum interval of 60 minutes, the mice were introduced to an alternative context that was visually and physically distinct from The Context to assess contextual memory specificity.

On the first probe, the alternative context (Novel1) was also a square chamber (20 cm × 20 cm) featuring only one transparent wall that revealed an arrow-shaped sign on the wall, which functioned as a visual cue. The floor was covered with black plastic and fresh bedding, the lighting was changed to red, and no white noise was present. The mice remained in Novel1 for 3 minutes. The chamber was cleaned before and between mice trials with 1% acetic acid, which served as a distinct olfactory cue.

On the second probe, the alternative context (Novel2) consisted of a rectangular chamber (23 cm × 17 cm) with entirely transparent walls. Signs with geometrical shapes were attached to the box walls and were visible to the mouse through the transparent chamber walls. The floor was covered with bedding, red lighting was used, and no white noise was played. The mice remained in Novel2 for 3 minutes. The chamber was cleaned with 1% acetic acid between mice.

The TSE software recorded locomotion and freezing behavior. Immobility for > 1 s was defined as freezing.

The experimental sessions were as follows:

- **Pre-shock**: The initial 3 minutes spent in The Context prior to the conditioning.
- **Post Shock**: The final 3 minutes in The Context immediately following the conditioning.
- **Recent memory**: The first probe session in The Context was conducted 7 days after the conditioning.
- **Novel 1**: The first session in an alternative context.
- **Remote memory**: The second probe session in The Context was conducted 21 days after the conditioning.
- **Novel 2**: The second session in an alternative context.

2.4 Calcium Imaging data Acquisition and Processing

During each behavioral task, we recorded calcium signals from the dCA using a miniaturized microscope (nVoke, Inscopix Inc). We selected an optimal field of view for each mouse and adjusted the imaging settings to achieve a good signal-to-noise ratio. The calcium signals were recorded at either 20 or 30 Hz. The miniscope was triggered using a TTL signal from Ethovision software for the OFT or TSE software for CFC.

2.4.1 Source Extraction

The calcium imaging data were processed using Inscopix Data Processing Software (IDPS), along with various Python packages (see section 2.6) and custom Python scripts. To enhance data analysis, we performed spatial down-sampling by a factor of 4 and temporal down-sampling by factors of 2 or 3. This process resulted in a final resolution of 3.128 microns per pixel and a sampling rate of 10 Hz. Following down-sampling, image frames were cropped to include only regions of interest (ROIs) containing visible neurons. In order to track the same cells across experimental paradigms (OFT and CFC), videos were concatenated into a single video prior to motion correction. The concatenated video was then motion corrected using the NoRMCorre algorithm (Pnevmatikakis et al., 2017), where both rigid and non-rigid motion correction were applied.

Subsequently, neuron footprints and activity traces, e.g. source extraction, were extracted using the open-source Constrained Nonnegative Matrix Factorization for the microendoscopic data

(CNMFe) package (Zhou et al., 2018) implanted in IDPS. The CNMFe algorithm was applied to extract single-neuron components from the down-sampled dataset, using the following parameter settings: a low-cut spatial value of 0.015Hz, a cell diameter of 6 pixel, a minimum correlation of 0.8, a minimum peak-to-noise ratio of 10, a Gaussian kernel of 3, and a pixel merging threshold of 0.7. While these parameters were generally consistent, some variation was needed between mice to account for individual differences in data quality and signal characteristics. These adjustments were made to ensure optimal neuronal signal detection while minimizing noise and artifacts.

The neuronal activity traces were extracted as dF/F and subsequently deconvolved using the OASIS algorithm (Friedrich et al., 2017) to estimate underlying calcium spiking activity. For calcium spike detection, we utilized a signal-to-noise ratio (SNR) of 6, categorizing these spikes as calcium spikes. Additionally, we performed calcium event detection, they are characterized by a rapid increase in amplitude followed by a prolonged decay back to baseline levels. We set the Event Threshold Factor to 6 and the decay time to 0.12 seconds, the estimated decay time for GCaMP8m (Zhang et al., 2023).
From the calcium events, we exported time points of onset of each event and the moment it peaked. This information enabled us to identify calcium bursts, which may include a single or multiple calcium events. The termination of a calcium event is marked when the dF/F returns to the baseline of that calcium burst, which was defined as below 10% of the lowest peak within a calcium burst.

A cleanup process was implemented to curate the neuron footprints and activity traces to eliminate non-neuronal spatial footprints and traces. To accomplish this, a Random Forest algorithm (specifically, Scikit-learn's ensemble RandomForestClassifier) was trained on a randomly chosen session from each mouse. Those sessions were manually labeled to distinguish between valid and invalid components.

The features provided to the Random Forest classifier were derived from the traces and spatial footprints. These included trace skewness, trace SNR, calcium spike rate, kurtosis, number of contour components, trace standard deviation, spatial footprint compactness, spatial footprint area, and spatial footprint circularity. As the manual labeling was biased towards valid components, the training data was balanced by randomly selecting an equal number of valid and invalid components. The Random Forest classifier was trained on ~350 data points and tested on ~350

data points, achieving an accuracy of 98%. This classification process ensured the exclusion of artifacts and noise, retaining only high-quality neuronal signals for downstream analysis.

However, one mouse had a low number of neurons and low SNR, and the Random Forest classifier could not accurately classify the neurons. Therefore, neurons were manually classified by visual inspection of the traces and spatial footprints for this mouse.

For further analysis, the dF/F traces were used for pre-event histograms, and the deconvolved calcium spikes were used for the remaining analysis.

2.4.2 Place Cells detection

The hippocampus is widely recognized for its function in encoding spatial information. This capability is linked to specific neurons called place cells; these cells exhibit location-specific firing patterns, creating a neural map of space that facilitates spatial navigation (O'Keefe & Dostrovsky, 1971). Place cells were identified by analyzing the mutual information (MI) between spatial position and calcium spikes. MI quantifies how knowing the spatial location reduces the uncertainty about the calcium spikes. Rate maps were smoothed using a Gaussian kernel with a standard deviation of 1.5 and location was binned into 2x2cm

The MI content was computed using:

$$MI(X,Y) = \sum_{x \in X} \sum_{y \in Y} p(x,y) \cdot \log\left(\frac{p(x,y)}{p(x) \cdot p(y)}\right)$$

Where:

- **X**: The set of spatial bins into which the environment is divided (occupancy map)
- **Y**: The binarized activity states of the neuron (active or inactive) (rate map)
- **p(x, y)**: The joint probability of observing the animal in spatial bin **x** and the neuron being in activity state **y**.
- **p(x)** and **p(y)**: The marginal probabilities of spatial bin occupancy and neuron activity, respectively.

A circular shuffling procedure was employed to assess the significance of the MI. Calcium spikes were shuffled 1000 times to construct a null distribution of MI values. Neurons were then classified as place cells if they met two criteria:

1. MI exceeded 95% of the shuffled null distributions
2. The neuron's calcium spike rate was greater than 0.01 Hz, e.g. at least 5 calcium spikes

Place cell detection was performed during periods of mobility. For the OFT, mobility periods were defined as intervals when the mouse was moving at a speed greater than 1.5 cm/s. The spatial bins were organized into a 20x20 grid, with each bin measuring 2x2.1 cm.

In The Context and Novel1 of CFC, bins were arranged in a grid of 10x10, with each bin measuring 2 cm by 2 cm. However, in Novel2, each bin measured 1.7 cm by 2.3 cm, but the arrangement remained a 10x10 grid. The mobility periods for CFC were defined as the inverse of freeze period. Specifically, the start of a mobility period was determined to be one second after the end of a freeze period, and the end of the mobility period was one second before the start of the next freezing period. Mobility periods less than 1 second apart were merged, and mobility periods with a duration of less than 2 seconds were removed.

The place field size was determined by counting the rate map bins adjacent to the maximum peak rate bin and surpassed the mean rate by more than 1.5 standard deviations (Schuette et al., 2020).

A place cell is considered stable across contiguous sessions if it meets the criteria for place cells in both sessions, shows a Spearman correlation greater than 0.5, and has a p-value of less than 0.05 (Kinsky et al., 2018).

2.4.3 Correlated calcium activity graph theory analysis

Calcium spikes from each neuron were binned into one-second bins. The Pearson correlation coefficient was calculated for each pair of neurons, with a threshold of 0.3 applied to identify correlated pairs. Next, a graph was created using the NetworkX Python package to visualize and analyze the structure of the neural correlations. For each neuron, we calculated the ratio of correlated pairs (number of pairs divided by the total number of cells in the field of view) and the clustering coefficient (number of edges among neighbors divided by the number of possible edges among neighbors) (Jimenez et al., 2020).

2.4.4 Defining Shock, Tone, Freeze, and Mobility Neuron

To identify neurons that were significantly responsive to shocks, tones, freeze periods, or mobility periods, we utilized a circular shuffling approach. For each neuron, the timing of its calcium spikes was shuffled across 1,000 iterations, and calcium spike rates were recalculated for specific behavioral epochs (shock, tone, freeze, or mobility) for each shuffle. This procedure generated a null distribution of calcium spike rates for each neuron and condition.

Neurons were classified as "shock neurons," "tone neurons," "freeze neurons," or "mobility neurons" if their calcium spike rate exceeded 95% of the shuffled null distributions for the corresponding behavioral condition.

Additional conditions and specific details included:

- **Tone Neurons**: Only the first tone presentation, which was untainted by shock association, was used. For circular calcium spike shuffling, only the period leading up to and including the tone presentation was considered. This ensured that the tone-evoked responses were attributed specifically to the tone and not contaminated by the shock.
- **Shock Neurons**: Both shock periods were included. To ensure robust estimation, these intervals were extended by an additional 10 seconds. This adjustment accounts for delayed or prolonged neuronal responses related to the shock.
- **Freeze and mobility neurons:** For pre-shock, the first 3 minutes, and for post-shock, the last three minutes of the conditioning session. For Novel1 and Novel2, the 3 minutes of each session were considered.

By applying these criteria, we ensured that the classification of neurons into shock, tone, freeze, and mobility categories was statistically robust and reflected their responsiveness to distinct behavioral and sensory stimulus.

2.4.5 Neuronal index discrimination

To better understand neuronal responses, we calculated the Neuronal Modulation Index (NMI) for each neuron. The NMI measures the degree to which a neuron’s activity is influenced by one episode compared to another. Its values range from -1 to 1.

The NMI was calculated using the following formula:

$$NMI = \frac{RX - RY}{RX + RY}$$

Where:

- **RX**: The calcium spike rate of the neuron during X episode.
- **RY**: The calcium spike rate of the neuron during the Y episode.

A positive NMI indicates that the neuron's activity increases in episode X relative to episode Y, while a negative NMI suggests reduced activity in episode X. Values near zero indicate little to no modulation.

2.5 Acquisition and processing of local field potentials and Action Potentials

Adult mice underwent anesthesia through an intraperitoneal injection of 1.2 mg/g body weight urethane (15% w/v; Sigma diluted in 0.9% NaCl). Initial anesthesia was administered using 5% isoflurane, which was subsequently reduced to 1.0–1.5% during the surgical procedure. A staggered 32-site silicon probe with a 25 μm inter-site distance and 177 μm^2 electrode surface (model A1x16-Poly3-5 mm-25s-177; NeuroNexus) was placed in the dCA1 region (AP: -2.45 mm, ML: +2.85 mm, DV: ~-1.2). Data from the probes were digitally filtered within a 0.5-9000 Hz bandpass and recorded as 16-bit integers using a 30 kHz sampling rate, facilitated by a SmartBox data acquisition system (NeuroNexus). The position of the probe, which had been pre-treated with a DiI-solution, was validated post-mortem on coronal slices.

2.5.1 Spike Sorting

We performed single-unit spike detection and sorting using Klusta-suite software (Rossant et al., 2016) and manually curated using Phy2.0 (https://github.com/cortex-lab/phy). Single-unit spike activities were obtained from raw signals for each electrode. Raw signals were band-pass–filtered (500 to 6000 Hz). The spike threshold level was set to > 4.5 median absolute deviations for the hippocampus probe shank (Rossant, Kadir et al. 2016). To ensure the quality of the isolated single units, we manually inspected the shape of spike waveforms, inter-spike intervals, and the shape of the autocorrelogram of spike times in Phy2. We only included units showing clear negative deflection in the spike waveform. In addition, units violating the refractory period (> 2ms) were excluded.

2.5.2 Cell Type Classification

We further inspected the isolated single-units with CellExplorer (Petersen et al., 2021). We classified the units into putative excitatory neurons and inhibitory interneurons based on the peak amplitude asymmetry index and trough-to-peak (Sirota et al., 2008). We classified inter-neurons as having a trough-to-peak < 0.385 ms and peak amplitude asymmetry index greater than 0 (Barthó et al., 2004; Stark et al., 2013). All neurons around the decision cut-off were carefully examined, and in case of doubt, the unit was excluded. Finally, only units with 300 or more spikes were used for further analysis.

2.6 Key resources table

REAGENT or RESOURCE	SOURCE	IDENTIFIER
Bacterial and virus strains		
pGP-AAV-syn-jGCaMP8m-WPRE	(Zhang et al., 2023)	RRID:Addgene_162375
Biological samples		
C57BL/6mice Arc/Arg3.1 Knockout	(Plath et al., 2006)	
Software and algorithms		
CustomPythoncodeforCa2+dataanalysis		
Python	Python.org	3.11.1
Numpy	Numpy.org	
Matplotlib	Matplotlib.org	
Seaborn	seaborn.pydata.org	
Pingouin		
Pynapple(PYthon Neural Analysis Package)	(Viejo et al., 2023)	
Deeplabcut	(Fujimori et al., 2020; Mathis et al., 2018)	
scipy	scipy.org	
KLUSTA	(Rossant et al., 2016)	
Phy2		
scikit-learn	scikit-learn.org	
Caiman	(Giovannucci et al., 2019)	
Matlab: Cellexpolare	(Petersen et al., 2021)	
Other		
GRINlens	GRINtech/Inscopix	1.0x4.0mmlens
1mLsyringe	Hamilton	
MicroInjectionpump		
Microendoscope+DataAcquisitionBox	Inscopix	nvoke
Recordingsystem	Intan	
32 channel headstage	Intan	
32 channel linear probe	NeuroNexus	A1x32-5mm-50-177

2.7 Statistical Analysis

All statistical analyses were performed using Python-Pingouin and MATLAB. Statistical tests used were as follows: Chi-square test, Mann–Whitney U test, and mixed-design analysis of variance with Sidak's post hoc test. The type of test is indicated in figure legends. A p-value below 0.05 was considered significant. P-values and, here possible, effect sizes (Cohen's d) are reported, with statistical significance denoted as follows: Between-genotype comparisons: $p < 0.05$ (*), $p < 0.01$ (**), $p < 0.001$ (**). Within-group comparisons: $p < 0.05$ (#), $p < 0.01$ (##), $p < 0.001$ (###). Non-significant differences: ns.

All graphs were generated with Python (Seaborn and Matplotlib), Adobe Illustrator (Version 29.5), and MATLAB R2023a (MathWorks). Line graphs are shown with mean ± S.E.M in shaded colors, and the markers indicate the mean values.

Results

3 Results

3.1 Preprocessing of Calcium Imaging Data

Miniscope-based calcium imaging has transformed neuroscience by enabling long-term observation of neuronal activity in freely moving animals. This method allows researchers to examine neural circuit dynamics in natural settings, providing significant insights into processes like memory acquisition, consolidation, and retrieval. Nevertheless, the reliability of calcium imaging data depends on thorough pre-processes to confirm that the signals observed genuinely reflect neuronal activity, not noise, motion artifacts, or misleading fluorescence variations (Stamatakis et al., 2021).

Miniscopes utilize genetically encoded calcium indicators (GECIs) to track calcium dynamics, which act as proxies for neuronal activity. Recent advancements focused on improving these indicators, notably within the GCaMP8 series. This series was developed through structure-guided mutagenesis of GCaMP6s, replacing the calmodulin (CaM) binding peptide, RS20-peptide, with a peptide based on endothelial nitric oxide synthase. As a result, GCaMP8 sensors achieve nearly tenfold faster fluorescence rise times compared to earlier versions, GCaMP6 and GCaMP7. Included in the GCaMP8 series are GCaMP8s (characterized by fast rise times, slow decay, and high sensitivity), GCaMP8f (featuring fast rise and fast decay), and GCaMP8m (which has a fast rise and medium decay). The GCaMP8m was utilized in this study. The validation of the GCaMP8 series involved in vitro and *in vivo* testing, in conjunction with simultaneous electrophysiology and calcium imaging, confirming their improved reflection of neuronal spiking. Functional validation across various species, such as in the mouse visual cortex and Drosophila neurons, showcased the indicators' robustness and adaptability. Impressively, *in vivo*, electrophysiology and two-photon calcium imaging were performed simultaneously in mouse V1 for functional validation (Zhang et al., 2023).

These indicators assess neuronal activity by monitoring calcium influx in cells. Therefor thorough preprocessing, motion correction, and quality control are critical to ensure that the signals accurately depict biologically relevant neuronal activity (Resendez et al., 2016). Mice were injected with AAV-Syn-jGCaMP8m-WPRE virus in the pyramidal layer of the right hemisphere of dCA1 and implanted with a GRIN lens above the virus injection site 10-14 days after the virus surgery (Figure 3.1-1.A-C)

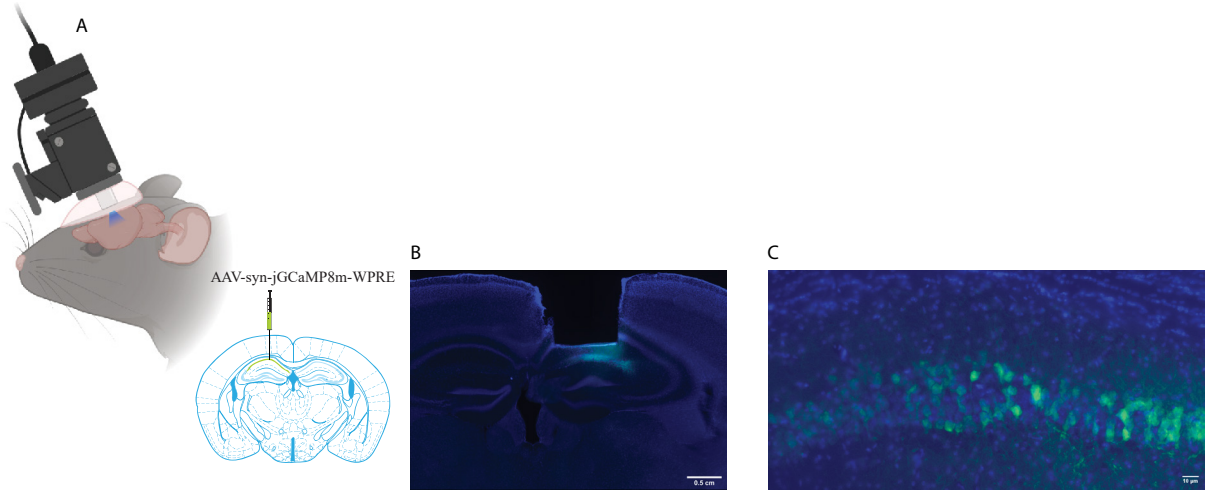


Figure 3.1-1 *In vivo* calcium imaging of dCA1 neurons expressing GCaMP8m in freely behaving mice. **A)** A miniature microscope with GRIN lens implanted above dCA1 neurons expressing jGCaMP8m. **B)** Representative confocal microscopic picture showing jGCaMP8m expression in dCA1 neurons where the GRIN lens was located **C)** confocal microscopic picture of jGCaMP8m expression in dCA1 neurons

This section gives a general overview of key pre-processing steps we used on the miniscope calcium imaging data. With the goal to minimize the inclusion of incorrectly identified artifacts or noise as meaningful neural activity.

3.1.1 Motion Correction

The first step in validating calcium imaging data is ensuring that the recording is stable. Due to the dynamic nature of freely behaving animals, head-mounted miniscopes are particularly susceptible to motion artifacts (Figure 3.1-2.A-B). Even slight head movements can cause shifts in the recorded field of view, leading to misalignment of neuronal signals. Here, we used the Motion correction algorithm NoRMCorre (Pnevmatikakis & Giovannucci, 2017) to realign images and reduce movement-related distortions. This algorithm works by detecting spatial shifts relative to a reference frame and compensating for them across frames.

Motion correction can be applied both within sessions and between sessions. Within-session correction involves a minor shift for aligning with a reference frame, while between-session alignments require a more prominent shift due to the detaching and reattaching of the miniscope. We reduced the influence of motion artifacts by implementing motion correction within and between sessions by concatenating all relevant sessions into a single session (Figure 3.1-2.D) (Ghandour et al., 2019).

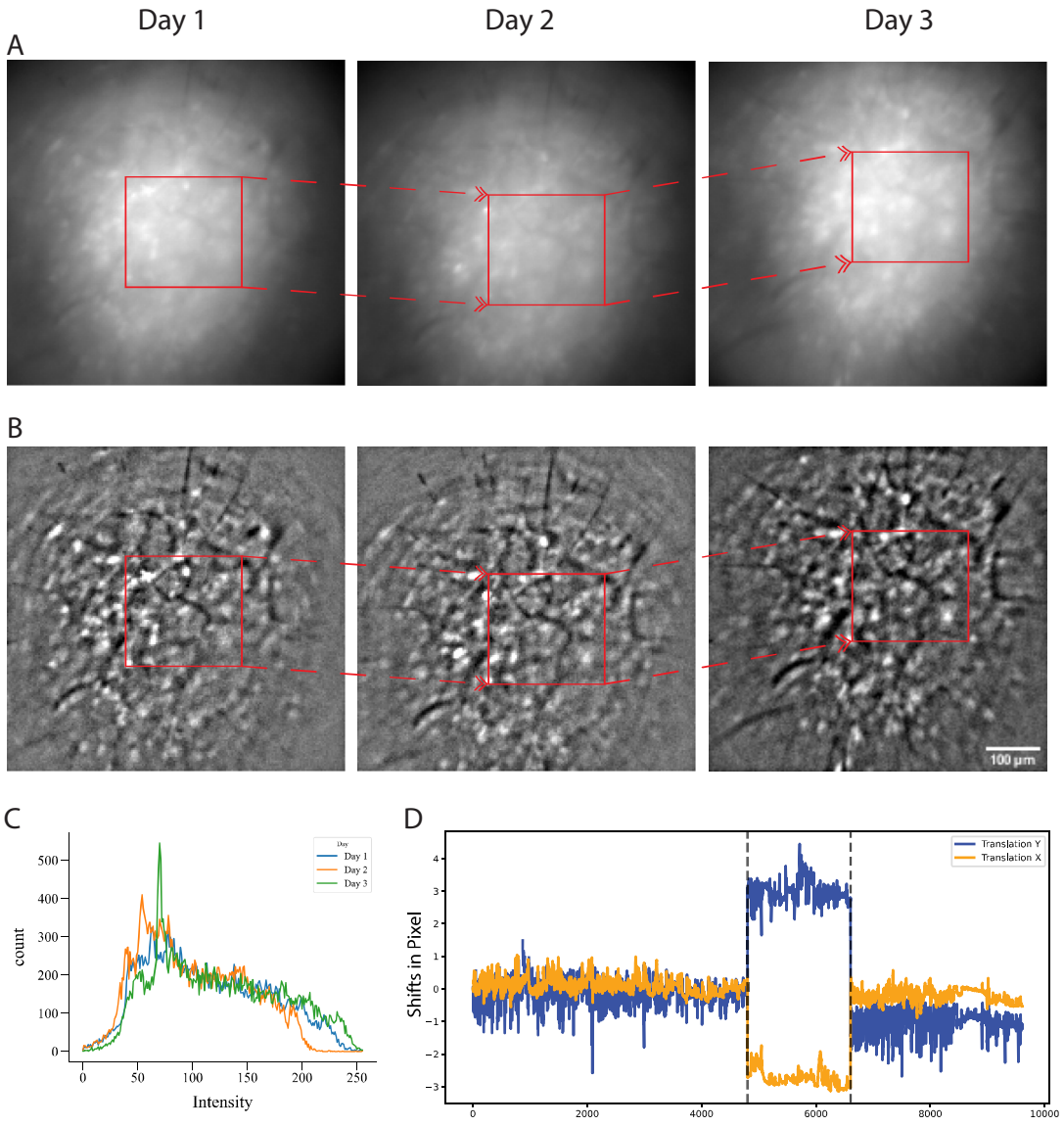


Figure 3.1-2 Motion Correction of Calcium Imaging Data. **A)** Raw calcium imaging data from various days from the same mouse. The red square illustrates how the field of view shifts due to the detection and reattachment of the miniscope. **B)** Identical to A but implementing a spatial Gaussian. **C)** The histogram corresponds to a random image from each session. **D)** The pixel shifts in both X and Y needed to correct each frame in the three sessions to align with the same reference frame.

3.1.2 Source Extraction

Calcium imaging data may experience interference from several sources of noise, such as background fluorescence, autofluorescence, and uneven illumination (Resendez et al., 2016; Stamatakis et al., 2021) (Figure 3.1-2 C). Employing filtering techniques can effectively eliminate this noise while retaining important neuronal signals. Here, we used band-pass filtering by subtracting a Gaussian-smoothed version of the frame from a less-smoothed version of the frame (Figure 3.1-2.B) (Zhou et al., 2018)

Following this, we conducted source extraction to obtain neuron footprints and activity traces using the open-source CNMFe package (Zhou et al., 2018), which is implemented in Inscopix data processing software (IDPS). We utilized the CNMFe algorithm to extract single-neuron components from the down-sampled, concatenated, motion-corrected, and spatially filtered calcium imaging data. The extracted neuron footprints and activity traces are significantly influenced by several parameters: the estimated diameter of the neuron, the correlation between adjacent pixels, and the minimum peak-to-noise ratio of a pixel when identifying new neuron centers (Figure 3.1-3).

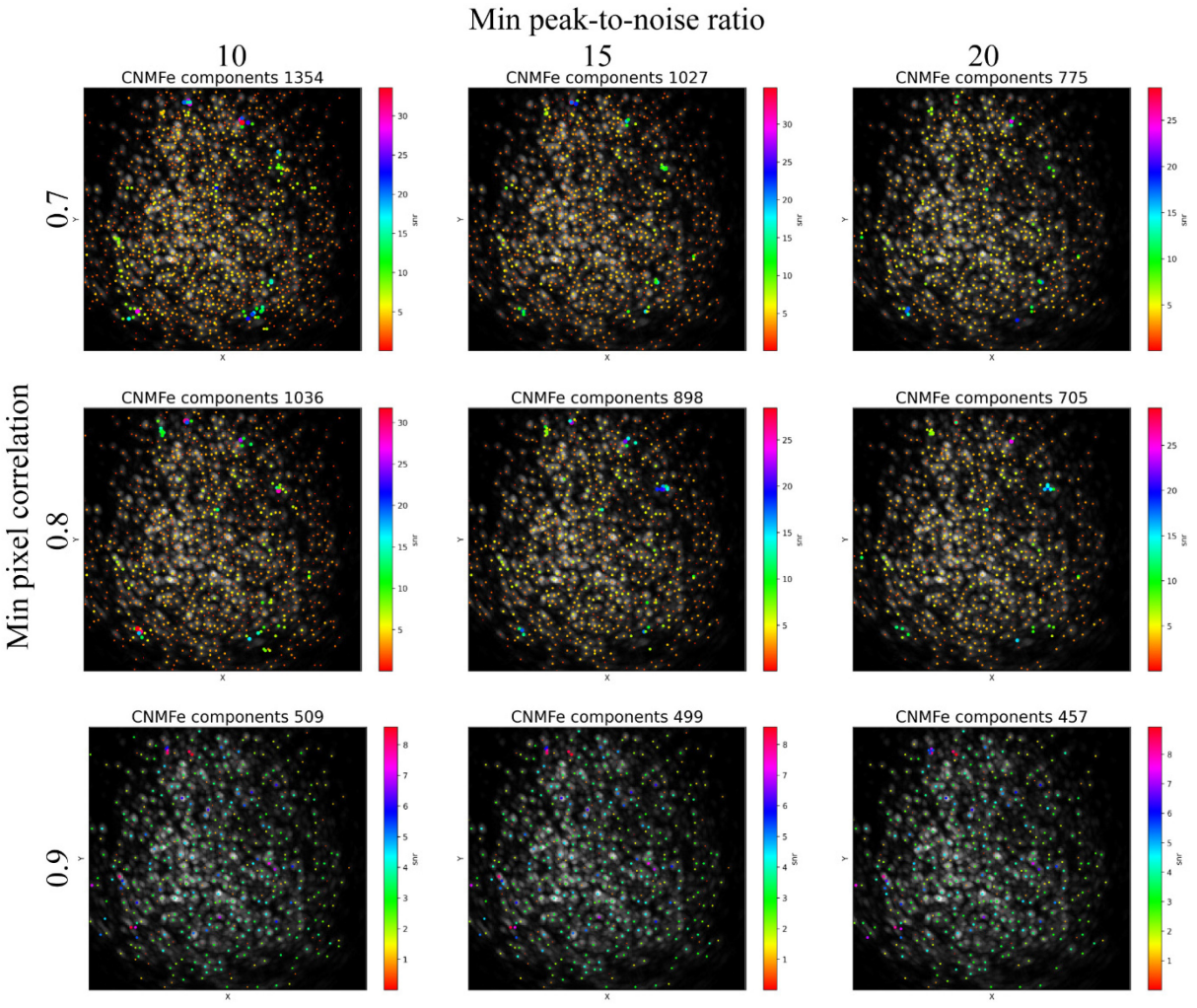


Figure 3.1-3 CNMFe parameters exploration. All plots use the same cell diameter of 5 pixels. The center plot was selected as the optimal parameter set for this particular mouse. Abbreviation; SNR : signal-to-noise ratio, min : minimum

Due to the absence of ground truth data, the determination of optimal parameters relied on thorough visual inspection of the extracted components. Since automated parameter selection was not feasible, we carefully examined each dataset to identify the most suitable settings that preserved meaningful signals while minimizing noise and artifacts (In Figure 3.1-3, the CNMFe parameters for the center plot were chosen as the most suitable). Furthermore, to reduce

variability among individual mice, we refined the preprocessing steps for each mouse. This included refining motion correction, background subtraction, and CNMFe extraction to ensure that each mouse's data was processed under the most appropriate conditions. By implementing this approach, we could enhance the reliability and comparability of the extracted neural activity across mice.

3.1.3 Random Forest Classifier

Even with optimization, CNMFe may still produce some false positives in the detected cell outputs, such as non-neuronal components. These can be removed through manual curation of the footprints and calcium traces. This curation process involves recognizing traces that lack stable baseline fluorescence (Resendez et al., 2016), calcium transient durations that do not align with the calcium indicator expressed (e.g., GCaMP8m), or spatial footprints that do not match the typical shapes and sizes of neurons (Figure 3.1-4.A). Although this manual curation helps decrease the number of false positives in CNMFe outputs, the visual inspection of thousands of extracted cells can be quite time-consuming.

To tackle this issue, we employed a semi-automated classification model built on random forest. This model aims to minimize the manual curation needed while still allowing for adjustments using manually labeled datasets. The model classifies components based on whether they should be included as neurons or excluded as non-neuronal components, utilizing features derived from the traces and spatial data footprints.

We manually classified a dataset of approximately 5,500 spatial footprints. This dataset was derived from a randomly selected session for each mouse, ensuring that at least one session from every mouse was incorporated into the classifier model.

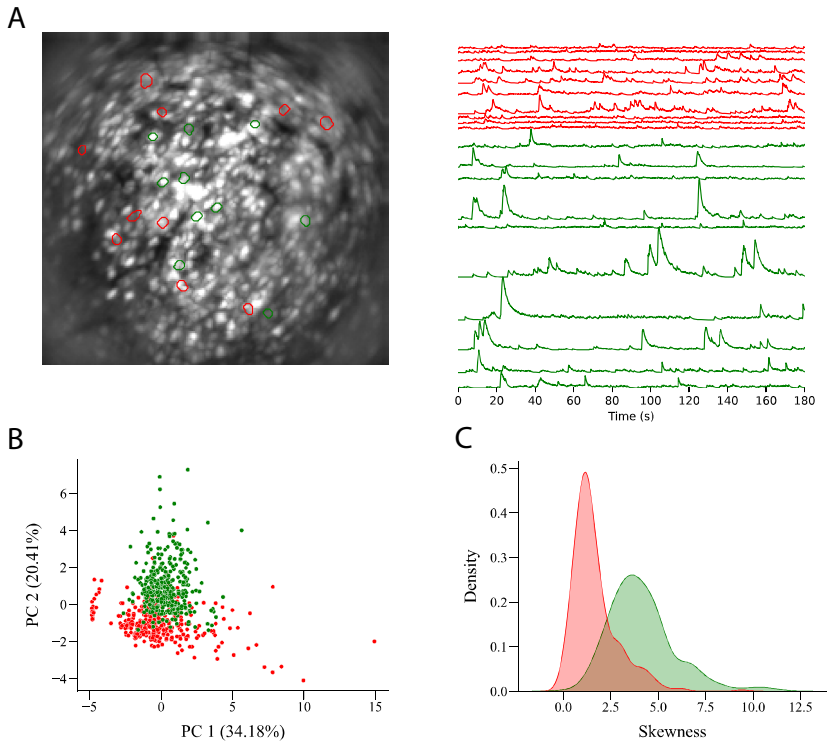


Figure 3.1-4 Manual correction of spatial footprints and traces. A) Left: The maximum projection of a single session overlaid with the spatial footprint for manually accepted (green) and rejected (red) components. Right: The activity of manually corrected components. B) The separation suggests distinct feature distributions between accepted and rejected components. D) The density of one feature used in the random forest model shown is the trace skewness separation, which reveals differing distributions for accepted and rejected components.

The features from traces included skewness, kurtosis, standard deviation, signal-to-noise ratio, and event rate. For footprint features, we included the number of contour components, circularity, compactness, perimeter, area, and eccentricity. Due to the skewness to watch valid accepted components (5,157) over rejected ones (350), the dataset was balanced by randomly selecting an equal count of accepted and rejected components. Principal Component Analysis (PCA) was employed to analyze the feature set and visualize the separation of accepted and rejected components (Figure 3.1-4.B). The findings indicated that the first principal component (PC1) accounted for 34% of the total variance, while the second principal component (PC2) explained 20%. This implies that most of the variability in the data is captured by these two components, suggesting that the selected features can effectively differentiate between the classes. Although there is a non-binary division in the PCA space, a clear distinction between accepted and rejected classes is observable. When plotting the density of all features (not shown), the skewness of the traces displayed the greatest differentiation between the two classes (Figure 3.1-4.C).

The random forest model was trained on 50% of the balanced dataset (e.g., 186 accepted and 163 rejected components) and demonstrated a high accuracy rate of 98% in predicting whether

a component should be included or excluded (Figure 3.1-5.A). This means that the model can effectively identify and filter out non-neuronal elements, thereby enhancing the quality and reliability of the extracted data.

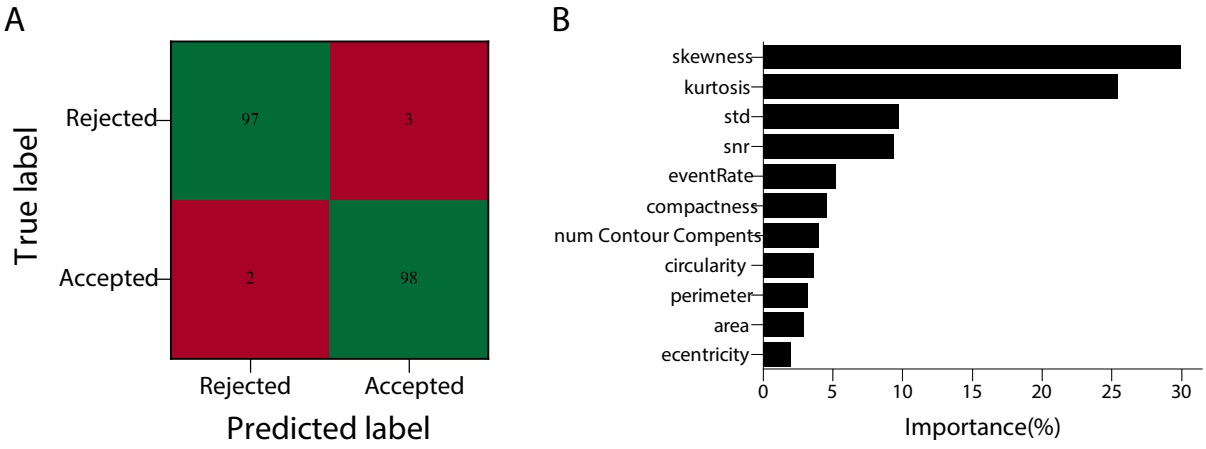


Figure 3.1-5 Performance and Feature Importance of the Random Forest Model. A) Confusion matrix for the Random Forest model, illustrating classification performance. B) Feature importance analysis, showing the contribution of different features to the model's decision-making.

The analysis of feature importance showed that trace features had the greatest importance, indicating they are vital in differentiating between accepted and rejected components. While footprint features also contributed to the model, their influence was notably smaller (Figure 3.1-6.B).

The use of a random forest classifier, informed by manual label footprints and traces, minimizes the chance of including non-neuronal elements.

3.1.4 Neural Activity

To derive conclusions from calcium imaging data, it is essential to quantify neural activity from these traces. Techniques such as spike deconvolution (Friedrich et al., 2017), calcium event detection (Jimenez et al., 2020), and area under the curve (AUC) analysis (Kobayashi & Matsuo, 2023) can be utilized. Deconvolution estimates the underlying calcium spike activity by computationally correcting for the slow calcium dynamics, while event detection identifies statistically significant fluorescence transients as discrete activity bursts. AUC, in contrast, provides a continuous measure of overall calcium activity over time, integrating signal intensity rather than detecting discrete events. While deconvolution offers higher temporal precision and event detection is robust against noise, AUC captures broader activity patterns.

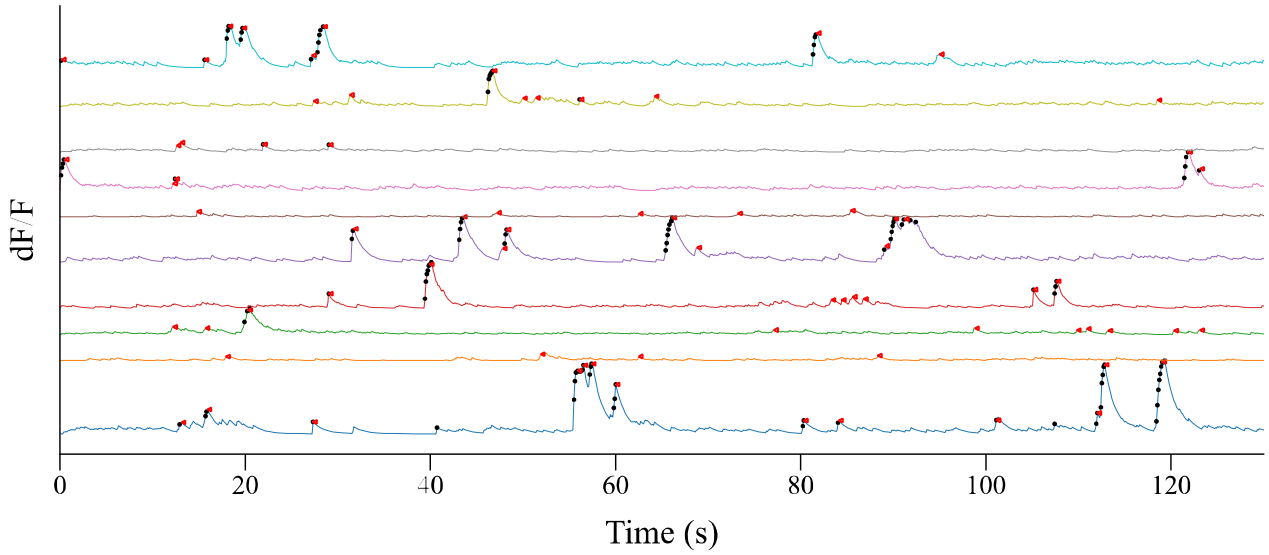


Figure 3.1-6 Representation of Calcium Activity. Calcium activity can be illustrated through various methods: spike deconvolution (black dots), calcium event detection (red triangles)

We utilized calcium spike detection due to its effective balance of sensitivity and robustness in different signal-to-noise environments. Calcium spike detection showed a better consistency with the average calcium fluorescence (see section 3.3.2)

3.2 Arc/Arg3.1 KO Mice Exhibit Reduced Exploratory Behavior over days

As an initial step in using miniscope calcium imaging to study the role of Arc/Arg3.1 in dCA1, we first examined the exploratory behavior of wildtype-control (WT) and Arc/Arg3.1 knockout (KO) mice in an open field arena. The open-field test (OFT) is a widely used method for assessing general locomotor activity, exploration, and anxiety-like behavior in rodents (Prut & Belzung, 2003; Walsh & Cummins, 1976). In this study, we compared the exploratory behavior of mice with GRIN lenses implanted (implanted) in the dCA1 to that of mice without lens implants (non-implanted), to inspect the impact of surgeries and microscope-carrying on mice behavior.

3.2.1 Distance Moved

During open-field exploration, we measured the distance traveled by non-implanted WT and KO mice without the miniscope (Figure 3.2-1.A-B, WT, n=11; KO, n=10) in a rectangular open-field box. Over three days, both genotypes displayed a significant decrease in distance traveled, indicating habituation to the environment.

Interestingly, KO mice showed a greater reduction in distance traveled compared to WT mice, suggesting a decrease in exploratory behavior (2ST-Sidak (*two-sample t-tests with Sidak correction for multiple comparisons*); OFT-day1, d=1.54, and $p<0.01$; OFT-day2, d=1.33 and $p<0.05$, Figure 3.2-1. A, C). This trend was consistent across all three days, with KO mice demonstrating lower locomotor activity, except for a not significant trend on OFT-day3.

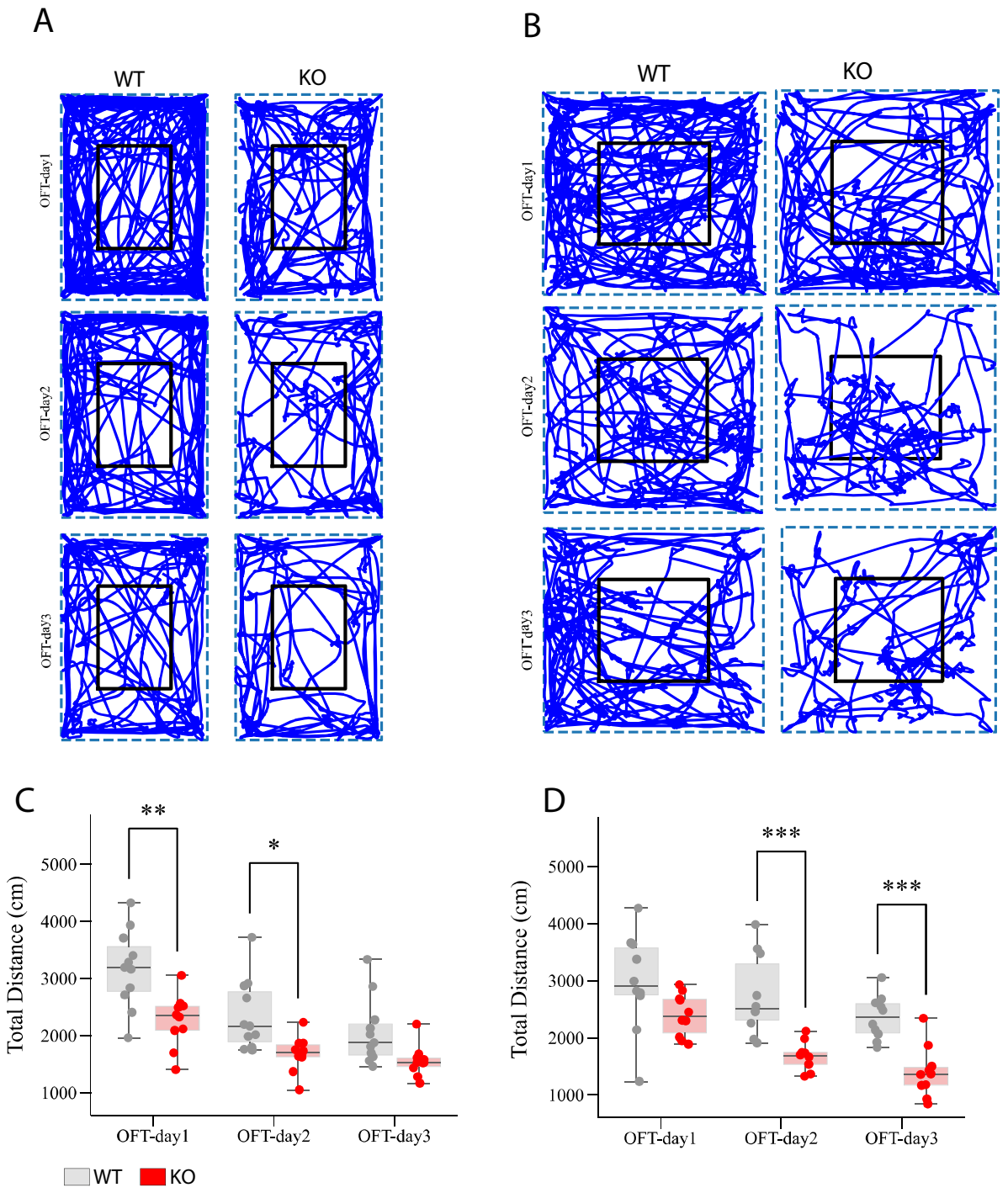


Figure 3.2-1 Total distance traveled. Trajectories of A) non-implanted and B) implanted mice in the open field, over three days of exploration. C) Non-implanted mice (Mixed-effect ANOVA: Genotype × OFT-day interaction, $F(2,38) = 0.95$, $p > 0.05$; Genotype effect, $F(1,19) = 21.41$, $p < 0.001$; OFT-day effect, $F(2,38) = 23.42$, $p < 0.001$; WT, n=11; KO, n=10, Stats-table 1) D) Implanted (Mixed-effect ANOVA: Genotype × OFT-day interaction, $F(2,36) = 2.1$, $p = 0.14$; Genotype effect, $F(1,18) = 20.19$, $p < 0.001$; OFT-day effect, $F(36) = 19.9$, $p < 0.001$; WT, n=10; KO, n=10, Stats-table 2)

The observed decrease in exploratory behavior among KO mice, in contrast to WT mice, was also evident in a cohort of mice that underwent surgeries and microscope carrying(implanted) (Figure 3.2-1.B,D, WT, n=10; KO, n=10) in the squared open-field arena. However, on the first

day, the distance traveled between the two genotypes showed no significant difference, though a trend was observed. In contrast, significant variations became apparent on the second and third days of exploration, with KO mice demonstrating lower locomotor activity than WT mice (2ST-Sidak; OFT-day2, d=2.02 and p<0.001; OFT-day3, d=2.32 and p<0.001, Figure 3.2-1. C).

We compared the non-implanted WT and KO mice cohort to their respective implanted mice over the three OFT-days. We found no significant differences in the total distance traveled for either genotype (WT Stats-table 3; KO Stats-table 4).

Since the two open-field arenas had different geometry, the time spent in the center is not directly comparable. The selection of the arena was accidental and imposes no merits.

3.2.2 Summary of Open Field Exploration

Even with a 3-gram extra weight placed on the mouse's head, the mice did not display any difference in movement compared to non-implanted mice over the three-day period. In summary, the surgical procedures, the lens, and miniscope mounting appeared to have close to no impact on the mobility and exploratory drive of the implanted mice. Supporting the use of this technique to study memory in WT and KO mice.

3.3 Calcium Dynamics in dCA1 and the Emergence of Place Cell

Recognizing the crucial role of place cells in spatial memory and navigation (Morris et al., 1982; Smith & Mizumori, 2006; Zinyuk et al., 2000). Place Cells are specifically activated when an animal occupies a particular location within its environment. We aimed to investigate how the absence of Arc/Arg3.1 might affect the generation of this place cell activity in the dCA1.

3.3.1 Reduced Calcium Spikes and Events in Arc/Arg3.1 KO

We identified populations of dCA1 neurons that were active during the three sessions of the OFT. The number of neurons observed in the dCA1 region was similar for both WT and KO mice, with no differences noted over the three days of exploration. On average, we detected 342 ± 235 neurons in the WT mice and 345 ± 235 neurons in the KO mice, resulting in a total of 1,883 neurons from 8 WT mice and 2,132 neurons from 10 KO mice (Figure 3.3-1. B). Some neurons exhibited consistent activation across all three days of OFT, whereas others were active on only two days, and a smaller subset showed activity exclusively on a single day (Figure 3.3-1.A). Approximately

75-80% of these neurons were active during any given session, with no significant difference between WT and KO mice (2-way ANOVA, F(2,2) = 0.40, p > 0.05, Figure 3.3-1.C)

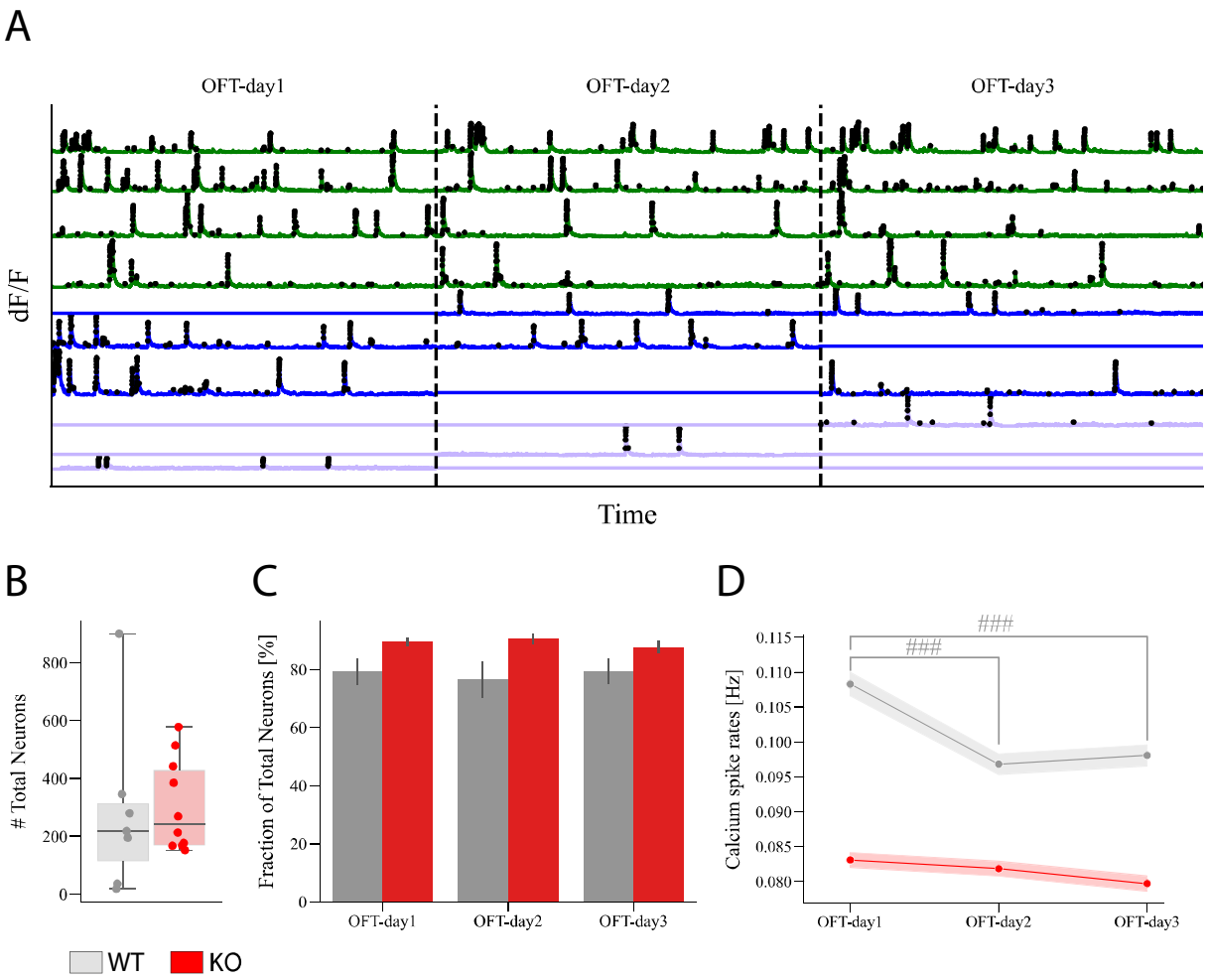


Figure 3.3-1 Number of neurons and their calcium spike rate in the open field task. A) Example of neurons that were activated all three days(green), two of the days(blue), or single days (purple) of OFT. Black dots are deconvolved calcium spikes. B) Total number of neurons detected for each mouse during the three days of the open field task. C) Fraction of active neurons each day in the open field task relative to the total detected neurons for each mouse (2-way ANOVA: Genotype × OFT-days interaction: F(1) = 0.40, p > 0.05, Genotype effect, F(2) = 17.4, p<0.001; OFT-day effect, F(2) = 0.05, p > 0.05,Stats-table 5). D) Calcium activity rate of active neurons in the open field task per day, with dots representing the group mean and shadows ±SEM. (2-way ANOVA: Genotype × OFT-days interaction: F(2,2) = 0.40, p < 0.001,Stats-table 6)

In contrast to the equal number of active neurons, the activity rates of WT and KO neurons were significantly different. Throughout the three days of exploration (Figure 3.3-1D) KO neurons displayed lower calcium spike rates (2-way ANOVA: F(2) = 0.40, p < 0.001). While the calcium spike rate of WT neurons decreased slightly over the three days (2ST-Sidak: OFT-day1 *vs* OFT-day2, *d*=0.16, p<0.001, OFT-day1 *vs* OFT-day3, *d*=0.14, p<0.001), the calcium spike rate of KO neurons remained relatively unchanged compared to the first day.

3.3.2 Absence of Small Calcium Events in Arc/Arg3.1 KO

To draw meaningful conclusions from calcium imaging data, quantifying neural activity from these recordings was crucial. As noted earlier (see 3.1.4), three primary methods typically exist for quantifying neural activity: spike deconvolution, calcium event detection, and mean AUC.

In this section, we reexamined the calcium spike rates (Figure 3.3-1.D) and added calcium event detection and calculated the mean AUC to enhance the result comparison (Figure 3.3-2).

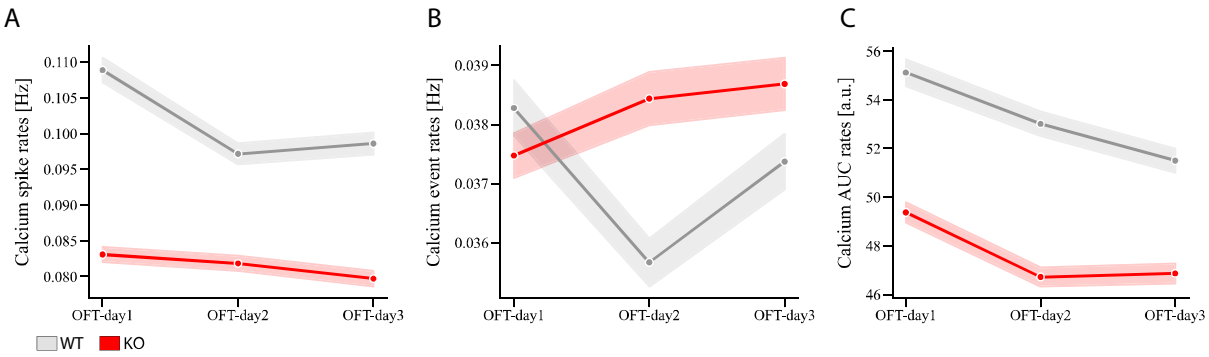


Figure 3.3-2 Various methods for quantifying calcium activity. A) Firing rates of calcium spikes. B) Firing rate of calcium events. C) Mean calcium AUC (area under the curve). Dots show means, shaded areas indicate ±SEM.

Interestingly, the rate of calcium events does not follow the same pattern observed in calcium AUC and calcium spike rates. In both the WT and KO groups, calcium AUC and spike rates exhibit the highest activity on OFT-day 1, with a decrease over the following days. Also, WT showed higher neural activity than KO across all three days. However, this trend is not reflected in calcium event rates, suggesting a distinct underlying dynamic in the calcium event detections. Initially, we noted that the calcium event rate in WT closely resembles that of KO on OFT-day1 and OFT-day3, but it is reduced on OFT-day2. Although KO experiences a minor, non-significant rise in calcium events across the days, WT displays a significant decline in OFT-day2 when compared to OFT-day1 and OFT-day3.

A question emerges: Why don't the rates of calcium events match the activity pattern of calcium spikes and the average calcium AUC?

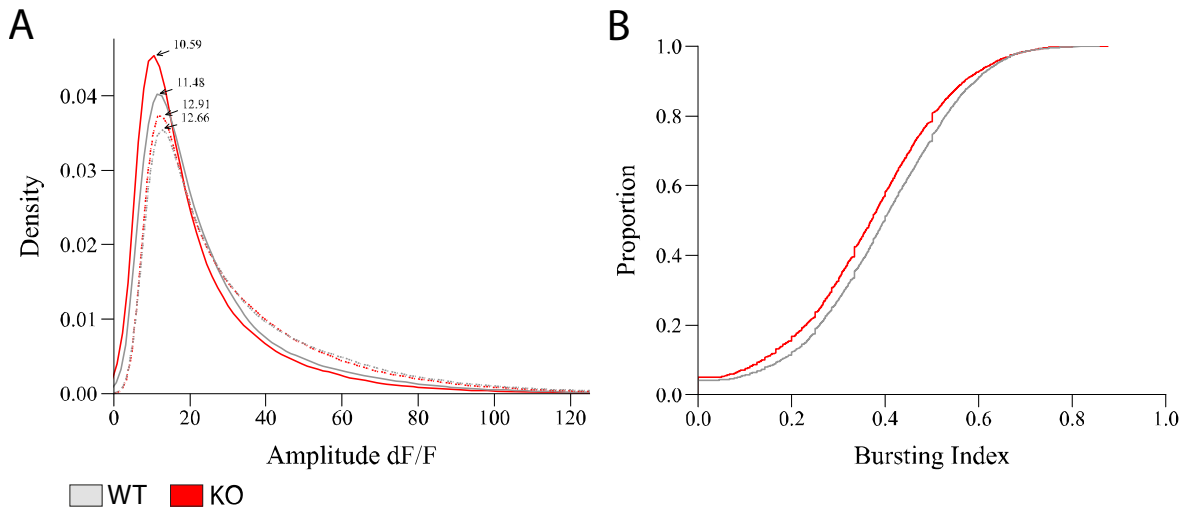


Figure 3.3-3 Calcium spikes' amplitude and bursting index. A) Calcium spikes (dashed line) and event (solid line). B) The bursting index based on the calcium spikes.

We began by assessing the amplitude of calcium spikes and the frequency of calcium events, as illustrated in Figure 3.3-3.A. Our analysis revealed a minor difference in the distribution of calcium spike amplitudes between WT and KO. However, it is noteworthy that the calcium events observed in the WT exhibited a larger amplitude compared to those in the KO. Suggesting that the event contains more calcium spikes, which is also evident by the bursting index (Figure 3.3-3.B), which in turn measures the fraction of calcium spikes that occur consecutively. The WT curve is shifted to the right of the KO, indicating that the WT has a higher burst index than the KO. Secondly, the calcium event curve of KO is shifted to the left, suggest that calcium events are generally smaller in KO compared to WT.

Neurons display various patterns of spike activity (Friedenberger et al., 2023), often occurring in bursts, which may generate particularly large and prolonged calcium influx, which we measured as a calcium event. Spike bursts (calcium events) can likewise occur with spaced but short intervals, leading to calcium events becoming calcium bursts. Here, a calcium burst is defined as the time from the onset of a calcium event until the calcium trace returns to baseline. This definition includes all intermediate peaks, such as calcium events, within one calcium burst (Figure 3.3-4.A).

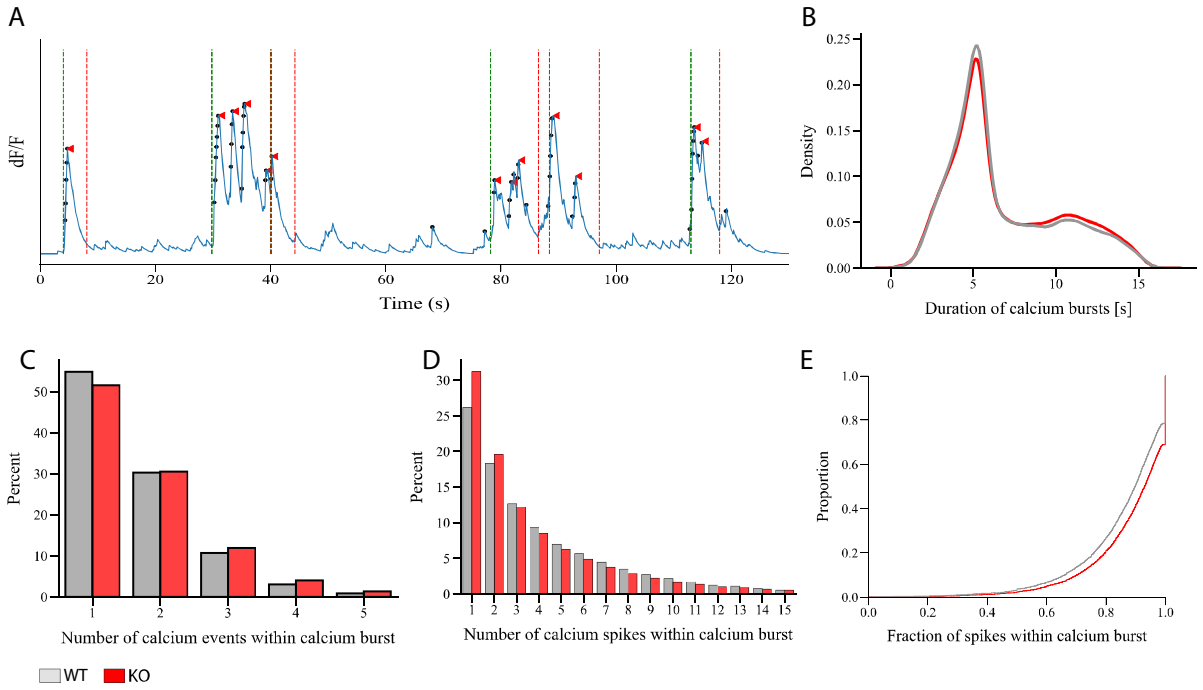


Figure 3.3-4 Calcium Burst. A) Detection of calcium bursts (calcium spikes (black dots), calcium events (red triangles), start and end of calcium burst (green and red dashed line respectively) B) Duration of each calcium burst C) Count of calcium events in every burst D) Count of calcium spike in every burst E) Fraction of calcium spikes within calcium burst

We initially observed that the duration of calcium bursts, which last up to 6 seconds, is similar for both WT and KO (Figure 3.3-4.B). However, between 6 to 12 seconds, WT shows a lower proportion of burst duration when compared to KO. For calcium bursts exceeding 12 seconds, WT and KO demonstrate comparable durations. This suggests that WT has shorter calcium bursts than KO.

But most calcium bursts consisted of either a single calcium event or two events (Figure 3.3-4.C), with very few bursts (< 2%) containing six or more events (data not shown). This distribution remains consistent across both WT and KO. However, a difference exists in the number of calcium spikes within each burst (Figure 3.3-4.D). In both groups, the majority of calcium bursts contained 1 to 3 calcium spikes. KO has a higher proportion of bursts with 1 to 3 spikes, while WT shows more bursts with four or more calcium spikes. This indicates that KO calcium bursts contain less calcium spikes than WT calcium bursts. However, as shown in the trace above, not all calcium spikes happen within a calcium burst. Therefore, we quantified the fraction of spikes that occurred during calcium event bursts (Figure 3.3-4.E). This shows that KO neurons exhibit a greater number of spikes during these bursts, meaning WT neurons display a higher percentage of spikes that occur outside of them.

In summary, two factors describe why WT neurons exhibit higher calcium spike rates than KO neurons. Although KO neurons experience longer calcium bursts, they also generate more

bursts with only 1-2 spikes. In contrast, WT neurons have a higher occurrence of bursts containing more than 3 spikes. And WT neurons produce a greater number of spikes outside of the calcium bursts.

3.3.3 Identification of Place Cells

Calcium imaging performed during open-field sessions allowed for the identification of place cells based on their unique spatial firing patterns during exploration. Place cell activity was quantified from epochs of exploration when the mouse moved at a speed greater than 1.5 cm/s. Additionally, for a neuron to be classified as a place cell, its calcium spike rates must exceed 0.01 Hz, and its mutual information should be higher than 95% of 1,000 shuffled MI values (Figure 3.3-5).

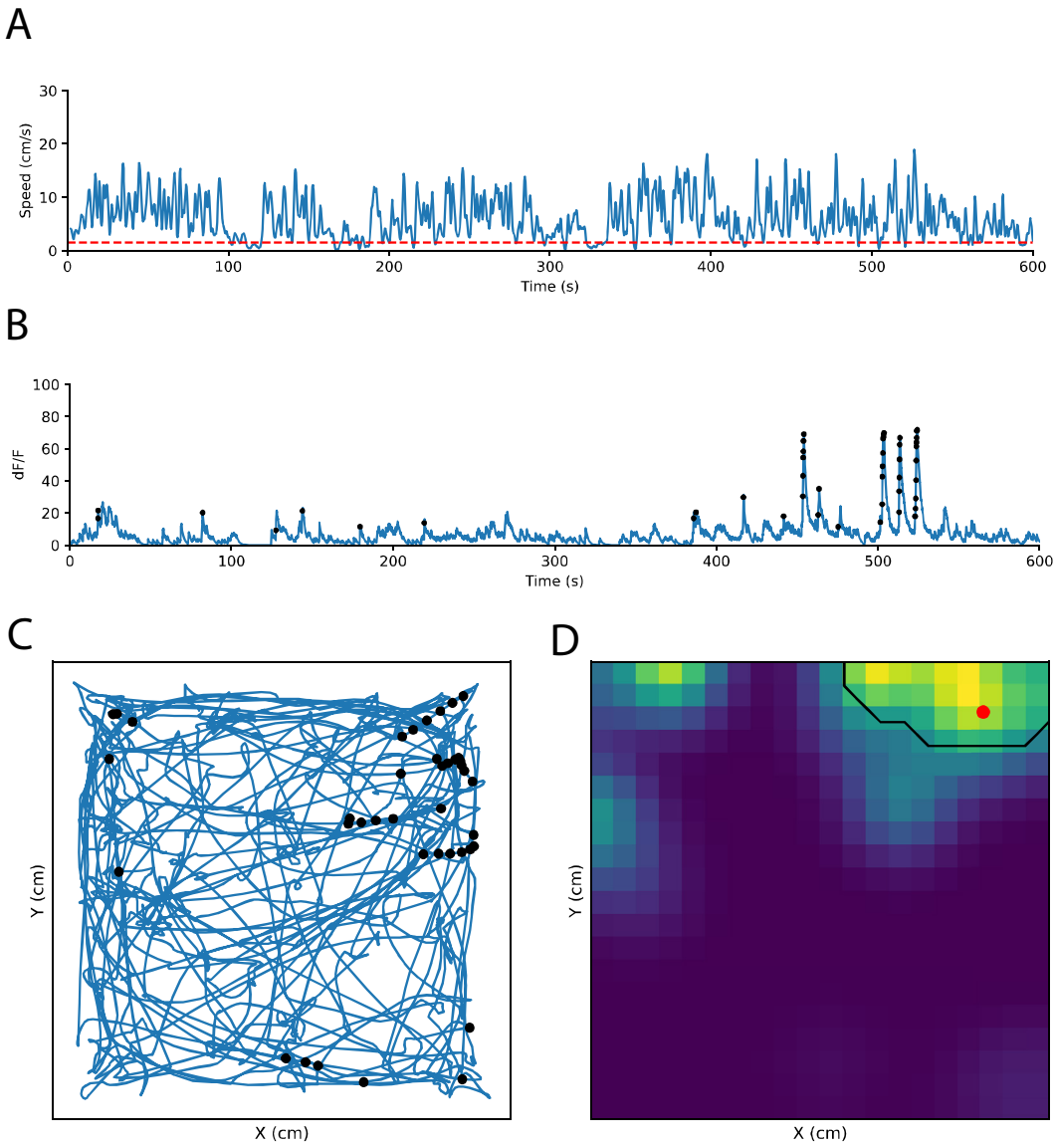


Figure 3.3-5 Example of a place cell in the open field. A) Shows the mouse's speed in the open field over time, with a red dashed line indicating the 1.5 cm/s threshold. B) An example trace (dF/F) for place cells identified in the open field is presented, where red dots represent the deconvolved spikes. C) The trajectory of the mouse in the open field is shown alongside the activity of calcium events. D) Normalized calcium event-rate maps are aligned to the mouse occupancy, with a red dot indicating the peak calcium event rate in the open field and a black contour delineating the place field for the specific place cell.

During the three days of observation, WT neurons showed a greater proportion of place cells than KO neurons (Figure 3.3-6.A), though this difference was only statistically significant for the OFT-day3 (Chi-square test, $\chi^2 = 1.51$, $p = 0.47$). In both the WT and KO groups, the proportion of place cells decreased slightly over time; however, the size of the place fields for place cell neurons remained constant and did not differ between the WT and KO groups (2-way ANOVA: $F(2) = 0.40$, $p < 0.001$,Figure 3.3-6.B).

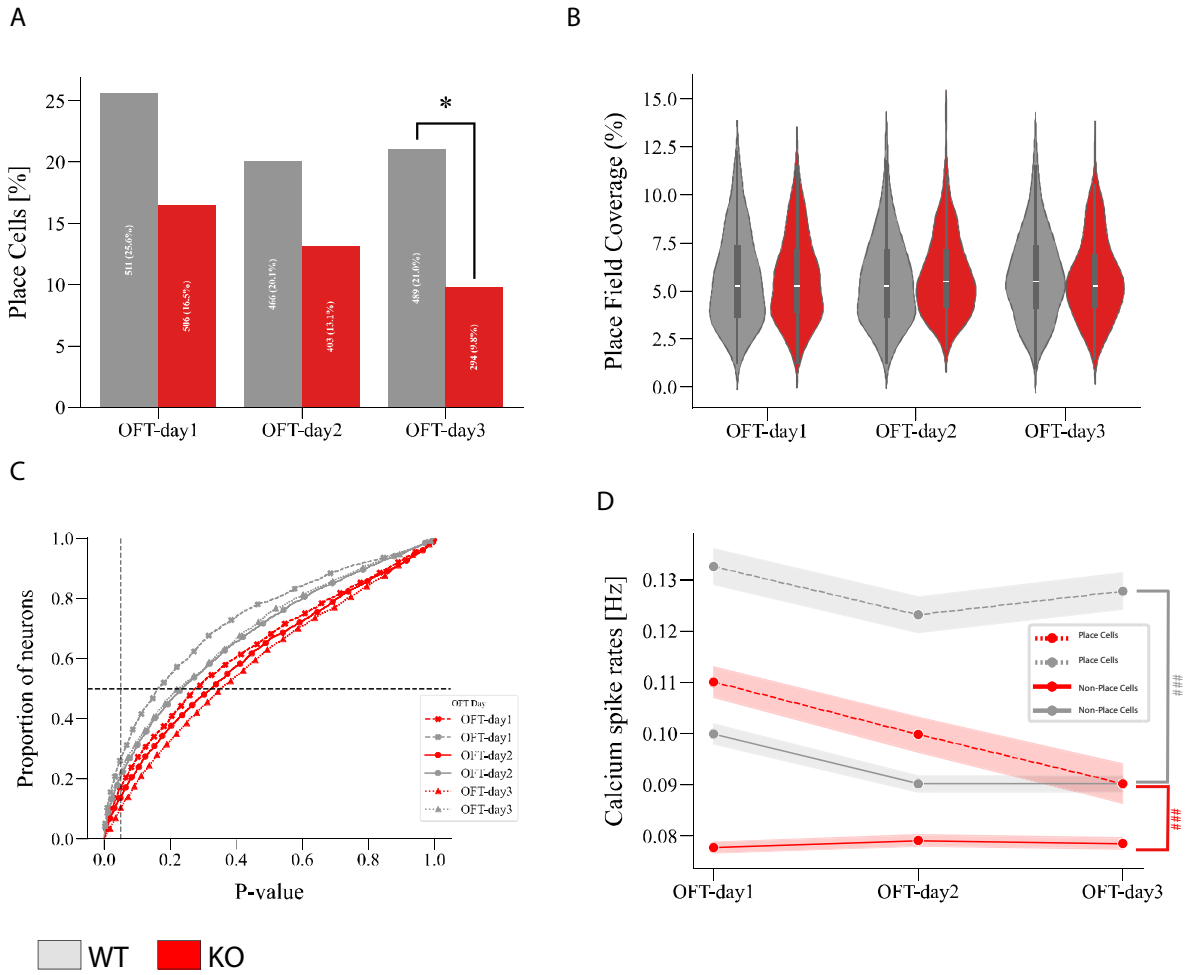


Figure 3.3-6 Place cells during the open field exploration task. A) The proportion of total neurons classified as place cells in each group (Chi-square test, * is p<0.05, Stats-table 7). B) The field size of identified place cells (2-way ANOVA: F(2) = 0.92, p >0.5, Stats-table 8). C) The mutual information p-values distribution for all neurons separated in days and groups, vertical line p-value (0.05), and horizontal dashed line (median). D) The firing rates of place cells compared to non-place cells, with dots representing the group mean and shadows ±SEM. (2-way ANOVA: WT, F(22) = 0.56, p < 0.001; KO, F(2,2) = 10, p < 0.001,Stats-table 9)

Despite the comparable proportion of place cells and place field size between groups, WT neurons displayed higher spatial tuning of place cells, as evidenced by the mutual information (MI) p-values distribution, defined as the fraction of shuffled MI values that exceeded the observed MI(Figure 3.3-6.C). The figures show that the whole distribution of WT p-values is left-shifted in the graph, and at higher p-values, WT distribution is separated more from the KO graphs. This became evident when looking at the median point (horizontal dashed line). Specifically, the median p-values were lower in WT neurons compared to KO neurons across all days: (OFT-day1: WT=0.15, KO=0.2; OFT-day2: WT=0.3, KO=0.35; (OFT-day3: WT=0.25, KO=0.6). These results suggest that while the quantity of place cells is similar between groups, spatial tuning is better preserved in the entire WT group.

The calcium spike rate of place cells was found to be significantly higher than that of other neurons in both WT and KO (2-way ANOVA: WT, $F(2) = 0.56$, $p < 0.001$; KO, $F(2,2) = 10$, $p < 0.001$, Figure 3.3-6D). This difference was consistent across all three days of exploration, indicating that place cells are generally more active than other neurons during open-field exploration.

Not all neurons exhibiting elevated calcium spike rates are classified as place cells; spatial tuning is a crucial criterion for identifying these cells. Specifically, only 15-40% of the neurons in each mouse with calcium spike rates above 0.01 Hz were categorized as place cells. In WT, about 50% of the neurons had calcium spike rates exceeding this threshold, while in KO, approximately 30% of the neurons did.

Only a small fraction of all neurons (10-25%) exhibited place cell properties, and there was no significant difference between WT and KO in their percentage or place field size. In contrast, the tuning and activity rates of WT place cells were higher than KO. What is evident is that place cells tended to have a higher firing rate than non-place cells for both WT and KO.

3.3.4 Reactivation and remapping of place cells

The ongoing discussion about place cells in the hippocampus focuses on their stability. Some studies indicate that place cells in mice and rats can maintain remarkable stability over long periods (Thompson & Best, 1990; Ziv et al., 2013). However, other research has shown that place cells in mice can be unstable over days, particularly when attention to specific landmarks is not required(Jeantet & Cho, 2012; Levy et al., 2021; Muzzio et al., 2009). This instability is exemplified by global remapping, which involves a complete reorganization of place fields when the animal is re-exposed to the same familiar environment (Figure 3.3-8A).

We examined the reactivation and remapping of place cells over three days (OFT-day1-3) in both WT and KO mice to evaluate the stability of spatial representations.

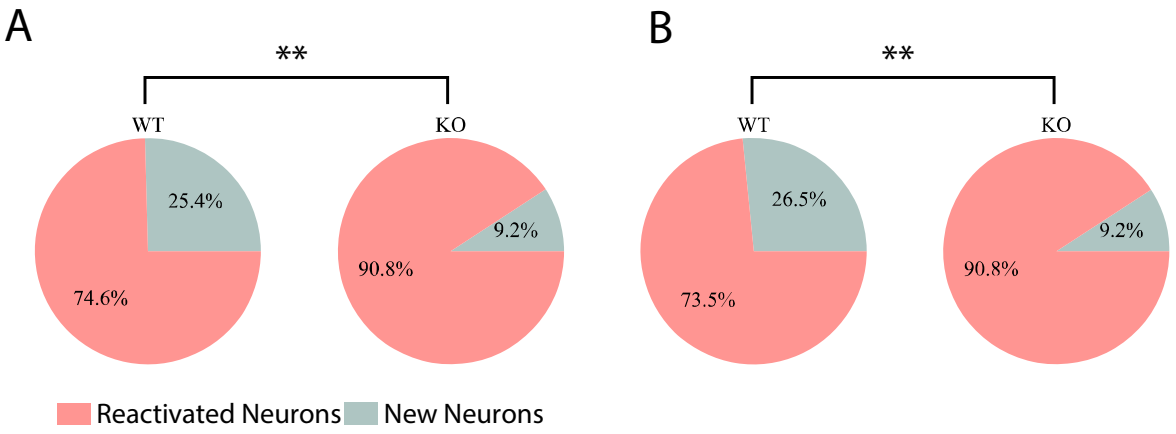


Figure 3.3-7 Proportion of reactivated neurons in OFT-day2 and OFT-day3. A) The proportion of neurons in OFT-day2 that were reactivated from OFT-day1. B) The proportion of neurons in OFT-day3 that were reactivated from OFT-day1 (Chi-square test, ** $p<0.01$)

We found that 74% of the total neurons active on OFT-day1 were reactivated on either OFT-day2 or OFT-day3 in WT. In contrast, the proportion of reactivated neurons in KO was significantly higher, at 90%, indicating a greater overall reactivation of neurons across days in the KO group (Chi-square test, OFT-day2 $\chi^2 = 8.05$, $p < 0.01$; OFT-day3 $\chi^2 = 9.14$, $p < 0.01$, Figure 3.3-7A-B). Focusing specifically on place cells, only 20–24% of the place cells active on OFT-day2 and OFT-day3 were also identified as place cells on OFT-day1. This percentage was similar for WT and KO, suggesting that most place cells were not consistently reactivated across days for both groups (Figure 3.3-8.B,C).

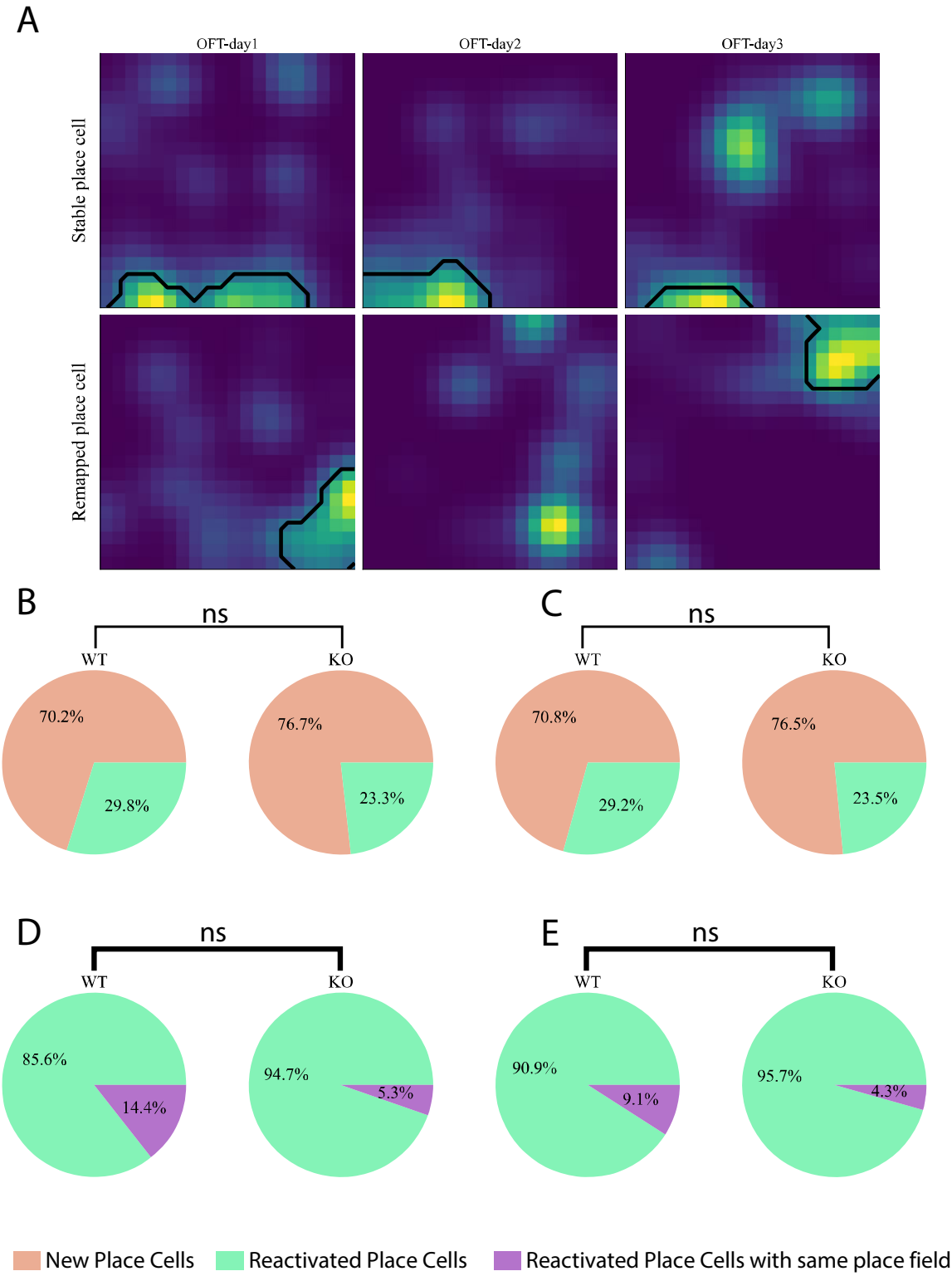


Figure 3.3-8 Place cell remapping in the OFT. A) The upper example illustrates a place cell that retains its properties while maintaining its place field. In contrast, the lower example shows a place cell identified on OFT-day 1, which did not function as a place cell on OFT-day 2. However, it was remapped as a place cell in a different place field on OFT-day 3. B) The proportion of place cells on OFT-day 2 that were reactivated from OFT-day 1. C) The proportion of place cells on OFT-day 3 that were reactivated from OFT-day 1.D) The proportion of reactivated place cells on OFT-day 2 that retained their place field from OFT-day 1. E) The proportion of reactivated place cells on OFT-day 3 that retained their place field from OFT-day 1 (B, C, D, and E Chi-square test, not significant at $p < 0.05$).

Additionally, only 4–15% of the reactivated place cells preserved their original place fields over time for both groups, representing just 3-20 neurons of all neurons (Figure 3.3-8.D,E). This low retention rate indicates significant global remapping of place cells between days for both WT and KO groups.

Overall, while reactivation of neurons was more prominent in KO, both groups exhibited significant remapping of place cells, suggesting a dynamic reorganization of spatial representations over the days.

3.3.5 Summary Open Field Test

Our goal was to determine whether the absence of Arc/Arg3.1 influenced the generation and stability of place cells, while KO mice exhibited a higher overall reactivation rate of neurons compared to WT mice, both groups demonstrated considerable remapping of place cells across days. These findings support existing studies that highlight the instability of place cells over time when strong spatial cues or attention to specific landmarks are lacking (Kentros et al., 2004; Muller & Kubie, 1987). Interestingly, when examining spatial tuning, the percentage of neurons with MI above the shuffled baseline, WT, showed a suggestive stronger ability to form spatial tuning compared to the KO. Additionally, Arc/Arg3.1 KO mice exhibited reduced calcium spike rates compared to WT.

These findings prompt a crucial question: Do KO mice show a reduction in electrical spikes compared to WT, or is this reduction exclusive to calcium spikes? To explore this, we performed *in vivo* local field potential recordings.

3.4 Conserved Electrical Spike Activity in Arc/Arg3.1 KO

We used silicon probes to record local field potentials (LFP) and unit spikes from the dCA1 region of the hippocampus of adult mice. The recordings were performed during urethane-induced sleep. Each recording session lasted between 90 and 120 minutes. Throughout the LFP recordings, we observed multiple REM cycles characterized by the presence of rapid eye movements (REM) and slow wave sleep (SWS) states, respectively. These were characterized by typical rhythms with a high theta/delta power ratio in REM and high delta power (ripple-rich) in the SWS epochs from the time-frequency spectrogram (Figure 3.4-1).

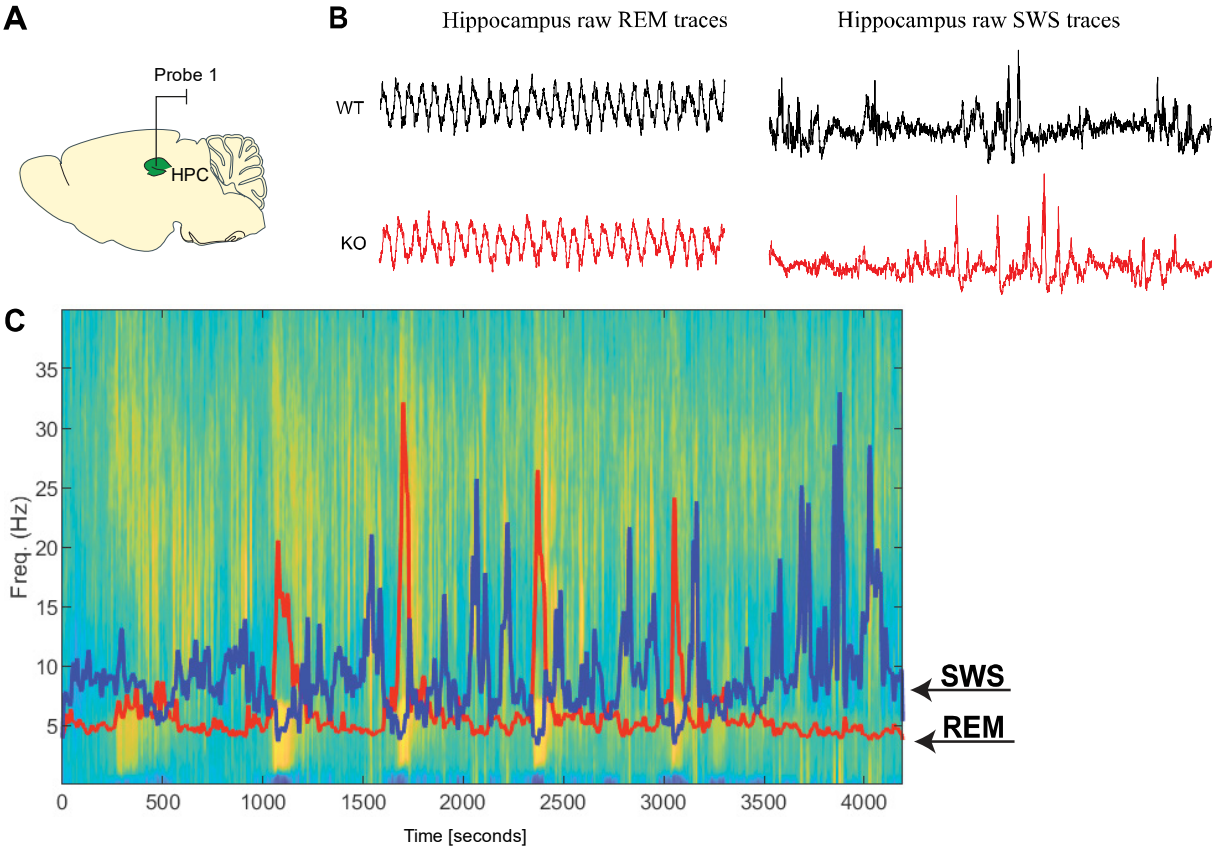


Figure 3.4-1 Local field potential recording in the CA1 A) Schematic of local field potential recording (LFP) B) Exemplary raw traces from hippocampus dCA1 REM-like sleep state and SWS (WT-black, KO red) C) Representative spectrogram from LFP recordings. Low-frequency power (0.2–1.2 Hz), indicative of putative SWS epochs (blue) ; and the theta-to-delta power ratio, a marker of rapid eye movement REM (red)

We conducted detailed spike sorting to investigate the neuronal activity within the dCA1 in WT and KO groups. For this purpose, we employed KLUSTA, a popular open-source software tool designed for automatic spike sorting of multi-channel (< 64 channels) data. The sorted spikes were then curated using the Phy2 GUI. We established strict criteria to isolate clusters, which included ensuring a clear refractory period in the auto-correlograms, minimal overlap in the feature space, and a consistent waveform shape across all the spikes in the clusters.

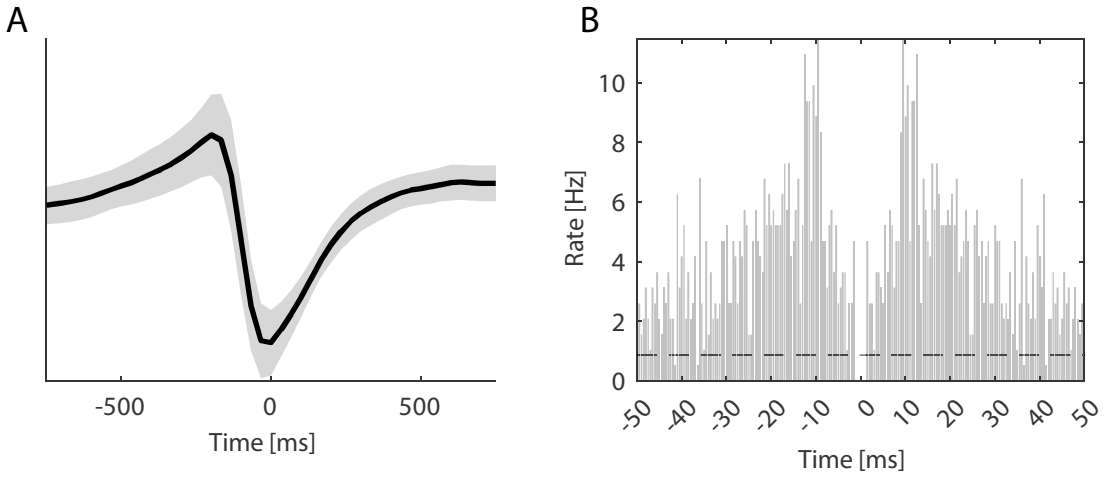


Figure 3.4-2 Example of an isolated neuron. A) The waveform of a well-isolated neuron by KLUSTA. B) The autocorrelogram for A.

Once clusters were validated, they were classified into putative excitatory or inhibitory neurons based on their spike waveform characteristics and firing patterns in CellExplorer. Typically, inhibitory neurons exhibit narrower and faster spike waveforms compared to the broader waveforms of excitatory neurons. Furthermore, excitatory neurons tend to have lower firing rates and less variability in inter-spike intervals compared to their inhibitory counterparts (Barthó et al., 2004). By applying these criteria and using a combination of waveform analysis and firing rate measurements, we were able to confidently classify the majority of neurons in our dataset (Figure **3.4-3**.C-D). A small fraction of neurons around the criteria borders were visually inspected and classified.

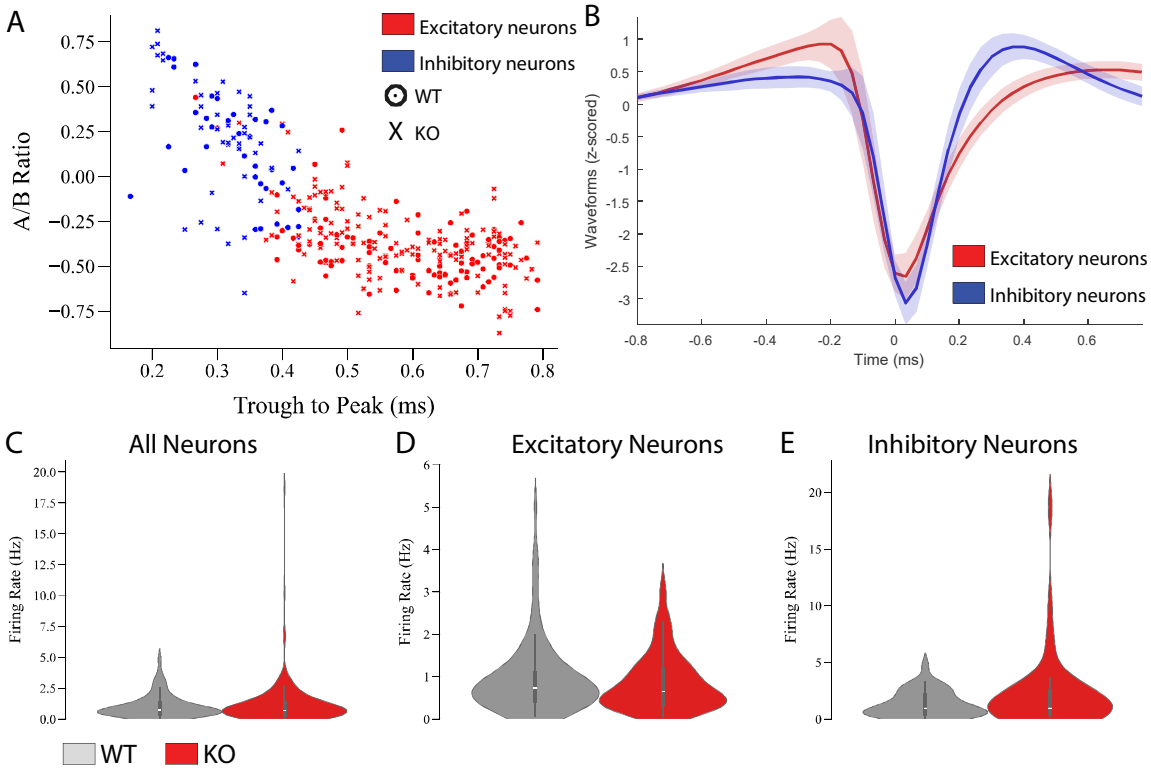


Figure 3.4-3 Firing rate of excitatory and inhibitory neurons. A) Scatter plot of A/B ratio and the trough-to-peak, showing a good separation of excitatory and inhibitory neurons B) Averaged waveform of the excitatory and inhibitory neurons C-E) The firing rates of all neurons (C), as well as those of excitatory(D) and inhibitory neurons (E) respectively (mann whitney non-significant)

This comprehensive approach to spike sorting and classification provided a robust framework for analyzing the firing rate differences between the WT and KO groups, enhancing our understanding of the impact of the lack of Arc/Arg3.1 on neuronal activity in the dCA1. In total, we classified 324 neurons in the dCA1(139 WT and 185 KO), where 242 were excitatory and 82 were inhibitory.

However, we found no notable differences in electrical spikes during urethane-induced sleep between the two groups (Figure 3.4-3.C-E). This finding aligns with earlier data collected from chronically implanted mice running on a circular track (Malkki et al., 2016).

3.5 Neural Activity Dynamics Are Largely Preserved During Fear Memory Acquisition in Arc/Arg3.1 KO

In this chapter, we expand our investigation to include aversive memory tasks, where a strong episodic memory is established through fear conditioning (O'Brien & Sutherland, 2007). Fear memory paradigms robustly activate neural circuits and enhance levels of plasticity to encode and consolidate the emotional and contextual components of the experience (Bliss & Lømo,

1973). The hippocampus, with its ability to encode contextual information and undergo robust synaptic plasticity(Liu et al., 2014), is believed to support the initial phase of contextual fear memory, however, its role in maintaining long-term synaptic plasticity is highly debated. Arc/Arg3.1 plays a crucial role in facilitating long-term synaptic changes within the hippocampal networks that support fear memory (Gao et al., 2018; Plath et al., 2006). However, an unanswered question remains: How does the lack of Arc/Arg3.1 disrupt these fear memory engrams?

In this part, we aimed to address this question by conducting longitudinal calcium imaging using head-mounted miniscopes in both WT and Arc/Arg3.1 KO mice. The mice underwent a contextual fear conditioning (CFC) paradigm, which included a conditioning phase on Day 1, followed by a first probe test conducted 7 days after conditioning and a second probe test 21 days after conditioning. At least one hour after each probe test, the mice were also exposed to an alternative novel environment to assess memory specificity (Figure 3.5-1)

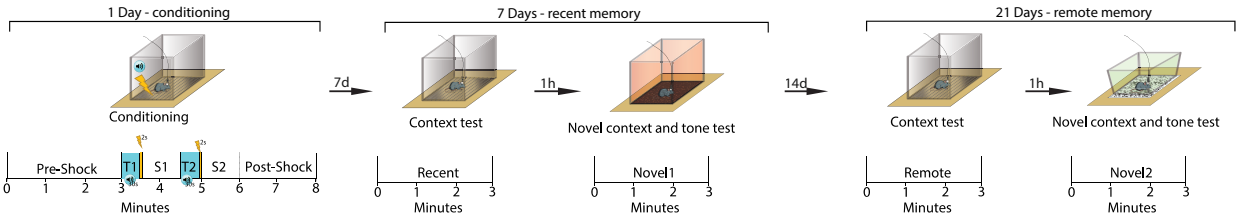


Figure 3.5-1 Contextual fear conditioning paradigm

3.5.1 Intact Behavioral Response During Contextual Fear Memory Acquisition in Arc/Arg3.1 KO

For the analysis of the conditioning session, we first focused on the freezing behavior and neuronal activity to assess how the absence of Arc/Arg3.1 may affect fear memory acquisition. The conditioning session was divided into six episodes (Figure 3.5-2.A). In the first 3-minute episode, the novel exposure to the context serves as the pre-shock, it is followed by a 28-seconds episode of tone display (Tone1, cyan), commencing with 2 seconds of the tone paired with an electrical foot shock (orange stripe, not considered a separate episode). Next is a 1-minute episode (S1), followed by a second 28(30)-second tone-shock pairing (Tone2). The session concludes with a final 3-minute episode (post-shock), of which the first minute was analyzed separately (S2) for comparisons with S1.

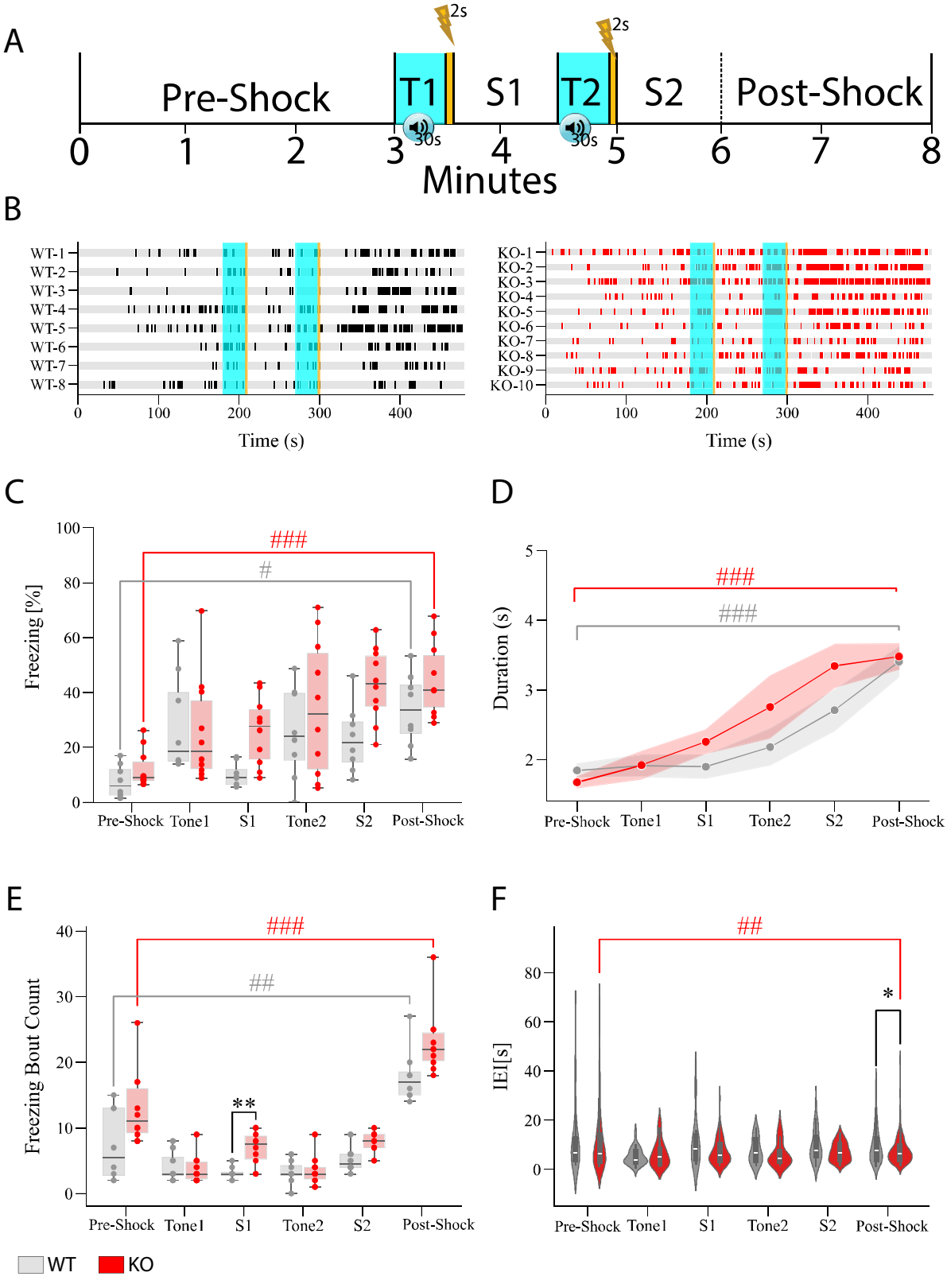


Figure 3.5-2 CFC: Behavioral response to fear conditioning. A) Illustration of the conditioning session. B) Freezing bouts during the conditioning session for all mice (WT, n=8; KO, n=10), WT is shown on the left and KO on the right. Tone presentation periods are highlighted in cyan, while shock periods are marked in orange. Grey indicates mobility periods, and red/black denote freeze bouts. C) Average percentage of freezing observed during fear acquisition (Mixed-effect ANOVA: Genotype × episode interaction, $F(5,80) = 0.08$, $p > 0.05$; Genotype effect, $F(1,16) = 4.02$, $p > 0.05$; episode effect, $F(5,80) = 15.67$, $p <$

0.001; WT, n=8; KO, n=10,Stats-table 10). D) Duration of each freezing bout (2-way ANOVA: Genotype × episode: $F(5) = 0.64$, $p > 0.05$, Genotype effect, $F(1) = 1.06$, $p > 0.05$; episode effect, $F(5) = 20.9$, $p < 0.001$,Stats-table 11). E) Freezing bout count for each mouse in the different episodes(paired two-sample t-tests with the Sidak correction) F) Inter event interval between freezing bouts for each episode (2-way ANOVA: Genotype × episode: $F(5) = 0.66$, $p > 0.05$, Genotype effect, $F(1) = 9.52$, $p < 0.001$; episode effect, $F(5) = 7.28$, $p < 0.001$, Stats-table 13)

An overall comparison of the total freezing times, revealed no significant differences between WT (n=8) and KO (n=10) mice (Mixed-effect ANOVA: Genotype × Episode interaction, $F(5,80) = 1.84$, $p > 0.05$, Figure 3.5-2.C), indicating that both groups displayed comparable levels of freezing across episodes. However, freezing behavior varied across episodes, primarily reflecting different responses to tone and shock stimuli (episode effect, $F(5,80) = 15.67$, $p < 0.001$, Figure 3.5-2 C). Importantly, for each group, post-shock freezing percentage was significantly higher than the pre-shock, indicating a shared response to the cumulative experience of the conditioning session and successful acquisition of the context/conditioning association (2ST-Sidak,pre- *vs* post-shock; WT: $d = -2.58$, $p < 0.01$; KO: $d = -3.09$, $p < 0.001$). To better capture the dynamics of the freezing responses of each group, we analyzed the duration, number of freezing bouts, and the intervals between them (Figure 3.5-2.D-F).

There is a noticeable increase in the duration of freezing bouts during the conditioning process. This increase was observed in both groups, with both demonstrating a notable rise in the length of freezing bouts (episode effect, $F(5) = 20.9$, $p < 0.001$, Figure 3.5-2.D). This is particularly clear when comparing the pre- and post-shock episodes (2ST-Sidak, pre- *vs* post-shock; WT: $d = -0.7$, $p < 0.001$; KO: $d = -0.77$, $p < 0.001$). This increase occurred abruptly in the post-shock period for WT mice, while KO mice exhibited a gradual increase across all episodes (Stats-table 11).

The number of freezing bouts was similar between WT and KO mice throughout all episodes, except during Session 1 (S1), where KO mice displayed a significantly higher number of bouts (2ST-Sidak,$d = -1.47$, $p < 0.05$). Within each group, both WT and KO mice demonstrated a significant increase in the number of freezing bouts in the post-shock episode compared to the pre-shock episode (2ST-Sidak, WT: $d = -1.79$, $p < 0.01$; KO: $d = -2.45$, $p < 0.001$).

Lastly, we considered the inter-event interval (IEI) of freezing bouts between WT and KO mice in each episode (Figure 3.5-2.F). During the pre-shock episode, both groups exhibited similar IEIs. In the post-shock episode, KO mice exhibited a significantly shorter IEI compared to WT mice (d=0.35, $p<0.05$).

In summary, even though WT and KO mice exhibited slightly different freezing patterns during the conditioning session, both groups showed similar learning of the context-shock association, as evidenced by the increased freezing behavior during the post-shock episode compared to the pre-shock episode, which was also reported in previous studies (Gao et al., 2018; Plath et al., 2006; Ploski et al., 2008).

3.5.2 Episode-Specific Neural Activity Modulation During Fear Memory Acquisition Is Mostly Intact in Arc/Arg3.1 KO

Calcium imaging was used to observe the activity of neuronal populations in the dCA1 region while acquiring contextual fear memory. This allowed us to identify and track individual neurons across various episodes of the conditioning session. We recorded 1560 neurons from 8 WT mice and 2179 neurons from 10 KO mice.

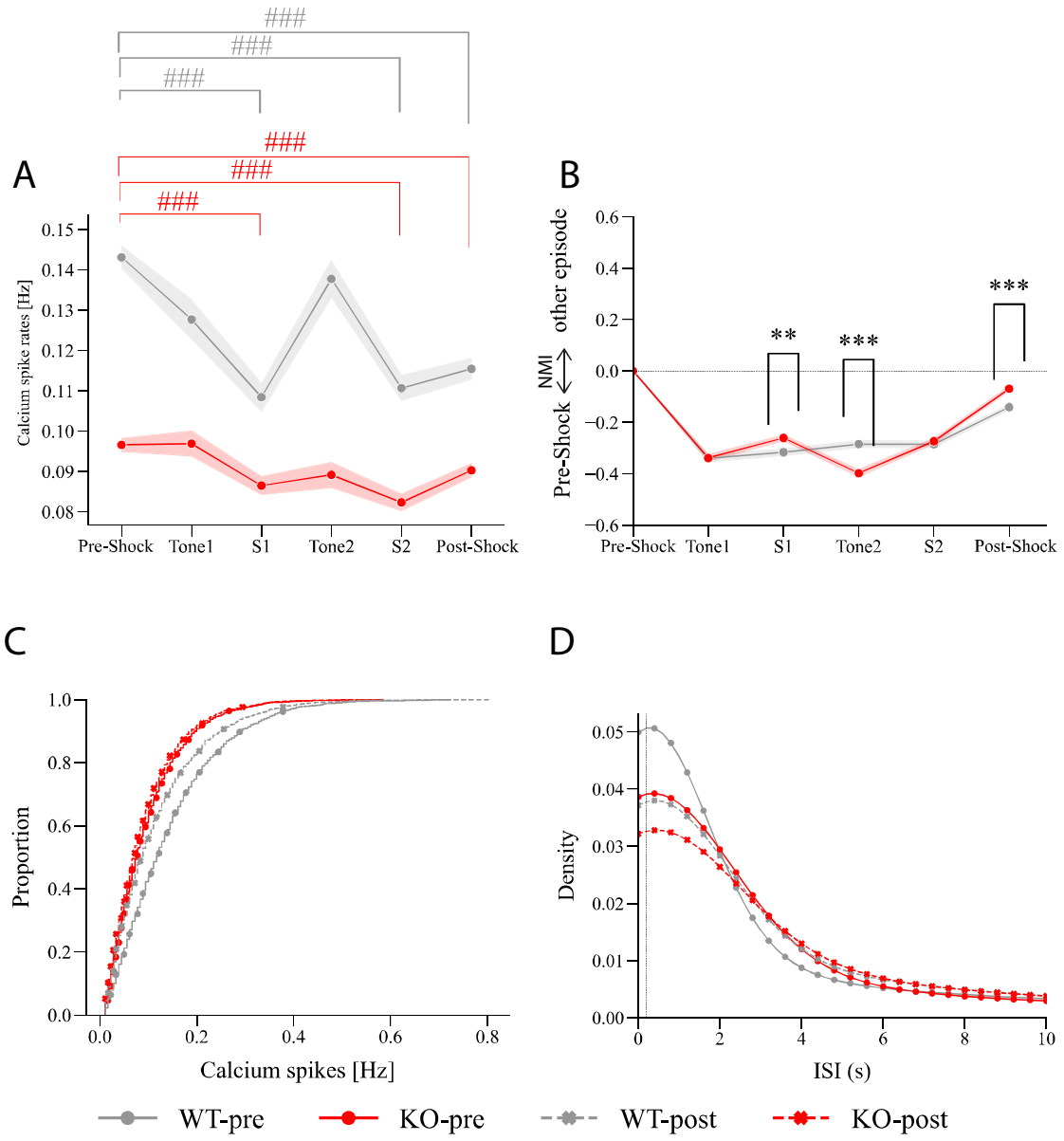


Figure 3.5-3 Calcium spike rates during fear acquisition. A) Rate of calcium spikes throughout conditioning episodes((Mixed-effect ANOVA: Genotype × episode interaction, $F(5,16895) = 10.35$, $p < 0.001$; Genotype effect, $F(1,3379) = 146.73$, $p < 0.001$; episode effect, $F(5,16895) = 24.08$, $p < 0.001$, Stats-table 14). B) Neural Modulation Index (NMI) of calcium spikes during the conditioning session, relative to pre-shock. The horizontal dashed line at 0 indicates no modulation (Mixed-effects ANOVA Genotype × Episode interaction $F(4,13516) = 20.88$, $p < 0.001$; Stats-table 15). C) Cumulative distribution of calcium spike during the pre- and post-shock conditions. D) Inter-spike interval (ISI) density of calcium spikes in the dCA1 region of the hippocampus, comparing the pre- and post-shock conditions. The vertical dashed line at 0.2 s indicates a reference threshold.

We observed that during the pre-shock episode, calcium spike rates were significantly higher in WT neurons compared to KO neurons (2ST-Sidak; pre-shock $d = 0.51$, $p < 0.001$, Figure 3.5-3A). This difference in spike activity between genotypes remains consistent across the subsequent conditioning episodes (Stats-table 14). Interestingly, calcium spike rates in both WT and KO neurons, decreased from the pre- to the post-shock episode (paired 2ST-Sidak; pre- *vs* post-shock, WT: $d = 0.32$, $p < 0.001$; KO: $d = 0.15$, $p < 0.001$)

The pronounced imbalance in calcium spike rates between WT and KO neurons does not allow a direct comparison of the rate modulation during the conditioning episodes between the groups. To account for this, we analyzed the modulation of spike activity in individual neurons relative to the pre-shock episode using a neuronal modulation index (NMI) instead (Figure 3.5-3B). The NMI is defined as $(R_X-R_Y)/(R_X+R_Y)$, where R_X represents calcium spike activity in a given episode and R_Y represents activity during the pre-shock. This approach focuses on relative changes in each neuron's activity compared to the pre-shock, as the absolute difference would be inherently biased by the initial difference between WT and KO neurons. A negative NMI indicates reduced neuronal activity relative to the pre-shock episode, while a positive index reflects increased activity. We observed that relative to the pre-shock episode, both WT and KO neurons exhibited a negative NMI in the post-shock episode, indicating an overall reduction in neuronal activity after the fear conditioning.

Additionally, we observed significant differences in the NMI between WT and KO mice during the S1, Tone2, and post-shock episodes (Figure 3.5-3C). In the S1 episode, WT neurons showed a larger negative NMI compared to KO neurons (2ST-Sidak, d = -0.11, $p < 0.01$). In the Tone2 episode, WT neurons exhibited a lower negative NMI compared to KO neurons (2ST-Sidak; d = 0.2, $p < 0.001$). No significant differences were observed in the NMI between WT and KO neurons during the Tone1 and S2 episodes. Interestingly, the NMI of WT neurons was largest negative during Tone1 and steadily increased throughout the conditioning session, while KO neurons showed more variable NMI indices during the session, with the biggest dip during Tone2. The NMI in the post-shock episode was lowest in WT neurons (2ST-Sidak; d = -0.18, $p < 0.001$), which indicates that WT mice had a higher reduction in calcium spike activity compared to KO mice at the end of the conditioning session.

The overall reduction in calcium spike activity in WT and KO neurons during the conditioning session is further supported by the cumulative distribution of calcium spike rates per neuron, between the pre- and post-shock episodes (Figure 3.5-3C). The cumulative distribution of calcium spikes in WT and KO neurons shifted to the left from the pre-shock compared to the post-shock episode, indicating a decrease in calcium spike activity in both genotypes. This shift was more pronounced in WT neurons, as evidenced by the stronger leftward shift of the WT curve compared to the KO curve.

Finally, we analyzed the inter-spike interval (ISI) between calcium spikes as a measure of instantaneous firing rates, in contrast to the previously presented mean firing rates. Such analysis could

reveal modulations in activity patterns, for example, a propensity for "burst-like" spiking. The density curves of ISI of WT and KO neurons during pre- and post-shock episodes are presented in Figure 3.5-3D. As described in the Methods section, the calcium images were down-sampled to 10Hz, effectively setting the shortest measurable interval between 2 subsequent calcium events to 0.2s. The ISI density curve of WT neurons during the pre-shock was higher than the corresponding KO ISI for intervals < 2s, indicating that WT neurons tended to generate calcium spikes within shorter intervals compared to KO neurons. During the post-shock episode, all ISI density curves were lower compared to pre-shock, reflecting a strong silencing of dCA1 neurons. Interestingly, in WT neurons, the ISI decreased strongly for short intervals but increased at longer ones, suggesting that the calcium-spiking pattern shifted from high ("burst") to low frequencies. KO neurons exhibited primarily a decrease of the shorter ISIs, reflecting a more selective silencing of high-frequency calcium spikes.

In summary: WT neurons exhibited significantly higher calcium spike rates compared to KO neurons during the pre-shock episode, with this difference persisting across conditioning episodes. Both WT and KO neurons showed a reduction in calcium spike activity from the pre-shock to the post-shock episode. The NMI revealed that WT neurons had a higher reduction in activity during the post-shock episode compared to KO neurons. Additionally, the ISI analysis indicated that WT neurons had shorter intervals between calcium spikes during the pre-shock episode, which shifted to longer intervals in the post-shock episode, suggesting a change from high to low-frequency spiking patterns.

3.5.3 Contextual Fear Conditioning Significantly Suppresses Neuronal Activity

As demonstrated in the previous section (3.5.23.5.2), the neuronal populations in both WT and KO mice exhibited an overall decrease in calcium activity following the context-shock association. Nonetheless, it remains unclear whether this decrease applied to all neurons or whether subpopulations of neurons were differentially affected. To further explore these possibilities, we analyzed the proportions of inhibited and excited neurons during the conditioning session and assessed whether the absence of Arc/Arg3.1 influences this distribution.

Neurons were classified as inhibited or excited based on their NMI between pre- vs post-shock, where a negative index indicates inhibition, and a positive index indicates excitation.

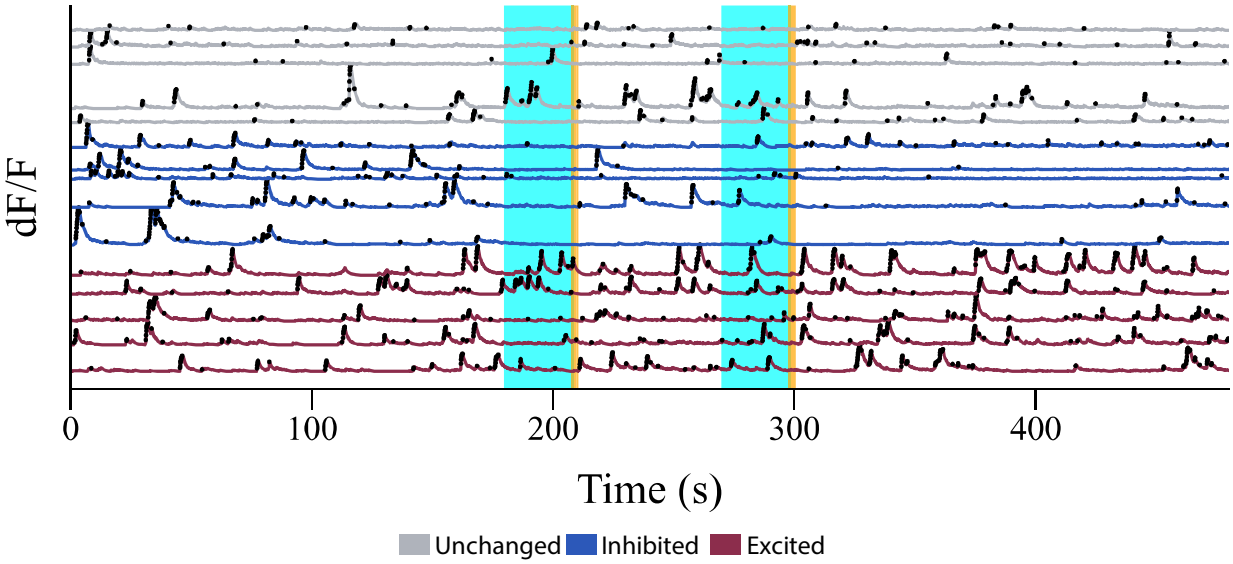


Figure 3.5-4 dF/F trace of inhibited or excited neurons post-conditioning. Example dF/F trace from neurons exhibiting different modulation durations during the conditioning session. Black dots on the trace indicate deconvolved calcium spikes. Tone presentation periods are highlighted in cyan, while shock periods are marked in orange

Figure 3.5-4 shows examples of neurons exhibiting excitation or inhibition relative to their pre-shock. For WT and KO mice, the proportion of inhibited neurons was notably higher than that of excited neurons (inhibited: WT = 67%, KO = 60.4%; excited: WT = 29.6%, KO = 36.1%, Figure 3.5-5.A). A small fraction of neurons remained unaffected by the conditioning (WT = 3.5%, KO = 3.5%). Consequently, no significant difference was observed in the proportion of inhibited vs excited neurons between WT and KO mice (Chi-square test, $\chi^2(2) = 1$, $p > 0.05$).

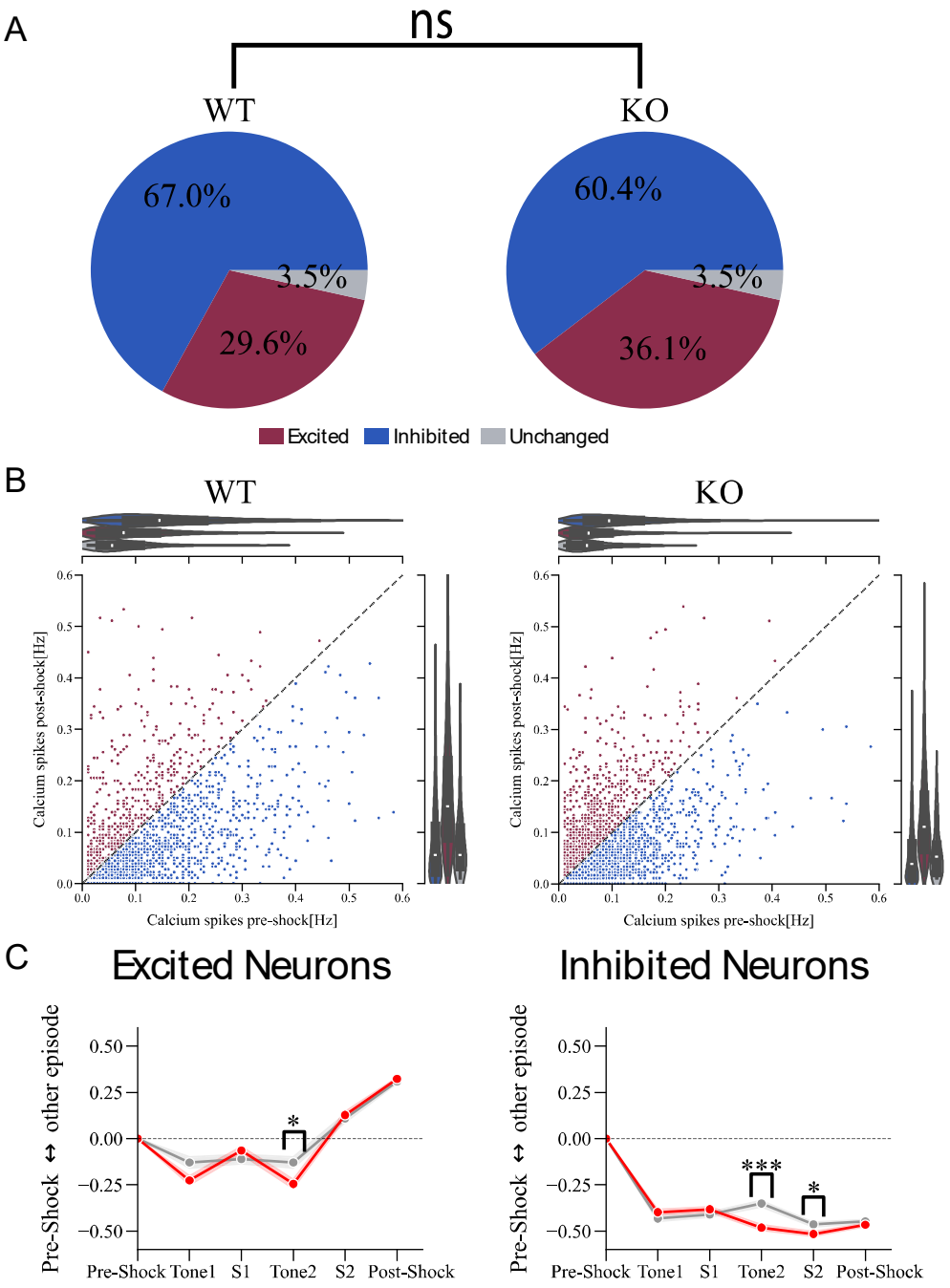


Figure 3.5-5 Calcium spike rate of excited and inhibited neurons post-conditioning. A) Proportion of neurons classified as excited or inhibited following the shock (Chi-square test, $\chi^2(2)=1$, $p > 0.05$). B) Calcium spike activity during the pre- and post-Shock periods, categorized as either excited or inhibited. C) Neuronal Discrimination Index for excited neurons (left) (Mixed-effects ANOVA Genotype × Episode interaction $F(4,4984) = 5.77$, $p < 0.001$; Stats-table 16) and inhibited neurons (right?) (Mixed-effects ANOVA Genotype × Episode interaction $F(4,8004) = 14.29$, $p < 0.001$; Stats-table 17).

We first asked whether the magnitude and direction of the activity modulation post-shock were related to the neurons' pre-shock activity rates. The data plotted in (Figure 3.5-5.B) shows that in both WT and KO mice, post-shock inhibited neurons typically had high pre-shock calcium spike rates. In contrast, post-shock excited neurons had generally low pre-shock calcium spike rates.

This pattern indicates that neurons with elevated activity prior to the shock were more likely to be inhibited afterwards, while those with lower pre-shock activity tended to become excited.

This observation was further supported by the NMI of calcium spikes in both excited and inhibited neurons (Figure 3.5-5.C). Notably, regardless of a neuron's classification as either excited or inhibited, the NMI decreased during the Tone1 episode compared to the pre-shock episode. However, excited neurons displayed a smaller negative NMI than inhibited neurons during the Tone1 episode. After the Tone1 episode, the NMI of excited neurons increased, while the NMI of inhibited neurons remained relatively unchanged. During the S2 episode, the excited neurons crossed the baseline and exhibited a positive NMI. In general, both genotypes exhibited a similar modulation pattern for both types of neurons during the conditioning phase.

However, an exception was observed during the Tone2 episode, where the NMI for both excited and inhibited neurons in WT neurons was significantly higher than that of KO (2ST-Sidak, excited neurons $d = 0.17$, $p < 0.01$; inhibited neurons $d = 0.27$, $p < 0.001$).

In summary, both genotypes showed that most neurons were inhibited after the shock, with 60–67% of neurons exhibiting this inhibition compared to 29–36% of neurons that were excited. Notably, all neurons demonstrated decreased calcium spike activity during the Tone1 episode. It was only during the S2 episode that the NMI for excited neurons surpassed the baseline and showed a positive NMI, while the NMI for inhibited neurons remained negative throughout the conditioning and afterwards. Additionally, the modulation indices for excited and inhibited neurons were similar between the WT and KO mice. This suggests that the absence of Arc/Arg3.1 does not significantly impact the calcium activity modulation of neurons in the dCA1 during the conditioning session.

3.5.4 Differential Neuronal Responses to Shock and Tone Stimuli

Tone and shock are auditory and somatosensory cues that are conveyed to the hippocampus mainly through the amygdala and the MEC and constitute features of the context in which they are presented (Phillips & LeDoux, 1992; Sun et al., 2024). As such, they are likely to be represented by the activity of dCA1 neurons during the conditioning episodes. This representation might specifically change following fear conditioning and, in theory, could contribute to memory engrams and memory consolidation. Here, we aimed to examine the responses of dCA1 neurons to tone and foot shock and assess whether the conditioning episodes modulate these

neurons. Tone neurons were identified as neurons with significantly higher calcium spike rates during the first tone representation compared with the rest of the pre-shock episode (see Methods for details), we omitted the second tone representation (Tone2), as it could already be associated with the shock. Shock neurons were detected from their significantly enhanced response to the shock (S1 and S2), compared with the rest of the complete conditioning episode (including pre-shock, Tone1, Tone2, and post-shock). We also extended the two-second shock duration by an extra ten-second window to capture any lingering calcium signals or delayed responses to the shock.

For defining neurons that were significantly responsive to shocks or tones (Figure 3.5-6.A), calcium spikes were circularly shuffled in time for individual neurons (1000 iterations), and shock or tone rates were re-calculated from those behavioral time periods to generate a null distribution of shock or tone calcium spikes rates for each neuron. A neuron was considered a shock-or tone-neuron if its calcium spike rate during those periods exceeded the 95th percentile of the null distribution.

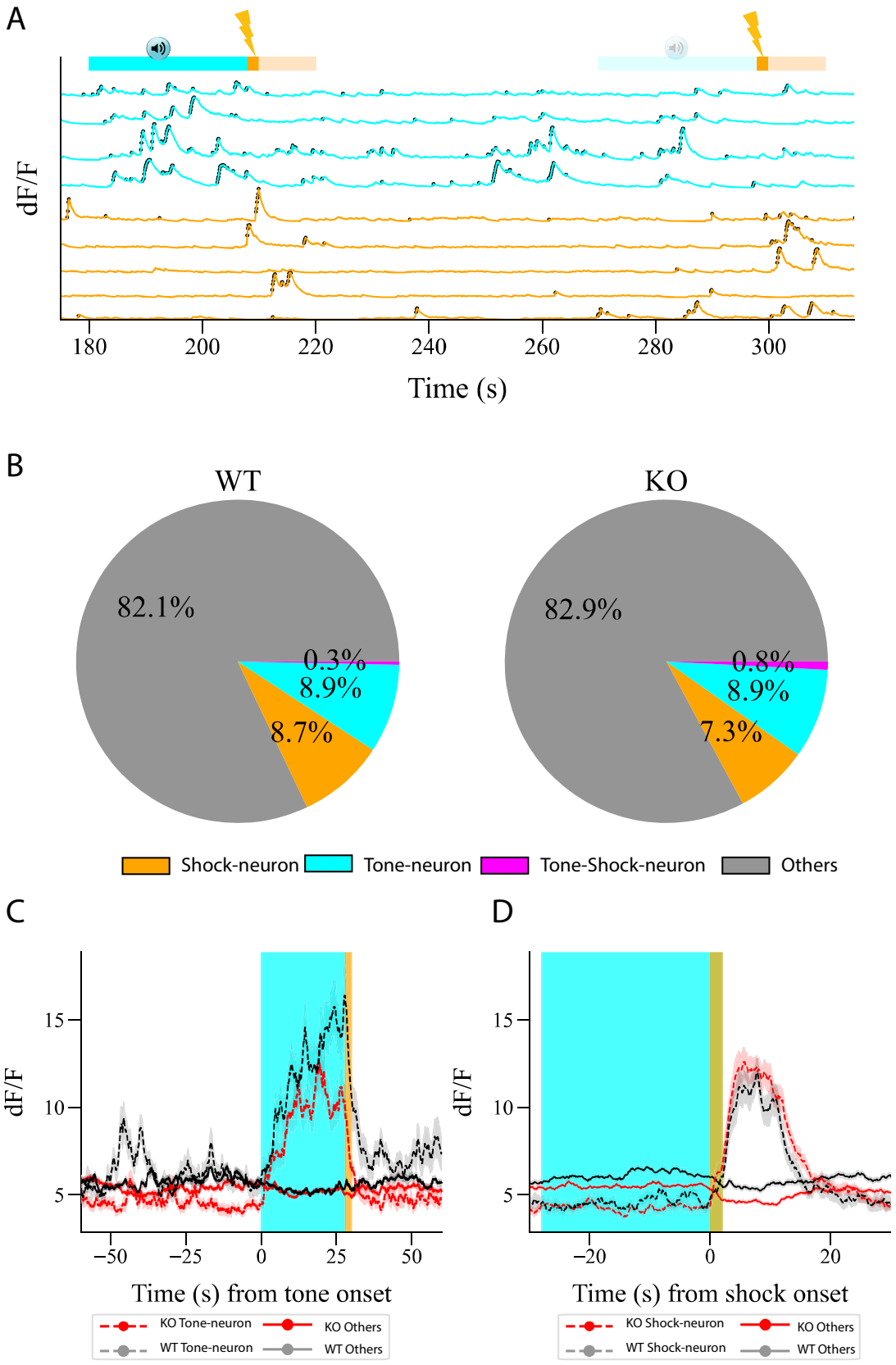


Figure 3.5-6 Shock-and tone-neurons. A) This example trace illustrates tone and shock-neurons. Note that the transparent tone (cyan) was not utilized to identify tone-neurons. The shaded orange (shock) represents an additional 10 seconds following the 2-second shock. B) The proportion of neurons responding to either tone, shock, or neither (Chi-square test, $\chi^2(3) = 0.34$, $p > 0.05$). C) Population dF/F of tone-neurons in comparison to other neurons. D) A similar comparison for shock-neurons.

After identifying neurons with significant responses to tone, shock (Figure 3.5-6.A), or both stimuli, we quantified their percentage in the total neuronal population of WT and KO (Figure 3.5-6.B). In both genotypes, the majority of neurons did not show significant responses to any of the stimuli. Specifically, 82.1% of WT neurons and 82.9% of KO neurons were non-responsive. A small percentage of neurons did respond to foot tone (WT: 8.9%, KO: 8.9%) or shock (WT: 8.7%, KO: 7.3%). An even smaller fraction of neurons responded to both stimuli (WT: 0.3%, KO: 0.8%). No significant differences were found between WT and KO mice in the proportions of neurons that responded to foot shock, tone, or neither stimulus (Chi-square test**,** $\chi^2(3) = 0.34$, $p = 0.95$). Calcium traces of either tone or shock neurons were averaged within genotypes (Figure 3.5-6.C), revealing different response patterns evoked by each stimulus. Tone neurons exhibited a gradual increase in calcium activity during the tone, followed by an immediate decrease once the tone ended. In contrast, shock neurons exhibited a gradual increase in calcium activity during the shock, peaking 5-12 seconds after the shock, before decreasing to baseline levels at 17 seconds after the shock.

As we have shown in section (3.5.3), the shock stimuli induced a widespread inhibition of calcium activity in most dCA1 neurons which persisted throughout the post-shock episode. We next asked whether the activity of Tone- and Shock neurons was differentially modulated pre- to post-shock. We analyzed the proportions of tone- and shock-neurons that were either inhibited or excited post-shock (Figure 3.5-7)

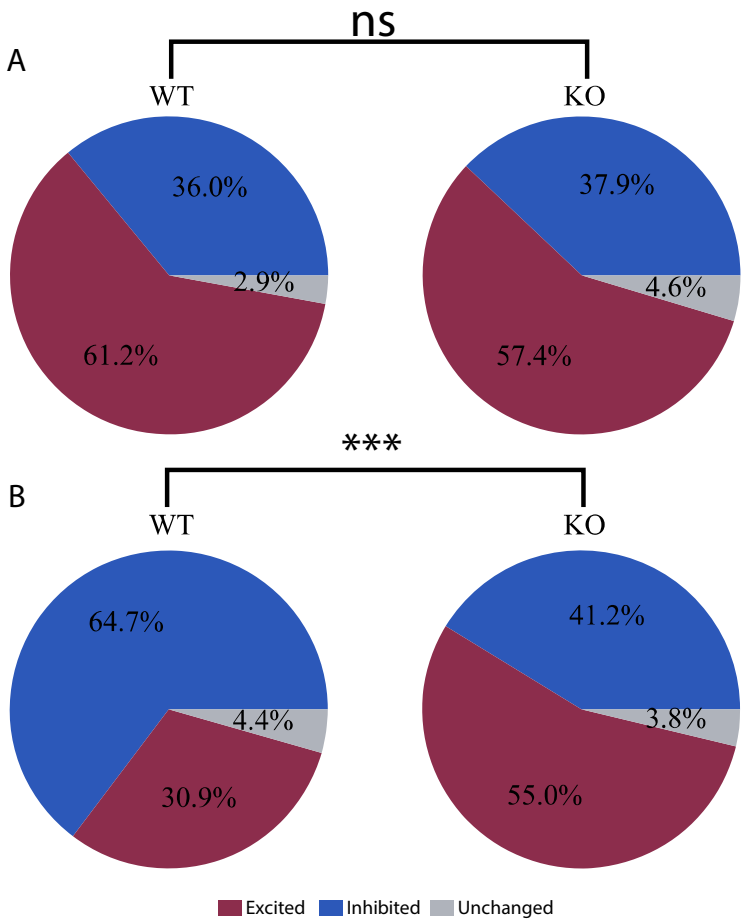


Figure 3.5-7 The proportion of inhibited versus excited tone- and shock-neurons. A) Tone-neurons (Chi-square test, $\chi^2 = 0.45$, $p > 0.05$). B) Shock-neurons (Chi-square test, $\chi^2 = 14.56$, $p < 0.001$).

In both WT and KO mice, the majority of Tone neurons responding were excited post-shock (WT: 61.2%, KO: 57.4%), while a third was inhibited (WT: 36%, KO:37.9%). There was no significant difference in the proportions of excited and inhibited tone-neurons between WT and KO mice (Chi-square test, $\chi^2(2) = 0.45$, $p > 0.05$).

In contrast, the proportions of inhibited and excited shock-neurons differed significantly between WT and KO mice (Chi-square test, $\chi^2(2) = 14.56$, $p < 0.001$). In WT mice, 64.7% of shock-neurons were inhibited, whereas only 41.2% of these neurons were inhibited in KO mice. Additionally, in WT mice, only 30.9% of shock-neurons exhibited excitation, compared to 55.0% in KO mice.

We identified dCA1 neurons with a preferred response to tone and foot shock sensory stimuli and analyzed their activity patterns during the conditioning session. We found that only a minority of dCA1 neurons displayed a sensory preference (18%) with roughly ~9% Tone and ~8% Shock, with a very small fraction responding to both (<1%). Previous studies have shown similar

findings, with one study reporting 11% of neurons responding to shock and 8% to tone(Zhou et al., 2020) and another study reporting 15% of neurons responding to shock (Mocle et al., 2024).

Response patterns to both stimuli were similar between WT and KO neurons, suggesting that sensory encoding in dCA1 is not grossly affected by loss of Arc/Arg3.1. Interestingly, the majority of tone-neurons were excited post-shock in both WT and KO mice, suggesting that their activity is modulated differently compared to the overall dCA1 neuron activity, potentially reflecting distinct modulation for these neurons. Furthermore, the conditioning modulated the activity of WT and KO Shock neurons differently. While most Shock neurons were inhibited in WT mice, they were excited in KO mice. This suggests that the absence of Arc/Arg3.1 may influence how neurons respond to foot shocks, resulting in excitation rather than inhibition in the post-shock period. Tone neurons likely play a role in auditory processing and may obtain inputs from auditory regions, while shock neurons are associated with pain-related stimuli and may derive inputs from pain pathways. The variation in modulation seen in KO mice suggests that Arc/Arg3.1 is vital for regulating the neural circuits involved in pain processing and may result in a changed neural response to foot shocks, despite similar freezing behavior as observed in the flinch test(Yang, 2024).

3.5.5 Impact of Shock on Behavior-Specific Neuronal Population Dynamics

Contextual fear memory tests build upon the innate behaviors of rodents in novel and unsafe environments. In neutral novel environments, rodents typically display heightened exploration and mobility with only short pauses for risk assessment. In contrast, in environments recognized by rodents as unsafe, they explore little and freeze for long time stretches. These behaviors are controlled by complex brain networks that encode for space, context, novelty, valence, and decision making (Izquierdo et al., 2016). The hippocampus encodes spatial and contextual information and receives direct input from cortical regions involved in decision making (i.e. anterior cingulate cortex) and subcortical regions signaling emotional states and fear (hypothalamus and amygdala, respectively). Thus, while the hippocampus does not directly control movement or freezing, it contains neurons whose activity is closely associated with these behaviors. To identify such neurons and investigate the relationship between their neuronal activity and behavior, we searched for neurons with distinct responses to freezing bouts and mobility during both pre-shock and post-shock episodes.

Freeze-neurons were defined as neurons exhibiting a significant increase in calcium spike activity during freezing bouts, while mobility-neurons were defined as neurons exhibiting a significant increase in calcium spike activity during mobility periods (Figure 3.5-8.A). Note that transition periods from freeze to mobility and vice versa were not included. For example, mobility start was defined as one second after freeze bouts stop and ends one second before freeze bouts start (Figure 3.5-2.A).

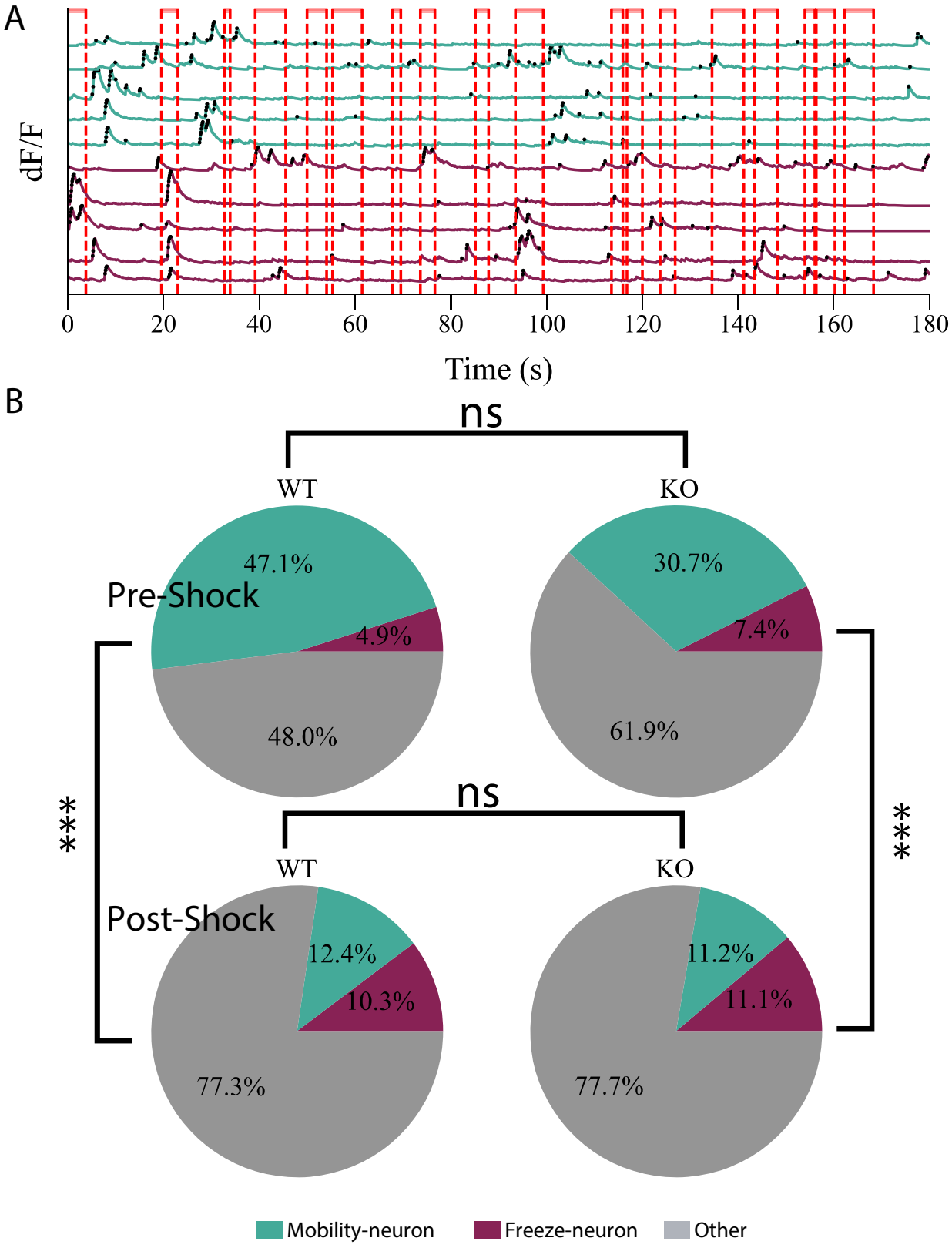


Figure 3.5-8 Mobility and freeze-neurons neurons. A) Representative mobility (green) and freeze (dark red) neuronal activity traces. Red bars indicate freeze bouts; dashed lines mark their start and end. B) Distributions of mobility- and freeze-neurons before and after shock in WT, left, and KO, right mice (Chi-square test, ***, $p < 0.001$).

The first question we asked was whether the ability to encode freezing and mobility states was affected in Arc/Arg3.1-KO. During the initial exploration of the novel context (pre-shock episode), 48% of WT neurons were not associated with any behavioral state (non-responsive). In contrast, this proportion was higher in KO mice at 61.9%. A small percentage of neurons was particularly active during freezing bouts (WT: 4.9%; KO: 7.4%), while a larger percentage was particularly active during periods of mobility (WT: 47.1%; KO: 30.7%). The differences in the proportions of freeze-, mobility-, or non-responsive neurons were not significantly different between WT and KO mice (Chi-square test, $\chi^2(2) = 5.65$, $p > 0.05$).

In the post-shock episode, these distributions shifted. Most neurons in either group were not selectively active in any behavioral state (non-responsive WT: 77.3%; KO:77.7%). The proportion of freeze-neurons increased in both WT and KO mice (WT: 10.3%; KO: 11.1%), whereas the proportion of mobility-neurons decreased (WT: 12.4%; KO: 11.5%). None of the proportions of freeze-, mobility-, or non-responsive neurons showed significant differences between WT and KO (Chi-square test, $\chi^2(2) = 0.09$, $p > 0.05$).
However, both groups exhibited a significant redistribution of freeze- and mobility-neurons in the post-shock episode compared to their pre-shock episode (Chi-square test, pre- *vs*. post-shock; WT: $\chi^2(2) = 28.96$, $p < 0.001$; KO: $\chi^2(2) = 11.68$, $p < 0.001$).

The extensive suppression of calcium activity in most dCA1 neurons during post-shock raises questions about its effects on mobility- and freeze-neurons. To answer this question, we analyzed the calcium spike rates of freeze- and mobility-neurons, as classified by post-shock episodes, comparing the pre- and post-shock episodes. Our observations revealed a significant decrease in the calcium spike rates of all neuron types (mobility, freeze, and non-responsive) in both WT and KO mice (Data not shown), indicating a general reduction in neuronal activity following the conditioning as shown earlier (Figure 3.5-3.A). The distribution of excited and inhibited neurons among the various neuron types reflected the overall neuronal population, with inhibited neurons making up approximately 65% and excited neurons about 35% (Data not shown).

Of course, a question remains whether neurons maintained their preference for a given behavioral state between the pre- and post-shock episodes (Figure 3.5-9). However, a small proportion of neurons that responded to freezing bouts during the pre-shock episode retained their freeze responsiveness status in the post-shock episode, contributing 8.2% of the WT and 11.3% of the KO to the post-shock freeze-neurons. The majority of post-shock freeze-neurons originated from those that were non-responsive to any behavioral states during the pre-shock episode (WT:

47.3%; KO: 56.9%) and from neurons that were previously responsive to mobility periods (WT: 44.5%; KO: 31.9%).

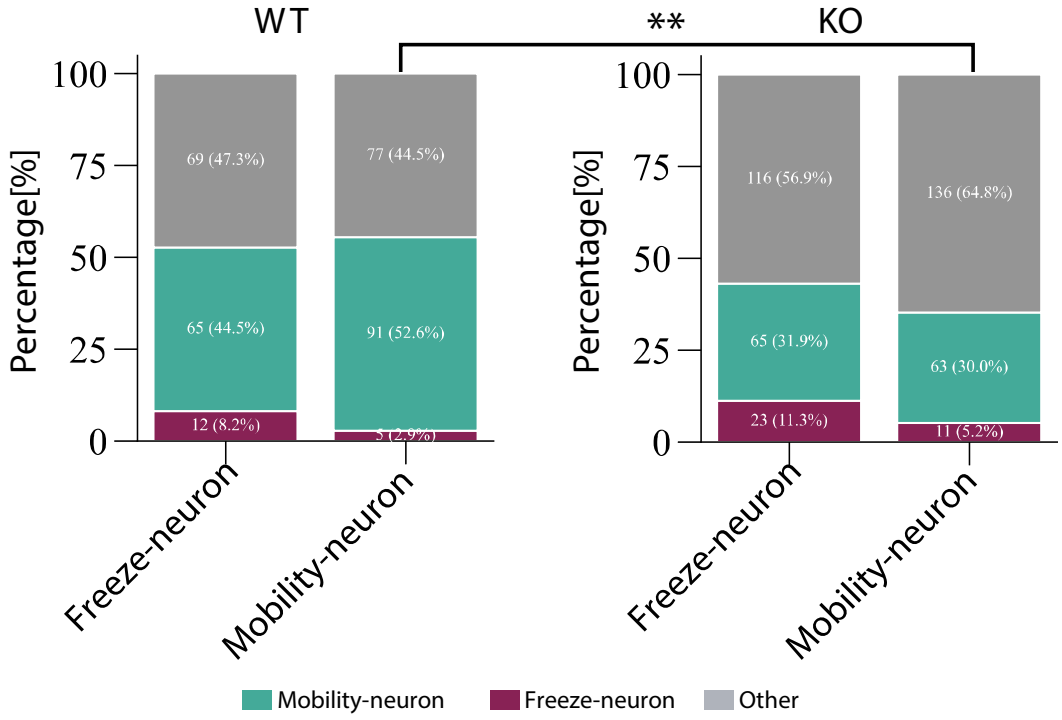


Figure 3.5-9 Remapping of freeze- and mobility-neurons post conditioning in WT and KO mice (Chi-square test, Freeze Neurons; $\chi^2(2) = 3.46$, $p > 0.05$; mobility neurons; $\chi^2(2) = 10.6$, $p < 0.01$).

A notable percentage of neurons that reacted during the mobility periods of the pre-shock episode continued to show mobility responsiveness in the post-shock episode (WT: 52.6%; KO: 30%). The remaining mobility-neurons in the post-shock phase were mainly those that had been non-responsive in the pre-shock episode (WT: 44.5%; KO: 64.8%) or had reacted during freezing bouts (WT: 2.9%; KO: 5.2%). This redistribution of mobility-neurons, showed a significant difference between WT and KO (Chi-square test χ^2 (2) = 10.6, $p < 0.01$).

To conclude our investigation into whether Arc/Arg3.1 might influence neuron response to behavioral states (mobility and freezing), we found no significant differences between WT and KO neurons in either the pre- or post-shock. Similar redistribution patterns were observed for WT and KO neurons in post-shock compared to the pre-shock episodes. Importantly, we noted a decrease in the number of mobility-neurons and an increase in the number of active freeze-neurons following the conditioning, in both genotypes. In the pre-shock episode, the neurons associated with freezing showed almost complete reshuffling in the post-shock episode, while 30-50% of the mobility-neurons in the pre-shock episode remained mobility-neurons in the post-shock episode.

This means 6-10% of the entire neuron population were mobility-neurons both in the pre- and post-shock episodes.

3.5.6 Contextual Fear Conditioning Drives Remapping of Place Cells

From a functional perspective, the most prominent feature of dCA1 neurons is their ability to encode space by forming place fields. Place fields are dynamic representations of space which can be modulated by sensory input, innate brain states and learning (Moser et al., 2008). During fear conditioning, place cells are engaged in the encoding of the environment and may also serve to encode complex context features (Donzis et al., 2013; Kobayashi & Matsuo, 2023; Schuette et al., 2020). We therefore examine how fear learning impacts the dynamics of place cells, specifically focusing on the stability and remapping of place fields. Our previous findings indicated that fear conditioning altered the neuronal activity of the dCA1, resulting in the formation of different subgroups of neurons that experience remapping following the shock. This leads us to wonder whether fear conditioning also reorganizes spatial coding to integrate emotional and contextual elements. Additionally, we are interested in whether Arc/Arg3.1 affects the formation of place cells during fear memory acquisition.

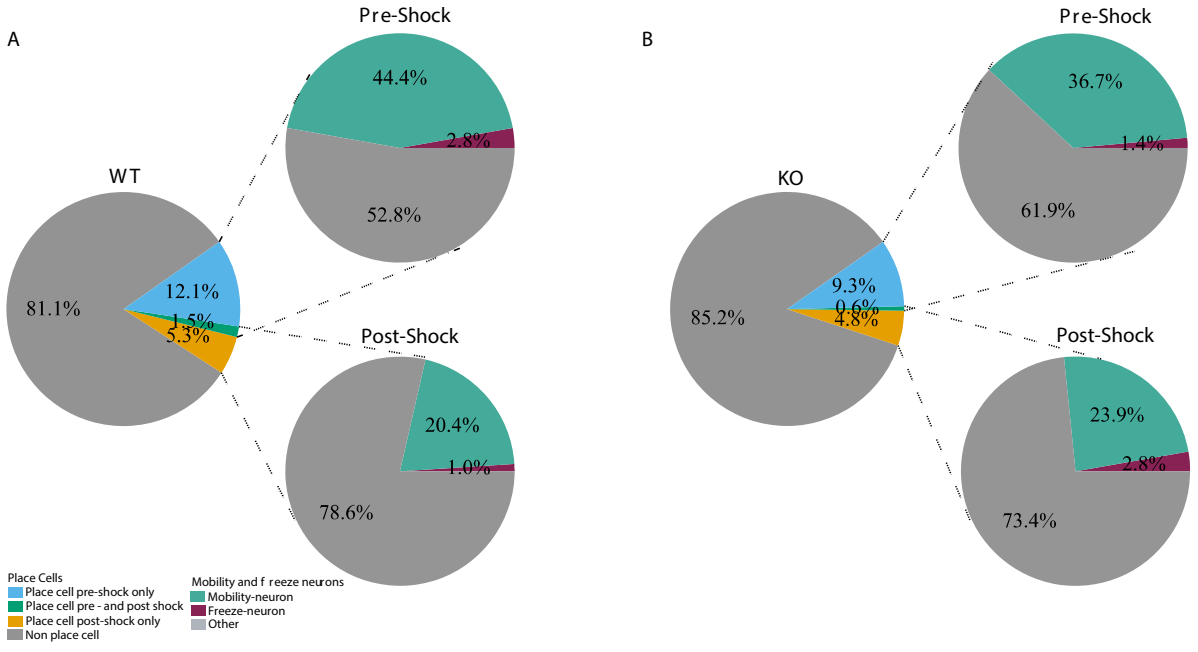


Figure 3.5-10 Place cells remap in the pre- to post-shock session. A) Place cell distributions for WT neurons before and after shock and how their neuronal activity correlates with behavioral changes. B) same as A but for KO neurons

The proportion of place cells in the dCA1 region of the hippocampus for WT and KO mice is presented in Figure 3.5-10. In the pre-shock episode, 13.6% of WT neurons and 9.9% of KO

neurons were identified as place cells. Following the shock episode, both WT and KO mice exhibited a reduction in the proportion of place cells (WT: 6.8%; KO: 5.4%). Only a small subset of neurons maintained their classification as place cells across both pre- and post-shock episodes (WT: 1.5%; KO: 0.6%), with no statistically significant difference between the groups (Chi-square test, χ^2 (3) = 0.83, $p > 0.05$). These results indicate that the absence of Arc/Arg3.1 does not significantly influence place cell formation in the dCA1 region during conditioning, while the stability of place cells decreases similarly in both genotypes after the shock.

We analyzed the behavioral categorization of place cells during these episodes. Since it is standard practice to classify place cells based on activity during movement, we focused exclusively on the subset of place cells associated with mobility rather than freezing. During the pre-shock episode, WT mice exhibited a higher proportion of mobility-related place cells (44.4%) compared to KO mice (36.7%). However, in the post-shock episode, the distribution of behavior-associated place cell categories became more similar between genotypes, with mobility-related place cells comprising 20.4% in WT and 23.9% in KO mice.

In total, only 10-14% of the overall neuron population was classified as place cells either during the pre-shock or the post-shock episode. The WT and KO neurons both demonstrated a reduced proportion of place cells following the shock, largely attributed to heightened freezing behavior. Curiously, only 36-45% of the identified place cells were classified as mobility neurons in the pre-shock episode, decreasing to 20-23% in the post-shock episode.

3.5.7 Summary of Fear Memory Acquisition

In summary, our study aimed to investigate the role of Arc/Arg3.1 in the encoding of contextual fear memory in the dCA1 region of the hippocampus. We conducted calcium imaging in WT and Arc/Arg3.1 KO mice during a contextual fear conditioning session. Our results revealed that the absence of Arc/Arg3.1 did not significantly affect the acquisition of fear memory, as both WT and KO mice exhibited similar freezing behavior patterns during the conditioning session. Nor did we observe major differences in the calcium activity modulation NMI during the conditioning besides the initial difference in the calcium spike rates. Additionally, we found that the majority of dCA1 neurons were inhibited following the conditioning, with around a third of neurons exhibiting excitation. The responses of dCA1 neurons to tone and foot shock stimuli were similar between WT and KO mice, suggesting that Arc/Arg3.1 does not grossly affect responses to sensory input in dCA1. Contrary to the general overall inhibition of dCA1

neurons, most tone-neurons were excited in both WT and KO. However, most shock-neurons were inhibited in the WT while excited in the KO.

Finally, we observed that fear conditioning led to a redistribution of mobility and freeze neurons in both WT and KO mice, with a decrease in the number of mobility neurons and an increase in the number of active freeze neurons following the conditioning. Our findings provide insights into the role of neural activity dynamics in encoding contextual fear memory in the dCA1 and highlight the complex interplay between neuronal activity and behavior during fear conditioning.

3.6 Disrupted Retrieval of Conditioned Fear Memory in Arc/Arg3.1 KO

In this part, we examined the impact of Arc/Arg3.1 on neural ensemble activity while retrieving contextual fear memories. We analyzed the activity of neurons in the dCA1 region during two time points: recent memory (7 days post-conditioning) and remote memory (21 days post-conditioning). Our goal was to determine whether Arc/Arg3.1 affects the stability of neural engrams during memory retrieval. Additionally, we investigated whether Arc/Arg3.1 influences the ability of neuronal activity to distinguish between familiar and novel contexts during both recent and remote memory. Previous research has established that Arc/Arg3.1 is crucial for memory consolidation. Mice lacking Arc/Arg3.1 display a deficit in long-term potentiation and memory consolidation(Gao et al., 2018; Plath et al., 2006). However, the specific role of Arc/Arg3.1 in neural activity during memory retrieval remains unclear.

3.6.1 Impaired Behavioral Response in Recent and Remote Memory in Arc/Arg3.1 KO

To assess the impact of Arc/Arg3.1 on memory recall, we analyzed the freezing behavior of WT and KO mice during the recent and remote memory tests and their freezing response to a novel context (Figure 3.5-1 and Figure 3.6-1.A). One notable observation is that WT mice exhibited a significant increase in freezing when re-exposed to the conditioning context, compared to KO mice. The observed trend was consistent in both recent and remote memory tests. In contrast, there was no difference in freezing when the mice were exposed to a novel context (Mixed-effect ANOVA: Genotype × Day interaction, $F(5,80) = 8.62, p < 0.001$, Figure 3.6-1.B).

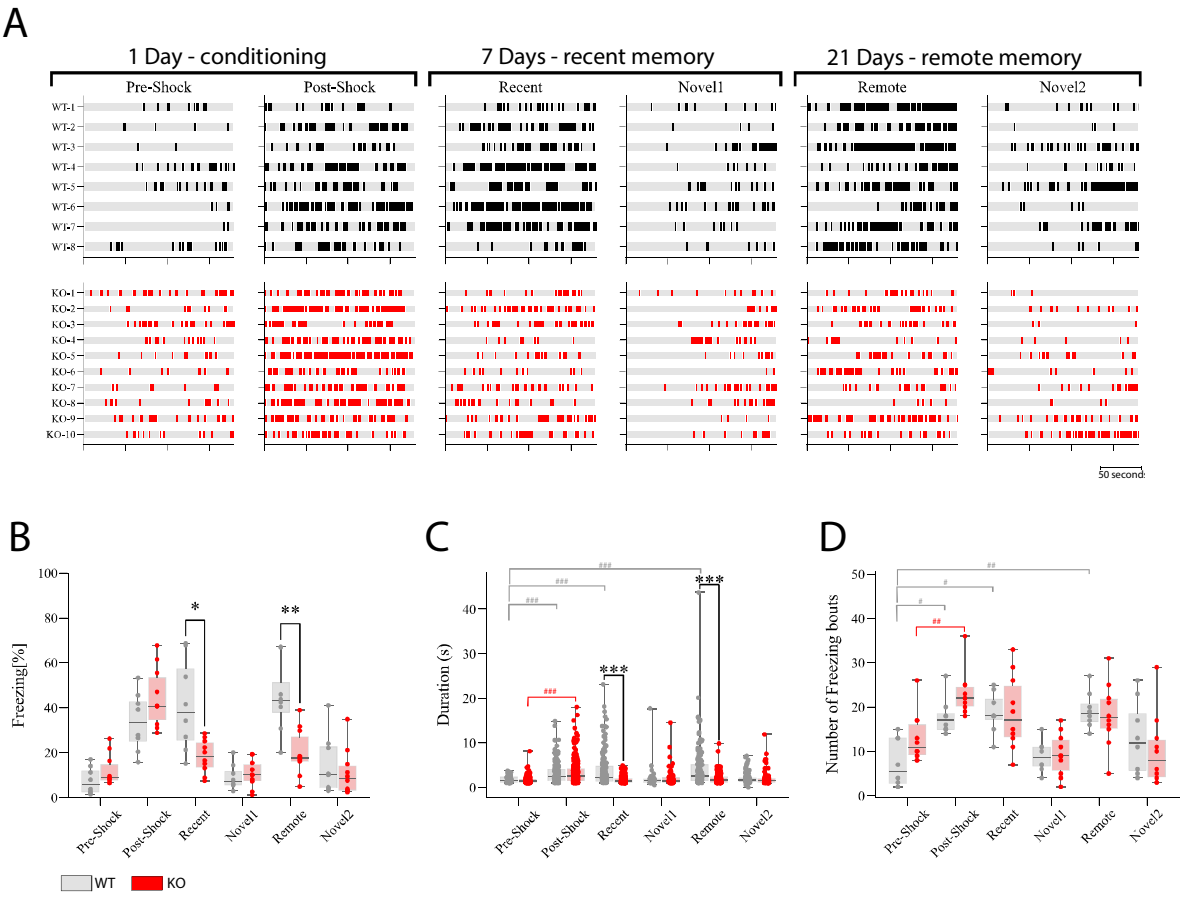


Figure 3.6-1 Freezing behavior in recent and remote memory test. A) Freezing bouts during the fear conditioning paradigm for all mice (WT, n=8; KO, n=10), WT is shown on the top row and KO on the bottom row. Grey indicates mobility periods, and red/black denote freeze bout**s.** B) Average percentage of freezing observed during recent and remote memory (Mixed-effect ANOVA: Genotype × Day , $F(5,80) = 8.62, p<0.0001$, n=8; KO, n=10,Stats-table 18) C) Duration of each freezing bouts (2-way ANOVA: Genotype × Day : $F(5) = 14.7$, $p < 0.001$, Stats-table 19) D) Freezing bout count for each mouse in the different episodes (Mixed-effect ANOVA: Genotype × Day, $F(5,80)=1.92$, $p>0.05$; Genotype effect, $F(1,16)=0.46$,$p>0.05$; day effect, $F(5,80)=16.47$,$p<0.001$,Stats-table 20)

We wondered if the increased freezing response observed is due to the same factors as those during the conditioning phase (Figure 3.5-2). The increased freezing during the post-shock episode was attributed to both an increase in the duration and the frequency of freezing bouts, compared to the pre-shock episode.

We next examined the duration of freezing bouts during both the recent and remote memory tests. WT mice showed a significant increase in the duration of freezing bouts during the recent memory test compared to KO mice. This significant increase was also evident during the remote memory test (2-way ANOVA: Genotype × Day : $F(5) = 14.7$, $p < 0.001$,Figure 3.6-1.C).

In the WT group, we observed a notable increase in freezing bout durations during both the remote and recent memory tests, compared to their exposure in the pre-shock episode (2ST-Sidak,

pre-shock *vs* Recent d = -0.62 p<0.001; pre-shock *vs* Remote d = -0.58 p<0.001). Conversely, the KO mice did not exhibit this pattern; their freezing bout durations remained consistent during the recent and remote memory tests, similar to the pre-shock episode.

We observed that KO mice did not significantly differ from WT mice in the number of freezing bouts during both recent and remote memory tests(Mixed-effect ANOVA: Genotype × Day, F(5,80)=1.92, p>0.05,Figure 3.6-1.C and Stats-table 20). However, within the WT group, there was a significant increase in the number of freezing bouts during the recent and remote memory compared to the pre-shock episode (2ST-Sidak, pre-shock *vs* Recent, d = -2.25, p < 0.05; pre-shock *vs* Remote d = -2.45, p < 0.01,Figure 3.6-1C). This indicates that WT mice exhibited more frequent freezing bouts during the remote memory test than in the earlier phases. In contrast, KO mice did not display this pattern; they showed similar freezing bouts during recent and remote memory tests as during the pre-shock episode. Additionally, when placed in an alternative context, WT exhibited a comparable number of freezing bouts as pre-shock.

In summary, WT mice showed a significantly greater tendency to freeze in conditioned environments compared to KO mice, with no noticeable increase in novel contexts. During both memory tests, WT mice had longer freezing durations than KO mice, with notable differences observed. Additionally, WT mice displayed more freezing bouts during the memory tests compared to their pre-shock phases, while KO mice did not exhibit this variability. Overall, WT mice demonstrated enhanced freezing behaviors primarily due to longer freezing bout durations rather than a higher frequency of freezing bouts. The absence of the Arc/Arg3.1 gene in KO mice is a critical factor in these observations. Arc/Arg3.1 is essential for synaptic plasticity and memory consolidation. In the absence of this gene, KO mice exhibit disrupted synaptic function, resulting in issues with memory formation and recall. This is evident by their diminished freezing behavior and lack of discrimination between familiar and novel contexts, as also previously demonstrated(Gao et al., 2018; Plath et al., 2006).

3.6.2 Impaired Modulation of Neural Activity in Memory Retention in Arc/Arg3.1 KO

As an initial step, our goal was to accurately quantify the total number of neurons recorded during the five experimental sessions. To monitor the same neurons across all sessions, we concatenated and processed the calcium videos (see methods section). By tracking neuronal activity across

multiple sessions, we can evaluate the stability and changes in neural activity related to both recent and remote memory retrieval.

We found that the total number of neurons recorded during the experiment was not significantly different between WT and KO mice. We recorded 2,717 neurons from 8 WT mice and 3,421 neurons from 10 KO mice (Figure 3.6-2A), with WT having a mean of 340 ± 253 neurons and KO having a mean of 342 ± 244 neurons. This suggests that the absence of Arc/Arg3.1 does not impact the number of neurons recorded. Additionally, there was no significant difference between the WT and KO groups in the fraction of total neurons activated per session, which consistently remained at 60%±10% (Figure 3.6-2.B).

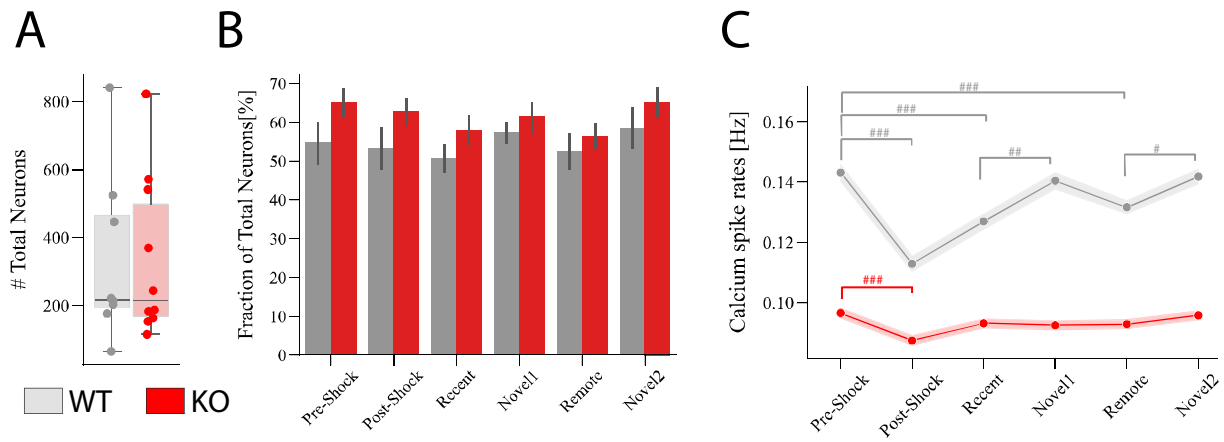


Figure 3.6-2 Neurons recorded during the CFC and their calcium spike rate. A) Total number of neurons per mouse throughout the entire CFC B) Fraction of total neurons active in any session of the CFC C) Calcium spike rate of neurons active in each session.(2-way ANOVA: Genotype × Sessions: $F(5) = 9.71$, $p < 0.001$,Stats-table 21)

In our bulk analysis, we calculated the mean calcium spike rate of neurons per mouse during the CFC-paradigm, focusing specifically on a 3-minute window from each session and the post-shock. We observed that the mean calcium spike rate of WT mice tended to be higher than that of KO mice during each session (data not shown). While this analysis offers a general overview of neuronal activity, using the average calcium spike rate per mouse presents several challenges and limitations that can obscure biologically meaningful insights. Averaging calcium spike rates across all neurons in a mouse overlooks the inherent heterogeneity of neuronal activity. Subsets of neurons may show significant differences in calcium spike rates or activity patterns that are critical for memory. This averaging dilutes the contributions from these important subsets, especially in systems like the hippocampus, where sparse coding is common and specific ensembles of neurons are responsible for memory encoding and retrieval.

Therefore, we looked at group-wise calcium spike rates where we compared the calcium spike rates of neurons in WT and KO mice during recent and remote memory tests and during exposure to a novel context. Our analysis revealed significant differences in calcium spike rates between WT and KO mice across the different sessions (2-way ANOVA: Genotype × Day $F(5)=9.71, p<0.001$, Figure 3.6-2.C). Notably, the change in calcium spike rate between familiar and novel context exposures was particularly striking. WT mice exhibited a significant decrease in calcium spike rate during each memory test compared to their calcium spike rates during novel context exposure (2ST-Sidak , Recent *vs* Novel1 $d = 0.5$, $p < 0.001$; Remote *vs* Novel2 $d = 0.6$, $p < 0.001$, Figure 3.6-2.C) and the pre-shock episode (Stats-table 21). In contrast, KO mice did not display this pattern; their calcium spike rates during both the recent and remote memory tests were comparable to those observed during novel context exposure. This indicates that WT mice exhibit context-specific modulation of neuronal activity, with a notable decrease in calcium spike rate during memory tests in familiar contexts when compared to novel context exposure. Conversely, the absence of Arc/Arg3.1 in KO mice appears to disrupt this context-specific modulation. Furthermore, the finding that WT mice demonstrated a significant decrease in calcium spike rates during familiar context exposure compared to novel exposure was reinforced by observations from the open field test, where WT mice in a non-aversive context also exhibited discriminating neuronal calcium spike rates between familiar and novel (Figure 3.3-1). These findings highlight the role of Arc/Arg3.1 in facilitating context-specific adjustments in neuronal activity during familiar situations, underscoring its significance for adaptive responses to new environments.

3.6.3 Behavior-Specific Neuronal Population Dynamics during the CFC

As a follow-up analysis, we examined the distribution of neuronal subtypes (neurons' preferred response to freezing or mobility bouts) during acquisition and recent and remote memory tests, as well as during novel context exposure. Our analysis indicated that both WT and KO mice demonstrated similar distributions of neuronal subtypes across the various sessions, as illustrated (Figure 3.6-3). The proportion of neurons classified as freeze-neurons remained consistent for both WT and KO mice during the recent and remote memory tests, as well as during novel context exposure, ranging from 5% to 10%. On the other hand, the percentage of neurons identified as mobility-neurons showed a slight decline during both recent and remote memory tests when compared to exposure to a novel context for each genotype. However, this was only a significant change between KO remote and Novel2 (Chi-square test: KO Remote *vs* Novel2 $\chi^2(2) = 11.7$, $p < 0.05$). These findings suggest that the absence of Arc/Arg3.1 does not significantly impact the

modulation of neuronal subtype distribution during memory tests or novel context exposure, nor does it affect the proportion of neurons classified as freeze-neurons or mobility-neurons. Instead, only the context modulates the proportion of neurons classified as mobility-neurons.

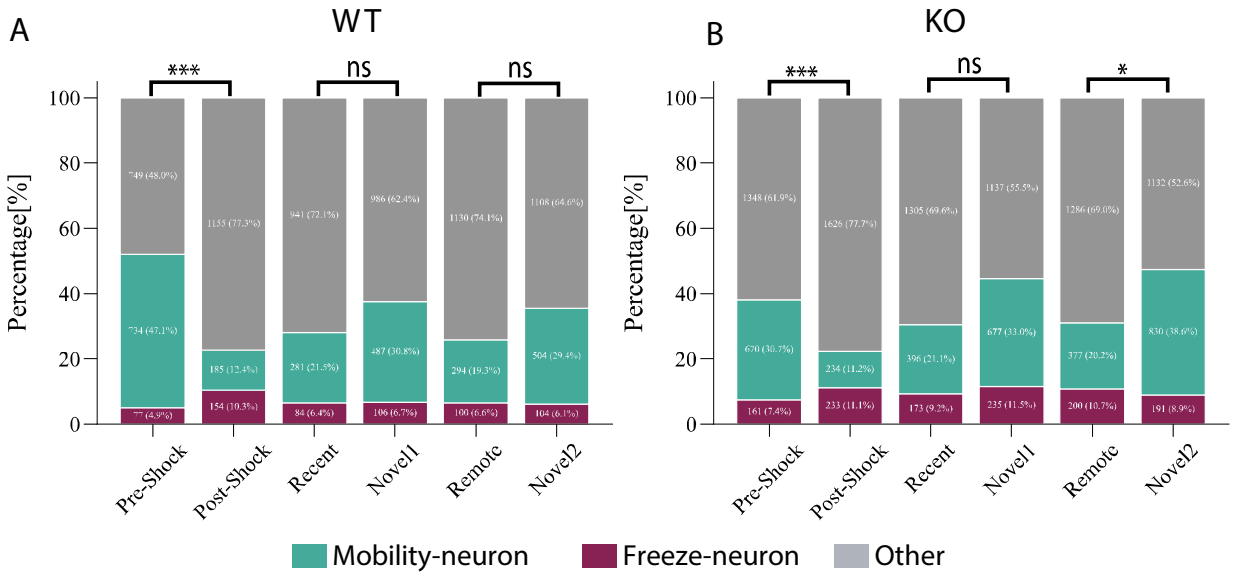


Figure 3.6-3 Mobility and freeze-neurons during the CFC sessionsA) for WT (Chi-square test, pre-shock vs post-Shock $\chi^2(2) = 29$, $p < 0.001$) B) for KO (Chi-square test,,pre-shock *vs* post-Shock $\chi^2(2) = 11.7$, $p < 0.001$; Remote *vs* Novel2 $\chi^2(2) = 11.7$, $p < 0.05$)

This finding is unexpected, as one might anticipate that the absence of Arc/Arg3.1 would have a significant impact on mobility-neurons, especially since KO mice do not exhibit the increased freezing behavior seen in WT mice in the context. This suggests that Arc/Arg3.1 may not be directly involved in context recognition but rather in encoding or retrieving the memory associated with that context.

3.6.4 Lack of Context-Dependent Modulation of Place Field Coverage in Arc/Arg3.1 KO

As demonstrated in a previous section (Figure **3.5-10**), the proportion of place cells in the dCA1 region of the hippocampus was not significantly different between WT and KO mice during the conditioning session. To further explore this, we investigated the contribution of Arc/Arg3.1 to the generation of place cell activity during recent and remote memory retention, focusing on context-specific dynamics. The results showed a notable decrease in the percentage of place cells during recent and remote memory retrieval compared to novel contexts (Figure **3.6-4**). However, differences are observed in how WT and KO mice retain their place cells across these sessions. WT mice demonstrated a greater ability to recruit and activate place cells in novel contexts. In

contrast, KO mice displayed little to no change in the proportion of active place cells. Undoubtedly, the reduction of place cells observed in the WT group during both recent and remote sessions is directly linked to the increased freezing and reduced firing rates in those sessions.

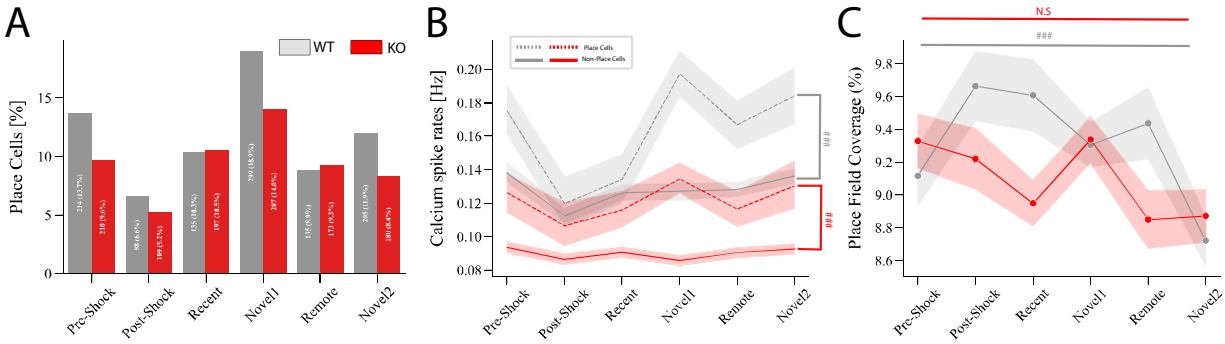


Figure 3.6-4 Place cell dynamics during the CFC sessions. A) Percentage place cells in the WT and KO in the different sessions B) Calcium spike rate of Place cells and NON-place cells (2-way ANOVA: WT, $F(5) = 9.47$, $p < 0.001$; KO, $F(5) = 3.96$, $p < 0.001$,Stats-table 22) C) Place Field size measure as the coverage of the total area

Identified place cells displayed significantly higher calcium spike rates than non-place cells in both WT and KO groups (2-way ANOVA: WT, $F(5) = 9.47$, $p < 0.001$; KO, $F(5) = 3.96$, $p < 0.001$, Figure 3.6-4B). This increase was particularly pronounced during sessions in a novel environment, demonstrating that place cells exhibit heightened activity in response to new surroundings. These results align with previous findings in the OFT (Figure 3.3-6), indicating that place cells are more active than other neurons in the hippocampus, especially in unfamiliar settings. Furthermore, this pattern is observed in both WT and KO mice, suggesting that Arc/Arg3.1 is not necessary for the increased activity of place cells in novel environments.

The size of place fields in WT and KO mice showed significant differences across sessions (Figure 3.6-4.C). In WT mice, place fields were larger during familiar exposure sessions compared to novel sessions (one-way ANOVA: $F(5) = 3.38$, $p < 0.001$). Conversely, KO mice exhibited no significant variation in place field size across sessions (one-way ANOVA: $F(5) = 2.11$, $p > 0.05$).

These findings suggest that Arc/Arg3.1 may influence the adaptation of place cells, enabling them to encode features of new environments while maintaining stability in familiar ones. While there is a decrease in the proportion of place cells in known settings, their field sizes increase. This pattern underscores the vital function of Arc/Arg3.1 in regulating the plasticity of the hippocampal network, allowing it to distinguish between familiar and neutral environments.

3.6.5 Coordinated Neural Activity is Impaired in Arc/Arg3.1 KO

Memory retrieval depends on synchronized neuronal activity within hippocampal circuits, particularly in the dCA1 area (O'Keefe & Krupic, 2021). The coordination of neuronal activity is believed to reflect crucial network-level encoding and retrieval processes that are essential for complex behavior. In dCA1, synchronization of neuronal ensembles is regarded as essential for memory encoding and retrieval. This synchronization, characterized by correlated activity among neurons, is thought to enhance the stability and strength of memory representations (Buzsáki & Draguhn, 2004; Eichenbaum, 2017b). The molecular mechanisms enabling ensemble synchronization from the perspective of memory, are not fully known. The key role Arc/Arg3.1 plays in regulating network oscillations in CA1, synaptic plasticity and memory consolidation (Plath et al 2006; Gao et al 2006), make it a key candidate to regulate memory-linked correlated activity patterns. However, whether Arc/Arg3.1 affects correlated activity in the process of memory consolidation remains unknown.

To address this question, we evaluated neuronal synchronization in dCA1, by applying graph-theoretical methods and utilizing Pearson correlation analysis. Neuronal pairs with a correlation coefficient exceeding 0.3 were considered functionally correlated (Figure 3.6-5.A), enabling us to create network representations of functional ensembles ((Jimenez et al., 2020; Ko et al., 2011)).

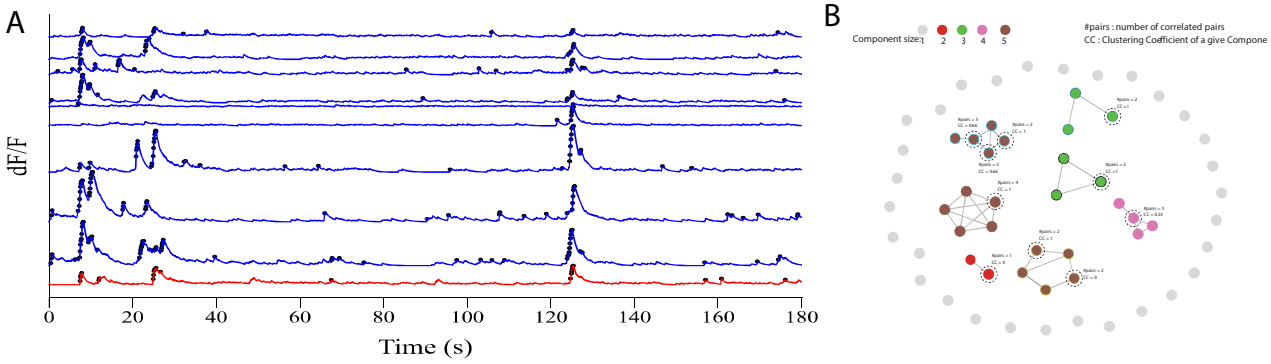


Figure 3.6-5 Example of correlated neurons A) Example of a neuron (red) with its correlations partners (blue) B) Graph connections metrics

We generated network correlation graphs for behavioral sessions by linking all correlated pairs and subsequently computed graph theory analysis metrics to assess individual neurons' participation in more complex correlated network activity (Figure 3.6-5.B). Our analysis focused on two graph theory metrics: the number of correlated pairs (corr-pairs) a neuron has and the degree to which a neuron's pairs were also correlated with one another, known as the clustering

coefficient (CC). The clustering coefficient can only be computed for a neuron in a group of three or more neurons.

Initially, we noted that around 90%±12% of both WT and KO groups in each session showed at least one correlated neuron. Of these, roughly 80%±12% were associated with a minimum of three neurons, which enables the calculation of the clustering coefficient.

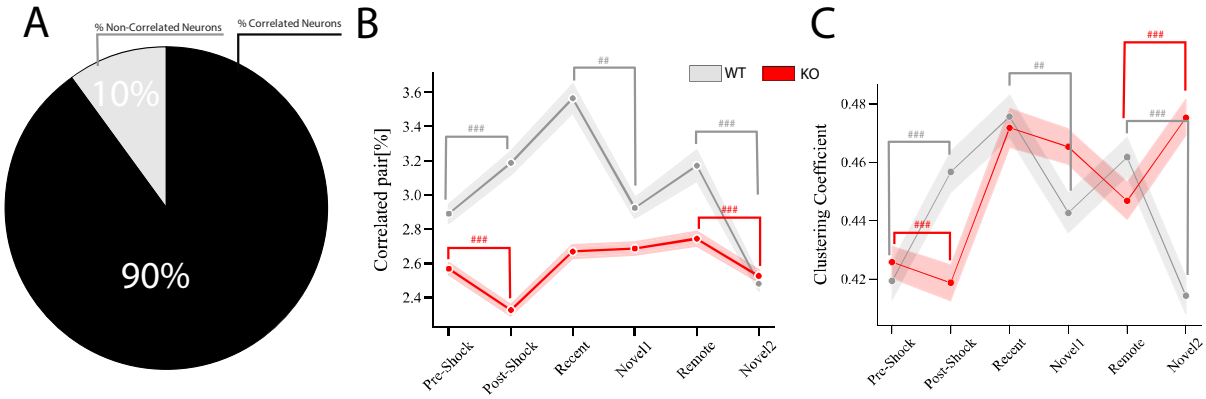


Figure 3.6-6 Calcium spike activity correlation A) Fraction of neurons that had at least one partner (2-way ANOVA: Genotype × Sessions: $F(5) = 28.15$, $p < 0.001$,Stats-table 23) B) Correlated pairs 2-way ANOVA: Genotype × Sessions: $F(5) = 13.82$, $p < 0.001$,Stats-table 24) .

Our analysis of correlated pairs revealed a notable uptick in WT neurons, specifically, in the conditioning session. WT neurons experienced a significant rise in correlated pairs when comparing the pre-shock phase to the post-shock phase, while KO neurons showed a considerable reduction in their correlated pairs. During the subsequent memory test, KO neurons did not display any significant changes between the recent and novel1 sessions. In contrast, WT neurons showed a marked difference; during the recent session, they had significantly more correlated pairs than both KO and novel1. This pattern persisted in the remote memory sessions.

Interestingly, we noted an increase in the CC that mirrored the trend of corr-pairs for WT neurons across the sessions. The CC of KO mice also reflected the trend in corr-pairs, with the exception of novel2, where CC increased. For both novel1 and novel2, KO exhibited a significant increase in CC compared to WT, whereas pre-shock revealed a significant decrease. However, there were no differences in pre-shock, recent, and remote memory.

Interestingly, both the corr-pairs and CC showed an increase for WT, while both decreased for the KO group. This indicates that although the KO and WT groups exhibited comparable

freezing behavior in the post-shock session, their neuron populations responded differently to the learning process.

In summary, the modulation of correlated pairs and CC is less effective in KO compared to WT. WT consistently showed a higher number of correlated pairs than KO, with context-specific variations observed across sessions, novel- vs familiar environments, similar to the CC. Conversely, KO showed no signs of context-specific modulation, indicating experiences in novel or familiar environments, depicting the lack of memory.

3.7 High-Excitability Identification and Tracking of Engram Neurons

As previously mentioned, "engram neurons" refer to groups of neurons that are crucial components of a specific memory engram. Engram neurons (1) are activated during the learning experience, (2) undergo physical or chemical modifications as a result, and (3) are reactivated when stimuli from that experience (or its components) are encountered again, which facilitates memory retrieval (Josselyn & Tonegawa, 2020). In this study, we tracked neurons activated during the conditioning session and subsequently reactivated in recent and remote memory tests. As shown by (Kim et al., 2014; Reijmers et al., 2007) engram neurons display increased excitability during conditioning, while (Mocle et al., 2024) defined engram neurons as those that show heightened activity during a retrieval session. Here we will examine engram neurons based on both definitions. We analyze the pre-shock and recent sessions by z-scoring the calcium spike rates in mice. Engram neurons are identified as those with a z-score greater than 0. This will provide three neuronal subgroups for the remaining sessions: engram, non-engram neurons, and "*new neurons*." New neurons refer to those not activated during the session that were used to define the engram.

3.7.1 Neural Reactivation Unaffected in Arc/Arg3.1 KO

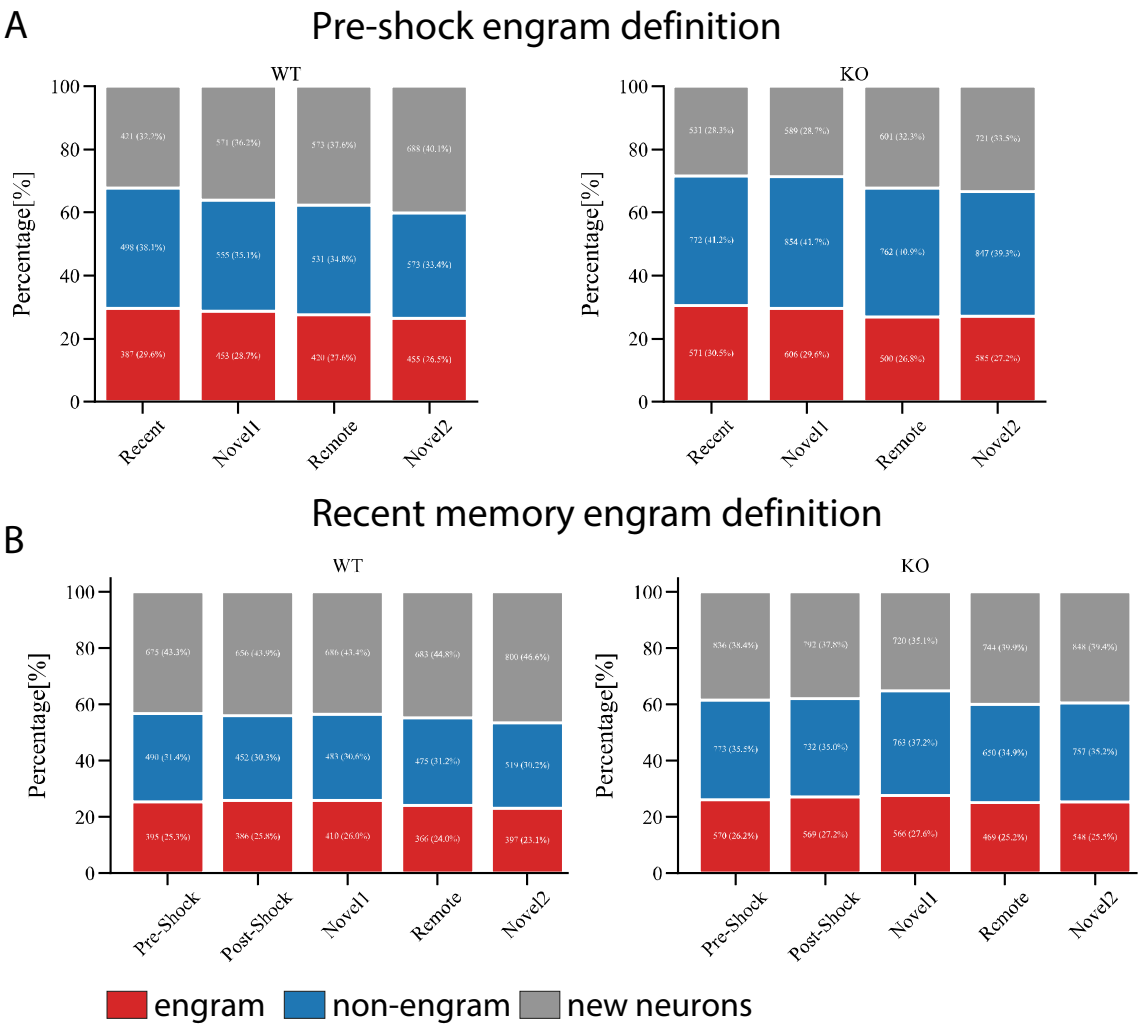


Figure 3.7-1 Neuron Reactivation A) The proportion of neurons activated during a session that were also activated in the pre-shock session. The reactivated neurons are classified into two categories: Engram, which has a z-scored calcium spike rate greater than 0, and Non-engram, which has a calcium spike rate less than 0. Neurons not identified in the pre-shock session were considered as part of the session under review. B) The same as A, but uses the neuron engram definition from the recent session (chi-square test not significant).

The number of detected cells was similar for both recent, remote, and novel sessions (Figure 3.6-2). Approximately 70% of the detected neurons in pre-shock sessions exhibited reactivation in WT and KO. This high reactivation rate was maintained across both familiar and novel context exposures, suggesting that most neurons active during conditioning remained active, irrespective of contextual novelty. Of the total detected neurons in each session, approximately 28±7% consistently represented engram neurons, and 36±9% of neurons were non-engram neurons. The remaining neurons (approximately 36±15%) represented *new neurons* that were inactive in the pre-shock session (Figure 3.7-1 -A).

When the engram neurons were based on the recent session, roughly 60% reactivation was observed in both retrospective and prospective sessions. It showed 27±9% for engram, 31±10% for non-engram, and 42±17% for new neurons (Figure 3.7-1-B). This stability in reactivation

percentage was consistent across sessions and genotypes, with no significant difference for either engram definition.

To investigate which neuronal groups' neuronal calcium spike rates are modulated by environmental context, as seen in the overall population activity. We assessed the activity of calcium spike rates across sessions and performed a one-way ANOVA within each neuronal group across sessions (Figure 3.7-2). For the engram neurons defined by the pre-shock session, the calcium spike rates during this session were excluded from the ANOVA. Those engram neurons were identified because of their heightened activity during that session. Including these calcium spike rates in the test would artificially inflate the apparent difference in activity, leading to a potentially spurious effect. Additionally, for the engram neurons defined by the recent session, the calcium spike rates from the recent session was excluded from the ANOVA.

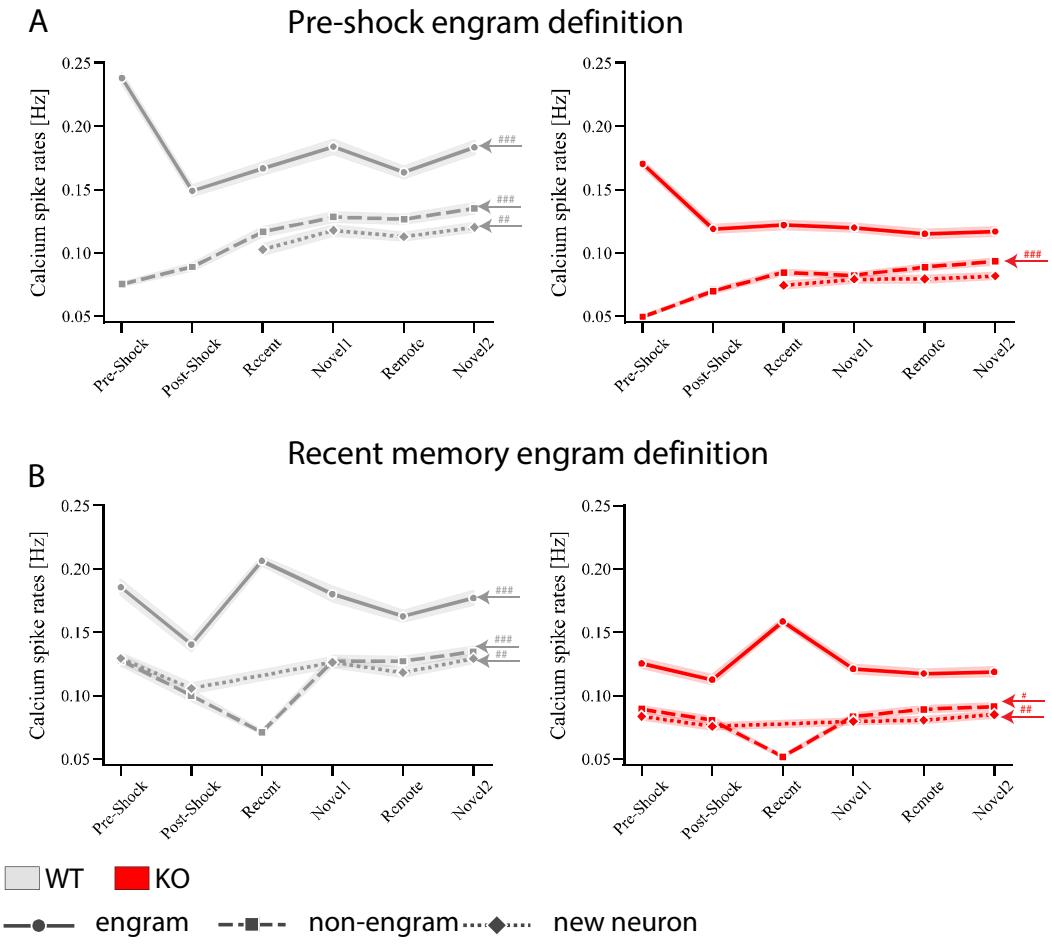


Figure 3.7-2 Calcium spike rate of Engram neurons A) The calcium spike rates of both Engram and non-engram neurons, as well as new neurons, are presented according to the definition of neuron engram from the pre-shock session. WT is shown on the left and KO on the right. B) The same as A, but uses the neuron engram definition from the recent session. A one-way ANOVA statistical test (Stats-table 25).

In WT neurons (Figure 3.7-2 A-left), calcium spike rates of all three neuronal groups showed significant modulation across sessions (one-way ANOVA: Engram neurons $F(4) = 10.29$, $p < 0.001$; Non-engram neurons $F(4) = 31.11$, $p < 0.001$; New neurons $F(3) = 3.88$, $p < 0.01$). All neuronal groups showed similar modulation as observed in the overall population activity. Interestingly, engram neurons consistently exhibited higher calcium spike rates in all sessions than the other neuronal groups and demonstrated the most extensive modulation.

In contrast (Figure 3.7-2 A-right), KO neurons displayed an almost constant calcium spike rate. Only non-engram neurons showed significant session-dependent modulation (one-way ANOVA Non-engram $F(4) = 21.42$, $p < 0.01$). This consistency in calcium spike rates is coherent with the overall population activity. Like for the WT, engram neurons in KO exhibited consistently higher calcium spike rates compared to the other neuronal groups.

A similar observation, when the engram is defined based on the recent session is shown in Figure 3.7-2 B and Stats-table 25.

This indicates that, even for neurons allocated to the engram, activity levels are sensitive to environmental context and that engram and newly active neurons are dynamically regulated depending on memory retrieval in the WT. At the same time, this is absent in the KO.

3.7.2 Loss of Coordinated Neural Activity in Arc/Arg3.1 KO in reactivated neurons

To further investigate the engram neurons, we assessed the correlation of calcium spike activity within each neuronal group by calculating the pairwise Pearson correlation coefficients for all neuron pairs within the same group across familiar and novel sessions (Figure 3.7-3). Here, we provide a descriptive summary of the results without reliance on statistical testing or inferential metrics.

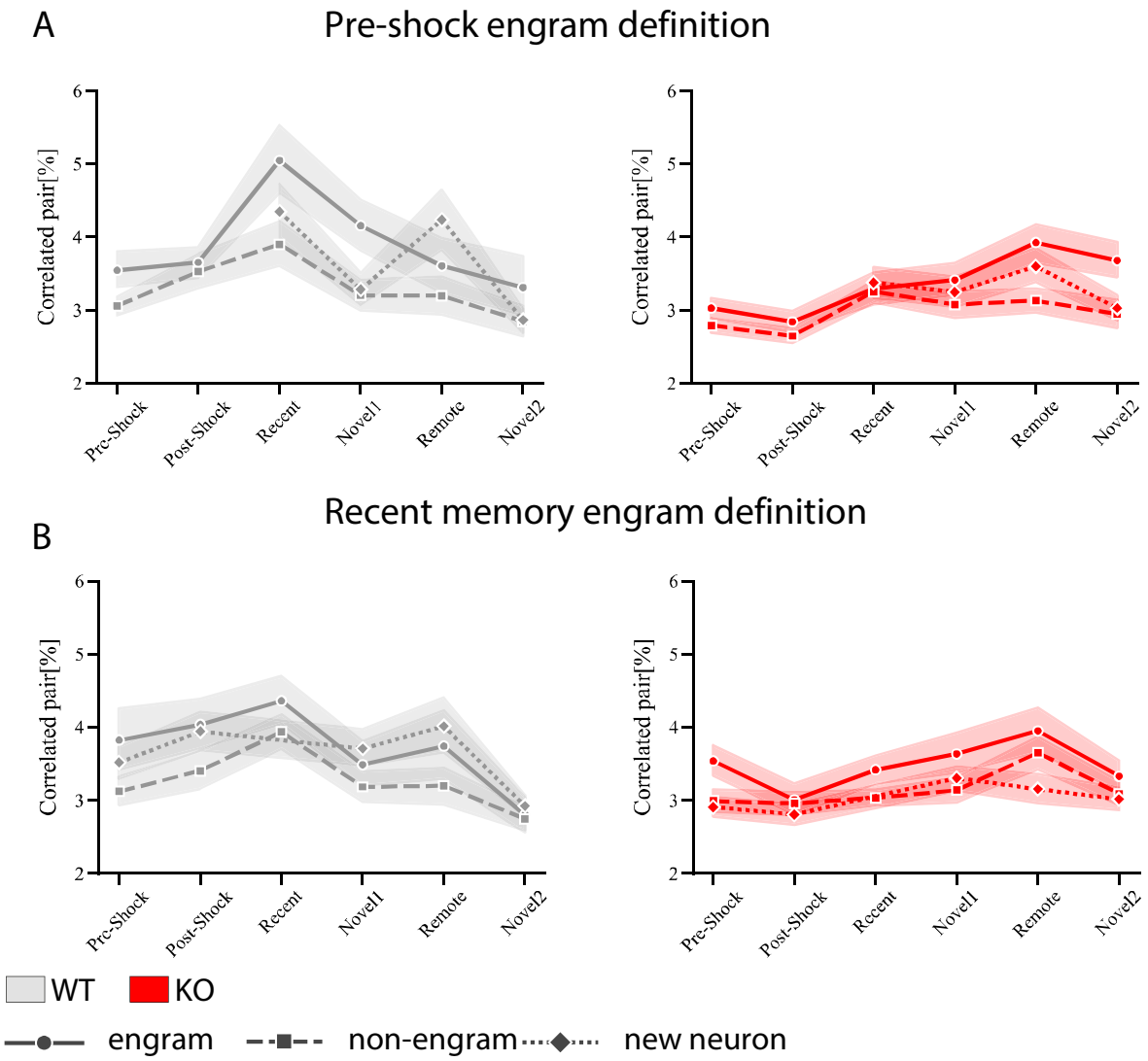


Figure 3.7-3 Correlated pairs within engram neurons. A) The fraction of correlated pairs within each neuron group. Engram and non-engram neurons and new neurons are presented according to the definition of neuron engram from the pre-shock session. WT is shown on the left and KO on the right. B) The same as A, but uses the neuron engram definition from the recent session

When the engram neurons are defined based on the pre-shock period. For WT, Engram neurons showed the highest corr-pairs in pre-shock, post-shock, and recent sessions. However, Engram neurons did not exhibit the heightened peak in the remote memory engram as seen in the overall corr-pairs, showing only a slight difference between remote and novel2. The non-engram neurons exhibited a trend similar to that of the engram neurons, but with lower corr-pair values. Notably, the newly formed neurons demonstrated modulation similar to the overall population, showing heightened corr-pairs during both recent and remote memory in comparison to novel1 and novel2, respectively (Figure 3.7-3 A-left).

In KO engram neurons, a decrease in corr-pairs was observed immediately after conditioning (post-shock session). This was followed by a substantial increase in corr-pairs, surpassing the

initial pre-shock levels. On the other hand, non-engram neurons showed weak modulation for both recent and remote memories. The new KO neurons displayed only increased corr-pairs during the remote session, but not in the recent, novel1, or novel2 sessions (Figure 3.7-3 A-Right).

When engram neurons are defined based on the recent session, WT engram neurons showed a modulation similar to the overall corr-pair modulation, where pre-shock < post-shock, recent > novel and remote > novel2. This tendency was also similar in the non-engram neurons. New neurons also showed pre-shock < post-shock and remote > novel2 (Figure 3.7-3 B-left). For KO, the engram neurons showed a decrease in the corr-pairs immediately after conditioning (post-shock session). This was followed by a substantial increase in corr-pairs, surpassing the initial pre-shock levels. This was also true for the non-engram neurons (Figure 3.7-3 B-Right).

These findings imply that two neuronal populations, where the first group is primarily important in the recent memory retrieval but not remote, and the second group plays a prominent role in both recent and remote memory retrieval in WT, which is absolutely in KO.

3.7.3 Reactivation of Shock and Tone-Responsive Neurons

During the conditioning session, the mice are exposed to both tone and shock, which allows us to identify a subset of neurons that were responsive to these stimuli (Figure 3.5-6). Here, we examine the reactivation dynamics of shock and tone-responsive neurons during recent and remote memory recall. Understanding how distinct components of a fear memory are re-engaged over time may provide insight into the processes that stabilize long-term memories.

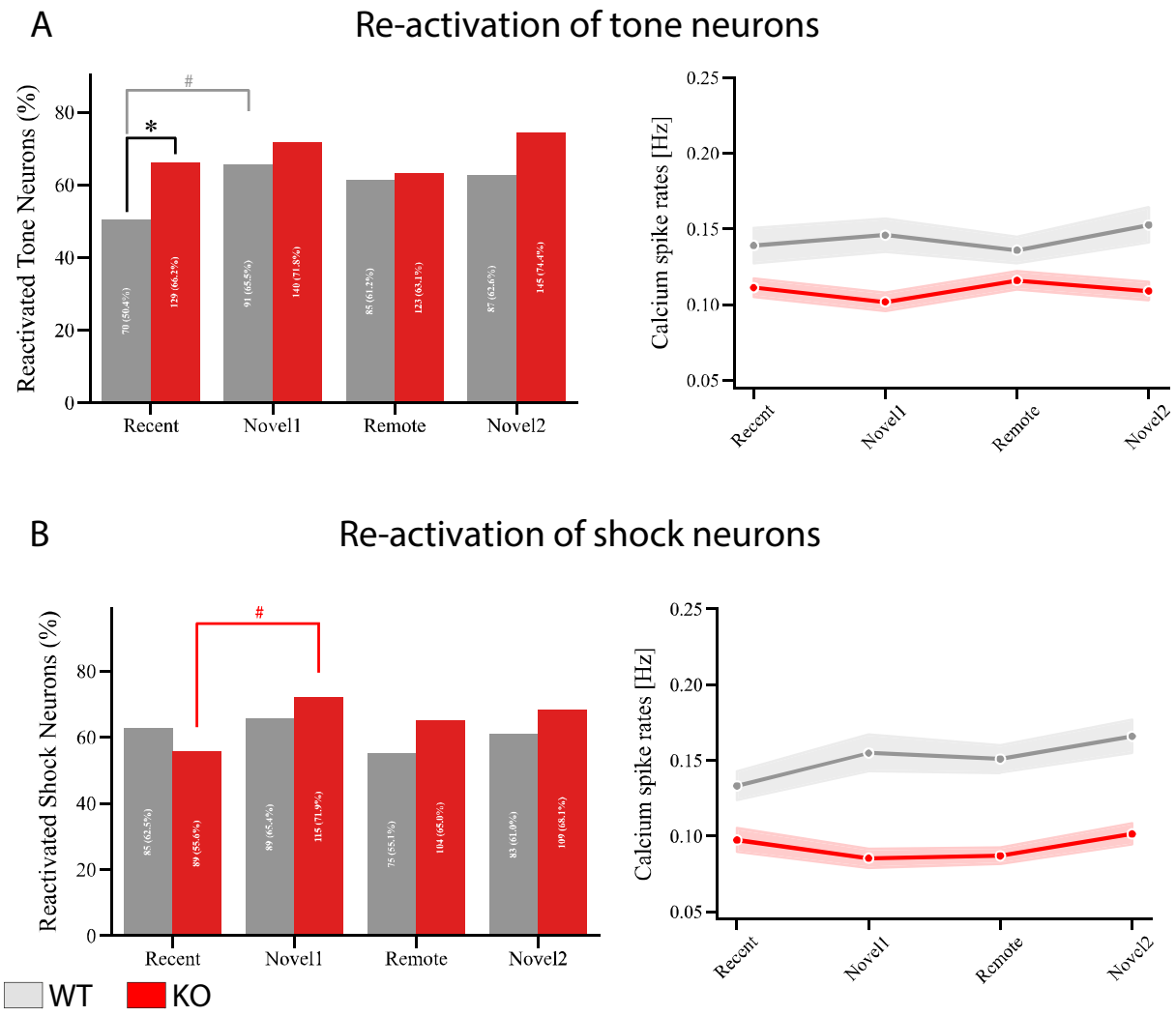


Figure 3.7-4 Reactivation of tone and shock neurons A) The fraction of reactivated Tone neurons in recent and remote sessions (left, chi-square test). The calcium rate of re-activated tone neurons (right, one-way anova). B) The same as for A but for shock neurons

WT neurons exhibited a reactivation of 64% ± 32% for tone-neurons, while KO tone-neurons showed a slightly higher reactivation of 77% ± 19%. Only during the recent session, a significant difference was observed, with a higher tone-reactivation in KO neurons ($\chi^2(1) = 4.08$, $p < 0.05$).

For shock neurons, WT showed a reactivation of 64% ± 33%, whereas KO neurons exhibited a slightly higher reactivation percentage of 75% ± 20%. Overall, no difference was noted in the reactivation of shock-neurons between WT and KO across the sessions.

The calcium spike rate dynamics of shock and tone-neurons were examined across the different sessions to understand how neuronal activity varied in context and novel exposure within these neurons.

For WT neurons, there was no significant difference in the calcium spike rate between tone-shock and tone-neurons, nor was there a significant variation across sessions. This indicates that the calcium spike rates of shock- and tone-neurons were relatively similar across sessions. The same was true for KO shock- and tone-neurons.

In summary, both shock and tone neurons exhibited comparable reactivation in KO and WT neurons, with no notable differences in calcium spike rate across the sessions for either neuron type or genotype.

3.7.4 Slight Reactivation of Place Cells

Understanding whether place cells remain active across different phases of memory retrieval is important for investigating their role in the stability and adaptability of context-dependent memory. Here, we examined whether neurons identified as place cells during encoding, either pre-shock or post-shock, continued to exhibit place-cell properties during the recent, remote, novel1, and novel2 tests. Furthermore, if a neuron was identified as a place cell in recent memory, it would still qualify as a place cell in retrospective and prospective sessions.

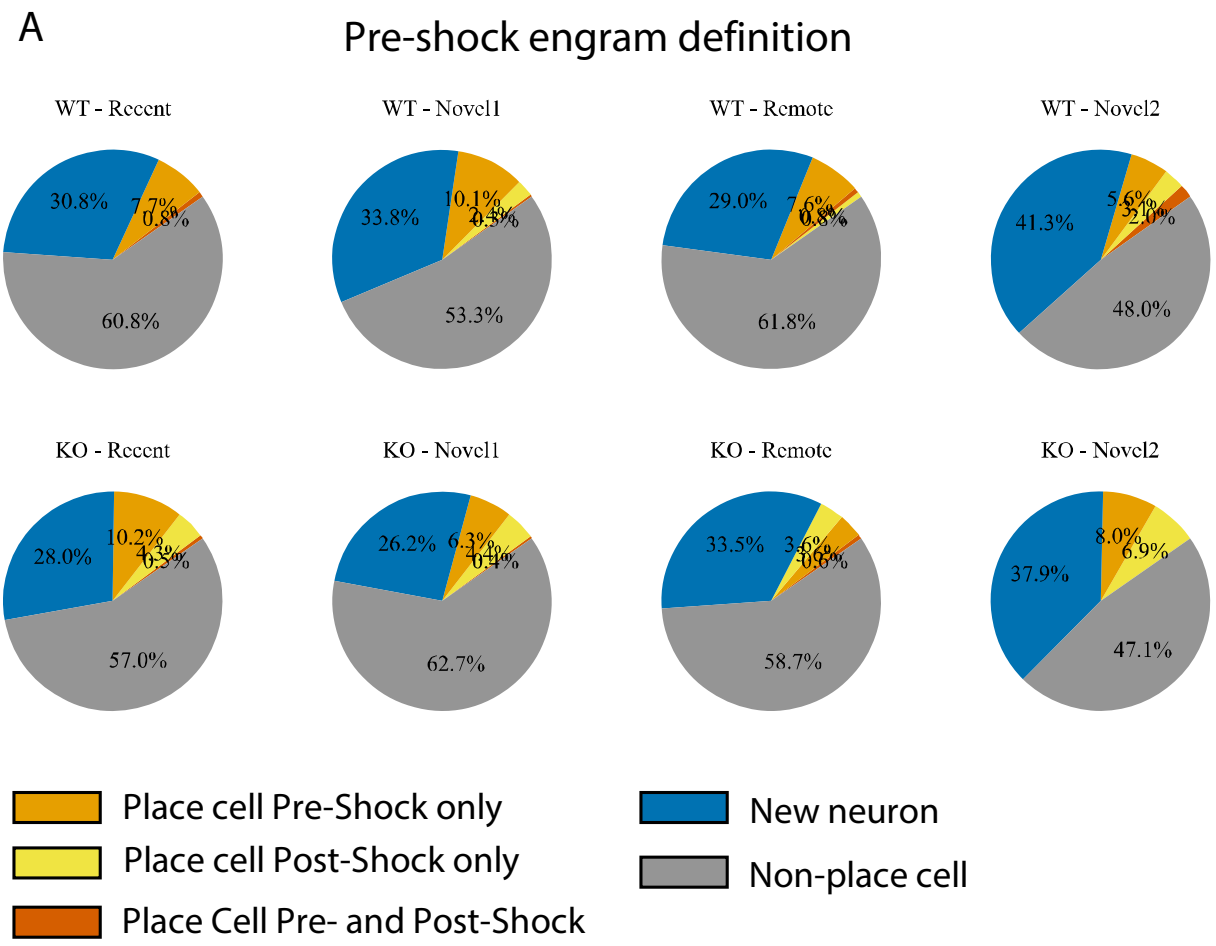


Figure 3.7-5 Place cell reactivation from the conditioning session

In WT neurons, pre-shock place cells demonstrated a small persistence across various sessions. These neurons showed reactivation of 7.7% in the recent session, 7.6% during the remote session, 10.1% in novel1, and 5.3% in novel2 of the place cells in each session. In contrast, post-shock place cells were less reactivated, comprising less than 1% in both the recent and remote sessions and under 4% in novel1 and novel2. More than 50% of the place cells were reactivated neurons that had not previously been classified as place cells, and approximately 30% of the place cells were new neurons. The proportion of reactivated non-place cells and new neurons classified as place cells was comparable between WT and KO. However, the KO neurons showed a higher fraction of post-shock place cell reactivation (Figure 3.7-5).

For engram neurons defined based on the recent session, the place cells reactivation was >5% for WT in the prospective session and < 5 % in retrospective sessions. The variability in KO, both retrospective and prospective, was minimal, ~8% of the place cells of a given day. For both WT and KO, a larger % of the place cells, 33-45%, are from new neurons (Figure 3.7-6).

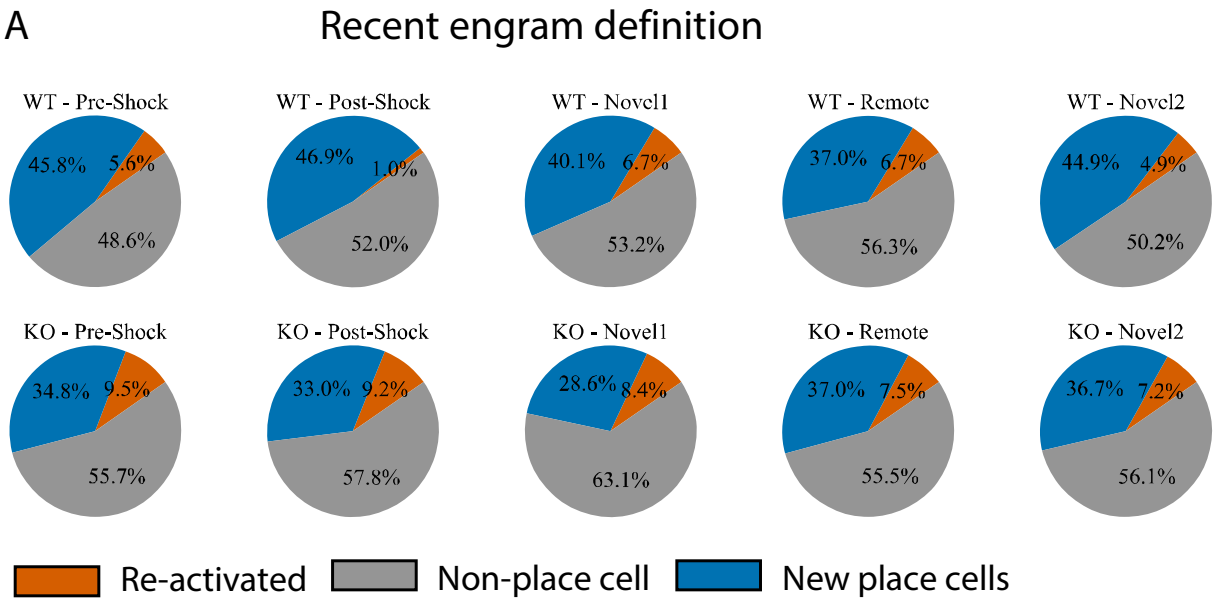


Figure 3.7-6 Place cell reactivation from the Recent session

In WT and KO, a greater percentage of place cells, ranging from 30-45%, originates from new neurons, reflecting the ratio of new neurons each day to the neuron count (Figure 3.7-5, Figure 3.7-6). This indicates that the place cells consist of both reactivated and newly activated neurons.

Discussion

4 Discussion

The dynamic signature of neuronal activity by which the hippocampus encodes and retrieves episodic memories is not well understood. In this study, we aimed to understand the role of Arc/Arg3.1 in memory engrams and how these engrams are encoded and reactivated during memory retrieval. Arc/Arg3.1 is recognized for its critical association with synaptic plasticity and memory consolidation. It is frequently used as a marker of neuronal activity and, in some studies, to tag neurons that become part of an engram. The removal of Arc/Arg3.1 from the brain has been shown to impair learning and memory, making our knockout mice a valuable tool for studying the role of Arc/Arg3.1 in memory engram encoding and retrieval. What is the impact of Arc/Arg3.1 on the life cycle of an engram, from encoding to retrieval? Here, we investigate which types of neurons become part of an engram, e.g. place cells, shock neurons, or freeze neurons.

4.1 Arc/Arg3.1 KO Mice Exhibit Reduced Exploratory Behavior in the Open Field Test

We observed that, after exposing the two mouse groups to the open field for three consecutive days, the KO group showed a significant reduction in exploration, as indicated by the total distance traveled (Figure 3.2-1). Previous research conducted in our lab found that KO mice did not exhibit changes in exploratory and emotional behaviors during the open field and elevated plus maze tests (Plath et al., 2006). However, this earlier study only assessed the exploratory behavior of the mice in a single exposure to an open-field arena. For our investigation, we placed the mice in the same arena for 10 minutes over three consecutive days. As in the previous study, during the first day, there was no difference between WT and KO. However, by the second day, we noticed that the KO mice displayed reduced movement and exploratory behavior compared to the WT mice. This pattern was also observed in mice without any lens implants, emphasizing that this difference is not due to surgical operations or miniscope carrying. Generally, a decrease in exploration over repeated exposures indicates good habituation to an environment. In our study, KO mice appeared to habituate to the arena more quickly than WT mice, prompting the question of whether KO mice truly habituate faster, or whether their lower exploratory drive might be the cause. Which only becomes apparent after the initial novelty drive has diminished. Our results are not in line with (Managò et al., 2016), who utilize a different generated Arc/Arg3.1 knockout mouse (Wang et al., 2006). They observed no differences in exploratory behavior between KO and WT mice, even after 1 hour in the open field. They used a different generated Arc/Arg3.1 knockout mouse, where a construct with an EGFP

and a Neo cassette was inserted immediately after the ATG start codon of the Arc/Arg3.1 gene. The findings reported by (Managò et al., 2016) were also questioned by colleagues from the lab in earlier studies (Gao et al., 2019).

4.2 Context-Dependent Modulation in Neural Activity

4.2.1 Disrupted Translation of Neural Activity to Calcium Signaling in Arc/Arg3.1 KO

Recording neural activity with fluorescence-based calcium indicators has become a widely used approach in neuroscience. Calcium can enter the cell body through various pathways, such as NMDA receptors, voltage-gated calcium channels (VGCC), nicotinic acetylcholine receptors (nAChR), and transient receptor potential type C channels (TRPCC). Or be released from internal stores, such as endoplasmic reticulum calcium and mitochondria. However, the influx through VGCC during the firing of an action potential is primarily what is recorded using somatic calcium imaging techniques (Ali & Kwan, 2020; Grienberger & Konnerth, 2012).

We observed a significant reduction in calcium spikes in KO neurons compared to WT neurons. Notably, this reduction was consistently observed across all behavioral paradigms, open field exploration, and contextual fear conditioning sessions. This suggests that the diminished neuronal activity in KO neurons is not merely a byproduct of behavioral state differences such as attention, arousal, or aversion, but rather reflects a more fundamental alteration in KO. This reduction was not apparent in the analysis of calcium events; it was only evident in calcium spikes and average calcium trace (Figure 3.3-2). Calcium spike deconvolution tries to estimate the underlying neural spike train from the calcium trace. While calcium event detection is more straightforward, it may overlook significant variations in firing patterns, spike totals, and neuronal coding. This method is unable to discern if a calcium event represents 4 spikes or 10; hence, it treats a large and a small event equally when both exceed a threshold. Consequently, calcium event detection might indicate no difference, whereas deconvolution uncovers a reduction in firing rates. *In vivo* electrophysiological recordings from both anaesthetized (Figure 3.4-3) and awake mice (Malkki et al., 2016) did not show any differences between the mean AP firing rates of WT and KO neurons, suggesting that the reduction in calcium spikes may stem from a deficit in calcium influx in KO neurons. The amplitude distributions of miniature excitatory postsynaptic currents (mEPSCs) were similar, and their frequency showed no significant variation (Plath et al., 2006). Additionally, the field excitatory postsynaptic potential (fEPSP) input/output function in KO mice remained unchanged (Plath et al., 2006).

One plausible explanation for the observed discrepancy between AP firing rate and calcium spike rates could stem from the differential integration of APs into detectable calcium transients in WT and KO. Specifically, multiple APs may be necessary to induce a sufficiently large increase in intracellular calcium levels to surpass the detection threshold of our miniscope imaging system in KO. Figure 3.3-3 shows that the smallest calcium events detected in WT mice exhibit dF/F, approximately half of what was observed in KO mice. This implies that the detection threshold for calcium events may selectively favor higher-amplitude transients in the KO group, effectively censoring smaller, subthreshold calcium fluctuations. Consequently, even if AP rates are comparable between WT and KO, the deconvolution of calcium traces will yield a higher frequency of detected calcium spikes in WT animals, since more of the AP-induced calcium influx exceeds the detection threshold.

This suggests that the reduction in calcium activity may inherently arise from impairments in the coupling between action potentials and calcium influx. In other words, Arc/Arg3.1 appears to be necessary to effectively translate AP into calcium signals, a process fundamental to activity-dependent plasticity. Arc/Arg3.1 might indirectly impact NMDA subunit composition, which would affect calcium permeability, since Arc/Arg3.1 protein is found in the postsynaptic density (PSD) and copurifies with the NMDA receptor complex. Alternatively, Arc/Arg3.1 knockout neurons could exhibit changes in ion channel distribution in dendrites. As Arc/Arg3.1 has been shown to regulate spine structure and actin dynamics, potentially reducing the effectiveness of dendritic spikes. Another possibility is that Arc/Arg3.1 influences the integration of synaptic input. Research has indicated that Arc/Arg3.1 impacts oscillatory network activity (Gao 2019), for example, shown as a decrease in theta power. The decrease in theta power observed in Arc/Arg3.1 KO mice indicates a wider impairment in afferent input and network synchronization, reducing excitatory drive to pyramidal neurons.

4.2.2 Downregulation of Neural Activity after Conditioning

WT and KO showed similar memory encoding as measured by the percentage of freezing during acquisition (Figure 3.6-1). One of the striking findings we observed was a decrease in calcium spike rates after conditioning. This was observed for both WT and KO, where 50-60% of the neurons were inhibited, while 30% showed excitation. However, this was not specific to either genotype. Studies using electrophysiological methods did not observe a significant change after immediately conditioning (Moita et al., 2004). While studies using *in vivo* calcium imaging suggested that activity increased immediately after footshock, but the number of active

neurons decreased (Roshchina et al., 2021).

A key analytic distinction lies in our treatment of neurons classified as inactive, those exhibiting no detectable calcium transients post-shock. For neurons classified as deactivated post-shock, calcium event rates were set to a nominal baseline, with the lowest detectable frequency being 1/1800 Hz based on our imaging sampling rate (10 Hz) and the duration of the post-shock session (180 seconds). This methodological choice emphasizes the contribution of neuronal silencing to the overall population response and ensures that suppression effects are not underestimated. While (Roshchina et al., 2021) excluded all inactive neurons from the average activity, they focused solely on the active ones. The total count of active neurons before the shock was 1.7 times higher than after the shock. Other studies using *in vivo* calcium imaging suggested that activity increased after conditioning (Kobayashi & Matsuo, 2023), while (Schuette et al., 2020) reported a decrease. Although it may seem that these results are inconsistent, the data show a high level of consistency. The discrepancy in conclusion arises from the definition of pre/post-shock. Schuette et al. (2020) examined activity at least 24 hours after conditioning, which serves as a resample of the 24-hour memory test. They observed a decrease in calcium activity, a natural response of the hippocampus that allows it to distinguish between familiar and novel environments (Cohen et al., 2017; Larkin et al., 2014; Wilson & McNaughton, 1993). (Kobayashi & Matsuo, 2023) recorded calcium activity 5 minutes after conditioning, thereby providing a closer temporal alignment to our recordings. They indicated that calcium activity increased after the shock. Yet, a deeper analysis of their data shows that repeated exposure of the mice to the conditioning environment before the shock led to adaptation and a simultaneous decrease in activity rates. Since the post-shock activity was compared to the last exposure, it appeared to report an increased rate, but compared to the first context-exposure, it was clearly reduced. Thus, when excluding adaptation effects, the results of Kobayashi et al resemble our own.

Moreover, it is crucial to emphasize that, although post-shock neural activity plays a key role in conditioning, it is rarely documented in detail in imaging or electrophysiological recording paradigms. Most studies emphasize baseline activity or immediate responses to stimuli, frequently cutting the recording period short within seconds after conditioning. A major factor behind this is the experimental design: to prevent prolonged contextual exposure and reduced associative learning by extinction, mice are taken out of the conditioning context just seconds after the conditioning. Though this is common in behavioral conditioning protocols, it unintentionally restricts the opportunity to record sustained or delayed neural dynamics following conditioning.

4.2.3 Impaired Context-Dependent Neuronal Activity in Arc/Arg3.1 KO

Our findings indicate that the hippocampus downregulates its calcium activity in a familiar environment (Larkin et al., 2014), and this downregulation is dependent on Arc/Arg3.1. For example, during the OFT, we observed that the calcium activity in KO neurons did not significantly decline on the second and third days despite a reduction in the distance moved. In contrast, WT exhibited a clear decrease in activity, which we attributed to the hippocampus response to a familiar environment. The hippocampus's ability to respond to novel environments became very evident during recent and remote memory tests in contextual fear conditioning (Figure 3.6-2). The calcium activity between recent and novel, and remote and novel2 in WT showed a clear environment-specific modulation, wherein calcium activity was decreased in the familiar environment and drastically increased in the novel environment. This modulation was not seen in the KO mice. Emphasizing the role of the hippocampus in recognizing a familiar environment that depends on Arc/Arg3.1. This function of the hippocampus has also been shown by numerous other studies utilizing calcium imaging (Jimenez et al., 2020; Lee & Han, 2023). The question is whether this reduction is solely seen in context-dependent memory, or also in other types of memory. This can be explored by subjecting animals to tests that do not involve the hippocampus. For example, studies have shown that hippocampal lesions do not prevent mice from forming tone-cued fear memories, indicating that this process may be hippocampus-independent (Phillips & LeDoux, 1992). Similarly, inhibiting protein synthesis in the hippocampus using anisomycin does not impair the retrieval of tone-associated fear memories, further supporting the idea that these memories rely on extra-hippocampal structures, such as the amygdala(Balleine et al., 2003). It would be interesting to analyze the tone-memory while observing the hippocampal activity, as it is known that Arc/Arg3.1 KO mice have deficits in amygdala-dependent memory tasks (Plath et al., 2006).

4.2.4 Impaired Formation of Coordinated Activity in Arc/Arg3.1 KO

Information stored in individual neurons is labile, but it can be reliably stored in networks of correlated neurons. The collective activity of a population of neurons, beyond the properties of individual cells, is critical for encoding and retrieval of memory engrams (Cheng & Frank, 2008). Both experimental data(Gonzalez et al., 2019) and computational models have proposed that synchronous activity within the hippocampus facilitates long-term synaptic plasticity for memory formation and retrieval.

Here we demonstrate that in WT mice, calcium activity is reduced in familiar environments (Post-shock, Recent and Remote sessions) and increased in novel ones (Pre-shock, Novel1, and Novel2 session). At the same time, the number of corr-pairs, which represents the synchronicity of neurons, is inversely modulated. This suggests that more neurons become correlated with each other despite a decrease in their calcium activity. Interestingly, this opposite modulation of the corr-pairs emerged already during the post-shock episode, when both WT and KO neurons experienced a strong suppression of activity, suggesting that synchronization and activity were governed by (partially) independent mechanisms. In addition, we observed the clustering coefficient, a measure reflecting the size of correlated neuron subgroups, likewise increases in accord with the corr-pairs. The inverse modulation of activity rates and correlated activity (corr-pairs and CC) not only distinguished between the encoding of a memorized context and the novel ones, it also clearly differentiated between WT and KO mice. We therefore argue that these two factors constitute, together, a clear signature of long-term memory ensembles.

The role of correlated network activity in encoding memory, had been addressed by a number of recent studies. The co-activation of neurons with synchronous activity persisted for several weeks. The likelihood that a neuron remains active across days is proportional to the number of neurons with which its activity is synchronized (Gonzalez et al., 2019) (Chen et al., 2023). The study by (Jimenez et al., 2020), identified some neuron types that were important for this correlation. They reported that during memory retrieval, a population of vCA1 neurons became correlated with shock-encoding neurons, and the magnitude of synchronized activity within this population was proportional to memory strength. (Kinsky et al., 2025) reported that the coactivation of freeze-predictive neurons increased significantly by 0–2 before freezing onset and (Ghandour et al., 2019) demonstrated that the synchronous activity exhibited by engram cells related to a single event does not originate from a single large group of neurons but instead results from the activity of multiple smaller sets of sub-ensembles.
This indicates that the identity of neurons in the observed enhanced co-activation could play a crucial role in memory retrieval. As detailed in the following section, we were able to identify multiple distinct neuronal subpopulations, including place cells, freeze-neurons, shock-encoding neurons, and tone-coding neurons. Some of these specialized cell types may drive elevated patterns of co-activation, thereby forming sub-ensembles that are critically involved in memory retrieval.

4.2.5 Coordinated Activity May be Supported by Early and Late Arc/Arg3.1 Expression

The concept of the engram is still hypothetical in neuroscience. Currently, there is no unified definition of an engram. Our approach to defining engram neurons primarily depends on the activity levels of neurons. Following the ideas of (Kim et al., 2014; Mocle et al., 2024; Reijmers et al., 2007), we have defined engram neurons as those that are highly activated either during the pre-shock activity or during the retrieval session. The fraction of reactivated engram neurons based on both the pre-shock session and recent session definition is consistent across sessions and genotypes. Proposing that simply reactivating highly active neurons does not suffice for accurate memory retrieval. Regardless of the specific engram used, engram neurons exhibited higher calcium spike rates than non-engram and newly formed neurons (Mocle et al., 2024). This was consistent for both WT and KO. However, engram neurons showed the largest calcium spike rate context-dependent modulation in WT, which is not seen in KO. Memory discrimination was seen in the neuronal group with the highest correlation activity. In the pre-shock-session definition, WT engram neurons showed a high correlation in the recent memory but continuously decreased in subsequent sessions. However, the new neuron showed a context-dependent modulation of the corr-pairs, like the overall corr-pairs. This modulation was not given in KO. This suggests that Arc/Arg3.1 coordinates the correlated activity of two neuronal populations, where the first group is primarily important in the recent memory retrieval but not remote, and the second group plays a prominent role in both recent and remote memory retrieval. During the conditioning session, a specific subset of neurons is activated, corresponding to the first Arc/Arg3.1 expression wave. In the offline state post-conditioning, a second wave of Arc/Arg3.1 expression occurs. As shown by (Nakayama et al., 2015), Arc/Arg3.1 expression increases immediately and 12 h after conditioning in CA1. This may serve dual purposes: reinforcing the initially activated neuronal ensemble and recruiting additional neurons that were not engaged during the pre-shock or initial learning episode.

These newly recruited neurons may be critical for the stabilization and long-term retention of the memory trace, thereby contributing to both recent and remote memory retrieval. This dual engagement may explain why engram cells identified using the recent session exhibit context-dependent modulation. They likely represent a heterogeneous population comprising both pre-shock neurons and newer neurons activated during the offline state.

4.3 dCA1 Sensory Encoding Remains Almost Intact in Arc/Arg3.1 KO

The ability of the hippocampus to link various stimuli plays a crucial role in long-term memory, though the mechanism by which neurons encode these associative memories remains unclear.

Here, we examined how the hippocampus encodes behaviorally relevant sensory and contextual information in both WT and KO mice. Consistent with prior literature, we identified functionally distinct neuronal populations, including place cells, tone-neurons, shock-neurons, and neurons selectively active during behavioral states such as mobility and freezing. These findings support the view of the hippocampus as a multimodal integrator, dynamically linking environmental cues with internal states to support memory formation.

4.3.1 Place Cell Development in a Non-Aversive Environment Unaffected in Arc/Arg3.1 KO

Our findings indicate that the percentage of place cells is comparable between WT and KO mice in the open fields (10-25%), suggesting that Arc/Arg3.1 did not affect the generation of place cells despite the decrease in calcium spike rate. However, we observed weakened spatial encoding in KO, which may be due to the reduced calcium spiking activity or the direct correlation with the reduced exploratory behavior observed in KO. Both of which can diminish the statistical significance in identifying a place cell. However, in a linear track experiment using the same Arc/Arg3.1 KO, there was likewise no difference in place cell size (Malkki et al., 2016). We generally observed a smaller fraction of place cells compared to other studies, (van der Veldt et al., 2021) observed >20% place cells in the open field, >25% in the linear track (Ziv et al., 2013), (Wirtshafter & Disterhoft, 2022) >70% in linear track. In the open-field tests, we relied exclusively on the mice's natural exploratory behaviors. Natural exploration declines rapidly in the absence of negative or positive rewards. The decline in exploration significantly reduces the chances of revisiting the same locations and hence limits the detection of place cells. In other studies, mice were typically deprived of food or water. During this experiment, mice foraged for food, milk, or sucrose solution, or were trained to run back and forth for water rewards at the ends of a linear track. This increases the chances for the mice to revisit the same locations multiple times.

4.3.2 Expansion of Place Field Coverage Drives Context-Dependent Memory

Across the various contextual fear conditioning, both WT showed a change in the fraction of place cells (5-19%). During novel exposure (pre-shock, novel1, and novel2), there is a slightly nonsignificant higher fraction of place cells compared to the familiar environment (post-shock, recent, and remote). This aligns with the notion that during repeated exposure to an environment, the number of place cells decreases (Kinsky et al., 2018). The decrease in WT can be

attributed to the decreased mobility associated with the recent and remote sessions. KO showed a change in the fraction of place cells, though to a lesser extent, aligned with the absence of diminished freezing in both recent and remote sessions. However, we noticed a distinct change in place field coverage based on whether the exposure was novel or familiar. In WT, place field coverage increased during exposure to the familiar environment compared to the novel one. This pattern was not observed in KO. This increase in place coverage occurred right after the conditioning, in the post-shock session, suggesting a rapid integration of contextual and emotional information in WT. Whereas KO showed a decrease in place cell coverage in the post-shock period. Expansion of place cell coverage might "bind" contextual elements more effectively, while insufficient expansion might prevent the association of spatial context with the conditioning, resulting in deficits in context-specific memory recall. In alignment with our data (Moita et al., 2004) reported an increase in place field size following shock. In contrast, fear conditioning was found to lead to a decrease in field size after conditioning day by (Schuette et al., 2020).

4.3.3 Mobility Neurons Exhibit Context-Dependent Variability

While place cell encoding is a central feature of the dCA1 region, it can also encode various other movement-related neurons. This includes a diverse range of mobility-neurons, such as place cells, speed cells, and border cells. Together, these neurons contribute to shaping the spatial map of the hippocampus(Behrens et al., 2018).

In the pre-shock session, 47% of WT neurons were mobility-neurons, compared to only 30.7% in KO neurons. Proposing that WT could incorporate additional mobility-related inputs, which are absent in KO. Following the conditioning, the percentage for both genotypes decreased significantly to approximately 11%, likely due to the increased freezing that occurred post-shock. In WT neurons, 52% of post-shock mobility neurons were also mobility neurons in the pre-shock. In contrast, for KO neurons, this percentage was significantly lower, around 30%. While there is no clear explanation for it, it is interesting that during pre-shock, WT has a higher percentage of neurons showing mobility-neurons, despite the fact that both WT and KO showed similar freezing levels in the pre-shock period. A possibility is that the reduced calcium spiking activity diminishes the statistical power in identifying mobility-neurons.

In the memory tests (recent, remote, novel1, and novel2), WT and KO showed comparable percentage variation in mobility-neurons, with higher percentages noted in novel1 and novel2 compared to recent and remote, respectively. This variation is not linked to memory, as WT has

significantly lower mobility in both recent and remote contexts compared to KO. However, the percentage of variation correlated with whether the environment is familiar or novel.

4.3.4 Conserved Freeze Neuron Activity in Arc/Arg3.1 KO

In contextual fear conditioning, freezing behavior in a context environment serves as an indicator of learning. Thus, we questioned whether we could identify freeze-neurons, such as those that exhibited heightened activity during freezing periods (Kinsky et al., 2025; Schuette et al., 2020). During the pre-shock session, freezing episodes were few and short in both WT and KO and concurrently, the percentage of freeze-neurons was low. Whereas, post-shock both WT and KO exhibited a 1.4-2-fold rise in the proportion of freeze neurons. Although there was an increase in freezing during both recent and remote memory tests, we found that the relative fraction of freeze neurons remained comparable to the pre-shock levels, not only for KO but also for WT. These findings suggest that the fraction of neurons classified as freeze neurons does not scale with the total duration of freezing behavior. This could reflect a categorical encoding strategy, where the presence of a behavioral state (e.g., freezing) is sufficient to engage a dedicated circuit, independent of its duration.

Interestingly, it was shown by (Schuette et al., 2020) that nearly 40% of the freeze neurons had sufficient spatial selectivity to qualify as place cells. However, they showed that freeze cells were responsive during freeze events across various locations in the context, suggesting that freeze-activated place cells independently indicate spatial location and freeze behavior, as freeze-activated place cells recruited by single freeze events shared no common spatial coding. The conjunction of freeze and place coding is a measure that we could not reproduce, although our definition of place cells aligns with Schuette's, the identification of freeze neurons differed. Schuettes characterized neurons as freeze-neurons by employing a generalized linear model (GLM) to identify cells that exhibited heightened calcium trace activity during freezing epochs, using freeze epochs as the predictor variable. For the GLM, they used the entire calcium trace, which can give a neuron a dual ability, acting as a freeze neuron and a place cell neuron. In our case, a neuron can either be classified as freeze- or mobility-neurons, but it can never be both. As a result, a significant portion of our neurons, approximately 65%, remained unclassified (Figure 3.6-3). These “other neurons” may possess both freeze neuron functionality and spatial coding capabilities as shown by Schutte. Another reason for the difference may arise from the definition of periods used to identify place cells. We excluded the transition between freezing and mobility to ensure that no trailing calcium spikes were included in the mobility period.

4.3.5 Intact Encoding of Conditioned and Unconditioned Stimuli in Arc/Arg3.1 KO

Here, we discuss how neurons in WT and KO dCA1 encode the association between conditioned stimuli (CS) and unconditioned stimuli (US). Our previous findings (Figure 3.5-3) indicated that both WT and KO generally suppressed their activity after the conditioning, primarily due to a reduction in response triggered by the tone introduction.

The tone and foot shock activated distinct small, non-overlapping groups of neurons. Approximately 8% of the neurons responded positively to either the tone or shock in both WT and KO groups, while neurons responding to both stimuli were scarce (<1%). This similarity between KO and WT suggests that the loss of Arc/Arg3.1 did not affect the number of sensory-specific neurons in CA1. Although the fraction preference of dCA1 neurons stayed consistent, their activity rates after the shock were affected differently. The majority (60%) of tone neurons were excited, and roughly 30% were inhibited, post-shock, in both WT and KO mice. In contrast, most shock neurons (60%) were inhibited in WT mice compared with only 30% in the KO. Both WT and KO mice displayed heightened freezing after the shock, suggesting that the activity of these neurons is not critical for the execution of freezing behavior. Instead, shock-neuron activity could be important for encoding of the aversive memory over longer time periods and its disruption could manifest as a deficit in contextual fear memory. In line with our observations, it has been shown that aversive stimuli activated dCA1 interneurons via cholinergic input, leading to the inhibition of pyramidal cells receiving aversive sensory excitation from the entorhinal cortex (Lovett-Barron et al., 2014). Recent studies highlight the significance of shock neurons as key hubs in memory retrieval. They are typically more co-activated with other neurons (Jimenez et al., 2020) and have a higher capacity for encoding spatial information (Mocle et al., 2024)

4.4 How does Arc/Arg3.1 affect context encoding and memory: a model

Our data indicates that Arc/Arg3.1 functions as a context-dependent modulator of neural activity, coordinating correlated activity between neurons in the dCA1 region related to episodic memory. During repeated exposure to a natural environment, calcium activity showed a slight decline compared to first exposure, which is not seen in the KO. During initial exposure to a novel environment or stimulus, Arc/Arg3.1 is rapidly induced in response. This results in the modification of synaptic strength through LTP. Repeated exposure to the same context

diminishes the need for dramatic changes in synaptic strength. This results in a reduction of synaptic plasticity after initial encoding. Synaptic connections become stronger and more stable, which reduces the overall network plasticity and spontaneous firing required to represent that environment. This becomes evident in the CFC, where the activity in familiar environments was significantly lower than in novel environments. However, this could also result from Arc/Arg3.1's function in memory consolidation, as Arc/Arg3.1 is important for the consolidation of LTP. Firstly, the rapid emergence (within minutes) of correlated activity aftershock was observed in WT but not KO, which is likely to reflect preexisting differences in hippocampal functional connectivity, as previously shown (Gao, 2018; Gao, 2019). Secondly, despite the decreased activity, WT showed increased corr pairs and the group size of correlated neurons. This may indicate the role of Arc/Arg3.1 in homeostatic synaptic scaling by modulating synaptic strengths to uphold network stability. In cultured hippocampal neurons, chemically induced LTP leads to a selective increase in correlated activity among Arc/Arg3.1-positive neurons (Jiang & VanDongen, 2021).

4.5 Experiment Limitation

Miniscope technology has revolutionized the field of neuroscience by enabling large-scale calcium imaging in freely behaving animals, providing unprecedented insights into neural dynamics. However, despite its advantages, several technical and analytical limitations must be considered when interpreting miniscope-derived data.

The use of GRIN lenses introduces optical aberrations, scattering, and out-of-focus fluorescence, which can reduce SNR and impair the ability to resolve densely packed neurons, as is the case in the dCA1. Therefore, optimizing the CNMFe for each mouse separately was necessary for us. Having the same parameters leads to many false-positive or false-negative neurons. However, changing the parameters for each can introduce inconsistencies. As the parameters are tuned based on visual inspection, subjective bias may have been introduced. Why other methods of extraction, like Suite2p(Pachitariu et al., 2017) and EXTRACT (Dinç et al., 2024), could have been used to benchmark the results.

Secondly, we use GCaMP to infer neuronal activity. We did not suspect that the viral injection of GCaMP would have different efficacy in WT and KO mice. Neither did we observe an obvious difference in the histology. However, the histology was performed on mice that had already been implanted, where the brain tissue was massed and damaged due to surgical

procedures. Therefore, it is necessary to conduct a systematic experiment comparing GCaMP efficacy in WT and KO mice.

Lastly, the question of dealing with inactive or deactivated neurons. For example, after the conditioning, there was a huge deactivation of neural activity. We used a nominal null calcium spike rate, giving all neurons without a detectable calcium spike a calcium spike rate of 1/1800 Hz. In comparison, studies as (Roshchina et al., 2021) excluded these neurons. We excluded inactive neurons when the miniscope was detached and reattached between sessions. However, neural inactivation can also be a code for encoding, as (Pérez-Ortega et al., 2024) suggested. They investigated responses of visual cortical neurons in awake mice. They identified neurons activated by the visual stimulus (termed "onensemble"), as well as neurons that are specifically inactivated (termed "offensemble"). In response to the visual stimuli, each ensemble (onsemble+offsemble) exhibited small trial-to-trial variability.

Interestingly, (Vanwalleghem et al., 2020) questioned the common assumption that neuronal activity measured through calcium indicators is exclusively non-negative. They propose that negative changes in baseline calcium influence neural activity, and reinforcing non-negativity may overlook genuine neuronal responses.

5 Future Perspectives

Investigating memory consolidation through in vivo calcium imaging and Arc/Arg3.1-KO presented a rich ground for future research.

Firstly, a particularly promising direction is the combined use of patch-clamp electrophysiology with calcium imaging. This enables direct recordings of AP spiking activity with calcium dynamics. This will allow us to more accurately deconvolve calcium spikes against underlying AP and refine interpretations of calcium-based neuronal activity. Here, we could utilize either viral-GCAMP-injected mice or chemical indicators like Fura-2. Additionally, it will be important to establish if the efficacy of viral-injected GCAMP differs between WT and KO.

Secondly, we have merely begun to explore the potential for analysis directions. We should consider what should happen to inactive neurons. Which neuron types show enlarged place fields? Which neurons are correlated, and do these correlations persist over several days, or do neurons change partners continuously? How large groups do neurons form? Can a decoder be used to predict freezing based on a subset of neurons' firing patterns?

Thirdly, to further conceptualize the neural activity within learning, consolidation, and retrieval, and the impact of Arc/Arg3.1 on these, longitudinal spatial memory tasks such as the Barnes

maze or Morris Water Maze could be employed. Unlike single-trial learning paradigms like contextual fear conditioning, these mazes will allow us to track multi-day learning, retention, and flexible/partial retrieval, thereby observing how neural representations evolve with learning, consolidation, and behavioral performance.

Appendix

6 Supplementary

6.1 Supplementary tables

Stats-table 1 Distance travelled with and without a miniscope: Mixed ANOVA for genotype X OFT-days Section 1: ANOVA Findings Section 2: Comparisons Between Groups; Section 3: Comparisons Within Groups - paired two-sample t-tests with the Sidak correction

Source	SS	DF1	DF2	MS	F	p-unc	np2
Genotype	7758962.37	1	19	7758962.37	21.41	0	0.53
Day	10545742.89	2	38	5272871.45	23.42	0	0.55
Interaction	426770.45	2	38	213385.22	0.95	0.4	0.05

Day	Day	A	B	mean(A)	std(A)	mean(B)	std(B)	T	dof	p-unc	p-corr	p-adjust	cohen
OFT-day1	OFT-day1	WT	KO	3163.67	687.2	2245.04	474.11	3.59	17.79	0	0.01	sidak	1.54
OFT-day2	OFT-day2	WT	KO	2319.02	616.04	1648.42	314.53	3.18	15.17	0.01	0.02	sidak	1.35
OFT-day3	OFT-day3	WT	KO	2012.2	574.29	1493.4	281.3	2.67	14.83	0.02	0.05	sidak	1.13

Genotype	A	B	mean(A)	std(A)	mean(B)	std(B)	T	dof	p-unc	p-corr	p-adjust	cohen
WT	OFT-day1	OFT-day2	3163.67	687.2	2319.02	616.04	2.94	10	0.01	0.04	sidak	1.29
WT	OFT-day1	OFT-day3	3163.67	687.2	2012.2	574.29	3.94	10	0	0.01	sidak	1.82
WT	OFT-day2	OFT-day3	2319.02	616.04	2012.2	574.29	2.08	10	0.06	0.18	sidak	0.52
KO	OFT-day1	OFT-day2	2245.04	474.11	1648.42	314.53	3.63	9	0.01	0.02	sidak	1.48
KO	OFT-day1	OFT-day3	2245.04	474.11	1493.4	281.3	6.41	9	0	0	sidak	1.93
KO	OFT-day2	OFT-day3	1648.42	314.53	1493.4	281.3	1.38	9	0.2	0.49	sidak	0.52

Stats-table 2 Mice with a miniscope: Mixed ANOVA for genotype X OFT-days Section 1: ANOVA Findings Section 2: Comparisons Between Groups; Section 3: Comparisons Within Groups - paired two-sample t-tests with the Sidak correction

Source	SS	DF1	DF2	MS	F	p-unc	np2
Genotype	11182409.01	1	18	11182409.01	20.19	0	0.53
Day	6585972.73	2	36	3292986.36	19.9	0	0.53
Interaction	695308.38	2	36	347654.19	2.1	0.14	0.1

Day	Day	A	B	mean(A)	std(A)	mean(B)	std(B)	T	dof	p-unc	p-corr	p-adjust	cohen
OFT-day1	OFT-day1	WT	KO	2965.36	855.76	2399.9	373.16	1.92	18	0.07	0.2	sidak	0.86
OFT-day2	OFT-day2	WT	KO	2736.44	703.83	1669.79	248.32	4.52	18	0	0	sidak	2.02
OFT-day3	OFT-day3	WT	KO	2354.94	382.18	1396.79	441.16	5.19	18	0	0	sidak	2.32

Genotype	A	B	mean(A)	std(A)	mean(B)	std(B)	T	dof	p-unc	p-corr	p-adjust	cohen
WT	OFT-day1	OFT-day2	2965.36	855.76	2736.44	703.83	1.1	9	0.3	0.66	sidak	0.29
WT	OFT-day1	OFT-day3	2965.36	855.76	2354.94	382.18	2.88	9	0.02	0.05	sidak	0.92
WT	OFT-day2	OFT-day3	2736.44	703.83	2354.94	382.18	1.93	9	0.09	0.23	sidak	0.67
KO	OFT-day1	OFT-day2	2399.9	373.16	1669.79	248.32	6.18	9	0	0	sidak	2.3
KO	OFT-day1	OFT-day3	2399.9	373.16	1396.79	441.16	5.38	9	0	0	sidak	2.46
KO	OFT-day2	OFT-day3	1669.79	248.32	1396.79	441.16	1.81	9	0.1	0.28	sidak	0.76

Stats-table 3 WT-control miniscope effect : Mixed ANOVA for miniscope(True/False) X OFT-days Section 1: ANOVA Findings Section 2: Comparisons Between Groups miniscope on(True) and miniscope off(False);

Source	SS	DF1	DF2	MS	F	p-unc	np2
MiniScope	551165.03	1	19	551165.03	0.78	0.39	0.04
Day	8541661.64	2	38	4270830.82	15.08	0	0.44
Interaction	1182843.46	2	38	591421.73	2.09	0.14	0.1

Day	A	B	mean(A)	std(A)	mean(B)	std(B)	T	dof	p-unc	p-corr	p-adjust	cohen
OFT-day1	FALSE	TRUE	3163.67	687.2	2965.36	855.76	0.58	17.3	0.57	0.92	sidak	0.26
OFT-day2	FALSE	TRUE	2319.02	616.04	2736.44	703.83	-1.44	18.03	0.17	0.42	sidak	-0.63
OFT-day3	FALSE	TRUE	2012.2	574.29	2354.94	382.18	-1.62	17.5	0.12	0.32	sidak	-0.7

Stats-table 4 Arc/Arg3.1-knockout miniscope effect : Mixed ANOVA for miniscope(True/False) X OFT-days Section 1: ANOVA Findings Section 2: Comparisons Between Groups miniscope on(True) and miniscope off(False);

Source	SS	DF1	DF2	MS	F	p-unc	np2
MiniScope	10562.39	1	18	10562.39	0.06	0.82	0
Day	8370993.87	2	36	4185496.93	40.2	0	0.69
Interaction	158295.48	2	36	79147.74	0.76	0.47	0.04

Day	A	B	mean(A)	std(A)	mean(B)	std(B)	T	dof	p-unc	p-corr	p-adjust	cohen
OFT-day1	FALSE	TRUE	2245.04	474.11	2399.9	373.16	-0.81	18	0.43	0.81	sidak	-0.36
OFT-day2	FALSE	TRUE	1648.42	314.53	1669.79	248.32	-0.17	18	0.87	1	sidak	-0.08
OFT-day3	FALSE	TRUE	1493.4	281.3	1396.79	441.16	0.58	18	0.57	0.92	sidak	0.26

Stats-table 5 Fraction of neurons active in a given day : 2-way ANOVA for Genotype X OFT-days. Section 1: ANOVA Findings Section 2: Comparisons Between Groups; Section 3: Comparisons Within Groups - unpaired two-sample t-tests with the Sidak correction

Source	SS	DF	MS	F	p-unc	np2
Genotype	1567.96	1	1567.96	17.4	0	0.27
Day	9.09	2	4.55	0.05	0.95	0
Genotype * Day	72.68	2	36.34	0.4	0.67	0.02
Residual	4234.59	47	90.1			

Day	Day	A	B	mean(A)	std(A)	mean(B)	std(B)	T	dof	p-unc	p-corr	p-adjust	cohen	A_count	B_count
OFT-day1	OFT-day1	WT	KO	79.27	11.31	89.64	3.51	-2.35	6.82	0.05	0.15	sidak	-1.36	7	10
OFT-day2	OFT-day2	WT	KO	76.6	16.93	90.67	4.44	-2.29	7.78	0.05	0.15	sidak	-1.21	8	10
OFT-day3	OFT-day3	WT	KO	79.31	11.26	87.75	5.64	-1.94	9.79	0.08	0.23	sidak	-0.99	8	10

Genotype	A	B	mean(A)	std(A)	mean(B)	std(B)	T	dof	p-unc	p-corr	p-adjust	cohen	A_count	B_count
KO	OFT-day1	OFT-day2	89.64	3.51	90.67	4.44	-0.57	18	0.57	0.92	sidak	-0.26	10	10
KO	OFT-day1	OFT-day3	89.64	3.51	87.75	5.64	0.9	18	0.38	0.76	sidak	0.4	10	10
KO	OFT-day2	OFT-day3	90.67	4.44	87.75	5.64	1.29	18	0.21	0.51	sidak	0.58	10	10
WT	OFT-day1	OFT-day2	79.27	11.31	76.6	16.93	0.36	12.25	0.72	0.98	sidak	0.18	7	8
WT	OFT-day1	OFT-day3	79.27	11.31	79.31	11.26	-0.01	12.72	0.99	1	sidak	0	7	8
WT	OFT-day2	OFT-day3	76.6	16.93	79.31	11.26	-0.38	14	0.71	0.98	sidak	-0.19	8	8

Stats-table 6 Calcium spike rate: 2-way ANOVA for Genotype X OFT-days . Section 1: ANOVA Findings Section 2: Comparisons Between Groups; Section 3: Comparisons Within Groups - unpaired two-sample t-tests with the Sidak correction

Source	SS	DF	MS	F	p-unc	np2
Genotype	1.44	1	1.44	333.55	0	0.02
Day	0.12	2	0.06	13.39	0	0
Genotype * Day	0.07	2	0.03	7.88	0	0
Residual	68	15769	0			

Day	Day	A	B	mean(A)	std(A)	mean(B)	std(B)	T	dof	p-unc	p-corr	p-adjust	cohen	A_count	B_count
OFT-day1	OFT-day1	WT	KO	0.11	0.08	0.08	0.06	12.46	3490.06	0	0	sidak	0.38	1993	3065
OFT-day2	OFT-day2	WT	KO	0.1	0.07	0.08	0.06	8.21	4451.63	0	0	sidak	0.23	2323	3071
OFT-day3	OFT-day3	WT	KO	0.1	0.07	0.08	0.06	9.85	4395.44	0	0	sidak	0.28	2324	2999

Genotype	A	B	mean(A)	std(A)	mean(B)	std(B)	T	dof	p-unc	p-corr	p-adjust	cohen	A_count	B_count
KO	OFT-day1	OFT-day2	0.08	0.06	0.08	0.06	0.82	6133.96	0.41	0.8	sidak	0.02	3065	3071
KO	OFT-day1	OFT-day3	0.08	0.06	0.08	0.06	2.22	6058.71	0.03	0.08	sidak	0.06	3065	2999
KO	OFT-day2	OFT-day3	0.08	0.06	0.08	0.06	1.41	6063.9	0.16	0.41	sidak	0.04	3071	2999
WT	OFT-day1	OFT-day2	0.11	0.08	0.1	0.07	5.06	4105.19	0	0	sidak	0.16	1993	2323
WT	OFT-day1	OFT-day3	0.11	0.08	0.1	0.07	4.45	4150.99	0	0	sidak	0.14	1993	2324
WT	OFT-day2	OFT-day3	0.1	0.07	0.1	0.07	-0.6	4641.57	0.55	0.91	sidak	-0.02	2323	2324

Stats-table 7 Proportion of Place cells over days : Chi-Square Test Results analyzing the relationship between the two Place cell vs Non-Place cells. Section 1: Evaluating the proportion of Place cells across days; Section 2: Assessing the proportion of Place cells within a group over days.

	chi2	p	dof
OFT-day1	1.987286925	0.158624844	1
OFT-day2	1.273742993	0.25906567	1
OFT-day3	4.017898274	0.045019783	1

	chi2	p	dof	Genotype
OFT-day1_vs_OFT-day2	0.594810576	0.440564905	1	WT
OFT-day1_vs_OFT-day2	0.225580679	0.634820228	1	KO
OFT-day1_vs_OFT-day3	0.361842787	0.547484576	1	WT
OFT-day1_vs_OFT-day3	1.424693728	0.232632381	1	KO
OFT-day2_vs_OFT-day3	0	1	1	WT
OFT-day2_vs_OFT-day3	0.265053029	0.606669715	1	KO

Stats-table 8 Place field size over days: 2-way ANOVA for Genotype X OFT-days . Section 1: ANOVA Findings Section 2: Comparisons Between Groups; Section 3: Comparisons Within Groups - unpaired two-sample t-tests with the Sidak correction

Source	SS	DF	MS	F	p-unc	np2
Genotype	1755.02	1	1755.02	1.44	0.23	0
Day	650.41	2	325.21	0.27	0.77	0
Genotype * Day	2243.94	2	1121.97	0.92	0.4	0
Residual	3254363.89	2663	1222.07			

Day	Day	A	B	mean(A)	std(A)	mean(B)	std(B)	T	dof	p-unc	p-corr	p-adjust	cohen	A_count	B_count
OFT-day1	OFT-day1	WT	KO	89.87	38.22	87.81	34.96	0.9	1008.68	0.37	0.75	sidak	0.06	511	506
OFT-day2	OFT-day2	WT	KO	87.51	35.79	88.29	31.15	-0.34	866.96	0.73	0.98	sidak	-0.02	466	403
OFT-day3	OFT-day3	WT	KO	90.56	35.31	86.66	31.9	1.59	666.58	0.11	0.3	sidak	0.11	489	294

Genotype	A	B	mean(A)	std(A)	mean(B)	std(B)	T	dof	p-unc	p-corr	p-adjust	cohen	A_count	B_count
KO	OFT-day1	OFT-day2	87.81	34.96	88.29	31.15	-0.22	895.64	0.83	0.99	sidak	-0.01	506	403
KO	OFT-day1	OFT-day3	87.81	34.96	86.66	31.9	0.47	658.6	0.64	0.95	sidak	0.03	506	294
KO	OFT-day2	OFT-day3	88.29	31.15	86.66	31.9	0.67	622.79	0.5	0.88	sidak	0.05	403	294
WT	OFT-day1	OFT-day2	89.87	38.22	87.51	35.79	1	974.31	0.32	0.69	sidak	0.06	511	466
WT	OFT-day1	OFT-day3	89.87	38.22	90.56	35.31	-0.3	996.77	0.76	0.99	sidak	-0.02	511	489
WT	OFT-day2	OFT-day3	87.51	35.79	90.56	35.31	-1.33	949.38	0.18	0.46	sidak	-0.09	466	489

Stats-table 9 Calcium rate place cells vs non-place cells . Section 1: ANOVA Findings Section for the WT mice 2: ANOVA Findings Section for the KO mice

Source	SS	DF	MS	F	p-unc	np2	genotype
Place Cell	1.35	1	1.35	258.07	0	0.04	WT
OFT-day	0.12	2	0.06	11.08	0	0	WT
Place Cell * OFT-day	0.01	2	0	0.56	0.57	0	WT
Residual	34.68	6634	0.01				WT

Source	SS	DF	MS	F	p-unc	np2	genotype
Place Cell	0.55	1	0.55	161.51	0	0.02	KO
OFT-day	0.01	2	0	0.8	0.45	0	KO
Place Cell * OFT-day	0.07	2	0.04	10.56	0	0	KO
Residual	31.34	9129	0				KO

Stats-table 10 Freezing percentage over the different conditioning episodes : Mixed ANOVA for genotype X episodes -days Section 1: ANOVA Findings Section 2: Comparisons Between Groups; Section 3: Comparisons Within Groups - paired two-sample t-tests with the Sidak correction

Source	SS	DF1	DF2	MS	F	p-unc	np2
Genotype	2514.83	1	16	2514.83	4.02	0.06	0.2
episode	10443.51	5	80	2088.7	15.67	0	0.49
Interaction	1375.02	5	80	275	2.06	0.08	0.11

episode	A	B	mean(A)	std(A)	mean(B)	std(B)	T	dof	p-unc	p-corr	p-adjust	cohen	A_count	B_count
Base	WT	KO	7.56	5.95	12.09	6.97	-1.49	15.9	0.16	0.64	sidak	-0.69	8	10
Tone1	WT	KO	28.16	17.7	26.07	19.43	0.24	15.67	0.81	1	sidak	0.11	8	10
S1	WT	KO	9.89	4.3	25.96	12.33	-3.84	11.61	0	0.01	sidak	-1.66	8	10
Tone2	WT	KO	25.32	16.69	34.46	24.81	-0.93	15.63	0.37	0.94	sidak	-0.42	8	10
S2	WT	KO	23.14	12.26	42.91	13.3	-3.27	15.62	0	0.03	sidak	-1.54	8	10
PostS	WT	KO	33.83	13.11	44.66	13.18	-1.74	15.18	0.1	0.48	sidak	-0.82	8	10

Genotype	A	B	mean(A)	std(A)	mean(B)	std(B)	T	dof	p-unc	p-corr	p-adjust	cohen	A_count	B_count
KO	Base	Tone1	12.09	6.97	26.07	19.43	-2.5	9	0.03	0.41	sidak	-0.96	10	10
KO	Base	S1	12.09	6.97	25.96	12.33	-3.87	9	0	0.06	sidak	-1.39	10	10
KO	Base	Tone2	12.09	6.97	34.46	24.81	-3.06	9	0.01	0.19	sidak	-1.23	10	10
KO	Base	S2	12.09	6.97	42.91	13.3	-8.46	9	0	0	sidak	-2.9	10	10
KO	Base	PostS	12.09	6.97	44.66	13.18	-9.03	9	0	0	sidak	-3.09	10	10
KO	Tone1	S1	26.07	19.43	25.96	12.33	0.02	9	0.99	1	sidak	0.01	10	10
KO	Tone1	Tone2	26.07	19.43	34.46	24.81	-1.35	9	0.21	0.97	sidak	-0.38	10	10
KO	Tone1	S2	26.07	19.43	42.91	13.3	-2.85	9	0.02	0.25	sidak	-1.01	10	10
KO	Tone1	PostS	26.07	19.43	44.66	13.18	-3.39	9	0.01	0.11	sidak	-1.12	10	10
KO	S1	Tone2	25.96	12.33	34.46	24.81	-1.34	9	0.21	0.97	sidak	-0.43	10	10
KO	S1	S2	25.96	12.33	42.91	13.3	-4.66	9	0	0.02	sidak	-1.32	10	10
KO	S1	PostS	25.96	12.33	44.66	13.18	-6.05	9	0	0	sidak	-1.47	10	10
KO	Tone2	S2	34.46	24.81	42.91	13.3	-1.34	9	0.21	0.97	sidak	-0.42	10	10
KO	Tone2	PostS	34.46	24.81	44.66	13.18	-1.78	9	0.11	0.82	sidak	-0.51	10	10
KO	S2	PostS	42.91	13.3	44.66	13.18	-0.56	9	0.59	1	sidak	-0.13	10	10
WT	Base	Tone1	7.56	5.95	28.16	17.7	-3.36	7	0.01	0.17	sidak	-1.56	8	8
WT	Base	S1	7.56	5.95	9.89	4.3	-1.16	7	0.29	0.99	sidak	-0.45	8	8
WT	Base	Tone2	7.56	5.95	25.32	16.69	-3.38	7	0.01	0.16	sidak	-1.42	8	8
WT	Base	S2	7.56	5.95	23.14	12.26	-3.72	7	0.01	0.11	sidak	-1.62	8	8
WT	Base	PostS	7.56	5.95	33.83	13.11	-5.58	7	0	0.01	sidak	-2.58	8	8
WT	Tone1	S1	28.16	17.7	9.89	4.3	2.7	7	0.03	0.37	sidak	1.42	8	8
WT	Tone1	Tone2	28.16	17.7	25.32	16.69	0.47	7	0.65	1	sidak	0.17	8	8
WT	Tone1	S2	28.16	17.7	23.14	12.26	0.67	7	0.53	1	sidak	0.33	8	8
WT	Tone1	PostS	28.16	17.7	33.83	13.11	-0.73	7	0.49	1	sidak	-0.36	8	8
WT	S1	Tone2	9.89	4.3	25.32	16.69	-2.62	7	0.03	0.41	sidak	-1.27	8	8
WT	S1	S2	9.89	4.3	23.14	12.26	-3.69	7	0.01	0.11	sidak	-1.44	8	8
WT	S1	PostS	9.89	4.3	33.83	13.11	-5.99	7	0	0.01	sidak	-2.45	8	8
WT	Tone2	S2	25.32	16.69	23.14	12.26	0.33	7	0.75	1	sidak	0.15	8	8
WT	Tone2	PostS	25.32	16.69	33.83	13.11	-1.18	7	0.28	0.99	sidak	-0.57	8	8
WT	S2	PostS	23.14	12.26	33.83	13.11	-8.65	7	0	0	sidak	-0.84	8	8

Stats-table 11 Freeze bouts duration: 2-way ANOVA for Genotype X episodes . Section 1: ANOVA Findings Section 2: Comparisons Between Groups; Section 3: Comparisons Within Groups - unpaired two-sample t-tests with the Sidak correction

Source	SS	DF	MS	F	p-unc	np2
Genotype	4.94	1	4.94	1.06	0.3	0
episode	486.64	5	97.33	20.9	0	0.1
Genotype * episode	14.81	5	2.96	0.64	0.67	0
Residual	4168.3	895	4.66			

episode	A	B	mean(A)	std(A)	mean(B)	std(B)	T	dof	p-unc	p-corr	p-adjust	cohen	A_count	B_count
Base	WT	KO	1.84	0.74	1.67	0.92	1.36	136.92	0.18	0.69	sidak	0.2	59	130
Tone1	WT	KO	1.91	0.9	1.92	1.24	-0.04	67.1	0.97	1	sidak	-0.01	33	38
S1	WT	KO	1.9	0.84	2.26	1.41	-1.5	71.62	0.14	0.59	sidak	-0.28	25	69
Tone2	WT	KO	2.18	1.34	2.76	2.65	-1.11	52.97	0.27	0.85	sidak	-0.26	26	35
S2	WT	KO	2.71	1.88	3.34	2.73	-1.48	108.38	0.14	0.6	sidak	-0.26	41	77
PostS	WT	KO	3.41	2.59	3.48	2.84	-0.26	321.63	0.8	1	sidak	-0.03	143	231

Genotype	A	B	mean(A)	std(A)	mean(B)	std(B)	T	dof	p-unc	p-corr	p-adjust	cohen	A_count	B_count
KO	Base	Tone1	1.67	0.92	1.92	1.24	-1.14	49.49	0.26	0.99	sidak	-0.25	130	38
KO	Base	S1	1.67	0.92	2.26	1.41	-3.11	99.29	0	0.04	sidak	-0.53	130	69
KO	Base	Tone2	1.67	0.92	2.76	2.65	-2.38	36.22	0.02	0.29	sidak	-0.74	130	35
KO	Base	S2	1.67	0.92	3.34	2.73	-5.2	86.25	0	0	sidak	-0.92	130	77
KO	Base	PostS	1.67	0.92	3.48	2.84	-8.89	304.62	0	0	sidak	-0.77	130	231
KO	Tone1	S1	1.92	1.24	2.26	1.41	-1.28	85.23	0.2	0.97	sidak	-0.25	38	69
KO	Tone1	Tone2	1.92	1.24	2.76	2.65	-1.71	47.28	0.09	0.78	sidak	-0.41	38	35
KO	Tone1	S2	1.92	1.24	3.34	2.73	-3.84	112.4	0	0	sidak	-0.61	38	77
KO	Tone1	PostS	1.92	1.24	3.48	2.84	-5.69	114.96	0	0	sidak	-0.58	38	231
KO	S1	Tone2	2.26	1.41	2.76	2.65	-1.04	44.04	0.3	1	sidak	-0.26	69	35
KO	S1	S2	2.26	1.41	3.34	2.73	-3.06	116.42	0	0.04	sidak	-0.49	69	77
KO	S1	PostS	2.26	1.41	3.48	2.84	-4.85	231.61	0	0	sidak	-0.47	69	231
KO	Tone2	S2	2.76	2.65	3.34	2.73	-1.08	67.79	0.28	0.99	sidak	-0.22	35	77
KO	Tone2	PostS	2.76	2.65	3.48	2.84	-1.49	46.65	0.14	0.9	sidak	-0.26	35	231
KO	S2	PostS	3.34	2.73	3.48	2.84	-0.38	134.68	0.71	1	sidak	-0.05	77	231
WT	Base	Tone1	1.84	0.74	1.91	0.9	-0.36	56.31	0.72	1	sidak	-0.08	59	33
WT	Base	S1	1.84	0.74	1.9	0.84	-0.28	40.57	0.78	1	sidak	-0.07	59	25
WT	Base	Tone2	1.84	0.74	2.18	1.34	-1.2	31.92	0.24	0.98	sidak	-0.35	59	26
WT	Base	S2	1.84	0.74	2.71	1.88	-2.8	48.7	0.01	0.1	sidak	-0.65	59	41
WT	Base	PostS	1.84	0.74	3.41	2.59	-6.59	185.99	0	0	sidak	-0.7	59	143
WT	Tone1	S1	1.91	0.9	1.9	0.84	0.05	53.55	0.96	1	sidak	0.01	33	25
WT	Tone1	Tone2	1.91	0.9	2.18	1.34	-0.88	41.82	0.38	1	sidak	-0.24	33	26
WT	Tone1	S2	1.91	0.9	2.71	1.88	-2.4	59.99	0.02	0.26	sidak	-0.52	33	41
WT	Tone1	PostS	1.91	0.9	3.41	2.59	-5.59	148.57	0	0	sidak	-0.63	33	143
WT	S1	Tone2	1.9	0.84	2.18	1.34	-0.9	42.25	0.37	1	sidak	-0.25	25	26
WT	S1	S2	1.9	0.84	2.71	1.88	-2.39	59.81	0.02	0.26	sidak	-0.52	25	41
WT	S1	PostS	1.9	0.84	3.41	2.59	-5.5	115.84	0	0	sidak	-0.62	25	143
WT	Tone2	S2	2.18	1.34	2.71	1.88	-1.34	64.01	0.19	0.95	sidak	-0.31	26	41
WT	Tone2	PostS	2.18	1.34	3.41	2.59	-3.6	65.12	0	0.01	sidak	-0.5	26	143
WT	S2	PostS	2.71	1.88	3.41	2.59	-1.91	88.02	0.06	0.6	sidak	-0.28	41	143

Stats-table 12 Frequency of freeze bouts for each episodes : Mixed ANOVA for genotype X episodes -days Section 1: ANOVA Findings Section 2: Comparisons Between Groups; Section 3: Comparisons Within Groups - paired two-sample t-tests with the Sidak correction

Source	SS	DF1	DF2	MS	F	p-unc	np2
Genotype	217.23	1	16	217.23	7.02	0.02	0.31
episode	3889.49	5	80	777.9	99.4	0	0.86
Interaction	138.28	5	80	27.66	3.53	0.01	0.18

episode	A	B	mean(A)	std(A)	mean(B)	std(B)	T	dof	p-unc	p-corr	p-adjust	cohen	A_count	B_count
Base	WT	KO	7.38	5.48	13	5.64	-2.14	15.33	0.05	0.26	sidak	-1.01	8	10
Tone1	WT	KO	4.12	2.3	3.8	2.15	0.31	14.66	0.76	1	sidak	0.15	8	10
S1	WT	KO	3.12	0.99	6.9	2.6	-4.22	12.05	0	0.01	sidak	-1.83	8	10
Tone2	WT	KO	3.25	1.83	3.5	2.32	-0.26	16	0.8	1	sidak	-0.12	8	10
S2	WT	KO	5.12	1.89	7.7	1.7	-3.01	14.36	0.01	0.05	sidak	-1.44	8	10
PostS	WT	KO	17.88	4.19	23.1	5.09	-2.39	15.97	0.03	0.16	sidak	-1.11	8	10

Genotype	A	B	mean(A)	std(A)	mean(B)	std(B)	T	dof	p-unc	p-corr	p-adjust	cohen	A_count	B_count
KO	Base	Tone1	13	5.64	3.8	2.15	6.31	9	0	0	sidak	2.16	10	10
KO	Base	S1	13	5.64	6.9	2.6	3.86	9	0	0.06	sidak	1.39	10	10
KO	Base	Tone2	13	5.64	3.5	2.32	7.4	9	0	0	sidak	2.2	10	10
KO	Base	S2	13	5.64	7.7	1.7	3.14	9	0.01	0.16	sidak	1.27	10	10
KO	Base	PostS	13	5.64	23.1	5.09	-6.57	9	0	0	sidak	-1.88	10	10
KO	Tone1	S1	3.8	2.15	6.9	2.6	-4.21	9	0	0.03	sidak	-1.3	10	10
KO	Tone1	Tone2	3.8	2.15	3.5	2.32	0.67	9	0.52	1	sidak	0.13	10	10
KO	Tone1	S2	3.8	2.15	7.7	1.7	-7.73	9	0	0	sidak	-2.01	10	10
KO	Tone1	PostS	3.8	2.15	23.1	5.09	-15.93	9	0	0	sidak	-4.94	10	10
KO	S1	Tone2	6.9	2.6	3.5	2.32	4.74	9	0	0.02	sidak	1.38	10	10
KO	S1	S2	6.9	2.6	7.7	1.7	-0.87	9	0.41	1	sidak	-0.36	10	10
KO	S1	PostS	6.9	2.6	23.1	5.09	-10.28	9	0	0	sidak	-4.01	10	10
KO	Tone2	S2	3.5	2.32	7.7	1.7	-5.66	9	0	0	sidak	-2.06	10	10
KO	Tone2	PostS	3.5	2.32	23.1	5.09	-16.95	9	0	0	sidak	-4.96	10	10
KO	S2	PostS	7.7	1.7	23.1	5.09	-10.02	9	0	0	sidak	-4.06	10	10
WT	Base	Tone1	7.38	5.48	4.12	2.3	1.56	7	0.16	0.93	sidak	0.77	8	8
WT	Base	S1	7.38	5.48	3.12	0.99	2.32	7	0.05	0.56	sidak	1.08	8	8
WT	Base	Tone2	7.38	5.48	3.25	1.83	2.64	7	0.03	0.4	sidak	1.01	8	8
WT	Base	S2	7.38	5.48	5.12	1.89	1.29	7	0.24	0.98	sidak	0.55	8	8
WT	Base	PostS	7.38	5.48	17.88	4.19	-4.84	7	0	0.03	sidak	-2.15	8	8
WT	Tone1	S1	4.12	2.3	3.12	0.99	0.98	7	0.36	1	sidak	0.57	8	8
WT	Tone1	Tone2	4.12	2.3	3.25	1.83	1.05	7	0.33	1	sidak	0.42	8	8
WT	Tone1	S2	4.12	2.3	5.12	1.89	-0.95	7	0.37	1	sidak	-0.48	8	8
WT	Tone1	PostS	4.12	2.3	17.88	4.19	-7.86	7	0	0	sidak	-4.07	8	8
WT	S1	Tone2	3.12	0.99	3.25	1.83	-0.16	7	0.88	1	sidak	-0.08	8	8
WT	S1	S2	3.12	0.99	5.12	1.89	-2.83	7	0.03	0.32	sidak	-1.33	8	8
WT	S1	PostS	3.12	0.99	17.88	4.19	-10.45	7	0	0	sidak	-4.85	8	8
WT	Tone2	S2	3.25	1.83	5.12	1.89	-2.09	7	0.07	0.69	sidak	-1.01	8	8
WT	Tone2	PostS	3.25	1.83	17.88	4.19	-8.77	7	0	0	sidak	-4.52	8	8
WT	S2	PostS	5.12	1.89	17.88	4.19	-11.61	7	0	0	sidak	-3.92	8	8

Stats-table 13 Inter-freezing bout-interval: 2-way ANOVA for Genotype X episodes . Section 1: ANOVA Findings Section 2: Comparisons Between Groups; Section 3: Comparisons Within Groups - unpaired two-sample t-tests with the Sidak correction

Source	SS	DF	MS	F	p-unc	np2
Genotype	544.54	1	544.54	9.52	0	0.01
episode	2080.57	5	416.11	7.28	0	0.04
Genotype * episode	188.19	5	37.64	0.66	0.66	0
Residual	45059.65	788	57.18			

episode	A	B	mean(A)	std(A)	mean(B)	std(B)	T	dof	p-unc	p-corr	p-adjust	cohen	A_count	B_count
Base	WT	KO	12.01	12.97	11.01	11.74	0.48	86.46	0.64	1	sidak	0.08	51	120
Tone1	WT	KO	5.2	3.29	6.34	5.22	-0.96	46.12	0.34	0.92	sidak	-0.26	25	28
S1	WT	KO	10.64	9.71	7.32	5.35	1.35	18.89	0.19	0.72	sidak	0.51	17	59
Tone2	WT	KO	7.56	5.05	6.2	4.92	0.89	38.37	0.38	0.94	sidak	0.27	19	25
S2	WT	KO	9.6	6.41	7.14	3.67	2.05	42.65	0.05	0.25	sidak	0.52	33	67
PostS	WT	KO	9.54	7.26	7.41	5.12	2.98	215.78	0	0.02	sidak	0.35	135	221

Genotype	A	B	mean(A)	std(A)	mean(B)	std(B)	T	dof	p-unc	p-corr	p-adjust	cohen	A_count	B_count
KO	Base	Tone1	11.01	11.74	6.34	5.22	3.2	97.4	0	0.03	sidak	0.43	120	28
KO	Base	S1	11.01	11.74	7.32	5.35	2.89	176.26	0	0.06	sidak	0.37	120	59
KO	Base	Tone2	11.01	11.74	6.2	4.92	3.3	89.29	0	0.02	sidak	0.44	120	25
KO	Base	S2	11.01	11.74	7.14	3.67	3.33	155.77	0	0.02	sidak	0.4	120	67
KO	Base	PostS	11.01	11.74	7.41	5.12	3.19	144.07	0	0.03	sidak	0.44	120	221
KO	Tone1	S1	6.34	5.22	7.32	5.35	-0.81	54.32	0.42	1	sidak	-0.18	28	59
KO	Tone1	Tone2	6.34	5.22	6.2	4.92	0.1	50.84	0.92	1	sidak	0.03	28	25
KO	Tone1	S2	6.34	5.22	7.14	3.67	-0.73	38.64	0.47	1	sidak	-0.19	28	67
KO	Tone1	PostS	6.34	5.22	7.41	5.12	-1.03	33.92	0.31	1	sidak	-0.21	28	221
KO	S1	Tone2	7.32	5.35	6.2	4.92	0.92	48.99	0.36	1	sidak	0.21	59	25
KO	S1	S2	7.32	5.35	7.14	3.67	0.22	100.85	0.83	1	sidak	0.04	59	67
KO	S1	PostS	7.32	5.35	7.41	5.12	-0.13	88.46	0.9	1	sidak	-0.02	59	221
KO	Tone2	S2	6.2	4.92	7.14	3.67	-0.86	34.47	0.4	1	sidak	-0.23	25	67
KO	Tone2	PostS	6.2	4.92	7.41	5.12	-1.16	30.2	0.26	0.99	sidak	-0.24	25	221
KO	S2	PostS	7.14	3.67	7.41	5.12	-0.49	151.07	0.62	1	sidak	-0.06	67	221
WT	Base	Tone1	12.01	12.97	5.2	3.29	3.53	61.8	0	0.01	sidak	0.63	51	25
WT	Base	S1	12.01	12.97	10.64	9.71	0.46	36.57	0.65	1	sidak	0.11	51	17
WT	Base	Tone2	12.01	12.97	7.56	5.05	2.06	67.79	0.04	0.48	sidak	0.39	51	19
WT	Base	S2	12.01	12.97	9.6	6.41	1.13	77.6	0.26	0.99	sidak	0.22	51	33
WT	Base	PostS	12.01	12.97	9.54	7.26	1.28	62.21	0.2	0.97	sidak	0.27	51	135
WT	Tone1	S1	5.2	3.29	10.64	9.71	-2.23	18.53	0.04	0.44	sidak	-0.82	25	17
WT	Tone1	Tone2	5.2	3.29	7.56	5.05	-1.78	29.23	0.09	0.74	sidak	-0.57	25	19
WT	Tone1	S2	5.2	3.29	9.6	6.41	-3.4	50.08	0	0.02	sidak	-0.83	25	33
WT	Tone1	PostS	5.2	3.29	9.54	7.26	-4.79	75.63	0	0	sidak	-0.64	25	135
WT	S1	Tone2	10.64	9.71	7.56	5.05	1.17	23.47	0.25	0.99	sidak	0.4	17	19
WT	S1	S2	10.64	9.71	9.6	6.41	0.4	23.41	0.69	1	sidak	0.14	17	33
WT	S1	PostS	10.64	9.71	9.54	7.26	0.45	18.32	0.66	1	sidak	0.15	17	135
WT	Tone2	S2	7.56	5.05	9.6	6.41	-1.26	45.07	0.21	0.97	sidak	-0.34	19	33
WT	Tone2	PostS	7.56	5.05	9.54	7.26	-1.5	29.66	0.14	0.9	sidak	-0.28	19	135
WT	S2	PostS	9.6	6.41	9.54	7.26	0.04	53.94	0.96	1	sidak	0.01	33	135

Stats-table 14 Calcium spike rates during the conditioning episodes . Mixed ANOVA for genotype X episodes -days Section 1: ANOVA Findings Section 2: Comparisons Between Groups; Section 3: Comparisons Within Groups - paired two-sample t-

tests with the Sidak correction

Source	SS	DF1	DF2	MS	F	p-unc	np2
Genotype	5.88	1	3379	5.88	146.73	0	0.04
episode	1.44	5	16895	0.29	24.08	0	0.01
Interaction	0.62	5	16895	0.12	10.35	0	0

episode	A	B	mean(A)	std(A)	mean(B)	std(B)	T	dof	p-unc	p-corr	p-adjust	cohen	A_count	B_count
Base	WT	KO	0.15	0.11	0.1	0.08	13.87	2452.13	0	0	sidak	0.51	1560	2179
Tone1	WT	KO	0.14	0.2	0.1	0.15	4.94	2567.9	0	0	sidak	0.18	1560	2179
S1	WT	KO	0.12	0.14	0.09	0.11	5.22	2663.13	0	0	sidak	0.19	1560	2179
Tone2	WT	KO	0.15	0.18	0.09	0.15	8.79	2687.31	0	0	sidak	0.32	1560	2179
S2	WT	KO	0.12	0.12	0.09	0.1	7.09	2665.25	0	0	sidak	0.26	1560	2179
PostS	WT	KO	0.12	0.1	0.09	0.08	8.01	2556.86	0	0	sidak	0.29	1434	1947

Genotype	A	B	mean(A)	std(A)	mean(B)	std(B)	T	dof	p-unc	p-corr	p-adjust	cohen	A_count	B_count
KO	Base	Tone1	0.1	0.08	0.1	0.15	-0.86	1946	0.39	1	sidak	-0.02	2179	2179
KO	Base	S1	0.1	0.08	0.09	0.11	3.65	1946	0	0	sidak	0.1	2179	2179
KO	Base	Tone2	0.1	0.08	0.09	0.15	2.03	1946	0.04	0.48	sidak	0.06	2179	2179
KO	Base	S2	0.1	0.08	0.09	0.1	4.13	1946	0	0	sidak	0.11	2179	2179
KO	Base	PostS	0.1	0.08	0.09	0.08	6.02	1946	0	0	sidak	0.15	2179	1947
KO	Tone1	S1	0.1	0.15	0.09	0.11	3.2	1946	0	0.02	sidak	0.09	2179	2179
KO	Tone1	Tone2	0.1	0.15	0.09	0.15	2.35	1946	0.02	0.25	sidak	0.07	2179	2179
KO	Tone1	S2	0.1	0.15	0.09	0.1	3.58	1946	0	0.01	sidak	0.1	2179	2179
KO	Tone1	PostS	0.1	0.15	0.09	0.08	4.39	1946	0	0	sidak	0.12	2179	1947
KO	S1	Tone2	0.09	0.11	0.09	0.15	-0.66	1946	0.51	1	sidak	-0.02	2179	2179
KO	S1	S2	0.09	0.11	0.09	0.1	0.17	1946	0.86	1	sidak	0	2179	2179
KO	S1	PostS	0.09	0.11	0.09	0.08	0.88	1946	0.38	1	sidak	0.02	2179	1947
KO	Tone2	S2	0.09	0.15	0.09	0.1	0.77	1946	0.44	1	sidak	0.02	2179	2179
KO	Tone2	PostS	0.09	0.15	0.09	0.08	1.38	1946	0.17	0.94	sidak	0.04	2179	1947
KO	S2	PostS	0.09	0.1	0.09	0.08	1.02	1946	0.31	1	sidak	0.02	2179	1947
WT	Base	Tone1	0.15	0.11	0.14	0.2	2.67	1433	0.01	0.11	sidak	0.09	1560	1560
WT	Base	S1	0.15	0.11	0.12	0.14	9.53	1433	0	0	sidak	0.27	1560	1560
WT	Base	Tone2	0.15	0.11	0.15	0.18	0.48	1433	0.63	1	sidak	0.01	1560	1560
WT	Base	S2	0.15	0.11	0.12	0.12	8.28	1433	0	0	sidak	0.25	1560	1560
WT	Base	PostS	0.15	0.11	0.12	0.1	11.17	1433	0	0	sidak	0.32	1560	1434
WT	Tone1	S1	0.14	0.2	0.12	0.14	3.66	1433	0	0	sidak	0.12	1560	1560
WT	Tone1	Tone2	0.14	0.2	0.15	0.18	-1.85	1433	0.06	0.63	sidak	-0.06	1560	1560
WT	Tone1	S2	0.14	0.2	0.12	0.12	2.74	1433	0.01	0.09	sidak	0.09	1560	1560
WT	Tone1	PostS	0.14	0.2	0.12	0.1	4.08	1433	0	0	sidak	0.13	1560	1434
WT	S1	Tone2	0.12	0.14	0.15	0.18	-6.09	1433	0	0	sidak	-0.19	1560	1560
WT	S1	S2	0.12	0.14	0.12	0.12	-1.24	1433	0.21	0.97	sidak	-0.04	1560	1560
WT	S1	PostS	0.12	0.14	0.12	0.1	-0.01	1433	0.99	1	sidak	0	1560	1434
WT	Tone2	S2	0.15	0.18	0.12	0.12	5.18	1433	0	0	sidak	0.17	1560	1560
WT	Tone2	PostS	0.15	0.18	0.12	0.1	6.64	1433	0	0	sidak	0.21	1560	1434
WT	S2	PostS	0.12	0.12	0.12	0.1	2.23	1433	0.03	0.32	sidak	0.04	1560	1434

Stats-table 15 NMI of calcium spike rates : Mixed ANOVA for genotype X episodes -days Section 1: ANOVA Findings Section 2: Comparisons Between Groups; Section 3: Comparisons Within Groups - paired two-sample t-tests with the Sidak correction

Source	SS	DF1	DF2	MS	F	p-unc	np2
Genotype	0.45	1	3379	0.45	0.87	0.35	0
episode	109.38	4	13516	27.34	120.43	0	0.03
Interaction	18.97	4	13516	4.74	20.88	0	0.01

episode	A	B	mean(A)	std(A)	mean(B)	std(B)	T	dof	p-unc	p-corr	p-adjust	cohen	A_count	B_count
Tone1	WT	KO	-0.32	0.58	-0.31	0.62	-0.48	3190.99	0.63	0.99	sidak	-0.02	1560	2179
S1	WT	KO	-0.29	0.49	-0.24	0.56	-3.09	3281.51	0	0.01	sidak	-0.11	1560	2179
Tone2	WT	KO	-0.25	0.56	-0.37	0.62	5.8	3244.73	0	0	sidak	0.2	1560	2179
S2	WT	KO	-0.23	0.49	-0.2	0.53	-1.85	3213	0.07	0.29	sidak	-0.06	1560	2179
PostS	WT	KO	-0.14	0.39	-0.07	0.39	-5.28	3104.65	0	0	sidak	-0.18	1434	1947

Genotype	A	B	mean(A)	std(A)	mean(B)	std(B)	T	dof	p-unc	p-corr	p-adjust	cohen	A_count	B_count
KO	Tone1	S1	-0.31	0.62	-0.24	0.56	-4.15	1946	0	0	sidak	-0.12	2179	2179
KO	Tone1	Tone2	-0.31	0.62	-0.37	0.62	3.4	1946	0	0.01	sidak	0.1	2179	2179
KO	Tone1	S2	-0.31	0.62	-0.2	0.53	-6.53	1946	0	0	sidak	-0.19	2179	2179
KO	Tone1	PostS	-0.31	0.62	-0.07	0.39	-15.32	1946	0	0	sidak	-0.46	2179	1947
KO	S1	Tone2	-0.24	0.56	-0.37	0.62	7.57	1946	0	0	sidak	0.23	2179	2179
KO	S1	S2	-0.24	0.56	-0.2	0.53	-2.44	1946	0.01	0.14	sidak	-0.07	2179	2179
KO	S1	PostS	-0.24	0.56	-0.07	0.39	-12.73	1946	0	0	sidak	-0.34	2179	1947
KO	Tone2	S2	-0.37	0.62	-0.2	0.53	-9.57	1946	0	0	sidak	-0.3	2179	2179
KO	Tone2	PostS	-0.37	0.62	-0.07	0.39	-19.46	1946	0	0	sidak	-0.58	2179	1947
KO	S2	PostS	-0.2	0.53	-0.07	0.39	-13.03	1946	0	0	sidak	-0.27	2179	1947
WT	Tone1	S1	-0.32	0.58	-0.29	0.49	-1.55	1433	0.12	0.73	sidak	-0.05	1560	1560
WT	Tone1	Tone2	-0.32	0.58	-0.25	0.56	-3.6	1433	0	0	sidak	-0.12	1560	1560
WT	Tone1	S2	-0.32	0.58	-0.23	0.49	-4.79	1433	0	0	sidak	-0.17	1560	1560
WT	Tone1	PostS	-0.32	0.58	-0.14	0.39	-10.99	1433	0	0	sidak	-0.36	1560	1434
WT	S1	Tone2	-0.29	0.49	-0.25	0.56	-2.34	1433	0.02	0.18	sidak	-0.08	1560	1560
WT	S1	S2	-0.29	0.49	-0.23	0.49	-3.87	1433	0	0	sidak	-0.13	1560	1560
WT	S1	PostS	-0.29	0.49	-0.14	0.39	-11	1433	0	0	sidak	-0.34	1560	1434
WT	Tone2	S2	-0.25	0.56	-0.23	0.49	-1.16	1433	0.25	0.94	sidak	-0.04	1560	1560
WT	Tone2	PostS	-0.25	0.56	-0.14	0.39	-6.7	1433	0	0	sidak	-0.23	1560	1434
WT	S2	PostS	-0.23	0.49	-0.14	0.39	-8.37	1433	0	0	sidak	-0.2	1560	1434

Stats-table 16 NMI of excited neurons : Mixed ANOVA for genotype X episodes -days Section 1: ANOVA Findings Section 2: Comparisons Between Groups; Section 3: Comparisons Within Groups - paired two-sample t-tests with the Sidak correction

Source	SS	DF1	DF2	MS	F	p-unc	np2
Genotype	1.04	1	1246	1.04	2.26	0.13	0
episode	248.53	4	4984	62.13	225.1	0	0.15
Interac-tion	6.37	4	4984	1.59	5.77	0	0

episode	A	B	mean(A)	std(A)	mean(B)	std(B)	T	dof	p-unc	p-corr	p-ad-just	co-hen	A_#	B_#
Tone1	WT	KO	-0.13	0.65	-0.23	0.7	2.46	1010.83	0.01	0.07	sidak	0.14	461	787
S1	WT	KO	-0.11	0.53	-0.06	0.6	-1.42	1062.48	0.16	0.57	sidak	-0.08	461	787
Tone2	WT	KO	-0.13	0.63	-0.25	0.7	3.03	1045.94	0	0.01	sidak	0.17	461	787
S2	WT	KO	0.11	0.51	0.13	0.52	-0.62	988.26	0.54	0.98	sidak	-0.04	461	787
Post-Shock	WT	KO	0.31	0.23	0.32	0.21	-1.02	897.04	0.31	0.84	sidak	-0.06	461	787

Genotype	A	B	mean(A)	std(A)	mean(B)	std(B)	T	dof	p-unc	p-corr	p-ad-just	co-hen	A_#	B_#

KO	Tone1	S1	-0.23	0.7	-0.06	0.6	-5.14	786	0	0	sidak	-0.25	787	787
KO	Tone1	Tone2	-0.23	0.7	-0.25	0.7	0.62	786	0.53	1	sidak	0.03	787	787
KO	Tone1	S2	-0.23	0.7	0.13	0.52	-12.12	786	0	0	sidak	-0.57	787	787
KO	Tone1	Post-Shock	-0.23	0.7	0.32	0.21	-21.92	786	0	0	sidak	-1.07	787	787
KO	S1	Tone2	-0.06	0.6	-0.25	0.7	5.96	786	0	0	sidak	0.28	787	787
KO	S1	S2	-0.06	0.6	0.13	0.52	-6.93	786	0	0	sidak	-0.34	787	787
KO	S1	Post-Shock	-0.06	0.6	0.32	0.21	-18.29	786	0	0	sidak	-0.86	787	787
KO	Tone2	S2	-0.25	0.7	0.13	0.52	-11.99	786	0	0	sidak	-0.6	787	787
KO	Tone2	Post-Shock	-0.25	0.7	0.32	0.21	-22.56	786	0	0	sidak	-1.1	787	787
KO	S2	Post-Shock	0.13	0.52	0.32	0.21	-10.92	786	0	0	sidak	-0.49	787	787
WT	Tone1	S1	-0.13	0.65	-0.11	0.53	-0.51	460	0.61	1	sidak	-0.03	461	461
WT	Tone1	Tone2	-0.13	0.65	-0.13	0.63	0	460	1	1	sidak	0	461	461
WT	Tone1	S2	-0.13	0.65	0.11	0.51	-6.17	460	0	0	sidak	-0.41	461	461
WT	Tone1	Post-Shock	-0.13	0.65	0.31	0.23	-14.29	460	0	0	sidak	-0.89	461	461
WT	S1	Tone2	-0.11	0.53	-0.13	0.63	0.54	460	0.59	1	sidak	0.03	461	461
WT	S1	S2	-0.11	0.53	0.11	0.51	-6.93	460	0	0	sidak	-0.42	461	461
WT	S1	Post-Shock	-0.11	0.53	0.31	0.23	-16.91	460	0	0	sidak	-1.03	461	461
WT	Tone2	S2	-0.13	0.63	0.11	0.51	-6.72	460	0	0	sidak	-0.42	461	461
WT	Tone2	Post-Shock	-0.13	0.63	0.31	0.23	-14.57	460	0	0	sidak	-0.93	461	461
WT	S2	Post-Shock	0.11	0.51	0.31	0.23	-8.62	460	0	0	sidak	-0.51	461	461

Stats-table 17 NMI of inhibited neurons: Mixed ANOVA for genotype X episodes -days Section 1: ANOVA Findings Section 2: Comparisons Between Groups; Section 3: Comparisons Within Groups - paired two-sample t-tests with the Sidak correction

Source	SS	DF1	DF2	MS	F	p-unc	np2
Genotype	2.16	1	2359	2.16	6.01	0.01	0
episode	14.35	4	9436	3.59	19.48	0	0.01
Interac-tion	10.52	4	9436	2.63	14.29	0	0.01

episode	A	B	mean(A)	std(A)	mean(B)	std(B)	T	dof	p-unc	p-corr	p-ad-just	co-hen	A #	B #
Tone1	WT	KO	-0.43	0.53	-0.4	0.57	-1.52	2306	0.13	0.5	sidak	-0.06	1045	1316
S1	WT	KO	-0.41	0.45	-0.38	0.51	-1.44	2339.89	0.15	0.56	sidak	-0.06	1045	1316
Tone2	WT	KO	-0.35	0.53	-0.48	0.56	5.78	2294.34	0	0	sidak	0.24	1045	1316
S2	WT	KO	-0.46	0.41	-0.52	0.42	3.01	2272.18	0	0.01	sidak	0.12	1045	1316
Post-Shock	WT	KO	-0.45	0.29	-0.47	0.31	1.46	2290.69	0.14	0.54	sidak	0.06	1045	1316

Genotype	A	B	mean(A)	std(A)	mean(B)	std(B)	T	dof	p-unc	p-corr	p-ad-just	co-hen	A #	B #
KO	Tone1	S1	-0.4	0.57	-0.38	0.51	-0.8	1315	0.43	1	sidak	-0.03	1316	1316
KO	Tone1	Tone2	-0.4	0.57	-0.48	0.56	4.33	1315	0	0	sidak	0.15	1316	1316
KO	Tone1	S2	-0.4	0.57	-0.52	0.42	6.41	1315	0	0	sidak	0.23	1316	1316
KO	Tone1	Post-Shock	-0.4	0.57	-0.47	0.31	4.11	1315	0	0	sidak	0.15	1316	1316

KO	S1	Tone2	-0.38	0.51	-0.48	0.56	4.94	1315	0	0	sidak	0.18	1316	1316
KO	S1	S2	-0.38	0.51	-0.52	0.42	7.51	1315	0	0	sidak	0.28	1316	1316
KO	S1	Post-Shock	-0.38	0.51	-0.47	0.31	5.46	1315	0	0	sidak	0.2	1316	1316
KO	Tone2	S2	-0.48	0.56	-0.52	0.42	1.78	1315	0.08	0.54	sidak	0.07	1316	1316
KO	Tone2	Post-Shock	-0.48	0.56	-0.47	0.31	-0.92	1315	0.36	0.99	sidak	-0.03	1316	1316
KO	S2	Post-Shock	-0.52	0.42	-0.47	0.31	-5.41	1315	0	0	sidak	-0.13	1316	1316
WT	Tone1	S1	-0.43	0.53	-0.41	0.45	-1.11	1044	0.27	0.95	sidak	-0.04	1045	1045
WT	Tone1	Tone2	-0.43	0.53	-0.35	0.53	-3.75	1044	0	0	sidak	-0.15	1045	1045
WT	Tone1	S2	-0.43	0.53	-0.46	0.41	1.63	1044	0.1	0.67	sidak	0.07	1045	1045
WT	Tone1	Post-Shock	-0.43	0.53	-0.45	0.29	0.92	1044	0.36	0.99	sidak	0.04	1045	1045
WT	S1	Tone2	-0.41	0.45	-0.35	0.53	-3.03	1044	0	0.02	sidak	-0.12	1045	1045
WT	S1	S2	-0.41	0.45	-0.46	0.41	3.12	1044	0	0.02	sidak	0.13	1045	1045
WT	S1	Post-Shock	-0.41	0.45	-0.45	0.29	2.59	1044	0.01	0.09	sidak	0.1	1045	1045
WT	Tone2	S2	-0.35	0.53	-0.46	0.41	5.93	1044	0	0	sidak	0.24	1045	1045
WT	Tone2	Post-Shock	-0.35	0.53	-0.45	0.29	5.93	1044	0	0	sidak	0.23	1045	1045
WT	S2	Post-Shock	-0.46	0.41	-0.45	0.29	-1.75	1044	0.08	0.57	sidak	-0.05	1045	1045

Stats-table 18 Freezing percentage over the different CFC days : Mixed ANOVA for genotype X episodes -days Section 1: ANOVA Findings Section 2: Comparisons Between Groups; Section 3: Comparisons Within Groups - paired two-sample t-tests.

Source	SS	DF1	DF2	MS	F	p-unc	np2
Genotype	866.22	1	16	866.22	3.92	0.07	0.2
Day	14643.91	5	80	2928.78	26.39	0	0.62
Interaction	4785.32	5	80	957.07	8.62	0	0.35

Day	Day	A	B	mean(A)	std(A)	mean(B)	std(B)	T	dof	p-unc	p-corr	p-adjust	cohen	A_count	B_count
Pre-Shock	Pre-Shock	WT	KO	7.56	5.95	12.09	6.97	-1.49	15.9	0.16	0.64	sidak	-0.69	8	10
Post-Shock	Post-Shock	WT	KO	33.83	13.11	44.66	13.18	-1.74	15.18	0.1	0.48	sidak	-0.82	8	10
Recent	Recent	WT	KO	41.19	20.5	18.41	7.41	2.99	8.47	0.02	0.09	sidak	1.55	8	10
Novel1	Novel1	WT	KO	9.2	5.64	10.61	6.21	-0.51	15.68	0.62	1	sidak	-0.24	8	10
Remote	Remote	WT	KO	44.67	16.12	20.2	10.34	3.72	11.4	0	0.02	sidak	1.86	8	10
Novel2	Novel2	WT	KO	14.94	13.23	11.21	10.28	0.65	13.03	0.52	0.99	sidak	0.32	8	10

Genotype	A	B	mean(A)	std(A)	mean(B)	std(B)	T	dof	p-unc	p-corr	p-adjust	cohen	A_count	B_count
KO	Pre-Shock	Post-Shock	12.09	6.97	44.66	13.18	-9.03	9	0	0	sidak	-3.09	10	10
KO	Pre-Shock	Recent	12.09	6.97	18.41	7.41	-2.9	9	0.02	0.23	sidak	-0.88	10	10
KO	Pre-Shock	Novel1	12.09	6.97	10.61	6.21	1.04	9	0.32	1	sidak	0.22	10	10
KO	Pre-Shock	Remote	12.09	6.97	20.2	10.34	-2.98	9	0.02	0.21	sidak	-0.92	10	10
KO	Pre-Shock	Novel2	12.09	6.97	11.21	10.28	0.25	9	0.81	1	sidak	0.1	10	10
KO	Post-Shock	Recent	44.66	13.18	18.41	7.41	6.43	9	0	0	sidak	2.45	10	10
KO	Post-Shock	Novel1	44.66	13.18	10.61	6.21	9.66	9	0	0	sidak	3.31	10	10
KO	Post-Shock	Remote	44.66	13.18	20.2	10.34	4.81	9	0	0.01	sidak	2.07	10	10
KO	Post-Shock	Novel2	44.66	13.18	11.21	10.28	6.78	9	0	0	sidak	2.83	10	10
KO	Recent	Novel1	18.41	7.41	10.61	6.21	5.11	9	0	0.01	sidak	1.14	10	10
KO	Recent	Remote	18.41	7.41	20.2	10.34	-0.61	9	0.56	1	sidak	-0.2	10	10
KO	Recent	Novel2	18.41	7.41	11.21	10.28	1.89	9	0.09	0.76	sidak	0.8	10	10
KO	Novel1	Remote	10.61	6.21	20.2	10.34	-3.3	9	0.01	0.13	sidak	-1.12	10	10
KO	Novel1	Novel2	10.61	6.21	11.21	10.28	-0.16	9	0.88	1	sidak	-0.07	10	10
KO	Remote	Novel2	20.2	10.34	11.21	10.28	3.36	9	0.01	0.12	sidak	0.87	10	10
WT	Pre-Shock	Post-Shock	7.56	5.95	33.83	13.11	-5.58	7	0	0.01	sidak	-2.58	8	8
WT	Pre-Shock	Recent	7.56	5.95	41.19	20.5	-5.63	7	0	0.01	sidak	-2.23	8	8
WT	Pre-Shock	Novel1	7.56	5.95	9.2	5.64	-0.49	7	0.64	1	sidak	-0.28	8	8
WT	Pre-Shock	Remote	7.56	5.95	44.67	16.12	-6.77	7	0	0	sidak	-3.05	8	8
WT	Pre-Shock	Novel2	7.56	5.95	14.94	13.23	-1.53	7	0.17	0.94	sidak	-0.72	8	8
WT	Post-Shock	Recent	33.83	13.11	41.19	20.5	-0.82	7	0.44	1	sidak	-0.43	8	8
WT	Post-Shock	Novel1	33.83	13.11	9.2	5.64	5.28	7	0	0.02	sidak	2.44	8	8
WT	Post-Shock	Remote	33.83	13.11	44.67	16.12	-1.32	7	0.23	0.98	sidak	-0.74	8	8
WT	Post-Shock	Novel2	33.83	13.11	14.94	13.23	3.17	7	0.02	0.21	sidak	1.43	8	8
WT	Recent	Novel1	41.19	20.5	9.2	5.64	3.81	7	0.01	0.09	sidak	2.13	8	8
WT	Recent	Remote	41.19	20.5	44.67	16.12	-0.41	7	0.7	1	sidak	-0.19	8	8
WT	Recent	Novel2	41.19	20.5	14.94	13.23	2.68	7	0.03	0.38	sidak	1.52	8	8
WT	Novel1	Remote	9.2	5.64	44.67	16.12	-4.88	7	0	0.03	sidak	-2.94	8	8
WT	Novel1	Novel2	9.2	5.64	14.94	13.23	-1.05	7	0.33	1	sidak	-0.56	8	8
WT	Remote	Novel2	44.67	16.12	14.94	13.23	6.47	7	0	0.01	sidak	2.02	8	8

Stats-table 19 2 Freeze bouts duration : 2-way ANOVA for Genotype × Sessions. Section 1: ANOVA Findings Section 2: Comparisons Between Groups; Section 3: Comparisons Within Groups - unpaired two-sample t-tests with the Sidak correction

Source	SS	DF	MS	F	p-unc	np2
Genotype	334.53	1	334.53	52.83	0	0.03
Day	604.93	5	120.99	19.11	0	0.06
Genotype * Day	465.57	5	93.11	14.7	0	0.04
Residual	10099.93	1595	6.33			

Day	Day	A	B	mean(A)	std(A)	mean(B)	std(B)	T	dof	p-unc	p-corr	p-adjust	cohen	A_count	B_count
Pre-Shock	Pre-Shock	WT	KO	1.84	0.74	1.67	0.92	1.36	136.92	0.18	0.69	sidak	0.2	59	130
Post-Shock	Post-Shock	WT	KO	3.41	2.59	3.48	2.84	-0.26	321.63	0.8	1	sidak	-0.03	143	231
Recent	Recent	WT	KO	3.95	3.98	1.76	0.78	6.64	158.06	0	0	sidak	0.81	150	188
Novel1	Novel1	WT	KO	1.87	2.02	2.05	1.82	-0.62	142.05	0.54	0.99	sidak	-0.1	71	93
Remote	Remote	WT	KO	4.18	4.73	2	1.18	5.57	169.16	0	0	sidak	0.66	154	182
Novel2	Novel2	WT	KO	2.05	1.28	2	1.56	0.25	193.08	0.8	1	sidak	0.04	105	101

Genotype	A	B	mean(A)	std(A)	mean(B)	std(B)	T	dof	p-unc	p-corr	p-adjust	cohen	A_count	B_count
KO	Pre-Shock	Post-Shock	1.67	0.92	3.48	2.84	-8.89	304.62	0	0	sidak	-0.77	130	231
KO	Pre-Shock	Recent	1.67	0.92	1.76	0.78	-0.91	246.93	0.37	1	sidak	-0.11	130	188
KO	Pre-Shock	Novel1	1.67	0.92	2.05	1.82	-1.85	125.44	0.07	0.64	sidak	-0.28	130	93
KO	Pre-Shock	Remote	1.67	0.92	2	1.18	-2.73	307.82	0.01	0.1	sidak	-0.3	130	182
KO	Pre-Shock	Novel2	1.67	0.92	2	1.56	-1.86	152.27	0.07	0.64	sidak	-0.26	130	101
KO	Post-Shock	Recent	3.48	2.84	1.76	0.78	8.81	271.53	0	0	sidak	0.79	231	188
KO	Post-Shock	Novel1	3.48	2.84	2.05	1.82	5.37	260.15	0	0	sidak	0.55	231	93
KO	Post-Shock	Remote	3.48	2.84	2	1.18	7.19	322.51	0	0	sidak	0.66	231	182
KO	Post-Shock	Novel2	3.48	2.84	2	1.56	6.1	313.2	0	0	sidak	0.59	231	101
KO	Recent	Novel1	1.76	0.78	2.05	1.82	-1.48	108.88	0.14	0.9	sidak	-0.24	188	93
KO	Recent	Remote	1.76	0.78	2	1.18	-2.25	311.53	0.03	0.32	sidak	-0.24	188	182
KO	Recent	Novel2	1.76	0.78	2	1.56	-1.42	127.16	0.16	0.92	sidak	-0.21	188	101
KO	Novel1	Remote	2.05	1.82	2	1.18	0.27	132.66	0.79	1	sidak	0.04	93	182
KO	Novel1	Novel2	2.05	1.82	2	1.56	0.23	181.99	0.82	1	sidak	0.03	93	101
KO	Remote	Novel2	2	1.18	2	1.56	0	164.39	1	1	sidak	0	182	101
WT	Pre-Shock	Post-Shock	1.84	0.74	3.41	2.59	-6.59	185.99	0	0	sidak	-0.7	59	143
WT	Pre-Shock	Recent	1.84	0.74	3.95	3.98	-6.22	172.91	0	0	sidak	-0.62	59	150
WT	Pre-Shock	Novel1	1.84	0.74	1.87	2.02	-0.08	91.54	0.93	1	sidak	-0.01	59	71
WT	Pre-Shock	Remote	1.84	0.74	4.18	4.73	-5.93	171.36	0	0	sidak	-0.58	59	154
WT	Pre-Shock	Novel2	1.84	0.74	2.05	1.28	-1.3	161.8	0.2	0.96	sidak	-0.18	59	105
WT	Post-Shock	Recent	3.41	2.59	3.95	3.98	-1.4	257.33	0.16	0.93	sidak	-0.16	143	150
WT	Post-Shock	Novel1	3.41	2.59	1.87	2.02	4.76	173.63	0	0	sidak	0.64	143	71
WT	Post-Shock	Remote	3.41	2.59	4.18	4.73	-1.76	240.69	0.08	0.71	sidak	-0.2	143	154
WT	Post-Shock	Novel2	3.41	2.59	2.05	1.28	5.43	218.72	0	0	sidak	0.64	143	105
WT	Recent	Novel1	3.95	3.98	1.87	2.02	5.17	217.91	0	0	sidak	0.6	150	71
WT	Recent	Remote	3.95	3.98	4.18	4.73	-0.44	295.85	0.66	1	sidak	-0.05	150	154
WT	Recent	Novel2	3.95	3.98	2.05	1.28	5.47	190	0	0	sidak	0.6	150	105
WT	Novel1	Remote	1.87	2.02	4.18	4.73	-5.13	222.07	0	0	sidak	-0.57	71	154
WT	Novel1	Novel2	1.87	2.02	2.05	1.28	-0.68	107.47	0.5	1	sidak	-0.11	71	105
WT	Remote	Novel2	4.18	4.73	2.05	1.28	5.31	184.28	0	0	sidak	0.57	154	105

Stats-table 20 Number of freezing bouts Mixed ANOVA for genotype X episodes -days Section 1: ANOVA Findings Section 2: Comparisons Between Groups; Section 3: Comparisons Within Groups - paired two-sample t-tests.

Source	SS	DF1	DF2	MS	F	p-unc	np2
Genotype	38.94	1	16	38.94	0.46	0.51	0.03
Day	2314.49	5	80	462.9	16.47	0	0.51
Interaction	269.41	5	80	53.88	1.92	0.1	0.11

Day	Day	A	B	mean(A)	std(A)	mean(B)	std(B)	T	dof	p-unc	p-corr	p-adjust	cohen	A_count	B_count
Pre-Shock	Pre-Shock	WT	KO	7.38	5.48	13	5.64	-2.14	15.33	0.05	0.26	sidak	-1.01	8	10
Post-Shock	Post-Shock	WT	KO	17.88	4.19	23.1	5.09	-2.39	15.97	0.03	0.16	sidak	-1.11	8	10
Recent	Recent	WT	KO	18.75	4.59	18.8	8.39	-0.02	14.4	0.99	1	sidak	-0.01	8	10
Novel1	Novel1	WT	KO	8.88	3.52	9.3	4.83	-0.22	15.91	0.83	1	sidak	-0.1	8	10
Remote	Remote	WT	KO	19.25	4.13	18.2	7.16	0.39	14.76	0.7	1	sidak	0.17	8	10
Novel2	Novel2	WT	KO	13.12	8.31	10.1	8.13	0.78	14.99	0.45	0.97	sidak	0.37	8	10

Genotype	A	B	mean(A)	std(A)	mean(B)	std(B)	T	dof	p-unc	p-corr	p-adjust	cohen	A_count	B_count
KO	Pre-Shock	Post-Shock	13	5.64	23.1	5.09	-6.57	9	0	0	sidak	-1.88	10	10
KO	Pre-Shock	Recent	13	5.64	18.8	8.39	-2.77	9	0.02	0.28	sidak	-0.81	10	10
KO	Pre-Shock	Novel1	13	5.64	9.3	4.83	3.08	9	0.01	0.18	sidak	0.7	10	10
KO	Pre-Shock	Remote	13	5.64	18.2	7.16	-2.15	9	0.06	0.61	sidak	-0.81	10	10
KO	Pre-Shock	Novel2	13	5.64	10.1	8.13	1	9	0.34	1	sidak	0.41	10	10
KO	Post-Shock	Recent	23.1	5.09	18.8	8.39	1.72	9	0.12	0.85	sidak	0.62	10	10
KO	Post-Shock	Novel1	23.1	5.09	9.3	4.83	7.51	9	0	0	sidak	2.78	10	10
KO	Post-Shock	Remote	23.1	5.09	18.2	7.16	1.63	9	0.14	0.89	sidak	0.79	10	10
KO	Post-Shock	Novel2	23.1	5.09	10.1	8.13	4.74	9	0	0.02	sidak	1.92	10	10
KO	Recent	Novel1	18.8	8.39	9.3	4.83	4.27	9	0	0.03	sidak	1.39	10	10
KO	Recent	Remote	18.8	8.39	18.2	7.16	0.24	9	0.82	1	sidak	0.08	10	10
KO	Recent	Novel2	18.8	8.39	10.1	8.13	2.5	9	0.03	0.4	sidak	1.05	10	10
KO	Novel1	Remote	9.3	4.83	18.2	7.16	-4.11	9	0	0.04	sidak	-1.46	10	10
KO	Novel1	Novel2	9.3	4.83	10.1	8.13	-0.29	9	0.78	1	sidak	-0.12	10	10
KO	Remote	Novel2	18.2	7.16	10.1	8.13	3.23	9	0.01	0.14	sidak	1.06	10	10
WT	Pre-Shock	Post-Shock	7.38	5.48	17.88	4.19	-4.84	7	0	0.03	sidak	-2.15	8	8
WT	Pre-Shock	Recent	7.38	5.48	18.75	4.59	-4.69	7	0	0.03	sidak	-2.25	8	8
WT	Pre-Shock	Novel1	7.38	5.48	8.88	3.52	-0.68	7	0.52	1	sidak	-0.33	8	8
WT	Pre-Shock	Remote	7.38	5.48	19.25	4.13	-6.27	7	0	0.01	sidak	-2.45	8	8
WT	Pre-Shock	Novel2	7.38	5.48	13.12	8.31	-1.96	7	0.09	0.76	sidak	-0.82	8	8
WT	Post-Shock	Recent	17.88	4.19	18.75	4.59	-0.35	7	0.73	1	sidak	-0.2	8	8
WT	Post-Shock	Novel1	17.88	4.19	8.88	3.52	6.42	7	0	0.01	sidak	2.33	8	8
WT	Post-Shock	Remote	17.88	4.19	19.25	4.13	-0.96	7	0.37	1	sidak	-0.33	8	8
WT	Post-Shock	Novel2	17.88	4.19	13.12	8.31	1.6	7	0.15	0.92	sidak	0.72	8	8
WT	Recent	Novel1	18.75	4.59	8.88	3.52	4.51	7	0	0.04	sidak	2.41	8	8
WT	Recent	Remote	18.75	4.59	19.25	4.13	-0.22	7	0.83	1	sidak	-0.11	8	8
WT	Recent	Novel2	18.75	4.59	13.12	8.31	1.29	7	0.24	0.98	sidak	0.84	8	8
WT	Novel1	Remote	8.88	3.52	19.25	4.13	-8.48	7	0	0	sidak	-2.7	8	8
WT	Novel1	Novel2	8.88	3.52	13.12	8.31	-1.43	7	0.2	0.96	sidak	-0.67	8	8
WT	Remote	Novel2	19.25	4.13	13.12	8.31	2.03	7	0.08	0.72	sidak	0.93	8	8

Stats-table 21 Firing rate during each session of CFC : 2-way ANOVA for Genotype × Sessions. Section 1: ANOVA Findings Section 2: Comparisons Between Groups; Section 3: Comparisons Within Groups - unpaired two-sample t-tests with the Sidak correction

Source	SS	DF	MS	F	p-unc	np2
Genotype	8.4	1	8.4	1181.51	0	0.05
Day	0.8	5	0.16	22.5	0	0.01
Genotype * Day	0.35	5	0.07	9.71	0	0
Residual	152.07	21378	0.01			

Day	Day	A	B	mean(A)	std(A)	mean(B)	std(B)	T	dof	p-unc	p-corr	p-adjust	cohen	A count	B count
Pre-Shock	Pre-Shock	WT	KO	0.14	0.11	0.1	0.08	14.42	2635.02	0	0	sidak	0.51	1560	2179
Post-Shock	Post-Shock	WT	KO	0.11	0.1	0.09	0.07	8.37	2632.18	0	0	sidak	0.3	1494	2093
Recent	Recent	WT	KO	0.13	0.09	0.09	0.07	11.45	2290.96	0	0	sidak	0.43	1306	1874
Novel1	Novel1	WT	KO	0.14	0.11	0.09	0.07	15.62	2556.65	0	0	sidak	0.55	1579	2049
Remote	Remote	WT	KO	0.13	0.08	0.09	0.07	14.64	2857.01	0	0	sidak	0.52	1524	1863
Novel2	Novel2	WT	KO	0.14	0.1	0.1	0.07	16.05	3038.81	0	0	sidak	0.54	1716	2153

Genotype	A	B	mean(A)	std(A)	mean(B)	std(B)	T	dof	p-unc	p-corr	p-adjust	cohen	A count	B count
KO	Pre-Shock	Post-Shock	0.1	0.08	0.09	0.07	3.93	4269.99	0	0	sidak	0.12	2179	2093
KO	Pre-Shock	Recent	0.1	0.08	0.09	0.07	1.5	4049.14	0.13	0.88	sidak	0.05	2179	1874
KO	Pre-Shock	Novel1	0.1	0.08	0.09	0.07	1.8	4211.51	0.07	0.67	sidak	0.06	2179	2049
KO	Pre-Shock	Remote	0.1	0.08	0.09	0.07	1.65	4039.99	0.1	0.79	sidak	0.05	2179	1863
KO	Pre-Shock	Novel2	0.1	0.08	0.1	0.07	0.35	4318.65	0.73	1	sidak	0.01	2179	2153
KO	Post-Shock	Recent	0.09	0.07	0.09	0.07	-2.52	3963.4	0.01	0.16	sidak	-0.08	2093	1874
KO	Post-Shock	Novel1	0.09	0.07	0.09	0.07	-2.28	4125.08	0.02	0.29	sidak	-0.07	2093	2049
KO	Post-Shock	Remote	0.09	0.07	0.09	0.07	-2.41	3954	0.02	0.22	sidak	-0.08	2093	1863
KO	Post-Shock	Novel2	0.09	0.07	0.1	0.07	-3.69	4232.25	0	0	sidak	-0.11	2093	2153
KO	Recent	Novel1	0.09	0.07	0.09	0.07	0.28	3895.83	0.78	1	sidak	0.01	1874	2049
KO	Recent	Remote	0.09	0.07	0.09	0.07	0.14	3733.54	0.89	1	sidak	0	1874	1863
KO	Recent	Novel2	0.09	0.07	0.1	0.07	-1.19	4003.75	0.23	0.98	sidak	-0.04	1874	2153
KO	Novel1	Remote	0.09	0.07	0.09	0.07	-0.14	3895.7	0.88	1	sidak	0	2049	1863
KO	Novel1	Novel2	0.09	0.07	0.1	0.07	-1.5	4199.76	0.13	0.89	sidak	-0.05	2049	2153
KO	Remote	Novel2	0.09	0.07	0.1	0.07	-1.34	4002.74	0.18	0.95	sidak	-0.04	1863	2153
WT	Pre-Shock	Post-Shock	0.14	0.11	0.11	0.1	8.01	3042.91	0	0	sidak	0.29	1560	1494
WT	Pre-Shock	Recent	0.14	0.11	0.13	0.09	4.33	2863.47	0	0	sidak	0.16	1560	1306
WT	Pre-Shock	Novel1	0.14	0.11	0.14	0.11	0.69	3131.08	0.49	1	sidak	0.02	1560	1579
WT	Pre-Shock	Remote	0.14	0.11	0.13	0.08	3.27	2923.75	0	0.02	sidak	0.12	1560	1524
WT	Pre-Shock	Novel2	0.14	0.11	0.14	0.1	0.34	3163.82	0.74	1	sidak	0.01	1560	1716
WT	Post-Shock	Recent	0.11	0.1	0.13	0.09	-3.93	2793.27	0	0	sidak	-0.15	1494	1306
WT	Post-Shock	Novel1	0.11	0.1	0.14	0.11	-7.44	3070.61	0	0	sidak	-0.27	1494	1579
WT	Post-Shock	Remote	0.11	0.1	0.13	0.08	-5.59	2920.13	0	0	sidak	-0.2	1494	1524
WT	Post-Shock	Novel2	0.11	0.1	0.14	0.1	-8.24	3152.5	0	0	sidak	-0.29	1494	1716
WT	Recent	Novel1	0.13	0.09	0.14	0.11	-3.69	2880.44	0	0	sidak	-0.14	1306	1579
WT	Recent	Remote	0.13	0.09	0.13	0.08	-1.41	2693.45	0.16	0.92	sidak	-0.05	1306	1524
WT	Recent	Novel2	0.13	0.09	0.14	0.1	-4.3	2930.79	0	0	sidak	-0.16	1306	1716
WT	Novel1	Remote	0.14	0.11	0.13	0.08	2.57	2991.76	0.01	0.14	sidak	0.09	1579	1524
WT	Novel1	Novel2	0.14	0.11	0.14	0.1	-0.4	3226.48	0.69	1	sidak	-0.01	1579	1716
WT	Remote	Novel2	0.13	0.08	0.14	0.1	-3.17	3229.91	0	0.02	sidak	-0.11	1524	1716

Stats-table 22 Calcium rate place cells vs non-place cells . Section 1: ANOVA Findings Section for the WT mice 2: ANOVA Findings Section for the KO mice

Source	SS	DF	MS	F	p-unc	np2	genotype
Base_PC	1.6	1	1.6	167.87	0	0.02	WT
Day	0.81	5	0.16	17.06	0	0.01	WT
Base_PC * Day	0.45	5	0.09	9.47	0	0.01	WT
Residual	87.52	9167	0.01				WT

Source	SS	DF	MS	F	p-unc	np2	genotype
Base_PC	1.18	1	1.18	236.06	0	0.02	KO
Day	0.09	5	0.02	3.67	0	0	KO
Base_PC * Day	0.1	5	0.02	3.96	0	0	KO
Residual	61.21	12199	0.01				KO

Stats-table 23 Correlated pairs across the sessions : 2-way ANOVA for Genotype × Sessions. Section 1: ANOVA Findings Section 2: Comparisons Between Groups; Section 3: Comparisons Within Groups - unpaired two-sample t-tests with the Sidak correction

Source	SS	DF	MS	F	p-unc	np2
Genotype	220.04	1	220.04	2.33	0.13	0
episode	2665.44	5	533.09	5.64	0	0.04
Genotype * episode	169.33	5	33.87	0.36	0.88	0
Residual	57024.92	603	94.57			

episode	A	B	mean(A)	std(A)	mean(B)	std(B)	T	dof	p-unc	p-corr	p-adjust	cohen	A_count	B_count
Base	WT	KO	12.01	12.97	11.01	11.74	0.48	86.46	0.64	1	sidak	0.08	51	120
Tone1	WT	KO	5.2	3.29	6.34	5.22	-0.96	46.12	0.34	0.92	sidak	-0.26	25	28
S1	WT	KO	10.64	9.71	7.32	5.35	1.35	18.89	0.19	0.72	sidak	0.51	17	59
Tone2	WT	KO	7.56	5.05	6.2	4.92	0.89	38.37	0.38	0.94	sidak	0.27	19	25
S2	WT	KO	9.6	6.41	7.14	3.67	2.05	42.65	0.05	0.25	sidak	0.52	33	67
PostS	WT	KO	12.01	12.97	11.01	11.74	0.48	86.46	0.64	1	sidak	0.08	51	120

Genotype	A	B	mean(A)	std(A)	mean(B)	std(B)	T	dof	p-unc	p-corr	p-adjust	cohen	A_count	B_count
KO	Base	Tone1	11.01	11.74	6.34	5.22	3.2	97.4	0	0.03	sidak	0.43	120	28
KO	Base	S1	11.01	11.74	7.32	5.35	2.89	176.26	0	0.06	sidak	0.37	120	59
KO	Base	Tone2	11.01	11.74	6.2	4.92	3.3	89.29	0	0.02	sidak	0.44	120	25
KO	Base	S2	11.01	11.74	7.14	3.67	3.33	155.77	0	0.02	sidak	0.4	120	67
KO	Base	PostS	11.01	11.74	11.01	11.74	0	238	1	1	sidak	0	120	120
KO	Tone1	S1	6.34	5.22	7.32	5.35	-0.81	54.32	0.42	1	sidak	-0.18	28	59
KO	Tone1	Tone2	6.34	5.22	6.2	4.92	0.1	50.84	0.92	1	sidak	0.03	28	25
KO	Tone1	S2	6.34	5.22	7.14	3.67	-0.73	38.64	0.47	1	sidak	-0.19	28	67
KO	Tone1	PostS	6.34	5.22	11.01	11.74	-3.2	97.4	0	0.03	sidak	-0.43	28	120
KO	S1	Tone2	7.32	5.35	6.2	4.92	0.92	48.99	0.36	1	sidak	0.21	59	25
KO	S1	S2	7.32	5.35	7.14	3.67	0.22	100.85	0.83	1	sidak	0.04	59	67
KO	S1	PostS	7.32	5.35	11.01	11.74	-2.89	176.26	0	0.06	sidak	-0.37	59	120
KO	Tone2	S2	6.2	4.92	7.14	3.67	-0.86	34.47	0.4	1	sidak	-0.23	25	67
KO	Tone2	PostS	6.2	4.92	11.01	11.74	-3.3	89.29	0	0.02	sidak	-0.44	25	120
KO	S2	PostS	7.14	3.67	11.01	11.74	-3.33	155.77	0	0.02	sidak	-0.4	67	120
WT	Base	Tone1	12.01	12.97	5.2	3.29	3.53	61.8	0	0.01	sidak	0.63	51	25
WT	Base	S1	12.01	12.97	10.64	9.71	0.46	36.57	0.65	1	sidak	0.11	51	17
WT	Base	Tone2	12.01	12.97	7.56	5.05	2.06	67.79	0.04	0.48	sidak	0.39	51	19
WT	Base	S2	12.01	12.97	9.6	6.41	1.13	77.6	0.26	0.99	sidak	0.22	51	33
WT	Base	PostS	12.01	12.97	12.01	12.97	0	100	1	1	sidak	0	51	51
WT	Tone1	S1	5.2	3.29	10.64	9.71	-2.23	18.53	0.04	0.44	sidak	-0.82	25	17
WT	Tone1	Tone2	5.2	3.29	7.56	5.05	-1.78	29.23	0.09	0.74	sidak	-0.57	25	19
WT	Tone1	S2	5.2	3.29	9.6	6.41	-3.4	50.08	0	0.02	sidak	-0.83	25	33
WT	Tone1	PostS	5.2	3.29	12.01	12.97	-3.53	61.8	0	0.01	sidak	-0.63	25	51
WT	S1	Tone2	10.64	9.71	7.56	5.05	1.17	23.47	0.25	0.99	sidak	0.4	17	19
WT	S1	S2	10.64	9.71	9.6	6.41	0.4	23.41	0.69	1	sidak	0.14	17	33
WT	S1	PostS	10.64	9.71	12.01	12.97	-0.46	36.57	0.65	1	sidak	-0.11	17	51
WT	Tone2	S2	7.56	5.05	9.6	6.41	-1.26	45.07	0.21	0.97	sidak	-0.34	19	33
WT	Tone2	PostS	7.56	5.05	12.01	12.97	-2.06	67.79	0.04	0.48	sidak	-0.39	19	51
WT	S2	PostS	9.6	6.41	12.01	12.97	-1.13	77.6	0.26	0.99	sidak	-0.22	33	51

Stats-table 24 Correlation coefficient for the conditioning sessions : 2-way ANOVA for Genotype × Sessions. Section 1: ANOVA Findings Section 2: Comparisons Between Groups; Section 3: Comparisons Within Groups - unpaired two-sample t-tests with the Sidak correction

Source	SS	DF	MS	F	p-unc	np2
Genotype	220.04	1	220.04	2.33	0.13	0
episode	2665.44	5	533.09	5.64	0	0.04
Genotype * episode	169.33	5	33.87	0.36	0.88	0
Residual	57024.92	603	94.57			

episode	A	B	mean(A)	std(A)	mean(B)	std(B)	T	dof	p-unc	p-corr	p-adjust	cohen	A_count	B_count
Base	WT	KO	12.01	12.97	11.01	11.74	0.48	86.46	0.64	1	sidak	0.08	51	120
Tone1	WT	KO	5.2	3.29	6.34	5.22	-0.96	46.12	0.34	0.92	sidak	-0.26	25	28
S1	WT	KO	10.64	9.71	7.32	5.35	1.35	18.89	0.19	0.72	sidak	0.51	17	59
Tone2	WT	KO	7.56	5.05	6.2	4.92	0.89	38.37	0.38	0.94	sidak	0.27	19	25
S2	WT	KO	9.6	6.41	7.14	3.67	2.05	42.65	0.05	0.25	sidak	0.52	33	67
PostS	WT	KO	12.01	12.97	11.01	11.74	0.48	86.46	0.64	1	sidak	0.08	51	120

Genotype	A	B	mean(A)	std(A)	mean(B)	std(B)	T	dof	p-unc	p-corr	p-adjust	cohen	A_count	B_count
KO	Base	Tone1	11.01	11.74	6.34	5.22	3.2	97.4	0	0.03	sidak	0.43	120	28
KO	Base	S1	11.01	11.74	7.32	5.35	2.89	176.26	0	0.06	sidak	0.37	120	59
KO	Base	Tone2	11.01	11.74	6.2	4.92	3.3	89.29	0	0.02	sidak	0.44	120	25
KO	Base	S2	11.01	11.74	7.14	3.67	3.33	155.77	0	0.02	sidak	0.4	120	67
KO	Base	PostS	11.01	11.74	11.01	11.74	0	238	1	1	sidak	0	120	120
KO	Tone1	S1	6.34	5.22	7.32	5.35	-0.81	54.32	0.42	1	sidak	-0.18	28	59
KO	Tone1	Tone2	6.34	5.22	6.2	4.92	0.1	50.84	0.92	1	sidak	0.03	28	25
KO	Tone1	S2	6.34	5.22	7.14	3.67	-0.73	38.64	0.47	1	sidak	-0.19	28	67
KO	Tone1	PostS	6.34	5.22	11.01	11.74	-3.2	97.4	0	0.03	sidak	-0.43	28	120
KO	S1	Tone2	7.32	5.35	6.2	4.92	0.92	48.99	0.36	1	sidak	0.21	59	25
KO	S1	S2	7.32	5.35	7.14	3.67	0.22	100.85	0.83	1	sidak	0.04	59	67
KO	S1	PostS	7.32	5.35	11.01	11.74	-2.89	176.26	0	0.06	sidak	-0.37	59	120
KO	Tone2	S2	6.2	4.92	7.14	3.67	-0.86	34.47	0.4	1	sidak	-0.23	25	67
KO	Tone2	PostS	6.2	4.92	11.01	11.74	-3.3	89.29	0	0.02	sidak	-0.44	25	120
KO	S2	PostS	7.14	3.67	11.01	11.74	-3.33	155.77	0	0.02	sidak	-0.4	67	120
WT	Base	Tone1	12.01	12.97	5.2	3.29	3.53	61.8	0	0.01	sidak	0.63	51	25
WT	Base	S1	12.01	12.97	10.64	9.71	0.46	36.57	0.65	1	sidak	0.11	51	17
WT	Base	Tone2	12.01	12.97	7.56	5.05	2.06	67.79	0.04	0.48	sidak	0.39	51	19
WT	Base	S2	12.01	12.97	9.6	6.41	1.13	77.6	0.26	0.99	sidak	0.22	51	33
WT	Base	PostS	12.01	12.97	12.01	12.97	0	100	1	1	sidak	0	51	51
WT	Tone1	S1	5.2	3.29	10.64	9.71	-2.23	18.53	0.04	0.44	sidak	-0.82	25	17
WT	Tone1	Tone2	5.2	3.29	7.56	5.05	-1.78	29.23	0.09	0.74	sidak	-0.57	25	19
WT	Tone1	S2	5.2	3.29	9.6	6.41	-3.4	50.08	0	0.02	sidak	-0.83	25	33
WT	Tone1	PostS	5.2	3.29	12.01	12.97	-3.53	61.8	0	0.01	sidak	-0.63	25	51
WT	S1	Tone2	10.64	9.71	7.56	5.05	1.17	23.47	0.25	0.99	sidak	0.4	17	19
WT	S1	S2	10.64	9.71	9.6	6.41	0.4	23.41	0.69	1	sidak	0.14	17	33
WT	S1	PostS	10.64	9.71	12.01	12.97	-0.46	36.57	0.65	1	sidak	-0.11	17	51
WT	Tone2	S2	7.56	5.05	9.6	6.41	-1.26	45.07	0.21	0.97	sidak	-0.34	19	33
WT	Tone2	PostS	7.56	5.05	12.01	12.97	-2.06	67.79	0.04	0.48	sidak	-0.39	19	51
WT	S2	PostS	9.6	6.41	12.01	12.97	-1.13	77.6	0.26	0.99	sidak	-0.22	33	51

Stats-table 25 Calcium Spike rate of reactivated neurons seperated in 3 groups(Engram, Non-engram and new neurons)

ddof1	ddof2	F	p-unc	np2	Genotype	Neuron Group	Neuron definition
4	2343	10,29	0	0,02	WT	engram	Pre-shock
3	2249	3,88	0,01	0,01	WT	new neuron	Pre-shock
4	2953	31,11	0	0,04	WT	non-engram	Pre-shock
4	3067	0,6	0,66	0	KO	engram	Pre-shock
3	2438	1,4	0,24	0	KO	new neuron	Pre-shock
4	4367	21,42	0	0,02	KO	non-engram	Pre-shock

4	1949	10,89	0	0,02	WT	engram	Recent-session
4	3495	7,19	0	0,01	WT	new neuron	Recent-session
4	2414	10,62	0	0,02	WT	non-engram	Recent-session
4	2717	1,94	0,1	0	KO	engram	Recent-session
4	3935	2,45	0,04	0	KO	new neuron	Recent-session
4	3670	3,41	0,01	0	KO	non-engram	Recent-session

6.2 Statement of Contributions

The research presented in this thesis, including the equipment and materials, was funded by a grant from the Schaller-Nikolich Foundation gGmbH to Dr. Dietmar Kuhl and Prof. Ora Ohana. I am deeply grateful to the foundation for granting me a PhD stipend and for their ongoing support.

For section 3.4 *Arc/Arg3.1 does not influence the electrical spikes*; Dr. Xiaoyu Yang performed *in vivo* LFP recording, and Dr. Ora Ohana performed manual curation of the spikes. AHAK performed subsequent post-hoc analysis.
For the remaining sections, AHAK performed all stages of *in vivo* miniscope calcium imaging, from surgery (virus injection, lens implants) to behavioral tests and data analysis.
I acknowledge the use of ChatGPT, developed by OpenAI, for assistance with code writing and English editing during the preparation of this Dissertation.

6.3 Acknowledgments

Completing this thesis has been a challenging journey, and I am immensely grateful to those who have supported me throughout this process.

First and foremost, I would like to express my greatest gratitude to my advisor Dr. Ora Ohana, for her invaluable guidance, PATIENCE, and expertise. Her insights and encouragement have been important in shaping this research, and I am fortunate to have had the opportunity to learn from her.

I am deeply grateful to my partner, Dr. Vanda Toth-Taksonyi, for her continuous support during the highs and lows of this journey. Thank you for all the adventures, whether we're punching each other in jiu-jitsu or stepping on each other's feet in dance classes, enjoying our travels, or spending lazy days watching TV.

I owe my deepest appreciation to my family, especially my parents and sisters. My parents have made sacrifices to provide me with the opportunities that led me here. Their unwavering belief in me and all their children, hard work, and endless support have shaped who I am today. I am forever grateful for everything they have done.

I sincerely thank all current and former group members. Their insightful advice and engaging discussions proved invaluable in helping me navigate my work challenges. I would also like to express my appreciation to Ute Süsens for her vital help in the lab and Priv.-Doz. Dr. Guido Hermey for his valuable guidance.

I want to extend a special thank you to Dani and Andres for their flexibility and for always being available when I reached out to try new foods and drinks, explore new places, or share lighthearted to existential conversations.

Finally, I thank to all those who have contributed, directly or indirectly, to my journey. Your support has significantly impacted me, whether through academic discussions, technical assistance, or encouraging words. I am genuinely thankful for the friendships that have helped me stay "almost" balanced and sane during this journey.

Thank you all.

7 Reference

Ali, F., & Kwan, A. C. (2020). Interpreting in vivo calcium signals from neuronal cell bodies, axons, and dendrites: a review. *Neurophotonics*, *7*(1), 011402. https://doi.org/10.1117/1.NPh.7.1.011402

Balleine, B. W., Killcross, A. S., & Dickinson, A. (2003). The Effect of Lesions of the Basolateral Amygdala on Instrumental Conditioning. *The Journal of Neuroscience*, *23*(2), 666. https://doi.org/10.1523/JNEUROSCI.23-02-00666.2003

Barthó, P., Hirase, H., Monconduit, L., Zugaro, M., Harris, K. D., & Buzsáki, G. (2004). Characterization of Neocortical Principal Cells and Interneurons by Network Interactions and Extracellular Features. *Journal of Neurophysiology*, *92*(1), 600-608. https://doi.org/10.1152/jn.01170.2003

Behrens, T. E. J., Muller, T. H., Whittington, J. C. R., Mark, S., Baram, A. B., Stachenfeld, K. L., & Kurth-Nelson, Z. (2018). What Is a Cognitive Map? Organizing Knowledge for Flexible Behavior. *Neuron*, *100*(2), 490-509. https://doi.org/https://doi.org/10.1016/j.neuron.2018.10.002

Benito, E., & Barco, A. (2010). CREB's control of intrinsic and synaptic plasticity: implications for CREB-dependent memory models. *Trends in Neurosciences*, *33*(5), 230-240. https://doi.org/10.1016/j.tins.2010.02.001

Bliss, T. V. P., & Lømo, T. (1973). Long-lasting potentiation of synaptic transmission in the dentate area of the anaesthetized rabbit following stimulation of the perforant path. *The Journal of Physiology*, *232*(2), 331-356. https://doi.org/https://doi.org/10.1113/jphysiol.1973.sp010273

Bostancıklıoğlu, M. (2020). An update on memory formation and retrieval: An engram-centric approach. *Alzheimer's & Dementia*, *16*(6), 926-937. https://doi.org/https://doi.org/10.1002/alz.12071

Bramham, C. R., Alme, M. N., Bittins, M., Kuipers, S. D., Nair, R. R., Pai, B., Panja, D., Schubert, M., Soule, J., Tiron, A., & Wibrand, K. (2010). The Arc of synaptic memory. *Experimental Brain Research*, *200*(2), 125-140. https://doi.org/10.1007/s00221-009-1959-2

Bramham, C. R., Worley, P. F., Moore, M. J., & Guzowski, J. F. (2008). The Immediate Early Gene Arc/Arg3.1: Regulation, Mechanisms, and Function. *The Journal of Neuroscience*, *28*(46), 11760. https://doi.org/10.1523/JNEUROSCI.3864-08.2008

Breijyeh, Z., & Karaman, R. (2020). Comprehensive Review on Alzheimer's Disease: Causes and Treatment. *Molecules*, *25*(24), 5789. https://www.mdpi.com/1420-3049/25/24/5789

Buzsáki, G. (2015). Hippocampal sharp wave-ripple: A cognitive biomarker for episodic memory and planning. *Hippocampus*, *25*(10), 1073-1188. https://doi.org/https://doi.org/10.1002/hipo.22488

Buzsáki, G., & Draguhn, A. (2004). Neuronal oscillations in cortical networks. *Science*, *304*(5679), 1926-1929. https://doi.org/10.1126/science.1099745

Buzsáki, G., Lai-Wo S, L., & Vanderwolf, C. H. (1983). Cellular bases of hippocampal EEG in the behaving rat. *Brain Research Reviews*, *6*(2), 139-171. https://doi.org/https://doi.org/10.1016/0165-0173(83)90037-1

Cai, D. J., Aharoni, D., Shuman, T., Shobe, J., Biane, J., Song, W., Wei, B., Veshkini, M., La-Vu, M., & Lou, J. (2016). A shared neural ensemble links distinct contextual memories encoded close in time. *Nature*, *534*(7605), 115-118.

Chen, L., Lin, X., Ye, Q., Nenadic, Z., Holmes, T. C., Nitz, D. A., & Xu, X. (2023). Anatomical organization of temporally correlated neural calcium activity in the hippocampal CA1 region. *iScience*, *26*(5), 106703. https://doi.org/https://doi.org/10.1016/j.isci.2023.106703

Cheng, S., & Frank, L. M. (2008). New Experiences Enhance Coordinated Neural Activity in the Hippocampus. *Neuron*, *57*(2), 303-313. https://doi.org/10.1016/j.neuron.2007.11.035

Choucry, A., Nomoto, M., & Inokuchi, K. (2024). Engram mechanisms of memory linking and identity. *Nature Reviews Neuroscience*, *25*(6), 375-392. https://doi.org/10.1038/s41583-024-00814-0

Chowdhury, S., Shepherd, J. D., Okuno, H., Lyford, G., Petralia, R. S., Plath, N., Kuhl, D., Huganir, R. L., & Worley, P. F. (2006). Arc/Arg3.1 Interacts with the Endocytic Machinery to Regulate AMPA Receptor Trafficking. *Neuron*, *52*(3), 445-459. https://doi.org/10.1016/j.neuron.2006.08.033

Citri, A., & Malenka, R. C. (2008). Synaptic Plasticity: Multiple Forms, Functions, and Mechanisms. *Neuropsychopharmacology*, *33*(1), 18-41. https://doi.org/10.1038/sj.npp.1301559

Cohen, J. D., Bolstad, M., & Lee, A. K. (2017). Experience-dependent shaping of hippocampal CA1 intracellular activity in novel and familiar environments. *Elife*, *6*, e23040. https://doi.org/10.7554/eLife.23040

Czerniawski, J., Ree, F., Chia, C., Ramamoorthi, K., Kumata, Y., & Otto, T. A. (2011). The Importance of Having Arc: Expression of the Immediate-Early Gene Arc Is Required for Hippocampus-Dependent Fear Conditioning and Blocked by NMDA Receptor Antagonism. *The Journal of Neuroscience*, *31*(31), 11200. https://doi.org/10.1523/JNEUROSCI.2211-11.2011

Dinç, F., Inan, H., Hernandez, O., Schmuckermair, C., Hazon, O., Tasci, T., Ahanonu, B. O., Zhang, Y., Lecoq, J., Haziza, S., Wagner, M. J., Erdogdu, M. A., & Schnitzer, M. J. (2024). Fast, scalable, and statistically robust cell extraction from large-scale neural calcium imaging datasets. *bioRxiv*, 2021.2003.2024.436279. https://doi.org/10.1101/2021.03.24.436279

Donzis, E. J., Rennaker, R. L., & Thompson, L. T. (2013). Fear conditioning alters neuron-specific hippocampal place field stability via the basolateral amygdala. *Brain Res*, *1525*, 16-25. https://doi.org/10.1016/j.brainres.2013.06.015

Doyon, J., & Benali, H. (2005). Reorganization and plasticity in the adult brain during learning of motor skills. *Curr Opin Neurobiol*, *15*(2), 161-167. https://doi.org/10.1016/j.conb.2005.03.004

Dudai, Y. (2004). The Neurobiology of Consolidations, Or, How Stable is the Engram? *Annual Review of Psychology*, *55*(Volume 55, 2004), 51-86. https://doi.org/https://doi.org/10.1146/annurev.psych.55.090902.142050

Dunsmoor, J. E., & Paz, R. (2015). Fear Generalization and Anxiety: Behavioral and Neural Mechanisms. *Biological Psychiatry*, *78*(5), 336-343. https://doi.org/https://doi.org/10.1016/j.biopsych.2015.04.010

Eichenbaum, H. (2016). Still searching for the engram. *Learning & behavior*, *44*(3), 209-222. https://doi.org/10.3758/s13420-016-0218-1

Eichenbaum, H. (2017a). Memory: Organization and Control. *Annual Review of Psychology*, *68*(Volume 68, 2017), 19-45. https://doi.org/https://doi.org/10.1146/annurev-psych-010416-044131

Eichenbaum, H. (2017b). Prefrontal–hippocampal interactions in episodic memory. *Nature Reviews Neuroscience*, *18*(9), 547-558. https://doi.org/10.1038/nrn.2017.74

Frankland, P. W., & Bontempi, B. (2005). The organization of recent and remote memories. *Nature Reviews Neuroscience*, *6*(2), 119-130. https://doi.org/10.1038/nrn1607

Friedenberger, Z., Harkin, E., Tóth, K., & Naud, R. (2023). Silences, spikes and bursts: Three-part knot of the neural code. *The Journal of Physiology*, *601*(23), 5165-5193. https://doi.org/https://doi.org/10.1113/JP281510

Fujimori, S., Ishikawa, T., & Watanabe, H. (2020, 13-16 Oct. 2020). Animal Behavior Classification Using DeepLabCut. 2020 IEEE 9th Global Conference on Consumer Electronics (GCCE),

Gao, M., Sossa, K., Song, L., Errington, L., Cummings, L., Hwang, H., Kuhl, D., Worley, P., & Lee, H.-K. (2010). A Specific Requirement of Arc/Arg3.1 for Visual Experience-Induced Homeostatic Synaptic Plasticity in Mouse Primary Visual Cortex. *The Journal of Neuroscience*, *30*(21), 7168. https://doi.org/10.1523/JNEUROSCI.1067-10.2010

Gao, X., Castro-Gomez, S., Grendel, J., Graf, S., Süsens, U., Binkle, L., Mensching, D., Isbrandt, D., Kuhl, D., & Ohana, O. (2018). Arc/Arg3.1 mediates a critical period for spatial learning and hippocampal networks. *Proceedings of the National Academy of Sciences*, *115*(49), 12531-12536. https://doi.org/doi:10.1073/pnas.1810125115

Gao, X., Grendel, J., Muhia, M., Castro-Gomez, S., Süsens, U., Isbrandt, D., Kneussel, M., Kuhl, D., & Ohana, O. (2019). Disturbed Prefrontal Cortex Activity in the Absence of Schizophrenia-Like Behavioral Dysfunction in Arc/Arg3.1 Deficient Mice. *The Journal of Neuroscience*, *39*(41), 8149. https://doi.org/10.1523/JNEUROSCI.0623-19.2019

Garner, A. R., Rowland, D. C., Hwang, S. Y., Baumgaertel, K., Roth, B. L., Kentros, C., & Mayford, M. (2012). Generation of a Synthetic Memory Trace. *Science*, *335*(6075), 1513-1516. https://doi.org/doi:10.1126/science.1214985

Ghandour, K., Ohkawa, N., Fung, C. C. A., Asai, H., Saitoh, Y., Takekawa, T., Okubo-Suzuki, R., Soya, S., Nishizono, H., Matsuo, M., Osanai, M., Sato, M., Ohkura, M., Nakai, J., Hayashi, Y., Sakurai, T., Kitamura, T., Fukai, T., & Inokuchi, K. (2019). Orchestrated ensemble activities constitute a hippocampal memory engram. *Nature Communications*, *10*(1), 2637. https://doi.org/10.1038/s41467-019-10683-2

Giovannucci, A., Friedrich, J., Gunn, P., Kalfon, J., Brown, B. L., Koay, S. A., Taxidis, J., Najafi, F., Gauthier, J. L., Zhou, P., Khakh, B. S., Tank, D. W., Chklovskii, D. B., & Pnevmatikakis, E. A. (2019). CaImAn an open source tool for scalable calcium imaging data analysis. *Elife*, *8*, e38173. https://doi.org/10.7554/eLife.38173

Gold, A. E., & Kesner, R. P. (2005). The role of the CA3 subregion of the dorsal hippocampus in spatial pattern completion in the rat. *Hippocampus*, *15*(6), 808-814. https://doi.org/https://doi.org/10.1002/hipo.20103

Gonzalez, W. G., Zhang, H., Harutyunyan, A., & Lois, C. (2019). Persistence of neuronal representations through time and damage in the hippocampus. *Science*, *365*(6455), 821-825. https://doi.org/doi:10.1126/science.aav9199

Grienberger, C., & Konnerth, A. (2012). Imaging Calcium in Neurons. *Neuron*, *73*(5), 862-885. https://doi.org/https://doi.org/10.1016/j.neuron.2012.02.011

Guzowski, J. F., Lyford, G. L., Stevenson, G. D., Houston, F. P., McGaugh, J. L., Worley, P. F., & Barnes, C. A. (2000). Inhibition of activity-dependent arc protein expression in the rat hippocampus impairs the maintenance of long-term potentiation and the consolidation of long-term memory. *J Neurosci*, *20*(11), 3993-4001. https://doi.org/10.1523/jneurosci.20-11-03993.2000

Guzowski, J. F., Miyashita, T., Chawla, M. K., Sanderson, J., Maes, L. I., Houston, F. P., Lipa, P., McNaughton, B. L., Worley, P. F., & Barnes, C. A. (2006). Recent behavioral history modifies coupling between cell activity and Arc gene transcription in hippocampal CA1 neurons. *Proceedings of the National Academy of Sciences*, *103*(4), 1077-1082.

Han, J.-H., Kushner, S. A., Yiu, A. P., Cole, C. J., Matynia, A., Brown, R. A., Neve, R. L., Guzowski, J. F., Silva, A. J., & Josselyn, S. A. (2007). Neuronal Competition and

Selection During Memory Formation. *Science*, *316*(5823), 457-460. https://doi.org/doi:10.1126/science.1139438
Han, J.-H., Kushner, S. A., Yiu, A. P., Hsiang, H.-L., Buch, T., Waisman, A., Bontempi, B., Neve, R. L., Frankland, P. W., & Josselyn, S. A. (2009). Selective erasure of a fear memory. *Science*, *323*(5920), 1492-1496.
Izquierdo, I., Furini, C. R. G., & Myskiw, J. C. (2016). Fear Memory. *Physiological Reviews*, *96*(2), 695-750. https://doi.org/10.1152/physrev.00018.2015
Jeantet, Y., & Cho, Y. H. (2012). Evolution of hippocampal spatial representation over time in mice. *Neurobiology of Learning and Memory*, *98*(4), 354-360. https://doi.org/https://doi.org/10.1016/j.nlm.2012.10.004
Jiang, Y., & VanDongen, A. M. J. (2021). Selective increase of correlated activity in Arc-positive neurons after chemically induced long-term potentiation in cultured hippocampal neurons. *eNeuro*, *8*(6). https://doi.org/10.1523/eneuro.0540-20.2021
Jimenez, J. C., Berry, J. E., Lim, S. C., Ong, S. K., Kheirbek, M. A., & Hen, R. (2020). Contextual fear memory retrieval by correlated ensembles of ventral CA1 neurons. *Nature Communications*, *11*(1), 3492. https://doi.org/10.1038/s41467-020-17270-w
Josselyn, S. A., & Tonegawa, S. (2020). Memory engrams: Recalling the past and imagining the future. *Science*, *367*(6473). https://doi.org/10.1126/science.aaw4325
Kentros, C. G., Agnihotri, N. T., Streater, S., Hawkins, R. D., & Kandel, E. R. (2004). Increased Attention to Spatial Context Increases Both Place Field Stability and Spatial Memory. *Neuron*, *42*(2), 283-295. https://doi.org/10.1016/S0896-6273(04)00192-8
Kesner, R. P., & Hunsaker, M. R. (2010). The temporal attributes of episodic memory. *Behavioural Brain Research*, *215*(2), 299-309. https://doi.org/https://doi.org/10.1016/j.bbr.2009.12.029
Kim, J., Kwon, J.-T., Kim, H.-S., Josselyn, S. A., & Han, J.-H. (2014). Memory recall and modifications by activating neurons with elevated CREB. *Nature Neuroscience*, *17*(1), 65-72. https://doi.org/10.1038/nn.3592
Kim, J. J., & Fanselow, M. S. (1992). Modality-Specific Retrograde Amnesia of Fear. *Science*, *256*(5057), 675-677. https://doi.org/doi:10.1126/science.1585183
Kinsky, N. R., Orlin, D. J., Ruesch, E. A., Kim, B., Coello, S., Diba, K., & Ramirez, S. (2025). Erasable hippocampal neural signatures predict memory discrimination. *Cell Reports*, *44*(3), 115391. https://doi.org/https://doi.org/10.1016/j.celrep.2025.115391
Kinsky, N. R., Sullivan, D. W., Mau, W., Hasselmo, M. E., & Eichenbaum, H. B. (2018). Hippocampal Place Fields Maintain a Coherent and Flexible Map across Long Timescales. *Current Biology*, *28*(22), 3578-3588.e3576. https://doi.org/https://doi.org/10.1016/j.cub.2018.09.037
Klinzing, J. G., Niethard, N., & Born, J. (2019). Mechanisms of systems memory consolidation during sleep. *Nature Neuroscience*, *22*(10), 1598-1610. https://doi.org/10.1038/s41593-019-0467-3
Ko, H., Hofer, S. B., Pichler, B., Buchanan, K. A., Sjöström, P. J., & Mrsic-Flogel, T. D. (2011). Functional specificity of local synaptic connections in neocortical networks. *Nature*, *473*(7345), 87-91. https://doi.org/10.1038/nature09880
Kobayashi, K. S., & Matsuo, N. (2023). Persistent representation of the environment in the hippocampus. *Cell Reports*, *42*(1), 111989. https://doi.org/https://doi.org/10.1016/j.celrep.2022.111989
Korb, E., & Finkbeiner, S. (2011). Arc in synaptic plasticity: from gene to behavior. *Trends in Neurosciences*, *34*(11), 591-598. https://doi.org/10.1016/j.tins.2011.08.007
Larkin, M. C., Lykken, C., Tye, L. D., Wickelgren, J. G., & Frank, L. M. (2014). Hippocampal output area CA1 broadcasts a generalized novelty signal during an object-place recognition task. *Hippocampus*, *24*(7), 773-783. https://doi.org/10.1002/hipo.22268

LeDoux, J. (2003). The Emotional Brain, Fear, and the Amygdala. *Cellular and Molecular Neurobiology*, *23*(4), 727-738. https://doi.org/10.1023/A:1025048802629
LeDoux, J. E. (1994). Emotion, Memory and the Brain. *Scientific American*, *270*(6), 50-57. http://www.jstor.org/stable/24942732
LeDoux, J. E. (2014). Coming to terms with fear. *Proceedings of the National Academy of Sciences*, *111*(8), 2871-2878.
LeDoux, J. E., Iwata, J., Cicchetti, P., & Reis, D. J. (1988). Different projections of the central amygdaloid nucleus mediate autonomic and behavioral correlates of conditioned fear. *The Journal of Neuroscience*, *8*(7), 2517. https://doi.org/10.1523/JNEUROSCI.08-07-02517.1988
Lee, A. K., & Wilson, M. A. (2002). Memory of Sequential Experience in the Hippocampus during Slow Wave Sleep. *Neuron*, *36*(6), 1183-1194. https://doi.org/https://doi.org/10.1016/S0896-6273(02)01096-6
Lee, H. S., & Han, J. H. (2023). Activity Patterns of Individual Neurons and Ensembles Correlated with Retrieval of a Contextual Memory in the Dorsal CA1 of Mouse Hippocampus. *J Neurosci*, *43*(1), 113-124. https://doi.org/10.1523/jneurosci.1407-22.2022
Levy, S. J., Kinsky, N. R., Mau, W., Sullivan, D. W., & Hasselmo, M. E. (2021). Hippocampal spatial memory representations in mice are heterogeneously stable. *Hippocampus*, *31*(3), 244-260. https://doi.org/https://doi.org/10.1002/hipo.23272
Link, W., Konietzko, U., Kauselmann, G., Krug, M., Schwanke, B., Frey, U., & Kuhl, D. (1995). Somatodendritic expression of an immediate early gene is regulated by synaptic activity. *Proc Natl Acad Sci U S A*, *92*(12), 5734-5738. https://doi.org/10.1073/pnas.92.12.5734
Liu, X., Ramirez, S., Pang, P. T., Puryear, C. B., Govindarajan, A., Deisseroth, K., & Tonegawa, S. (2012). Optogenetic stimulation of a hippocampal engram activates fear memory recall. *Nature*, *484*(7394), 381-385. https://doi.org/10.1038/nature11028
Liu, X., Ramirez, S., Redondo, R. L., & Tonegawa, S. (2014). Identification and Manipulation of Memory Engram Cells. *Cold Spring Harb Symp Quant Biol*, *79*, 59-65. https://doi.org/10.1101/sqb.2014.79.024901
Louie, K., & Wilson, M. A. (2001). Temporally Structured Replay of Awake Hippocampal Ensemble Activity during Rapid Eye Movement Sleep. *Neuron*, *29*(1), 145-156. https://doi.org/10.1016/S0896-6273(01)00186-6
Lovett-Barron, M., Kaifosh, P., Kheirbek, M. A., Danielson, N., Zaremba, J. D., Reardon, T. R., Turi, G. F., Hen, R., Zemelman, B. V., & Losonczy, A. (2014). Dendritic Inhibition in the Hippocampus Supports Fear Learning. *Science*, *343*(6173), 857-863. https://doi.org/doi:10.1126/science.1247485
Lyford, G. L., Yamagata, K., Kaufmann, W. E., Barnes, C. A., Sanders, L. K., Copeland, N. G., Gilbert, D. J., Jenkins, N. A., Lanahan, A. A., & Worley, P. F. (1995). Arc, a growth factor and activity-regulated gene, encodes a novel cytoskeleton-associated protein that is enriched in neuronal dendrites. *Neuron*, *14*(2), 433-445.
Malkki, H. A., Mertens, P. E., Lankelma, J. V., Vinck, M., van Schalkwijk, F. J., van Mourik-Donga, L. B., Battaglia, F. P., Mahlke, C., Kuhl, D., & Pennartz, C. M. (2016). Effects of Arc/Arg3.1 gene deletion on rhythmic synchronization of hippocampal CA1 neurons during locomotor activity and sleep. *Neurobiol Learn Mem*, *131*, 155-165. https://doi.org/10.1016/j.nlm.2016.03.021
Managò, F., Mereu, M., Mastwal, S., Mastrogiacomo, R., Scheggia, D., Emanuele, M., De Luca, M. A., Weinberger, D. R., Wang, K. H., & Papaleo, F. (2016). Genetic Disruption of Arc/Arg3.1 in Mice Causes Alterations in Dopamine and Neurobehavioral Phenotypes Related to Schizophrenia. *Cell Rep*, *16*(8), 2116-2128. https://doi.org/10.1016/j.celrep.2016.07.044

Maren, S. (1999). Neurotoxic or electrolytic lesions of the ventral subiculum produce deficits in the acquisition and expression of Pavlovian fear conditioning in rats. *Behavioral Neuroscience*, *113*(2), 283-290. https://doi.org/10.1037/0735-7044.113.2.283

Mathis, A., Mamidanna, P., Cury, K. M., Abe, T., Murthy, V. N., Mathis, M. W., & Bethge, M. (2018). DeepLabCut: markerless pose estimation of user-defined body parts with deep learning. *Nature Neuroscience*, *21*(9), 1281-1289. https://doi.org/10.1038/s41593-018-0209-y

McCurry, C. L., Shepherd, J. D., Tropea, D., Wang, K. H., Bear, M. F., & Sur, M. (2010). Loss of Arc renders the visual cortex impervious to the effects of sensory experience or deprivation. *Nature Neuroscience*, *13*(4), 450-457.

McGaugh, J. L. (2004). THE AMYGDALA MODULATES THE CONSOLIDATION OF MEMORIES OF EMOTIONALLY AROUSING EXPERIENCES. *Annual Review of Neuroscience*, *27*(Volume 27, 2004), 1-28. https://doi.org/https://doi.org/10.1146/annurev.neuro.27.070203.144157

Messaoudi, E., Kanhema, T., Soulé, J., Tiron, A., Dagyte, G., da Silva, B., & Bramham, C. R. (2007). Sustained Arc/Arg3. 1 synthesis controls long-term potentiation consolidation through regulation of local actin polymerization in the dentate gyrus in vivo. *Journal of Neuroscience*, *27*(39), 10445-10455.

Miller, E. K., & Cohen, J. D. (2001). An integrative theory of prefrontal cortex function. *Annu Rev Neurosci*, *24*, 167-202. https://doi.org/10.1146/annurev.neuro.24.1.167

Minatohara, K., Akiyoshi, M., & Okuno, H. (2016). Role of Immediate-Early Genes in Synaptic Plasticity and Neuronal Ensembles Underlying the Memory Trace [Review]. *Frontiers in molecular neuroscience*, *8*. https://doi.org/10.3389/fnmol.2015.00078

Mocle, A. J., Ramsaran, A. I., Jacob, A. D., Rashid, A. J., Luchetti, A., Tran, L. M., Richards, B. A., Frankland, P. W., & Josselyn, S. A. (2024). Excitability mediates allocation of pre-configured ensembles to a hippocampal engram supporting contextual conditioned threat in mice. *Neuron*, *112*(9), 1487-1497.e1486. https://doi.org/https://doi.org/10.1016/j.neuron.2024.02.007

Moita, M. A., Rosis, S., Zhou, Y., LeDoux, J. E., & Blair, H. T. (2004). Putting fear in its place: remapping of hippocampal place cells during fear conditioning. *J Neurosci*, *24*(31), 7015-7023. https://doi.org/10.1523/jneurosci.5492-03.2004

Morris, R. G. M., Garrud, P., Rawlins, J. N. P., & O'Keefe, J. (1982). Place navigation impaired in rats with hippocampal lesions. *Nature*, *297*(5868), 681-683. https://doi.org/10.1038/297681a0

Morris, R. G. M., Schenk, F., Tweedie, F., & Jarrard, L. E. (1990). Ibotenate Lesions of Hippocampus and/or Subiculum: Dissociating Components of Allocentric Spatial Learning. *European Journal of Neuroscience*, *2*(12), 1016-1028. https://doi.org/https://doi.org/10.1111/j.1460-9568.1990.tb00014.x

Moser, E. I., Kropff, E., & Moser, M. B. (2008). Place cells, grid cells, and the brain's spatial representation system. *Annu Rev Neurosci*, *31*, 69-89. https://doi.org/10.1146/annurev.neuro.31.061307.090723

Muller, R. U., & Kubie, J. L. (1987). The effects of changes in the environment on the spatial firing of hippocampal complex-spike cells. *The Journal of Neuroscience*, *7*(7), 1951. https://doi.org/10.1523/JNEUROSCI.07-07-01951.1987

Muzzio, I. A., Kentros, C., & Kandel, E. (2009). What is remembered? Role of attention on the encoding and retrieval of hippocampal representations. *The Journal of Physiology*, *587*(12), 2837-2854. https://doi.org/https://doi.org/10.1113/jphysiol.2009.172445

Nadel, L., & Moscovitch, M. (1997). Memory consolidation, retrograde amnesia and the hippocampal complex. *Curr Opin Neurobiol*, *7*(2), 217-227. https://doi.org/10.1016/s0959-4388(97)80010-4

Nakayama, D., Iwata, H., Teshirogi, C., Ikegaya, Y., Matsuki, N., & Nomura, H. (2015). Long-delayed expression of the immediate early gene Arc/Arg3.1 refines neuronal circuits to perpetuate fear memory. *J Neurosci*, *35*(2), 819-830. https://doi.org/10.1523/jneurosci.2525-14.2015

Navabpour, S., Kwapis, J. L., & Jarome, T. J. (2020). A neuroscientist's guide to transgenic mice and other genetic tools. *Neuroscience & Biobehavioral Reviews*, *108*, 732-748. https://doi.org/https://doi.org/10.1016/j.neubiorev.2019.12.013

Neves, G., Cooke, S. F., & Bliss, T. V. P. (2008). Synaptic plasticity, memory and the hippocampus: a neural network approach to causality. *Nature Reviews Neuroscience*, *9*(1), 65-75. https://doi.org/10.1038/nrn2303

O'Brien, J., & Sutherland, R. J. (2007). Evidence for episodic memory in a pavlovian conditioning procedure in rats. *Hippocampus*, *17*(12), 1149-1152. https://doi.org/https://doi.org/10.1002/hipo.20346

O'Keefe, J., & Krupic, J. (2021). Do hippocampal pyramidal cells respond to nonspatial stimuli? *Physiological Reviews*, *101*(3), 1427-1456. https://doi.org/10.1152/physrev.00014.2020

Ortega-de San Luis, C., & Ryan, T. J. (2022). Understanding the physical basis of memory: Molecular mechanisms of the engram. *Journal of Biological Chemistry*, *298*(5), 101866. https://doi.org/https://doi.org/10.1016/j.jbc.2022.101866

Pachitariu, M., Stringer, C., Dipoppa, M., Schröder, S., Rossi, L. F., Dalgleish, H., Carandini, M., & Harris, K. D. (2017). Suite2p: beyond 10,000 neurons with standard two-photon microscopy. *bioRxiv*, 061507. https://doi.org/10.1101/061507

Park, S., Park, J. M., Kim, S., Kim, J.-A., Shepherd, J. D., Smith-Hicks, C. L., Chowdhury, S., Kaufmann, W., Kuhl, D., & Ryazanov, A. G. (2008). Elongation factor 2 and fragile X mental retardation protein control the dynamic translation of Arc/Arg3. 1 essential for mGluR-LTD. *Neuron*, *59*(1), 70-83.

Pérez-Ortega, J., Akrouh, A., & Yuste, R. (2024). Stimulus encoding by specific inactivation of cortical neurons. *Nature Communications*, *15*(1), 3192. https://doi.org/10.1038/s41467-024-47515-x

Perry, R. J., & Hodges, J. R. (1999). Attention and executive deficits in Alzheimer's disease: A critical review. *Brain*, *122*(3), 383-404. https://doi.org/10.1093/brain/122.3.383

Petersen, P. C., Siegle, J. H., Steinmetz, N. A., Mahallati, S., & Buzsáki, G. (2021). CellExplorer: A framework for visualizing and characterizing single neurons. *Neuron*, *109*(22), 3594-3608.e3592. https://doi.org/https://doi.org/10.1016/j.neuron.2021.09.002

Phillips, R., & LeDoux, J. (1992). Differential contribution of amygdala and hippocampus to cued and contextual fear conditioning. *Behavioral Neuroscience*, *106*(2), 274.

Plath, N., Ohana, O., Dammermann, B., Errington, M. L., Schmitz, D., Gross, C., Mao, X., Engelsberg, A., Mahlke, C., Welzl, H., Kobalz, U., Stawrakakis, A., Fernandez, E., Waltereit, R., Bick-Sander, A., Therstappen, E., Cooke, Sam F., Blanquet, V., Wurst, W.,…Kuhl, D. (2006). Arc/Arg3.1 Is Essential for the Consolidation of Synaptic Plasticity and Memories. *Neuron*, *52*(3), 437-444. https://doi.org/https://doi.org/10.1016/j.neuron.2006.08.024

Ploski, J. E., Pierre, V. J., Smucny, J., Park, K., Monsey, M. S., Overeem, K. A., & Schafe, G. E. (2008). The activity-regulated cytoskeletal-associated protein (Arc/Arg3.1) is required for memory consolidation of pavlovian fear conditioning in the lateral amygdala. *J Neurosci*, *28*(47), 12383-12395. https://doi.org/10.1523/jneurosci.1662-08.2008

Pnevmatikakis, E. A., & Giovannucci, A. (2017). NoRMCorre: An online algorithm for piecewise rigid motion correction of calcium imaging data. *Journal of Neuroscience Methods*, *291*, 83-94. https://doi.org/https://doi.org/10.1016/j.jneumeth.2017.07.031

Prut, L., & Belzung, C. (2003). The open field as a paradigm to measure the effects of drugs on anxiety-like behaviors: a review. *European Journal of Pharmacology*, *463*(1), 3-33. https://doi.org/https://doi.org/10.1016/S0014-2999(03)01272-X

Raber, J., Arzy, S., Bertolus, J. B., Depue, B., Haas, H. E., Hofmann, S. G., Kangas, M., Kensinger, E., Lowry, C. A., Marusak, H. A., Minnier, J., Mouly, A.-M., Mühlberger, A., Norrholm, S. D., Peltonen, K., Pinna, G., Rabinak, C., Shiban, Y., Soreq, H.,…Boutros, S. W. (2019). Current understanding of fear learning and memory in humans and animal models and the value of a linguistic approach for analyzing fear learning and memory in humans. *Neuroscience & Biobehavioral Reviews*, *105*, 136-177. https://doi.org/https://doi.org/10.1016/j.neubiorev.2019.03.015

Ramirez, S., Liu, X., Lin, P.-A., Suh, J., Pignatelli, M., Redondo, R. L., Ryan, T. J., & Tonegawa, S. (2013). Creating a False Memory in the Hippocampus. *Science*, *341*(6144), 387-391. https://doi.org/doi:10.1126/science.1239073

Rao, V. R., Pintchovski, S. A., Chin, J., Peebles, C. L., Mitra, S., & Finkbeiner, S. (2006). AMPA receptors regulate transcription of the plasticity-related immediate-early gene Arc. *Nature Neuroscience*, *9*(7), 887-895. https://doi.org/10.1038/nn1708

Rashid, A. J., Yan, C., Mercaldo, V., Hsiang, H.-L., Park, S., Cole, C. J., De Cristofaro, A., Yu, J., Ramakrishnan, C., Lee, S. Y., Deisseroth, K., Frankland, P. W., & Josselyn, S. A. (2016). Competition between engrams influences fear memory formation and recall. *Science*, *353*(6297), 383-387. https://doi.org/doi:10.1126/science.aaf0594

Reijmers, L. G., Perkins, B. L., Matsuo, N., & Mayford, M. (2007). Localization of a stable neural correlate of associative memory. *Science*, *317*(5842), 1230-1233. https://doi.org/10.1126/science.1143839

Resendez, S. L., Jennings, J. H., Ung, R. L., Namboodiri, V. M., Zhou, Z. C., Otis, J. M., Nomura, H., McHenry, J. A., Kosyk, O., & Stuber, G. D. (2016). Visualization of cortical, subcortical and deep brain neural circuit dynamics during naturalistic mammalian behavior with head-mounted microscopes and chronically implanted lenses. *Nat Protoc*, *11*(3), 566-597. https://doi.org/10.1038/nprot.2016.021

Roshchina, M. A., Smirnov, I. V., Isaev, A. B., Roshchin, M., Borodinova, A. A., Aseyev, N. A., & Balaban, P. M. (2021). INVESTIGATION OF CA1 NEURONAL ACTIVITY DURING CONTEXT FEAR CONDITIONING WITH MINIATURE FLUORESCENCE MICROSCOPES. *Opera Med Physiol.*, *8*(3), 52-58. https://doi.org/10.24412/2500-2295-2021-3-52-58

Rossant, C., Kadir, S. N., Goodman, D. F. M., Schulman, J., Hunter, M. L. D., Saleem, A. B., Grosmark, A., Belluscio, M., Denfield, G. H., Ecker, A. S., Tolias, A. S., Solomon, S., Buzsáki, G., Carandini, M., & Harris, K. D. (2016). Spike sorting for large, dense electrode arrays. *Nature Neuroscience*, *19*(4), 634-641. https://doi.org/10.1038/nn.4268

Roy, D. S., Park, Y.-G., Kim, M. E., Zhang, Y., Ogawa, S. K., DiNapoli, N., Gu, X., Cho, J. H., Choi, H., Kamentsky, L., Martin, J., Mosto, O., Aida, T., Chung, K., & Tonegawa, S. (2022). Brain-wide mapping reveals that engrams for a single memory are distributed across multiple brain regions. *Nature Communications*, *13*(1), 1799. https://doi.org/10.1038/s41467-022-29384-4

Schmidt, B., Marrone, D. F., & Markus, E. J. (2012). Disambiguating the similar: The dentate gyrus and pattern separation. *Behavioural Brain Research*, *226*(1), 56-65. https://doi.org/https://doi.org/10.1016/j.bbr.2011.08.039

Schuette, P. J., Reis, F. M. C. V., Maesta-Pereira, S., Chakerian, M., Torossian, A., Blair, G. J., Wang, W., Blair, H. T., Fanselow, M. S., Kao, J. C., & Adhikari, A. (2020). Long-Term Characterization of Hippocampal Remapping during Contextual Fear Acquisition and Extinction. *The Journal of Neuroscience*, *40*(43), 8329. https://doi.org/10.1523/JNEUROSCI.1022-20.2020

Scoville, W. B., & Milner, B. (2000). Loss of recent memory after bilateral hippocampal lesions. 1957. *J Neuropsychiatry Clin Neurosci*, *12*(1), 103-113. https://doi.org/10.1176/jnp.12.1.103

Shepherd, J. D., Rumbaugh, G., Wu, J., Chowdhury, S., Plath, N., Kuhl, D., Huganir, R. L., & Worley, P. F. (2006). Arc/Arg3. 1 mediates homeostatic synaptic scaling of AMPA receptors. *Neuron*, *52*(3), 475-484.

Sirota, A., Montgomery, S., Fujisawa, S., Isomura, Y., Zugaro, M., & Buzsáki, G. (2008). Entrainment of neocortical neurons and gamma oscillations by the hippocampal theta rhythm. *Neuron*, *60*(4), 683-697. https://doi.org/10.1016/j.neuron.2008.09.014

Smith, D. M., & Mizumori, S. J. Y. (2006). Hippocampal place cells, context, and episodic memory. *Hippocampus*, *16*(9), 716-729. https://doi.org/https://doi.org/10.1002/hipo.20208

Squire, L. R., & Wixted, J. T. (2011). The cognitive neuroscience of human memory since H.M. *Annu Rev Neurosci*, *34*, 259-288. https://doi.org/10.1146/annurev-neuro-061010-113720

Stamatakis, A. M., Resendez, S. L., Chen, K. S., Favero, M., Liang-Guallpa, J., Nassi, J. J., Neufeld, S. Q., Visscher, K., & Ghosh, K. K. (2021). Miniature microscopes for manipulating and recording in vivo brain activity. *Microscopy (Oxf)*, *70*(5), 399-414. https://doi.org/10.1093/jmicro/dfab028

Stark, E., Eichler, R., Roux, L., Fujisawa, S., Rotstein, Horacio G., & Buzsáki, G. (2013). Inhibition-Induced Theta Resonance in Cortical Circuits. *Neuron*, *80*(5), 1263-1276. https://doi.org/https://doi.org/10.1016/j.neuron.2013.09.033

Steward, O., Wallace, C. S., Lyford, G. L., & Worley, P. F. (1998). Synaptic Activation Causes the mRNA for the IEG Arc to Localize Selectively near Activated Postsynaptic Sites on Dendrites. *Neuron*, *21*(4), 741-751. https://doi.org/https://doi.org/10.1016/S0896-6273(00)80591-7

Steward, O., & Worley, P. F. (2001). A cellular mechanism for targeting newly synthesized mRNAs to synaptic sites on dendrites. *Proceedings of the National Academy of Sciences*, *98*(13), 7062-7068. https://doi.org/doi:10.1073/pnas.131146398

Steward, O., & Worley, P. F. (2001). Selective targeting of newly synthesized Arc mRNA to active synapses requires NMDA receptor activation. *Neuron*, *30*(1), 227-240.

Sun, D., Shaik, N. E. K., Unnithan, R. R., & French, C. (2024). Hippocampal cognitive and relational map paradigms explored by multisensory encoding recording with wide-field calcium imaging. *iScience*, *27*(1). https://doi.org/10.1016/j.isci.2023.108603

Tanaka, Kazumasa Z., Pevzner, A., Hamidi, Anahita B., Nakazawa, Y., Graham, J., & Wiltgen, Brian J. (2014). Cortical Representations Are Reinstated by the Hippocampus during Memory Retrieval. *Neuron*, *84*(2), 347-354. https://doi.org/10.1016/j.neuron.2014.09.037

Teber, I., Köhling, R., Speckmann, E.-J., Barnekow, A., & Kremerskothen, J. (2004). Muscarinic acetylcholine receptor stimulation induces expression of the activity-regulated cytoskeleton-associated gene (ARC). *Molecular Brain Research*, *121*(1), 131-136. https://doi.org/https://doi.org/10.1016/j.molbrainres.2003.11.017

Thompson, L. T., & Best, P. J. (1990). Long-term stability of the place-field activity of single units recorded from the dorsal hippocampus of freely behaving rats. *Brain Research*, *509*(2), 299-308. https://doi.org/https://doi.org/10.1016/0006-8993(90)90555-P

Tonegawa, S., Pignatelli, M., Roy, D. S., & Ryan, T. J. (2015). Memory engram storage and retrieval. *Current Opinion in Neurobiology*, *35*, 101-109. https://doi.org/https://doi.org/10.1016/j.conb.2015.07.009

Tunney, C., Thorson, E., & Chen, W. (2021). Following and Avoiding Fear-Inducing News Topics: Fear Intensity, Perceived News Topic Importance, Self-Efficacy, and News

Overload. *Journalism Studies*, *22*(5), 614-632. https://doi.org/10.1080/1461670X.2021.1890636

van der Veldt, S., Etter, G., Mosser, C.-A., Manseau, F., & Williams, S. (2021). Conjunctive spatial and self-motion codes are topographically organized in the GABAergic cells of the lateral septum. *PLOS Biology*, *19*(8), e3001383. https://doi.org/10.1371/journal.pbio.3001383

Vanwalleghem, G., Constantin, L., & Scott, E. K. (2020). Calcium Imaging and the Curse of Negativity. *Front Neural Circuits*, *14*, 607391. https://doi.org/10.3389/fncir.2020.607391

Viejo, G., Levenstein, D., Skromne Carrasco, S., Mehrotra, D., Mahallati, S., Vite, G. R., Denny, H., Sjulson, L., Battaglia, F. P., & Peyrache, A. (2023). Pynapple, a toolbox for data analysis in neuroscience. *Elife*, *12*, RP85786. https://doi.org/10.7554/eLife.85786

Walsh, R. N., & Cummins, R. A. (1976). The Open-Field Test: a critical review. *Psychol Bull*, *83*(3), 482-504.

Waltereit, R., Dammermann, B., Wulff, P., Scafidi, J., Staubli, U., Kauselmann, G., Bundman, M., & Kuhl, D. (2001). Arg3. 1/Arc mRNA induction by Ca2+ and cAMP requires protein kinase A and mitogen-activated protein kinase/extracellular regulated kinase activation. *Journal of Neuroscience*, *21*(15), 5484-5493.

Wang, K. H., Majewska, A., Schummers, J., Farley, B., Hu, C., Sur, M., & Tonegawa, S. (2006). In vivo two-photon imaging reveals a role of arc in enhancing orientation specificity in visual cortex. *Cell*, *126*(2), 389-402.

Waung, M. W., Pfeiffer, B. E., Nosyreva, E. D., Ronesi, J. A., & Huber, K. M. (2008). Rapid translation of Arc/Arg3. 1 selectively mediates mGluR-dependent LTD through persistent increases in AMPAR endocytosis rate. *Neuron*, *59*(1), 84-97.

Wilson, M. A., & McNaughton, B. L. (1993). Dynamics of the Hippocampal Ensemble Code for Space. *Science*, *261*(5124), 1055-1058. https://doi.org/doi:10.1126/science.8351520

Wirtshafter, H. S., & Disterhoft, J. F. (2022). In Vivo Multi-Day Calcium Imaging of CA1 Hippocampus in Freely Moving Rats Reveals a High Preponderance of Place Cells with Consistent Place Fields. *The Journal of Neuroscience*, *42*(22), 4538. https://doi.org/10.1523/JNEUROSCI.1750-21.2022

Yang, X. (2024). *Expression of Arc/Arg3. 1 in GABAergic neurons and in hippocampal-septal circuits, regulates Learning, memory and stress-related disorders* Staats-und Universitätsbibliothek Hamburg Carl von Ossietzky].

Ying, S.-W., Futter, M., Rosenblum, K., Webber, M. J., Hunt, S. P., Bliss, T. V., & Bramham, C. R. (2002). Brain-derived neurotrophic factor induces long-term potentiation in intact adult hippocampus: requirement for ERK activation coupled to CREB and upregulation of Arc synthesis. *Journal of Neuroscience*, *22*(5), 1532-1540.

Yiu, Adelaide P., Mercaldo, V., Yan, C., Richards, B., Rashid, Asim J., Hsiang, H.-Lin L., Pressey, J., Mahadevan, V., Tran, Matthew M., Kushner, Steven A., Woodin, Melanie A., Frankland, Paul W., & Josselyn, Sheena A. (2014). Neurons Are Recruited to a Memory Trace Based on Relative Neuronal Excitability Immediately before Training. *Neuron*, *83*(3), 722-735. https://doi.org/10.1016/j.neuron.2014.07.017

Zhang, H., & Bramham, C. R. (2021). Arc/Arg3.1 function in long-term synaptic plasticity: Emerging mechanisms and unresolved issues. *Eur J Neurosci*, *54*(8), 6696-6712. https://doi.org/10.1111/ejn.14958

Zhang, Y., Rózsa, M., Liang, Y., Bushey, D., Wei, Z., Zheng, J., Reep, D., Broussard, G. J., Tsang, A., Tsegaye, G., Narayan, S., Obara, C. J., Lim, J.-X., Patel, R., Zhang, R., Ahrens, M. B., Turner, G. C., Wang, S. S. H., Korff, W. L.,…Looger, L. L. (2023). Fast and sensitive GCaMP calcium indicators for imaging neural populations. *Nature*, *615*(7954), 884-891. https://doi.org/10.1038/s41586-023-05828-9

Zhou, P., Resendez, S. L., Rodriguez-Romaguera, J., Jimenez, J. C., Neufeld, S. Q., Giovannucci, A., Friedrich, J., Pnevmatikakis, E. A., Stuber, G. D., Hen, R., Kheirbek, M. A., Sabatini, B. L., Kass, R. E., & Paninski, L. (2018). Efficient and accurate extraction of in vivo calcium signals from microendoscopic video data. *Elife*, *7*, e28728. https://doi.org/10.7554/eLife.28728

Zhou, Y., Qiu, L., Wang, H., & Chen, X. (2020). Induction of activity synchronization among primed hippocampal neurons out of random dynamics is key for trace memory formation and retrieval. *The FASEB Journal*, *34*(3), 3658-3676. https://doi.org/https://doi.org/10.1096/fj.201902274R

Zinyuk, L., Kubik, S., Kaminsky, Y., Fenton, A. A., & Bures, J. (2000). Understanding hippocampal activity by using purposeful behavior: Place navigation induces place cell discharge in both task-relevant and task-irrelevant spatial reference frames. *Proceedings of the National Academy of Sciences*, *97*(7), 3771-3776. https://doi.org/doi:10.1073/pnas.97.7.3771

Ziv, Y., Burns, L. D., Cocker, E. D., Hamel, E. O., Ghosh, K. K., Kitch, L. J., Gamal, A. E., & Schnitzer, M. J. (2013). Long-term dynamics of CA1 hippocampal place codes. *Nature Neuroscience*, *16*(3), 264-266. https://doi.org/10.1038/nn.3329